PEOPLE'S DEMOCRATIC REPUBLIC OF ALGERIA

MINISTRY OF HIGHER EDUCATION AND SCIENTIFIC RESEARCH

UNIVERSITY OF ECHAHID HAMMA LAKHDAR EL-OUED

جامعة الشهيد حمّه لخضر - الوادي
Université Echahid Hamma Lakhdar - El-Oued

Faculty of Technology

Department of Electrical Engineering

Thesis

Submitted in partial fulfillment of the requirements for Doctorate degree

Option: Telecommunications Networks

Presented by **BEDDIAF SAFIA**

Theme

Effect Reduction of Hardware Impairment on the NOMA System

Jury:

President	Ajgou Riad	Professor	University of El-Oued
Director	Khelil Abdellatif	Associate Professor	University of El-Oued
Examiner	Aounallah Naceur	Professor	University of Ouargla
Examiner	Merah Hocine	Associate Professor	University of Laghouat
Examiner	Medjouri Abdelkader	Professor	University of El-Oued

September 2023

بسم الله الرحمن الرحيم

Acknowledgements

I want to take a moment to extend my heartfelt appreciation and deep gratitude to my thesis supervisor, Khelil Abdellatif. Their steadfast support, invaluable guidance, and unwavering dedication have been the bedrock of my research journey. Khelil Abdellatif has been an exemplary mentor, shaping the course of this research project with their expertise, insights, and unwavering commitment. Their constructive feedback, scholarly wisdom, and unwavering encouragement have significantly enhanced the quality of my work.

I am equally grateful to Pr. Khaled Rabie, Pr. Halim Yanikomeroglu, and particularly Dr. Ferdi Kara for their invaluable contributions and guidance throughout this research endeavor. Their expertise and insights have added a multifaceted dimension to my work, and their support has been instrumental in its success.

I extend my sincere thanks to the members of the jury who graciously agreed to be a part of this humble endeavor. I am indebted to certain individuals and friends who provided unwavering support, enabling us to navigate obstacles optimistically. To all of you, my heartfelt gratitude.

This thesis is dedicated to my father, who can take pride in seeing the culmination of years of sacrifices and hardships that have helped me progress in life. May God bless this work with success. Thank you, Dad, for instilling in me noble values, providing education, and unwavering support.

I also want to express my gratitude to my mother, whose tireless efforts, love, unwavering support, sacrifices, and invaluable advice have been the pillars of my journey. Through this modest work, I hope to convey the depth of my feelings and eternal gratitude for all that you've done.

To my brothers Walid, Ilyes, Younes, and Hassen, and my sisters Dalel, Amina, and Soundous, who have consistently embodied perseverance, courage, and generosity in my life.

To my little angels, Iyed, Melissa, Roya, Yousra, Louai, Maria, and Anais, who bring boundless joy and inspiration.

Lastly, I extend my appreciation to my friends and colleagues at the University of Echahid Hamma Lakhdar, El-Oued, and all those who have supported me throughout this period. Your camaraderie and support have been invaluable.

Dedication

I dedicate this work to my parents:

Your unwavering support and love have been my inspiration throughout this journey. This thesis is a tribute to your boundless encouragement and belief in my potential.

In honor of my beloved brothers and sister, Whose love and unwavering support have lit my path, I appreciate your constant encouragement and inspiration.

To all my friends and those who have helped and continuously encouraged me, I extend my best wishes for continued success.

Thanks

Beddiaf Safia

Abstract

The rapid expansion of wireless communication systems has ushered in a new era marked by soaring demands for faster data rates, reduced latency, and improved spectral efficiency. To meet these demands, the Non-Orthogonal Multiple Access (NOMA) system has emerged as a game-changing technology. NOMA enables multiple users to share the same time-frequency resources, significantly enhancing system capacity and efficiency. Within NOMA, the power domain (PD-NOMA), where users share resources with different power allocation coefficients, has attracted particular interest. This approach employs successive interference canceler (SIC) to mitigate interference and has great potential for applications in 5G and beyond, leading to extensive research on its achievable rates and outage probabilities.

In real communication systems, transceivers play a pivotal role by facilitating both the transmission and reception of signals. However, due to the intricate nature of their internal components and the inherent complexity of the manufacturing process, it is quite common for transceivers to exhibit hardware imperfections and non-ideal behavior. Several contributing factors give rise to this non-ideal operation, particularly in radio frequency (RF) transceivers. These hardware impairments (HWI) manifest across various stages of the transceiver's operation, non-linear behavior in high-power amplifiers, the presence of phase noise, and imbalances in the in-phase and quadrature (I/Q) components within the RF front-end.

The motivation for our research stems from two primary concerns: NOMA and HWI. Our work is driven by the objective of exploring and understanding the performance such as capacity, outage probability (OP), ergodic capacity (EC), and bit error rate (EC) of NOMA systems operating in the presence of HWI. This research seeks to provide realistic conditions, where hardware imperfections can significantly impact the system's overall efficiency and reliability. By addressing these critical issues, our study aims to contribute to the enhancement of NOMA-based communication systems and their practical implementation in a range of applications.

In the initial segment of this thesis, we delve into the impact of HWI and IQI on conventional NOMA systems. Our analysis assumes that users communicate directly with the source, and we focus on deriving mathematical expressions to quantify these effects over a Rayleigh fading channel. To validate the accuracy of our findings, we conduct comprehensive computer simulations.

Subsequently, we explore the synergistic potential of combining NOMA with cooperative communication techniques to enhance spectral efficiency. This novel approach, known as Cooperative NOMA (CNOMA), represents a promising avenue for improving the performance of wireless communication systems.

In CNOMA, we consider two distinct concepts: CNOMA without the presence of direct links and CNOMA with direct links between users. In both scenarios, we investigate the influence of various hardware impairments, including HWI and IQI, on critical performance metrics such as BER, OP, and EC. By systematically examining these metrics in the presence of hardware imperfections, we aim to gain a comprehensive understanding of how CNOMA can thrive in real-world conditions, ultimately contributing valuable insights to the field of wireless communications.

Finally, the thesis concludes by delving into a comprehensive discussion of the results obtained. It not only highlights the opportunities and challenges revealed but also offers valuable insights that can shape the direction of future research endeavors in this field.

Keywords: Bit error rate (BER), Ergodic capacity (EC), Hardware impairment (HWI), Imperfect channel state information (ipCSI), Imperfect successive interference canceler (ipSIC), In-phase and quadrature-phase imbalance (IQI), Non-orthogonal multiple access (NOMA), and Outage probability (OP).

Résumé

L'expansion rapide des systèmes de communication sans fil a ouvert une nouvelle ère marquée par une demande croissante de débits de données plus rapides, de latence réduite et d'efficacité spectrale améliorée. Pour répondre à ces exigences, le système d'accès multiple non orthogonal (NOMA) est apparu comme une technologie révolutionnaire. NOMA permet à plusieurs utilisateurs de partager les mêmes ressources temps-fréquence, améliorant ainsi considérablement la capacité et l'efficacité du système. Dans le cadre de NOMA, le domaine de puissance (PD)-NOMA, où les utilisateurs partagent des ressources avec des coefficients d'allocation de puissance différents, suscite un intérêt particulier. Cette approche utilise un annulateur d'interférences successives (SIC) pour atténuer les interférences et présente un potentiel considérable pour les applications en 5G et au-delà, ce qui a conduit à des recherches approfondies sur ses taux réalisables et ses probabilités de panne.

Dans les systèmes de communication réels, les émetteurs-récepteurs jouent un rôle central en facilitant à la fois la transmission et la réception des signaux. Cependant, en raison de la nature complexe de leurs composants internes et de la complexité inhérente au processus de fabrication, il est assez courant que les émetteurs-récepteurs présentent des imperfections matérielles et un comportement non idéal. Plusieurs facteurs contributifs donnent lieu à cette opération non idéale, notamment dans les émetteurs-récepteurs radiofréquence (RF). Ces altérations matérielles (HWI) se manifestent à des étapes différentes de l'opération de l'émetteur-récepteur, telles que le comportement non linéaire dans les amplificateurs haute puissance, la présence de bruit de phase, et les déséquilibres entre les composantes en phase et en quadrature (I/Q) dans la partie RF.

La motivation de notre recherche découle de deux aspects principales : NOMA et HWI. Notre travail est guidé par l'objectif d'explorer et de comprendre les performances telles que la capacité, la probabilité d'indisponibilité (OP), la capacité ergodique (EC) et le taux d'erreur binaire (EC) des systèmes NOMA fonctionnant en présence de HWI. Cette recherche vise à fournir des conditions réalistes, où les imperfections matérielles peuvent avoir un impact significatif sur l'efficacité et la fiabilité globales du système. En abordant ces questions cruciales, notre étude vise à contribuer à l'amélioration des systèmes de communication basés sur NOMA et à leur mise en œuvre pratique dans diverses applications.

Dans la première partie de cette thèse, nous explorons l'impact des imperfections matérielles (HWI) et de l'imbalance en phase et en quadrature (IQI) sur les systèmes NOMA conventionnels. Notre analyse suppose que les utilisateurs communiquent directement avec la source, et nous nous concentrons sur l'élaboration d'expressions mathématiques pour quantifier ces effets sur un canal de propagation de Rayleigh. Pour valider la précision de nos résultats, nous menons des simulations informatiques approfondies.

Par la suite, nous explorons le potentiel synergique de la combinaison de NOMA avec des techniques de communication coopérative pour améliorer l'efficacité spectrale. Cette approche novatrice, connue sous le nom de Cooperative NOMA (CNOMA), représente une voie prometteuse pour améliorer les performances des systèmes de communication sans fil.

Dans le cadre du CNOMA, nous considérons deux concepts distincts : le CNOMA sans la présence de liaisons directes et le CNOMA avec des liaisons directes entre les utilisateurs. Dans les deux scénarios, nous étudions l'influence de diverses imperfections matérielles, notamment les HWI et les IQI, sur des métriques de performance critiques telles que le BER, l'OP et l'EC. En examinant systématiquement ces métriques en présence d'imperfections matérielles, notre objectif est de comprendre de manière globale comment le CNOMA peut prospérer dans des conditions du monde réel, contribuant ainsi à des informations précieuses dans le domaine des communications sans fil.

Enfin, la thèse se conclut en approfondissant une discussion complète des résultats obtenus. Elle met en lumière non seulement les opportunités et les défis révélés, mais offre également des connaissances précieuses qui peuvent orienter la direction des futures recherches dans ce domaine.

Mots-clés : Taux d'erreur binaire (BER), Capacité ergodique (EC), Altération matérielle (HWI), Information d'état de canal imparfaite (ipCSI), Annulateur d'interférences successives imparfait (ipSIC), Déséquilibre en phase et en quadrature (IQI), Accès multiple non orthogonal (NOMA) et Probabilité de panne (OP).

ملخص

فتح التوسع السريع لأنظمة الاتصالات اللاسلكية حقبة جديدة تميزت بالطلب المتزايد على معدلات بيانات أسرع وتقليل زمن الوصول وتحسين الكفاءة الطيفية. لتلبية هذه المتطلبات ، ظهر نظام الوصول المتعدد غير المتعامد (NOMA) كتقنية تطورية. تسمح NOMA لعدة مستخدمين بمشاركة نفس موارد التردد الزمني ، وبالتالي تحسين قدرة النظام وكفاءته بشكل كبير. كجزء من NOMA ، مجال الطاقة (PD-NOMA) ، المستخدمين أو تقاسم الموارد مع مختلف معاملات توزيع الطاقة، يثير إريت كثافة العمليات معين. يستخدم هذا النهج أداة إلغاء التداخل المتتالية (SIC)لتقييم التدخلات ويظهر إمكانات كبيرة للتطبيقات في الجيل ٥ وما بعده ، مما يؤدي إلى بحث مكثف حول معدلاته القابلة للتحقيق واحتمالات الانقطاع.
في أنظمة الاتصالات الحقيقية ، تلعب أجهزة الإرسال والاستقبال دورا محوريا من خلال تسهيل إرسال واستقبال الإشارات. ومع ذلك ، نظرا للطبيعة المعقدة لمكوناتها الداخلية والتعقيد المتأصل في عملية التصنيع ، فمن الشائع جدا أن تظهر أجهزة الإرسال والاستقبال عيوبا في الأجهزة وسلوكا غير مثالي. تؤدي العديد من العوامل المساهمة إلى ظهور هذه العملية غير المثالية ، لا سيما في أجهزة الإرسال والاستقبال ذات التردد اللاسلكي(RF). تتجلى هذه الإعاقات في الأجهزة (HWI)عبر مراحل مختلفة من تشغيل جهاز الإرسال والاستقبال ، والسلوك غير الخطي في مكبرات الصوت عالية الطاقة ، ووجود ضوضاء الطور ، والاختلالات في مكونات الطور والتربيع (I/Q) داخل الواجهة الأمامية للترددات اللاسلكية.

الدافع وراء بحثنا ينبع من اهتمامين رئيسيين: NOMA و HWI. يرتكز عملنا على هدف استكشاف وفهم الأداء مثل السعة واحتمالية الانقطاع (OP) والسعة المريحة (EC) ومعدل خطأ البت (EC) لأنظمة NOMA التي تعمل في وجود HWI. يسعى هذا البحث إلى توفير ظروف واقعية، حيث يمكن أن تؤثر عيوب الأجهزة بشكل كبير على كفاءة النظام وموثوقيته بشكل عام. ومن خلال معالجة هذه القضايا الحاسمة، تهدف دراستنا إلى المساهمة في تعزيز أنظمة الاتصالات القائمة على NOMA وتنفيذها العملي في مجموعة من التطبيقات.

في الجزء الأول من هذه الأطروحة، نتعمق في تأثير HWI و IQI على أنظمة NOMA التقليدية. يفترض تحليلنا أن المستخدمين يتواصلون مباشرة مع المصدر، ونركز على استخلاص التعبيرات الرياضية لتحديد هذه التأثيرات عبر قناة خبو رايلي. للتحقق من دقة النتائج التي توصلنا إليها، نقوم بإجراء عمليات محاكاة حاسوبية شاملة.

وبعد ذلك، نستكشف الإمكانات التآزرية للجمع بين NOMA وتقنيات الاتصال التعاوني لتعزيز الكفاءة الطيفية. يمثل هذا النهج الجديد، المعروف

باسم NOMA التعاوني (CNOMA)، وسيلة واعدة لتحسين أداء أنظمة الاتصالات اللاسلكية.

في CNOMA، نعتبر مفهومين متميزين: CNOMA بدون وجود روابط مباشرة و CNOMA مع روابط مباشرة بين المستخدمين. في كلا السيناريوهين، نقوم بالتحقيق في تأثير حالات قصور الأجهزة المختلفة، بما في ذلك HWI و IQI، على مقاييس الأداء المهمة مثل BER و OP و EC. ومن خلال الفحص المنهجي لهذه المقاييس في ظل وجود عيوب في الأجهزة، فإننا نهدف إلى الحصول على فهم شامل لكيفية ازدهار CNOMA في ظروف العالم الحقيقي، مما يساهم في النهاية برؤى قيمة في مجال الاتصالات اللاسلكية.

وأخيرا، تختتم الرسالة بالخوض في مناقشة شاملة للنتائج التي تم الحصول عليها. فهو لا يسلط الضوء على الفرص والتحديات التي تم الكشف عنها فحسب، بل يقدم أيضاًا رؤى قيمة يمكن أن تشكل اتجاه المساعي البحثية المستقبلية في هذا المجال.

الكلمات المفتاحية: معدل خطأ البت (BER)، السعة المريحة (EC)، ضعف الأجهزة (HWI)، معلومات حالة القناة غير الكاملة (ipCSI)، أداة إلغاء التداخل المتتالي غير الكامل (ipSIC)، اختلال التوازن في الطور والطور التربيعي (IQI)، غير - الوصول المتعدد المتعامد (NOMA)، واحتمال الانقطاع (OP).

Contents

List of Figures

List of Abbreviations

5G	5th Generation
ABER	Average Bit Error Rate
AF	Amplify-Forward
AWGN	Additive White Gaussian Noise
BER	Bit Error Rate
BS	Base Station
CD-NOMA	Code Domaine-NOMA
CDMA	Code Division Multiple Access
CNOMA	Cooperative Non-Orthogonal Multiple Access
CPE	Common Phase Error
CDF	Cumulative Distribution Function
CSI	Channel State Information
e2e	End-2-End
EC	Ergodic Capacity
HD	Half Duplex
HPA	High-Power Amplifier
HWI	Hardware Impairment
ICI	Inter-Carrier Interference

IOT	Internet Of Things
ipCSI	Imperfect Channel State Information
ipSIC	Imperfect Successive Interference Canceler
IQI	In-Phase and Quadrature Imbalance
IRR	Image Rejection ratio
LO	Local Oscillator
MIMO	Multiple-Input Multiple-Output
ML	Maximum Likelihood
MRC	Maximum Ratio Combining
NOMA	Non-Orthogonal Multiple Access
OP	Outage Probability
PA	Power Allocation
PD-NOMA	Power Domaine-NOMA
PHN	Phase Noise
RB	Resource Block
RF	Radio Frequency
RIS	Reconfigurable Intelligent Surfaces
Rx	Receiver
SC	Selection Combinig
SIC	Successive Interference Canceler
SIMO	Single-Input Multiple-Output
SINR	Signal-to-Interference plus Noise Ratio
SNR	Signal-to-Noise Ratio

SR	Selection relay
Tx	Transmitter
UAV	Uncrewed Aerial Vehicle

List of Symbols

w: Additive white Gaussian noise

h_i: Channel coefficient of the link at i

e: Channel estimation error

$F_X(.)$: Cumulative Distribution Function of X

$\tilde{h}_i$: Estimation channel coefficient

$\xi_{t/r}$: Gain imbalances at the TX/RX

η_r: Independent distortion noise parameters at the receiver

η: Independent distortion noise parameters at the transceiver

η_t: Independent distortion noise parameters at the transmitter

ς: Imperfect successive interference canceler coefficient

η: Independent distortion noise parameters at the transceiver

$\mu_{t/r}$: IQI coefficients at the TX/RX

$\nu_{t/r}$: IQI coefficients at the TX/RX

k_r: Level of impairment at the receiver

k: Level of impairment at the transceiver

k_t: Level of impairment at the transmitter

$P_i(out)$: Outage Probability of i

$\Upsilon_{t/r}$: Phase imbalances at the TX/RX

α: Power allocation

y_i: Received signal at i

P_r: Transmit power of relay

P_s: Transmit power of source

General introduction

The progression of communication technology, beginning with conventional analog phone calls to the current 5G era, has been driven by the necessity to address the unique technological requirements of each successive generation. In the present context, with the emergence of 5G technology, the primary aim is to establish an extensively interconnected society that highly values rapid data transmission speeds and minimal network latency. The main factor in this evolution is the growth in the utilization of the mobile Internet and the Internet of Things (IoT), which require a higher level of data transfer rates. Additionally, 5G provides the basis for the seamless integration of IoT devices, augmented security measures, and protocols to safeguard privacy. As the deployment of 5G progresses, researchers are concurrently exploring the possibilities presented by 6G technology, highlighting a persistent dedication to meeting the demands of an interconnected world powered by data [1, 2].

Within a cellular network's framework, the fundamental connection is established using radio access technology, operationalized through a network module recognized as the radio access network (RAN). The RAN employs a specific channel access method to establish connections between mobile devices and the core network. A crucial factor in enhancing system capacity is the effective design of a multiple access (MA) technique. These techniques can be classified into orthogonal and non-orthogonal approaches. Orthogonal multiple access (OMA) techniques revolve around the allocation of resources in an orthogonal manner to serve multiple users. These techniques encompass a range of strategies, including frequency-division multiple access (FDMA), time-division multiple access (TDMA), code-division multiple access (CDMA), and orthogonal frequency-division multiple access (OFDMA). In an OMA framework, the allocation of resources orthogonalizes communication, minimizing intra-cell interference. As a result, the retrieval of information from multiple users becomes streamlined with reduced complexity. However, it's crucial to serve several users in the OMA system due to a limited number of orthogonal resources [3, 4].

On the other hand, Non-orthogonal multiple access (NOMA) introduces the concept of interuser interference within resource allocation, enabling multiple users to be accommodated using a shared resource block. To counteract the impact of this interference, techniques like successive interference canceler (SIC) are employed, aiming to mitigate and manage the overlapping transmissions effectively [5]. In this regard, the NOMA has the capacity to substantially enhance spectral efficiency, achieve high throughput at the cell edges, reduce reliance on detailed channel feedback, and minimize transmission latency. As a result, NOMA emerges as a technology that can greatly enhance the capacity of wireless networks by accommodating a substantially higher quantity of connected devices.

However, In communication systems, transceivers play a crucial role in both transmitting and receiving signals. However, due to the intricate nature of their internal components and the complexity of the manufacturing process, it's common for transceivers to exhibit hardware imperfections and non-ideal behavior. Several factors contribute to the non-ideal operation of radio frequency (RF) transceivers. These hardware impairments manifest across various stages, including the analog-to-digital converters' imperfections, non-linear behavior in high-power amplifiers, the presence of phase noise, and imbalances in the in-phase and quadrature (I/Q) components within the RF front-end. Collectively, these impairments significantly impact the overall system performance and can result in signal distortion, posing challenges for signal processing [6].

This thesis focuses on the impact of HWIs on NOMA systems stems from the increasing demand for high-efficiency communication solutions. NOMA has emerged as a powerful contender due to its exceptional spectral efficiency and capacity to support a multitude of connections simultaneously. However, the real-world deployment of NOMA systems introduces the complexity of hardware imperfections that can disrupt their envisioned advantages. Understanding these impacts is essential to ensuring that the promises of NOMA are effectively realized in practical applications. By comprehensively evaluating how noise, nonlinearities, imbalances, and other hardware-related issues influence NOMA's performance, we can develop strategies to mitigate these challenges and enhance the robustness and reliability of NOMA systems. Ultimately, this exploration is integral to harnessing the full potential of NOMA and advancing its contribution to next-generation communication networks.

The structure of the manuscript is organized into six chapters, each addressing distinct aspects of the topic:

Chapter 1 serves as a foundational introduction to the conventional Non-Orthogonal Multiple Access (NOMA) system, encompassing both its downlink and uplink configurations. However, the desire for extensive mobility and broader coverage prompts the introduction of cooperative communication. This integration leads to a comprehensive study of cooperative NOMA (CNOMA) in both downlink and uplink contexts, aiming to enhance the system's capabilities. Yet, a prevalent oversight in many analyses involves assuming ideal transmitter-receiver hardware structures, a representation that doesn't align with the practical realities of transceiver operations. In practical applications, these devices commonly suffer from hardware impairments, notably including issues like In-phase Quadrature-phase Imbalance (IQI), Phase Noise (PHN), and High Power Amplifier (HPA) imperfections. These imperfections play a significant role in affecting the overall performance of the system but are often disregarded in theoretical models, despite their ubiquitous presence in real-world transceivers.

Chapter 2 marks our initial investigation into the impact of Hardware Impairments (HWI) on downlink and uplink NOMA systems, specifically over the Rayleigh fading channel. The first section of this chapter focuses on evaluating the downlink NOMA system's performance in the presence of both HWI and imperfect channel state information (ipCSI). Our examination encompasses crucial metrics like outage probability (OP), ergodic capacity (EC), and bit error rate (BER) within this context. Additionally, the second section delves into the uplink NOMA system's behavior under the influence of HWI and ipCSI, concentrating on the implications for both OP and EC. To start, we initially derive the received signal of the NOMA network, considering both near and far users, accounting for the presence of HWI and ipCSI. Following this, we derive the expression for the signal-to-interference-plus-noise ratio (SINR) of the system. Furthermore, we develop precise closed-form expressions for both the OP, EC, and BER of users in the downlink NOMA network. Thereafter, the expressions of the OP and EC for the uplink NOMA for both users. This analysis extends to thoroughly investigating the effects of HWI and ipCSI, incorporating different power allocation schemes. To validate the accuracy of these derived expressions, we present simulation results that demonstrate the performance of the NOMA system under the influence of HWI and ipCSI, confirming the reliability and effectiveness of our analytical findings.

Chapter 3 marks our second significant contribution, delving into the impact of In-phase Quadrature-phase Imbalance (IQI) on both the uplink and downlink aspects of direct Non-

Orthogonal Multiple Access (NOMA). Here, we meticulously examine practical scenarios involving transmitter IQI (TX IQI), receiver IQI (RX IQI), and the combined TX/RX IQI scenario. Our analysis delves into the evaluation of IQI implications in the context of NOMA, particularly focusing on OP and EC. The primary contribution of this investigation unfolds in three sequential steps. Firstly, we introduce the presence of IQI impairments affecting the transmitter, receiver, and both components. Secondly, we provide the SNIR for each individual case, delineating the impact of IQI on the performance of the downlink and uplink NOMA system. Lastly, we derive the OP of the considered system and complement our analysis by evaluating its performance through simulations, ensuring a comprehensive understanding of the effects of IQI on the NOMA framework.

Chapter 4 marks our third significant contribution, delving deeply into the impact of Hardware Impairments (HWI) in cooperative downlink NOMA systems. This investigation covers a range of scenarios, including downlink NOMA, cooperative NOMA without a direct link, and with a direct NOMA link. We meticulously analyze the effects of imperfect successive interference canceller (ipSIC) and ipCSI at transceivers. Our main focus is on detailing OP and BER expressions in downlink NOMA across varied scenarios, considering the practical constraints posed by HWI, ipCSI, and ipSIC and their combined effect on system performance. Additionally, this chapter contributes to a comprehensive understanding of system behavior in diverse conditions, offering insights into how HWIs influence the reliability and efficiency of cooperative downlink NOMA systems. Our emphasis on OP and BER highlights both the challenges and opportunities for implementation, aligning theoretical concepts with practical implications.

Chapter 5 introduces an extensive analysis of the impact of IQI on cooperative NOMA systems with a direct link. Employing the Maximum Ratio Combining (MRC) method to merge signals from both the direct and cooperative links, we aim to understand how IQI influences system performance, specifically in terms of OP and throughput metrics. This study also incorporates considerations of ipCSI to add a layer of realism. Our comprehensive exploration involves deriving end-to-end (e2e) OP and throughput metrics under the influence of IQI and ipCSI. Moreover, we delve into a comparison between our model and conventional NOMA, particularly examining the impact of factors like Image Rejection Ratio (IRR) and power allocation on the system's performance. Recognizing the significance of relay distance in affecting user performance, we further evaluate how this distance influences CNOMA performance in the presence of IQI and ipCSI. To validate our findings, comprehensive Monte-Carlo simulations are presented, confirming the accuracy of the derived expressions.

Chapter 6 represents a crucial exploration into the performance of the Up-link Single-Input Multiple-Output Cooperative NOMA (SIMO-CNOMA) system over the Rayleigh fading channel. This segment introduces five key contributions, emphasizing the evaluation of the system's OP and throughput metrics. Notably, this analysis stands out for its consideration of often overlooked practical constraints like ipCSI and ipSIC in previous uplink studies. This chapter meticulously investigates a practical multi-user uplink NOMA scheme affected by HWI, ipCSI, and ipSIC. Utilizing the Selection Relay (SR) technique and employing Single-Input Multiple-Output (SIMO) setups, we aim to optimize system performance. Through the derivation of OP and system throughput metrics, validated by comprehensive computer simulations, we reveal insights into the impact of HWI and ipCSI parameters on system performance, particularly in high SNR conditions. Furthermore, our comprehensive analysis delves into the influence of crucial system parameters—HWI, ipCSI, relay numbers, and antenna number on the OP and system throughput performance within the considered schemes. Despite efforts to increase antennas and relays, our findings uncover a limitation imposed by HWI and ipCSI, resulting in a significant degradation of the system's performance.

In the conclusion section, we summarize the key findings and insights gained throughout the research. Furthermore, we provide an overview of the potential avenues for future research in the domain of NOMA. As well as HWIs that warrant attention and exploration in upcoming studies.

Chapter 1

An overview of the non orthogonal multiple access and hardware impairment

1.1 Introduction

Non-orthogonal multiple access (NOMA) is a promising technology for future wireless networks due to its ability to efficiently support massive connectivity. NOMA allows multiple users to share the same frequency resources simultaneously, departing from traditional orthogonal access schemes. This non-orthogonal approach enhances spectral efficiency, a critical factor in accommodating numerous users within limited frequency bands. NOMA's potential to maximize spectrum utilization positions it as a key player in addressing the connectivity needs of dense network deployments and the growing demand for wireless communication.

The interplay between cooperative communication focused on extensive mobility and wide coverage, and NOMA, designed to boost spectral efficiency in upcoming wireless networks, has become a subject of considerable attention. The combination and mutual influence of these two fundamental physical layer techniques hold significant promise and have therefore attracted substantial interest in the realm of wireless network advancements.

On the other hand, H hardware impairment (HWI) is a critical consideration in the field of communication systems and technology. It encompasses a wide range of factors and challenges that can significantly impact the quality and reliability of these systems. These impairments can arise from various sources, including components like transmitters, receivers, amplifiers, and the characteristics of communication channels. Understanding HWI is essential because it plays a fundamental role in determining the overall performance and resilience of communication technologies in today's complex and demanding communication environments.

In this chapter, we will provide a thorough exploration of NOMA, CNOMA and simultaneously investigate the diverse aspects of HWI that have a significant impact on the performance of communication systems.

1.2 Direct NOMA system

1.2.1 Code-domain NOMA

Code-domain NOMA (CD-NOMA) is a multiple-access technique that allows multiple users to share the same frequency band simultaneously. It uses user-specific spreading sequences (either sparse sequences or non-orthogonal cross-correlation sequences of the low correlation coefficient) to separate signals in the frequency domain. The receiver performs successive interference cancellations to separate and decode the different signals. This allows for an increased number of users and higher spectral efficiency compared to traditional multiple-access techniques [1, 7].

1.2.2 Power-domain NOMA

Power-domain NOMA (PD-NOMA) superposes multiple users in the power domain and exploits the channel gain difference between the multiplexed users. At the transmitter, the signals from various users are superposed and transmitted over the same channels (time-frequency resources). At the receiver, multiuser detection algorithms, such as successive interference cancellation (SIC), are used to detect the desired signals. The receiver first decodes the signal with the highest power level and then cancels the interference from that signal to decode the next signal with the lower power level [8, 1, 9].

1.2.3 Downlink PD-NOMA

To clarify the concept of NOMA, we can use an example of a downlink transmission involving users, as illustrated in Fig. 1.1. The base station (BS) can simultaneously serve the users using the same time, code, or frequency resources, but with varying power levels. The BS

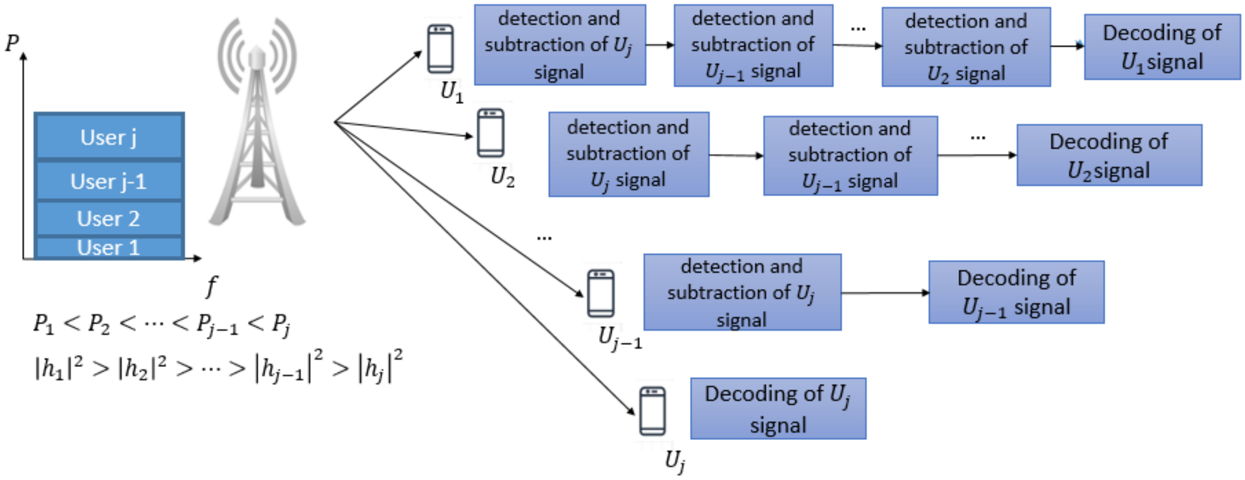

Figure 1.1: System model of downlink NOMA.

will transmit a composite signal that contains two distinct messages for each user, respectively. In conventional schemes, NOMA allocates more transmission power to users with poor channel conditions, specifically to the user with the weaker channel condition. This enables the weaker user to detect its message directly by treating the other user's information as noise. Meanwhile, the user with the stronger channel condition in NOMA needs to detect their partner's message first, subtract it from their received signal, and then decode their information using successive interference cancellation (SIC) [8, 10]. The received signal at the users can be represented as:

$$y_i = h_i \sqrt{P_s} SC + n, \tag{1.1}$$

where P_s is the transmit power of the Base station (BS), $SC = \sum_{i=1}^{J} \sqrt{\alpha_i} x_i$ is the superimposed coding signal transmitted by the BS with different α_i power allocation (PA) coefficient according to the channel gain $E|h_2| > E|h_1|$ with $P_J < P_{J-1}$, x_i is the message for users and n is the additive white Gaussian noise (AWGN) with zero mean and variance N_0 [9].

1.2.4 Uplink PD-NOMA

In uplink NOMA transmission, multiple users transmit their own uplink signals to the base station (BS) in the same resource block (RB). Unlike in downlink NOMA, where different transmit power levels are assigned to different users, in uplink NOMA, the transmit power levels of users are determined by their channel conditions. This means that users with better channel conditions may transmit at higher power levels, while users with weaker channel

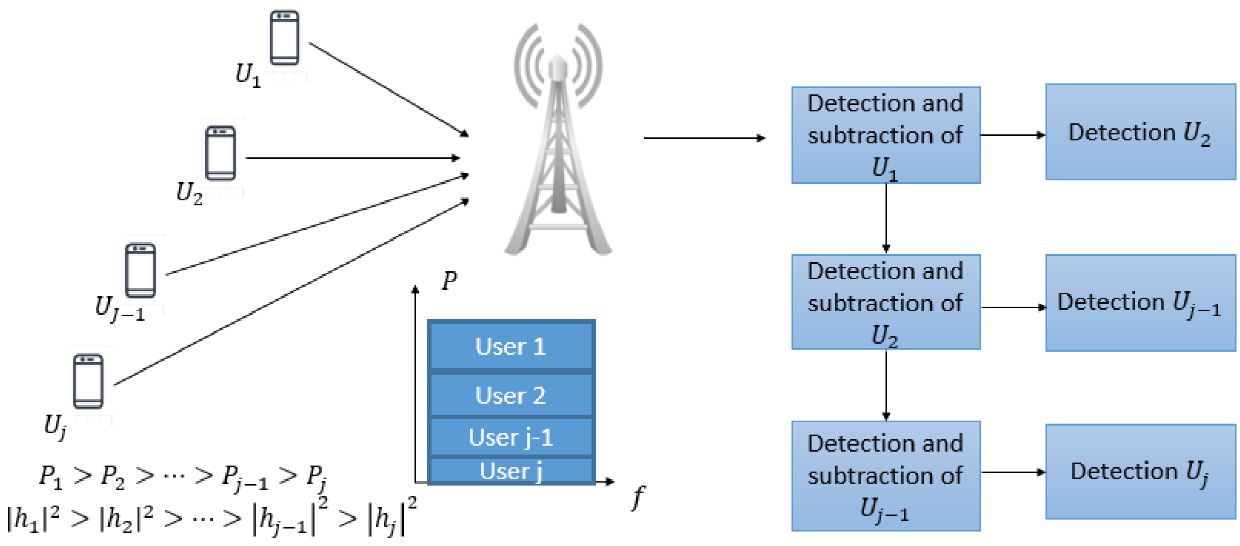

Figure 1.2: System model of uplink NOMA.

conditions transmit at lower power levels [11]. As shown in Fig. 1.2, the SIC is carried out at the base station (BS) to detect the signals from multiple users. it starts with the detection of the signal from the strongest user U_1, treating the signal from the other user as interference.

Once the signal from the User is detected and decoded, the BS re-modulates the recovered signal and subtracts the interference imposed by the strong User from the received signal to detect the signal from the weaker user. This process continues iteratively, with the BS detecting and canceling the signals of stronger users to improve the detection performance of weaker users [9]. In the uplink NOMA scenario, the received signal at the BS can be given as:

$$y_i = \sum_{i=1}^{J} h_i \sqrt{\alpha_i} x_i + n. \tag{1.2}$$

1.3 Cooperative NOMA

Cooperative communication aims to provide extensive mobility and wide coverage, while NOMA is designed to enhance spectral efficiency in future wireless networks. Consequently, the interplay between these two fundamental physical layer techniques has garnered significant attention. Within Cooperative NOMA (CNOMA) schemes, two distinct configurations exist: In the first one, the relay nodes play a crucial role in enhancing critical performance indicators. In the second, the relay nodes are primarily utilized to extend network coverage. However, the majority of literature focuses on the latter configuration, where direct links are

obstructed by various obstacles or impediments.
Cooperative communication, distinct from typical point-to-point communication, employs relays that actively participate in transmitting and receiving signals for multiple devices, whether they are dedicated or utilize inactive network users. This approach is categorized into two key concepts: amplify-and-forward (AF) and decode-and-forward (DF) [12].

1.3.1 Downlink CNOMA

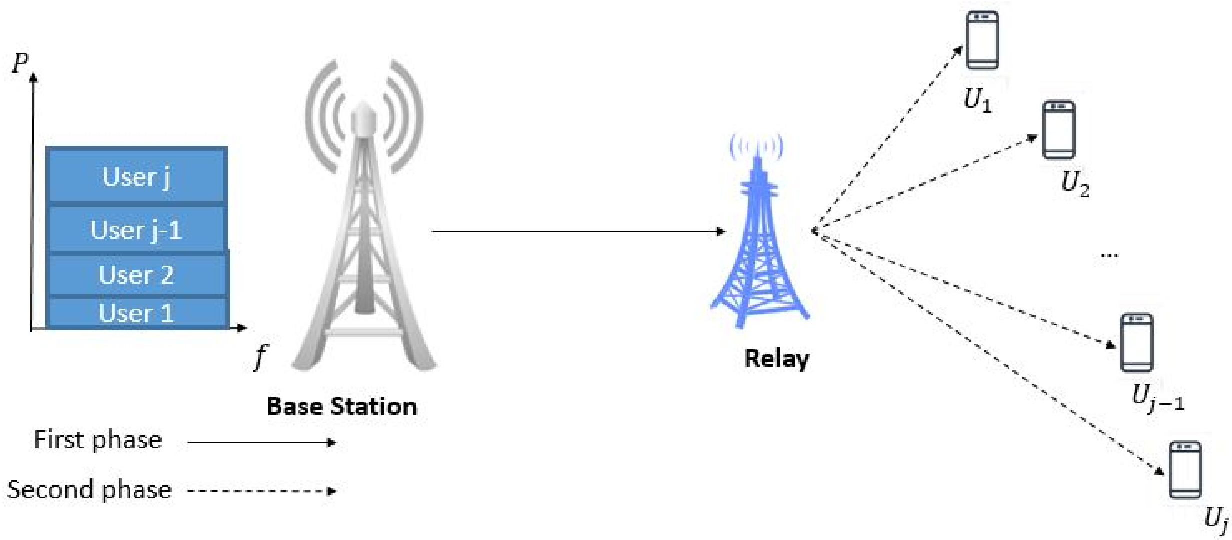

Figure 1.3: System model of downlink CNOMA.

we consider a downlink CNOMA which consists of BS, DF relay, and users as demonstrated in Fig. 1.3. In the first phase The BS employs SC and sends the combined symbols of multiple users over the same resource block, as the downlink NOMA approach. The signal received by users during the initial phase is represented as follows:

$$y_r = h_r\sqrt{P_s}SC + n, \tag{1.3}$$

where h_r is the channel coefficient between the BS and relay.

During the second phase, the relay node re-encodes and combines the signals of all users into a new SC signal, mirroring the base station's approach, and subsequently transmits it to the users at its power level. Then, the relay forwards it by its power to the users. The received signal at the users can be presented as:

$$y_i = \sqrt{P_r}X_{SC}\ h_i + n, \quad i = 1, 2, 3, ..., j, \tag{1.4}$$

where h_i is the channel coefficient between the relay and i^{th} users, P_r is the transmit power of the relay node.

1.3.2 Uplink CNOMA

Fig 1.4 represents an uplink CNOMA which consists of a BS, DF relay, and users. In the first phase, the users transmit their signals simultaneously to the relay. Then, the received signal at the relay can be given as:

$$y_r = \sqrt{P_t}\ \sum_{i=1}^{j}(h_i\ \sqrt{\alpha_i}x_i) + n, \qquad k = 1, 2, 3, ..., i. \tag{1.5}$$

where x_i and h_i are the transmit signal and the channel coefficient from the users to relay, respectively.

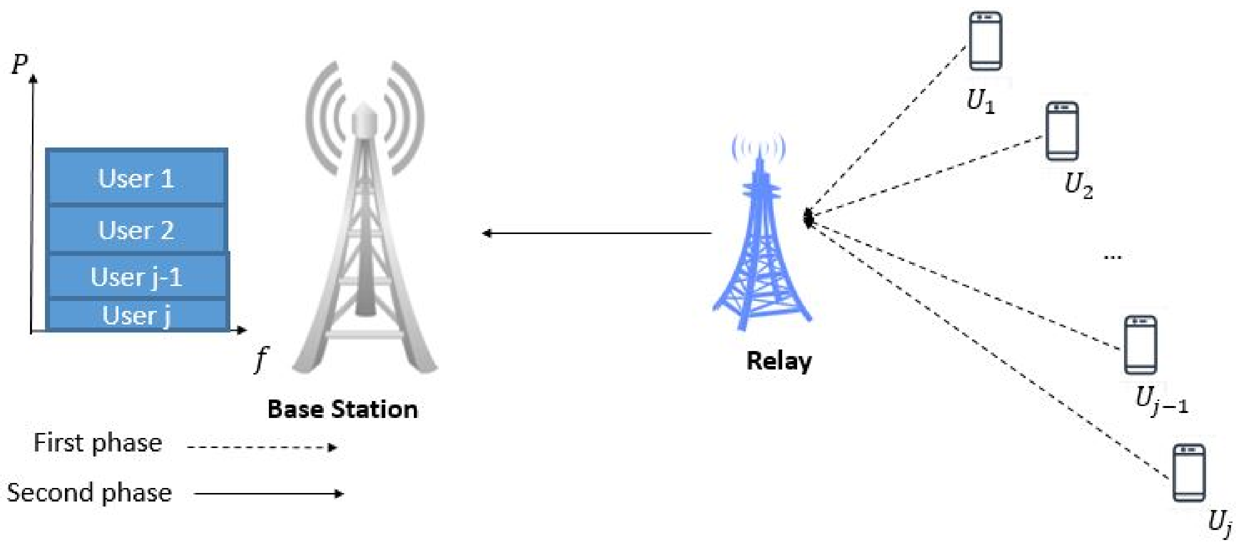

Figure 1.4: System model of Uplink CNOMA.

1.4 RF Analog Impairments

Radio-frequency (RF) equipment is a critical component in the vast network of interconnected devices that allow communication between individual devices and their base stations (BS). Direct conversion transceivers are becoming a solution for RF front-end design due to their ability to meet stringent design goals such as low cost, low power dissipation, improved efficiency, and performance. Direct conversion transceivers provide these benefits by reducing the overall complexity of the system, reducing noise, and enabling digital signal processing of the baseband signals. The use of direct conversion transceivers enhances the performance and efficiency of RF equipment by improving communication in the massive network of interconnected devices [13].

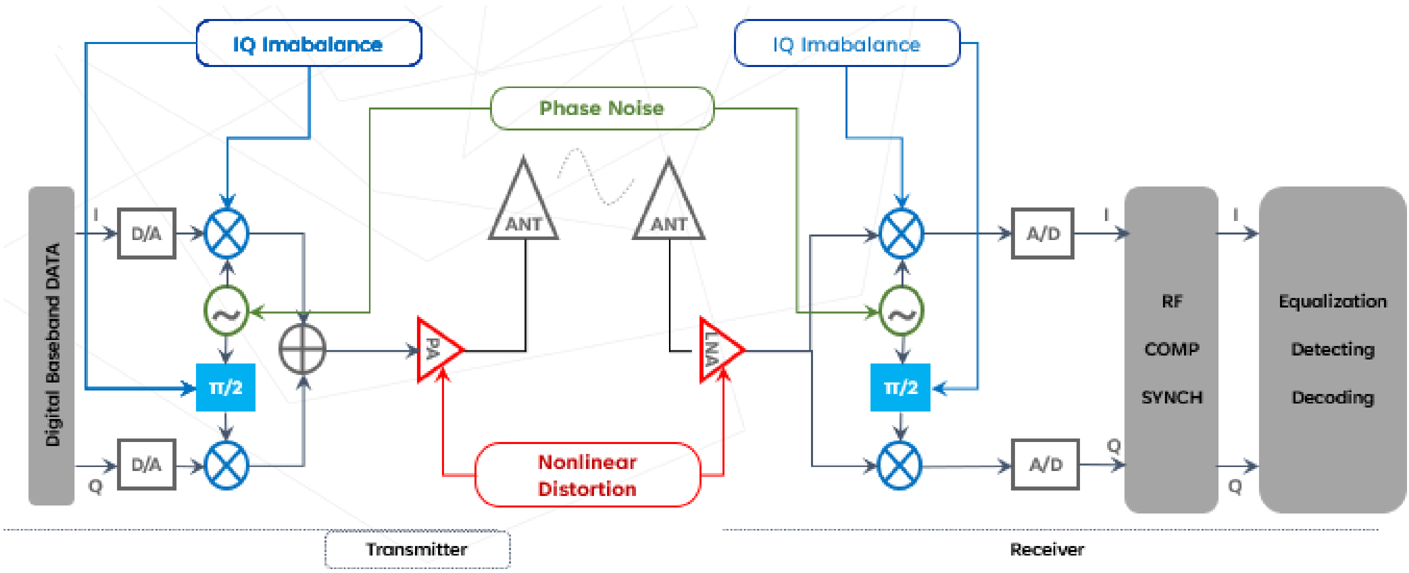

Figure 1.5: Block diagram of communication transceiver.

A generic wireless transceiver is depicted in Fig. 1.5 and is composed of three key blocks: the analog block, the digital block, and their interface [14, 15]. The analog block represents the RF front-end of the transmitter (TX) and receiver (RX) and typically includes components such as the antenna array, the TX power amplifier, the RX low noise amplifier, and possible mixers and filters. The digital block includes all baseband signal processing, including tasks such as coding, interleaving, and modulation at the transmitter, as well as diversity management, synchronization, and decoding at the receiver. The interface between these two blocks is accomplished through the use of a digital-to-analog converter (DAC) and an analog-to-digital converter (ADC), which perform the necessary mapping between signals and symbols in each domain [16].

Non-idealities in electronic devices can cause deviations from expected behavior such as temperature fluctuations, pressure, and component mismatches which impact the performance of the system. In communication systems, these deviations can manifest as hardware impairments such as high-power amplifier (HPA) [17], in-phase and quadrature imbalance (IQI) [18], and phase noise (PN) [19]. These impairments can reduce the quality and reliability of the communication signal, leading to decreased system performance [20].

1.4.1 Hardware Impairment

In the studies of wireless communication, the assumption of ideal transmitter-receiver hardware structures is frequently made, despite the fact that this is often unrealistic in practical applications. In reality, hardware impairments are commonly present as in Fig. 1.6 in transceivers, such as IQI, PHN, and HPA imperfections. These non-ideal characteristics are a significant contributing factor to the performance degradation observed in wireless communications [21]. Such impairment can cause [22].

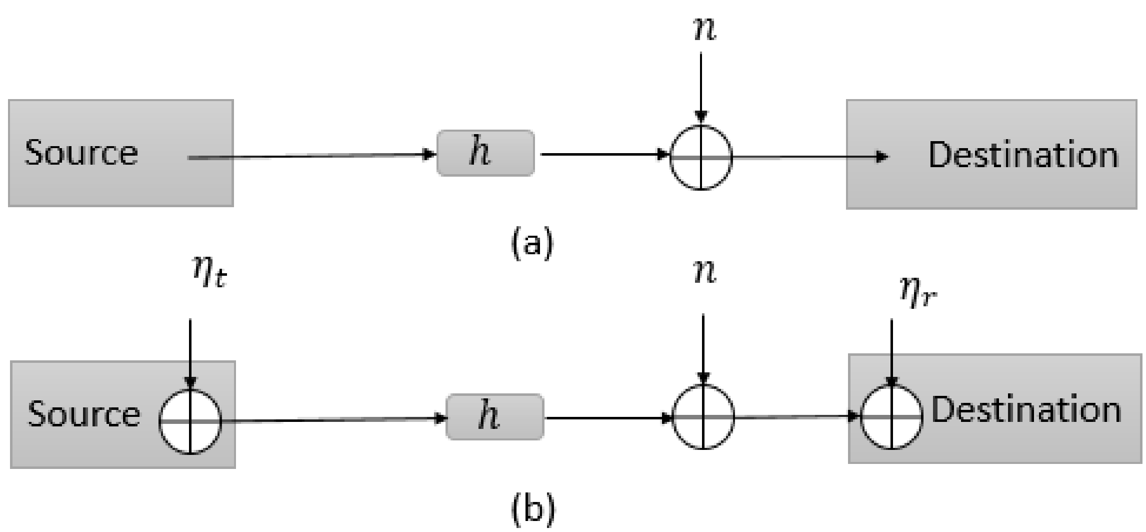

Figure 1.6: (a) Transmission bloc with ideal hardware (b) Transmission bloc with non-ideal hardware.

- a difference between the originally transmitted signal and the signal received.
- Distort the received signal during the processing of detection.

In an ideal scenario, the received signal can be modeled as:

$$y = hx + n, \tag{1.6}$$

where h, x, n are statistically independent referring to channel coefficient, transmit signal, and AWGN. However, the transceiver hardware impairment is defined using a generalized channel model that creates distortion noises added at both the transmitter and receiver sides. The received signal considering the nonideal hardware can be presented as [23]:

$$y = h(x + \eta_t) + \eta_r + n, \tag{1.7}$$

where η_t and η_r are the independent distortion noise parameters at the transmitter and receiver, respectively. The distortion noises are given as [24, 25]:

$$\eta_t \sim \mathcal{CN}(0,\ k_t^2 P), \eta_r \sim \mathcal{CN}(0,\ k_r^2 P), \tag{1.8}$$

where P is the total transmitted power, k_t and k_r represent the level of impairment at the transmitter and receiver, respectively. Then, (1.7) can be characterized as:

$$y = h(x + \eta) + n, \tag{1.9}$$

where η is the independent distortion noise at the transceiver with

$$\eta \sim \mathcal{CN}(0,\ k^2 P), \tag{1.10}$$

k^2 is the HWI level at the transceiver. The overall impact of the HWI transceiver can be characterized as in [22] by

$$k = \sqrt{k_t^2 + k_r^2}. \tag{1.11}$$

1.4.2 In-phase and quadrature-phase imbalance

A major source of impairments in wireless communication systems is a mismatch between the in-phase (I) and quadrature-phase (Q) branches, or equivalently between the real and imaginary parts of the complex signal at both transmitter (up-conversion) and receiver (down-conversion) [26, 27, 28].

Model (IQI)

In the up and down-conversion process of the transceiver, the incoming signal in the I-path is mixed with a local oscillator at the carrier frequency, while the Q-path signal is mixed with a local oscillator that has a 90-degree phase shift. Ideally, the I and Q paths should be perfectly matched, but in reality, this is not the case. Imperfections in the hardware components or manufacturing processes can result in differences between the two paths, causing I and Q imbalance [29]. Fig. 1.7 presents the transmitter and receiver IQI. Thus the phase and/or

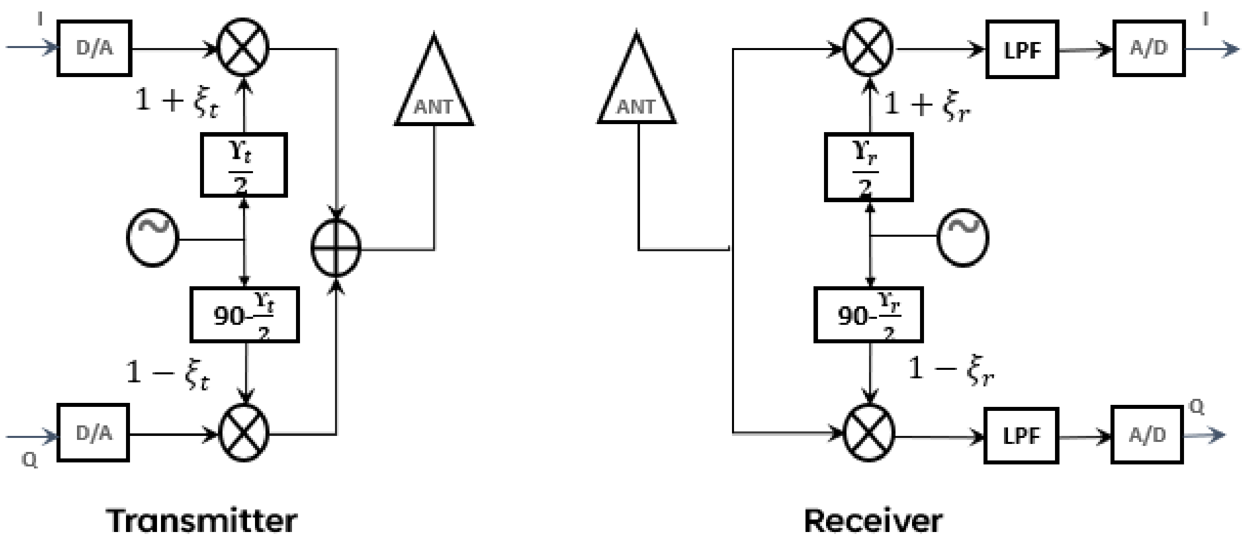

Figure 1.7: IQI models for transceiver.

amplitude imbalance between the phase and phase branches is modeled as:

$$x_{IQI} = \mu_{t/r} S + \nu_{t/r} S^*. \tag{1.12}$$

where S is the baseband transmit signal, * is the conjugation, $\mu_{t/r}$ and $\nu_{t/r}$ are the IQI coefficients at the TX/RX respectively, We can see that in the absence of IQI, μ_t=μ_r= 1 and ν_t=ν_r= 0. The parameter IQI is expressed as: [30]

$$\begin{aligned}
\mu_t &= \frac{1}{2}(1+\xi_t \exp(j\Upsilon_t)),\\
\nu_t &= \frac{1}{2}(1-\xi_t \exp(-j\Upsilon_t)),\\
\mu_r &= \frac{1}{2}(1+\xi_r \exp(-j\Upsilon_r)),\\
\nu_r &= \frac{1}{2}(1-\xi_r \exp(j\Upsilon_r)),
\end{aligned} \tag{1.13}$$

with $\xi_{t/r}$ and $\Upsilon_{t/r}$ are the gain and the phase imbalances levels and j is the unit of the imaginary $j = \sqrt{-1}$. The received signal in the presence of IQI in both transmitter and receiver can be presented as:

$$y^{IQI} = \mu_r(\tilde{h}(\mu_t S + \nu_t S^*) + n) + \nu_r(\tilde{h}(\mu_t S + \nu_t S^*) + n)^*. \tag{1.14}$$

1.4.3 Phase noise effects

Phase noise should be carefully considered in the design of communication and other systems that rely on stable, accurate oscillators. The phase noise of the local oscillators at both the transmitter and receiver can have a significant impact on the performance of the system. Phase noise is a random process caused by fluctuations in the frequency of the local oscillator (LO). These fluctuations result in undesired variations in the amplitude and frequency of the signal, causing phase noise distortion [31].

The phase noise is popularly modeled as Wiener–Levy (random walk) process (from one symbol to another), and the process can be given as:

$$\phi_m = \phi_{m-1} + \omega_m \tag{1.15}$$

where ω_m is denoted as the walk's step size and is represented by a zero-mean Gaussian random variable with a variance of $2\Pi\beta T$ [32].

The power spectrum of an ideal oscillator would exhibit a precise, impulse-like shape at the intended frequency. Nevertheless, in the presence of phase noise in the system, the spectrum becomes broader and takes on a Lorentzian shape. The characterization of phase noise is determined by the ratio of the peak carrier signal to the noise at a specific offset from the carrier, as depicted in Figure 1.18

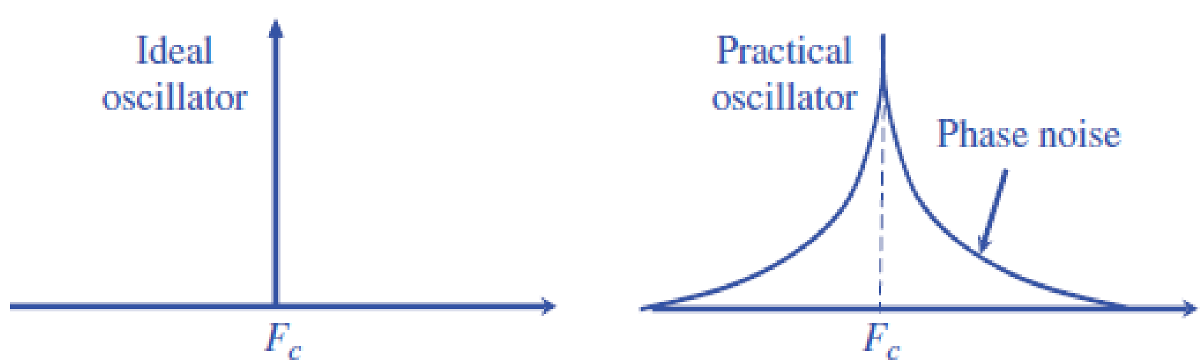

Figure 1.8: Spectra of ideal and practical oscillators, demonstrating the impact of phase noise.

1.4.4 Nonlinear power amplifier

The power amplifier (PA) is a critical component of a transmitter in a wireless communication system. Its main function is to boost the signal level from the low-power stage of the transmitter to the level required for successful transmission to the receiver. Ideally, the PA should have a linear input-output relationship, meaning that the output signal is a precise representation of the input signal. However, in practice, all power amplifiers have some level of non-linearity, which causes non-linear distortion in the output signal. This distortion can have a significant impact on the system's performance and overall quality of communication [33, 29].

The system-level depiction outlines the attributes of the amplifier, with a focus on a memoryless nonlinearity assumption. This implies that the Power Amplifier's (PA) output signal only relies on the current input signal. The inherent nature of the PA involves a dependence on amplitude, signifying that the distortion is directly influenced by the amplitude of the input signal. The characterization of a memoryless PA model involves assessing amplitude-to-amplitude distortions (AM-AM) (amplitude to amplitude)and amplitude-to-phase distortions (AM-PM) (amplitude to phase).

Typically, AM/AM and AM/PM curves are used to model the distortion of the PA, the output of the PA can be given as:

$$y^{PA} = AM(A(t)) \exp(j[\varphi(t) + PM(A(t))], \tag{1.16}$$

where AM(A(t)) is the amplitude-to-amplitude (AM-AM) representing the PA output amplitude as a function of the input signal amplitude and PM(A(t)) is the amplitude-to-phase (AM-PM) representing the PA output phase as a function of the input signal amplitude. The AM/AM results in amplitude distortion, while the AM/PM causes a phase shift in the output signal [34].

Initially, Figure 1.9 illustrates the characteristic and definition of the PA operation point. It is evident that at lower input power levels, the output power of PA demonstrates near linearity in relation to the input power. However, as the input power rises, the AM/AM of the PA curve progressively exhibits more nonlinearity. Eventually, when the input power no longer influences a change in output power, the amplifier reaches its saturation point [29]. Several parameters are used to describe the efficiency of a power amplifier [16], including:

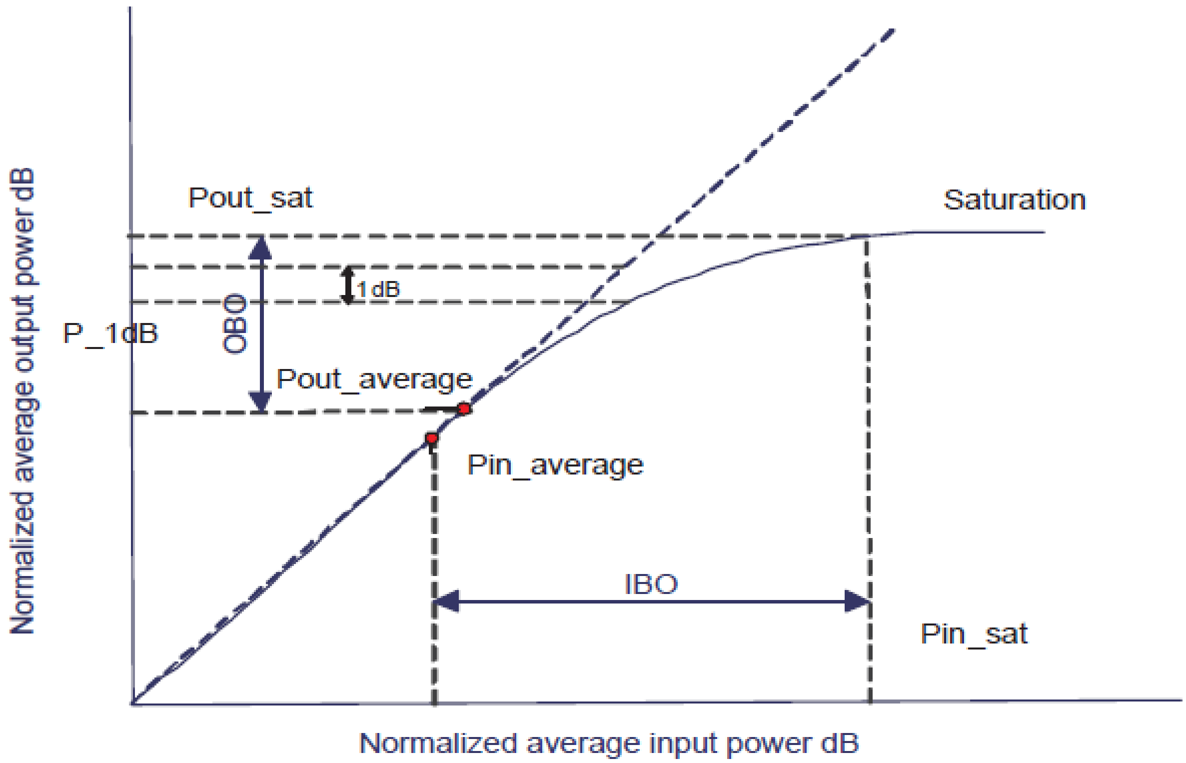

Figure 1.9: Input/output characteristic of PA.

Input Back-Off (IBO): It is a measure of the difference between the input saturation power and the input average power and provides information about the operating point of the power amplifier and its utilization efficiency

Output Back-Off (OBO): refers to the difference between the output saturation power and the output average power of the power amplifier. It provides information about the output power of the power amplifier and how efficiently it is being utilized.

1.4.4.1 PA Performance Parameters

The PA is defined by certain parameters that describe its performance.

1. **Output power**: It is an important metric that determines the overall performance of the amplifier and its ability to drive the load effectively. The output power is usually specified at a particular load impedance (RL) and is a key factor in determining the maximum signal strength that can be delivered to the antenna in a wireless communication system. The output power also affects the amplifier's efficiency, linearity, and

stability [35, 36].

2. **Peak-to-Average Power Ratio (PAPR)**: The average power (Po, avg) of an amplifier is defined as the average of its instantaneous output power over one modulation period. Meanwhile, peak output power $(Po, peak)$ refers to the maximum power delivered to a load within the desired frequency band. The Peak-to-Average Power Ratio (PAPR) is a metric that quantifies the variability of the amplifier's output power, and it is determined by dividing the peak output power by the average output power and expressing the result in decibels (dB) as follows:

$$PAPR = 10 \log 10 \frac{(Po, peak)}{(Po, avg)}. \tag{1.17}$$

A high PAPR can cause various issues in wireless communication and broadcasting systems, such as increased power handling requirements, reduced system efficiency, and signal distortion [37, 38].

3. **P1dB point**: The P1dB is a measure of the linearity of an amplifier. It refers to the input power level at which the output power starts to deviate from a linear relationship by 1 dB, indicating the start of compression of the input signal. The P1dB point is an important specification for amplifiers, as it provides information on the maximum input power the amplifier can handle without significant distortion. The higher the P1dB point, the more input power the amplifier can handle before output power deviates from linearity [39].

4. **The Adjacent Channel Power Ratio**: The Adjacent Channel Power Ratio (ACPR) is a performance metric used to quantify the amount of energy that leaks into adjacent frequency channels as a result of nonlinearity in a Power Amplifier (PA). It is expressed as the ratio of power in the desired signal to the power in the adjacent channel contaminated by intermodulation products. The Adjacent Channel Power Ratio (ACPR) is calculated as the ratio of the power that leaks into adjacent channels from the main channel to the root-mean-squared (rms) power of the main channel signal [35].

1.4.5 ADC/DAC impairment

The Analog-to-Digital Converter (ADC) and Digital-to-Analog Converter (DAC) serve as the boundary between the analog and digital domains. A standard ADC is composed of a sampler and a quantizer, with the sampling rate standing out as a key attribute. A limitation arises in meeting the sampling rate criteria, necessitating that the signal bandwidth before ADC remains below half of the sampling rate, as dictated by the Nyquist theorem

$$f_s \geq 2f_{max} \tag{1.18}$$

where f_{max} and f_s are maximum frequency and the sampling rate.
To prevent aliasing, the signal undergoes low-pass filtering, also known as anti-aliasing filtering. This process involves removing high-frequency components, effectively limiting the signal bandwidth before sampling.

After the proper sampling of the analog signal, the quantizer transforms these discrete samples into bits, with the word length determining the resolution of (ADC) and influencing quantization error. Each additional bit contributes a 6 dB increase in dynamic range to the receiver. Besides quantization noise, the performance of ADCs is impacted by distortions arising from static and dynamic nonlinearity features [32].
The structure of a generalized DAC includes a DAC register, a resistor string, and subsequent output buffer amplifier blocks [40]. In a standard DAC, bits are transformed into a sequence of impulses, which are subsequently handled by a reconstruction filter using some interpolation method to interpolate data between these impulses. Much like ADCs, the key attributes of DACs encompass resolution, maximum sampling rate, monotonicity, dynamic range, and phase distortion. examining a system that transforms an N-bit digital number into an analog signal with a range spanning from V_{min} to V_{max}, we can express the resolution v as follows:

$$V = \frac{V_{max} - V_{min}}{2^N - 1} \tag{1.19}$$

where 2^N is the number of levels in the system

1.4.6 Thermal noise

Thermal noise arises from the stochastic movement of free electrons within a conductor, induced by thermal agitation and directly correlated with the conductor's temperature. This random electron motion gives rise to fluctuating currents, resulting in the manifestation of a random noise voltage across the terminals of the conductor. This phenomenon is prevalent in various electrical components, including resistors, capacitors, inductors, and transistors, as it stems from the thermal excitement of electrons in conductive materials. The intensity of the noise power is contingent upon both the temperature and the bandwidth of the system. The thermal noise is quantified through its average power, denoted as P_{ave},

$$P_{avg} = 4KTB \tag{1.20}$$

where (T) is temperature of the conductor and (B) is the frequency bandwidth considered in the measurement, K is Boltzmann's constant with $K = 1.3 \times 10^{23} J/K$ [41, 32].
The thermal noise distribution exhibits a Gaussian nature, and its spectrum is independent of frequency.

1.5 Conclusion

In this chapter, we delved into the foundational aspects of NOMA and explored its integration with cooperative communication. Additionally, we investigated the various types of Hardware Impairment (HWI). Our exploration began with the definition of NOMA and CNOMA, followed by a comprehensive examination of different facets of the NOMA system, including its diverse links. Moreover, we conducted a detailed analysis of various HWI types, highlighting their potential challenges to communication system quality and reliability.

In the next chapter, we will investigate the critical influence of HWI on the performance of NOMA.

Chapter 2

Effect of the Hardware Impairment on the NOMA system

2.1 Introduction

The increasing demands of mobile internet and the emergence of the Internet of Things (IoT) require massive connectivity and high spectral efficiency in future wireless networks 5G and beyond. In response to these challenges, non-orthogonal multiple access (NOMA) has recently been introduced as an effective solution [42]. The principal idea behind NOMA is that multiple users can share the same source block (frequency/time/code) with different power allocations based on their channel conditions. At the receiver, successive interference cancellation (SIC) is applied to decode the superimposed transmitted signal [1, 43]. Significant attention has been devoted to studying the performance analysis of NOMA in literature. However, the outage probability of downlink and uplink NOMA communication with fading channels has been investigated in [44]. Additionally, [45] discussed the fundamentals of NOMA and its capacity limits in terms of energy efficiency, spectral efficiency, and sum capacity. Furthermore, the authors of [46, 47] derived the exact closed-form expression for the bit error rate in downlink NOMA under SIC errors over Rayleigh fading channels.

On the other hand, the performance of the proposed system can be affected by non-ideal processes in the radiofrequency (RF) transceiver, such as in-phase and quadrature imbalance (IQI), phase noise (PHN), and high-power amplifier (HPA), which can cause several degradations in system performance [48]. In [23], the authors presented the impact of hardware impairment (HWI) on dual-hop relaying in terms of outage probability (OP) and ergodic capacity (EC). Similarly, [22] provided an analysis of the performance of a cognitive Special Modulation Multiple-Input Multiple-Output (MIMO) system in the presence of HWI and imperfect channel state information (ipCSI). However, within the context of the NOMA network, the impact of HWI in NOMA-based relaying over the Nakagami-m fading channel is considered in [49]. Subsequently, the OP and EC of full-duplex (FD) NOMA networks under HWI are determined in [50]. Furthermore, in real communication systems, it isn't easy to achieve perfect channel state information (CSI), necessitating the study of the impact of ipCSI on NOMA system performance. In [51], the authors derived a closed-form approximation for the average sum rate and OP for a NOMA system with ipCSI. Additionally, [52] investigates the impact of imperfect CSI on the uplink NOMA system in terms of OP, while [53, 54] presents the performance of energy harvesting (EH) cooperative NOMA in the presence of ipCSI. Moreover, the closed-form expression of the bit error rate (BER) for the NOMA system under ipCSI is provided in [55, 56].

2.2 Motivations and contributions

Based on the previous investigation above, it is evident that HWI and ipCSI are the primary factors contributing to the performance degradation of the NOMA network. However, it is worth noting that the exact closed-form expression of the BER for the NOMA system in the presence of HWI and ipCSI over a Rayleigh fading channel has not been addressed in the aforementioned studies. In addition, this chapter examines the performance of the downlink and uplink NOMA systems in terms of OP, EC, and BER. Specifically, the analysis focuses on the scenario where direct transmission is assumed between the base station (BS) and the users. Then, the principal contributions of this chapter are summarized as Firstly, the obtention of the received signal of the downlink and uplink NOMA network considering both the near and far users, taking into account the presence of HWI and ipCSI. Subsequently, we derive the expression for the signal-to-interference-plus-noise ratio (SINR) of the two considered systems. Next, the derivation of the exact closed-form expressions for both the OP and BER of the users in the NOMA network. These expressions accurately characterize the impact of imperfections for any signal-to-noise ratio (SNR) value. Furthermore, the effects of HWI and ipCSI by considering different power allocation schemes are investigated in this chapter.

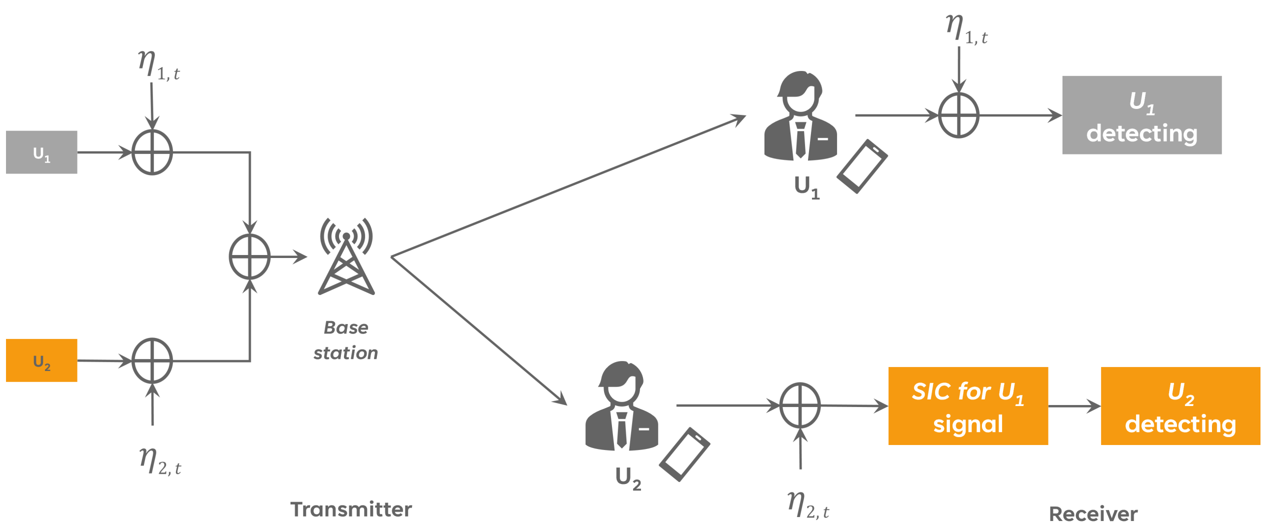

Figure 2.1: System model downlink NOMA under HWI.

2.3 System model of the downlink NOMA

We consider the downlink NOMA system, which consists of a (BS) and two users i.e. the far user U_1, and the near user U_2. We assume that the nodes are equipped with a single antenna. The transmission is linked directly between the BS and users over the Rayleigh fading channel. The BS transmits the superimposed signal to the users with different levels of power. According to NOMA protocol, the received signal at the i^{th} users can be defined as:

$$y_i = h_i(\sqrt{\alpha_1 P} x_1 + \sqrt{\alpha_2 P} x_2) + n, \ i = S1, S2 \tag{2.1}$$

where h_i is the channel coefficient, $n \sim \mathcal{CN}(0, N_o)$ is the additive white Gaussian noise (AWGN), P is the total transmitted power, x_i is the transmit signal for user i and α_1, α_2 are the power allocation coefficients of the U_1 and U_2, respectively.

2.3.1 NOMA with HWI and ipCSI

We consider a downlink NOMA network with HWI, as depicted in Fig. 2.1. We assume that all nodes are equipped with a single antenna. Also, direct communication can be established between the BS and users. Assuming non-ideal hardware in the NOMA system, the receiver signal at the i^{th} user is presented as in [57]:

$$y_i = h_i(\sqrt{\alpha_1 P} x_1 + \sqrt{\alpha_2 P} x_2 + \eta_i) + n, \ i = S1, S2 \tag{2.2}$$

where η_i is the independent distortion noise $\eta_i \sim \mathcal{CN}(0, k_i^2 P)$ and k is the HWI level at the transceiver. The ipCSI is modeled using channel estimation.
However, the channel coefficient is defined as [58]:

$$h_i = \tilde{h}_i + e, \tag{2.3}$$

where $\tilde{h}_i$ represent the estimation channel coefficient and e is the channel estimation error, modeled as $e \sim \mathcal{CN}(0, \sigma_e^2)$. Noted that $\tilde{h}_i$ and e are independent distributed [59] consequently, we can write $\sigma_e = E[|h_i|^2] - E[|\tilde{h}_i|^2]$. Thus, considering a perfect SIC, the receiver signal affected by HWI and ipCSI is obtained as follows

$$y_i = \tilde{h}_i(\sqrt{\alpha_1 P}x_1 + \sqrt{\alpha_2 P}x_2 + \eta_i) + e(\sqrt{\alpha_1 P}x_1 + \sqrt{\alpha_2 P}x_2 + \eta_i) + n, \tag{2.4}$$

The instantaneous signal-to-interference-plus-noise ratio (SINR) for the far user is obtained as:

$$\gamma_{S1} = \frac{|\tilde{h}_1|^2 \alpha_1 P}{|\tilde{h}_{S1}|^2 \alpha_2 P + |\tilde{h}_{S1}|^2 k_{S1}^2 P + \sigma_e^2 k_{S1}^2 P + \sigma_e^2 P + N_o}. \tag{2.5}$$

The received SINR for U_2 to decode U_1's signal is given as:

$$\gamma_{S2\rightarrow S1} = \frac{|\tilde{h}_{S2}|^2 \alpha_1 P}{|\tilde{h}_{S2}|^2 \alpha_2 P + |\tilde{h}_{S2}|^2 k_{S2}^2 P + \sigma_e^2 k_{S2}^2 P + \sigma_e^2 P + N_o}. \tag{2.6}$$

Then, assuming the perfect SIC, the SINR of the U_2 is:

$$\gamma_{S2} = \frac{|\tilde{h}_{S2}|^2 \alpha_2 P}{|\tilde{h}_{S2}|^2 k_{S2}^2 P + \sigma_e^2 k_{S2}^2 P + \sigma_e^2 P + N_o}. \tag{2.7}$$

2.4 Performance analysis of the downlink NOMA

2.4.1 Outage probability analysis

In this part, we derive the analytical expression of the OP of the downlink NOMA system under HWI and ipCSI over the Rayleigh fading channel. The probability density function (PDF) and cumulative distribution function (CDF) of the channel power gain $\varphi_i = E|\tilde{h}_i|^2$

are given respectively as [60, eq. (7,8)]:

$$f_{x_i}(x_i) = \frac{1}{\varphi_i} \exp\left(-\frac{x_i}{\varphi_i}\right), \tag{2.8}$$

$$F_{x_i}(x_i) = 1 - \exp\left(-\frac{x_i}{\varphi_i}\right). \tag{2.9}$$

Outage probability of U_1

Assuming an ipCSI, the OP of the U_1 can be given as [61]:

$$P_{out,1} = Pr(\gamma_{S1} \leq \gamma_{th,1}), \tag{2.10}$$

where $\gamma_{th,1}$ is the threshold at the U_1.

$$\begin{aligned} P_{out,1} &= Pr\left(|\tilde{h}_{S1}|^2 \leq \frac{\gamma_{th,1}(\sigma_e^2 k_{S1}^2 P + \sigma_e^2 P + N_o)}{(\alpha_1 - \gamma_{th,1}\alpha_2 - \gamma_{th,1}k_{S1}^2)P}\right) \\ &= \int_0^{\frac{\gamma_{th,1}(\sigma_e^2 k_{S1}^2 P + \sigma_e^2 P + N_o)}{(\alpha_1 - \gamma_{th,1}\alpha_2 - \gamma_{th,1}k_{S1}^2)P}} \frac{1}{\phi_{S1}} \exp\left(-\frac{y}{\phi_{S1}}\right) \mathrm{d}y. \end{aligned} \tag{2.11}$$

Following the evaluation of the integral, we get

$$P_{out,1} = 1 - \exp\left(-\frac{1}{\phi_{S1}} \frac{\gamma_{th,1}(\sigma_e^2 k_{S1}^2 P + \sigma_e^2 P + N_o)}{(\alpha_1 - \gamma_{th,1}\alpha_2 - \gamma_{th,1}k_{S1}^2)P}\right). \tag{2.12}$$

Outage probability of U_2

The OP of the near user can be determined as:

$$P_{out,2} = 1 - Pr(min(\gamma_{S2\to S1}, \gamma_{S2} > \gamma_{th,2})), \tag{2.13}$$

where $\gamma_{th,2}$ is the threshold at the U_2. Based on the [61], due to the fact that $\gamma_{S2\to S1}, \gamma_{S2}$ are independent (2.13) can be written as

$$P_{out,2} = 1 - Pr(\gamma_{S2\to S1} > \gamma_{th,2}) \times Pr(\gamma_{S2} > \gamma_{th,2}), \tag{2.14}$$

where

$$\begin{aligned} Pr(\gamma_{S2\to S1} > \gamma_{th,2}) &= Pr\left(|\tilde{h}_{S2}|^2 \le \frac{\gamma_{th,2}(\sigma_e^2 k_{S2}^2 P + \sigma_e^2 P + N_o)}{(\alpha_1 - \gamma_{th,2}\alpha_2 - \gamma_{th,2}k_{S2}^2)P}\right) \\ &= \int_0^{\frac{\gamma_{th,2}(\sigma_e^2 k_{S2}^2 P + \sigma_e^2 P + N_o)}{(\alpha_1 - \gamma_{th,2}\alpha_2 - \gamma_{th,2}k_{S2}^2)P}} \frac{1}{\phi_{S2}} \exp\left(-\frac{y}{\phi_{S2}}\right) \mathrm{d}y \\ &= \exp\left(-\frac{1}{\phi_{S2}} \frac{\gamma_{th,2}(\sigma_e^2 k_{S2}^2 P + \sigma_e^2 P + N_o)}{(\alpha_1 - \gamma_{th,2}\alpha_2 - \gamma_{th,2}k_{S2}^2)P}\right), \end{aligned} \tag{2.15}$$

and

$$\begin{aligned} Pr(\gamma_{S2} > \gamma_{th,2}) &= Pr\left(|\tilde{h}_{S2}|^2 \le \frac{\gamma_{th,2}(\sigma_e^2 k_{S2}^2 P + \sigma_e^2 P + N_o)}{(\alpha_2 - \gamma_{th,2}k_{S2}^2)P}\right) \\ &= \int_0^{\frac{\gamma_{th,2}(\sigma_e^2 k_{S2}^2 P + \sigma_e^2 P + N_o)}{(\alpha_2 - \gamma_{th,2}k_{S2}^2)P}} \frac{1}{\phi_{S2}} \exp\left(-\frac{y}{\phi_{S2}}\right) \mathrm{d}y \\ &= \exp\left(-\frac{1}{\phi_{S2}} \frac{\gamma_{th,2}(\sigma_e^2 k_{S2}^2 P + \sigma_e^2 P + N_o)}{(\alpha_2 - \gamma_{th,2}k_{S2}^2)P}\right), \end{aligned} \tag{2.16}$$

Substituting (2.15) and (2.16) into (2.14) we obtain

$$P_{out,2} = 1 - \exp\left(-\frac{1}{\phi_{S2}} \frac{\gamma_{th,2}(\sigma_e^2 k_{S2}^2 P + \sigma_e^2 P + N_o)}{(\alpha_1 - \gamma_{th,2}\alpha_2 - \gamma_{th,2}k_{S2}^2)P}\right) \exp\left(-\frac{1}{\phi_{S2}} \frac{\gamma_{th,2}(\sigma_e^2 k_{S2}^2 P + \sigma_e^2 P + N_o)}{(\alpha_2 - \gamma_{th,2}k_{S2}^2)P}\right). \tag{2.17}$$

2.4.2 Ergodic capacity of the downlink NOMA

In this subsection, we derive the EC of the users of the downlink NOMA system under the HWI and ipCSI. The achievable rates of the U_1 and U_2 according to SINR are presented, respectively as:

$$R_1 = (1 + \gamma_{S1}), \tag{2.18}$$

$$R_2 = (1 + \gamma_{S2}). \tag{2.19}$$

The ergodic capacity of individual users is calculated by averaging the achievable rates across instantaneous channel coefficients as

$$C_1 = \int_0^{\infty} log_2(1 + \gamma_{S1}) p_{\delta_1}(\delta_1) d_{\delta_1}, \tag{2.20}$$

$$C_2 = \int_0^{\infty} log_2(1 + \gamma_{S2}) p_{\delta_2}(\delta_2) d_{\delta_2}, \tag{2.21}$$

where $\delta_i|\tilde{h_i}|^2$ and $p_{\delta_i}(\delta_i)$ is the PDF of δ_i.
Reminding as in [62] that $\int_0^\infty = log_2(1+x)f_x(x)dx = \frac{1}{ln2}\int_0^\infty \frac{1-F_X(x)}{1+x}dx$, where $F_X(.)$ is are the CDFs of X.

Hence the EC of the U_1 and U_2 under ipCSI and HWI can be expressed, respectively as:

$$C_1 = \frac{1}{ln2}\int_0^{\frac{\alpha_1}{\alpha_2+k_{S1}^2}} \frac{\frac{\exp(x(\sigma_e^2 P+\sigma_e^2 P k_{S1}^2+N_o))}{\phi_{S1}(\alpha_1-x\alpha_2-xk_{S1}^2)P}}{1+x}dx, \tag{2.22}$$

$$C_2 = \frac{1}{ln2}\int_0^{\frac{\alpha_2}{k_{S2}^2}} \frac{\frac{\exp(x(\sigma_e^2 P+\sigma_e^2 P k_{S2}^2+N_o))}{\phi_{S2}(\alpha_2-xk_{S2}^2)P}}{1+x}dx. \tag{2.23}$$

To the best of the author's knowledge, there is no known analytical solution for equations (2.22) and (2.23). However, it can be easily computed using software tools such as MATLAB, MAPLE, and MATHEMATICA.

2.4.3 Bit error rate of the downlink NOMA

In this part, we derive the expression of the BER to evaluate the performance of the NOMA system under HWI and ipCSI. We analyze the expression of BER for the downlink NOMA system at the users, assuming the BPSK-BPSK modulation for both users. The BER for ideal Downlink NOMA with BPSK-BPSK modulation is derived in [46]. However, we can present the BER for NOMA with HWI and ipCSI.

2.4.3.1 Bit error rate of U_1

The error probability at the U_1 by considering the ML decision rule can be given as: [46]:

$$\begin{aligned} P_1(e) =& \frac{1}{2}\Big[Pr\Big(n + (\sqrt{\alpha_1 P} - \sqrt{\alpha_2 P} + \eta_{S1})e + \tilde{h_{S1}}\eta_{S1} \geq (\sqrt{\alpha_1 P} - \sqrt{\alpha_2 P})\tilde{h_{S1}}\Big) + \\ & Pr\Big(n + (\sqrt{\alpha_1 P} + \sqrt{\alpha_2 P} + \eta_{S1})e + \tilde{h_{S1}}\eta_{S1} \geq (\sqrt{\alpha_1 P} + \sqrt{\alpha_2 P})\tilde{h_{S1}}\Big). \end{aligned} \tag{2.24}$$

However, the expression of the error probability can be represented using the Gaussian Q function as:

$$P_1(e) = \frac{1}{2}\left[Q(\sqrt{\Gamma_1}) + Q(\sqrt{\Gamma_2})\right], \tag{2.25}$$

where

$$\Gamma_1 = \frac{(\sqrt{\alpha_1 P}-\sqrt{\alpha_2 P})\tilde{|h_{S1}|^2}}{\frac{N_o}{2}+((\sqrt{\alpha_1 P}-\sqrt{\alpha_2 P})^2+k_{S1}^2 P)\sigma_e^2+k_{S1}^2 P\tilde{|h_{S1}|^2}},\ \Gamma_2 = \frac{(\sqrt{\alpha_1 P}+\sqrt{\alpha_2 P})\tilde{|h_{S1}|^2}}{\frac{N_o}{2}+((\sqrt{\alpha_1 P}+\sqrt{\alpha_2 P})^2+k_{S1}^2 P)\sigma_e^2+k_{S1}^2 P\tilde{|h_{S1}|^2}}.$$

Then, the final expression of the BER at the far user is obtained as:

$$P_1^{avg}(e) = \frac{1}{4}\left[\left(1-\sqrt{\frac{\bar{\Gamma_1}}{2+\bar{\Gamma_1}}}\right)+\left(1-\sqrt{\frac{\bar{\Gamma_2}}{2+\bar{\Gamma_2}}}\right)\right], \tag{2.26}$$

where

$$\bar{\Gamma_1} = \frac{(\sqrt{\alpha_1 P}-\sqrt{\alpha_2 P})E[\tilde{|h_{S1}|^2}]}{\frac{N_o}{2}+((\sqrt{\alpha_1 P}-\sqrt{\alpha_2 P})^2+k_{S1}^2 P)\sigma_e^2+k_{S1}^2 PE[\tilde{|h_{S1}|^2}]},\ \bar{\Gamma_2} = \frac{(\sqrt{\alpha_1 P}+\sqrt{\alpha_2 P})E[\tilde{|h_{S1}|^2}]}{\frac{N_o}{2}+((\sqrt{\alpha_1 P}+\sqrt{\alpha_2 P})^2+k_{S1}^2 P)\sigma_e^2+k_{S1}^2 PE[\tilde{|h_{S1}|^2}]}.$$

Proof Please see Appendix A.

2.4.3.2 Bit error rate of U_2

The error probability of the near user is given as the sum of two cases due to the SIC process involved. Thus, assuming an imperfect channel state information, the BER at near user is given as:

$$P_2(e) = P_2(e|correct) + P_2(e|error), \tag{2.27}$$

where $P_2(e|correct)$ and $P_2(e|error)$ are the probability of error of the near user when the far user is decoding correctly and erroneously at the near user, respectively.

$$P_2(e|correct) = \frac{1}{2}\Bigg[P\Bigg(n + \left(\sqrt{\alpha_1 P} - \sqrt{\alpha_2 P} + \eta_{S2}\right) e + \tilde{h_{S2}}\eta_{S2} \leq \left(\sqrt{\alpha_1 P} - \sqrt{\alpha_2 P}\right) \tilde{h_{S2}}\Bigg)$$
$$\times P\Bigg(n + \left(\sqrt{\alpha_1 P} + \sqrt{\alpha_2 P} + \eta_{S2}\right) e + \tilde{h_{S2}}\eta_{S2} \leq$$
$$- \sqrt{\alpha_2 P}\tilde{h_{S2}}|n + \left(\sqrt{\alpha_1 P} - \sqrt{\alpha_2 P} + \eta_{S2}\right) e + \tilde{h_{S2}}\eta_{S2} \leq \left(\sqrt{\alpha_1 P} - \sqrt{\alpha_2 P}\right) \tilde{h_{S2}}\Bigg)$$
$$+ P\Bigg(n + \left(\sqrt{\alpha_1 P} + \sqrt{\alpha_2 P} + \eta_{S2}\right) e + \tilde{h_{S2}}\eta_{S2} \leq \left(\sqrt{\alpha_1 P} + \sqrt{\alpha_2 P}\right) \tilde{h_{S2}}\Bigg)$$
$$\times P\Bigg(n + \left(\sqrt{\alpha_1 P} + \sqrt{\alpha_2 P} + \eta_{S2}\right) e + \tilde{h_{S2}}\eta_{S2} \leq$$
$$\sqrt{\alpha_2 P}\tilde{h_{S2}}|n + \left(\sqrt{\alpha_1 P} + \sqrt{\alpha_2 P} + \eta_{S2}\right) e + \tilde{h_{S2}}\eta_{S2} \leq \left(\sqrt{\alpha_1 P} + \sqrt{\alpha_2 P}\right) \tilde{h_{S2}}\Bigg)\Bigg]. \tag{2.28}$$

Then, the error probability at near user depends on the probability of erroneous detection of far user defined as:

$$P_2(e|error) = \frac{1}{2}\Bigg[P\Bigg(n + \left(\sqrt{\alpha_1 P} - \sqrt{\alpha_2 P} + \eta_{S2}\right) e + \tilde{h_{S2}}\eta_{S2} \geq \left(\sqrt{\alpha_1 P} - \sqrt{\alpha_2 P}\right) \tilde{h_{S2}}\Bigg)\times$$
$$P\Bigg(n + \left(\sqrt{\alpha_1 P} - \sqrt{\alpha_2 P} + \eta_{S2}\right) e + \tilde{h_{S2}}\eta_{S2} \leq$$
$$(2\sqrt{\alpha_1 P} - \sqrt{\alpha_2 P})\tilde{h_{S2}}|n + \left(\sqrt{\alpha_1 P} - \sqrt{\alpha_2 P} + \eta_{S2}\right) e\tilde{h_{S2}}\eta_{S2} \geq \left(\sqrt{\alpha_1 P} - \sqrt{\alpha_2 P}\right) \tilde{h_{S2}}\Bigg)+$$
$$P\Bigg(n + \left(\sqrt{\alpha_1 P} + \sqrt{\alpha_2 P} + \eta_{S2}\right) e + \tilde{h_{S2}}\eta_{S2} \geq \left(\sqrt{\alpha_1 P} + \sqrt{\alpha_2 P}\right) \tilde{h_{S2}}\Bigg)$$
$$\times P\Bigg(n + \left(\sqrt{\alpha_1 P} + \sqrt{\alpha_2 P} + \eta_{S2}\right) e + \tilde{h_{S2}}\eta_{S2} \geq (2\sqrt{\alpha_1 P} - \sqrt{\alpha_2 P})\tilde{h_{S2}}|n+$$
$$\left(\sqrt{\alpha_1 P} + \sqrt{\alpha_2 P} + \eta_{S2}\right) e + \tilde{h_{S2}}\eta_{S2} \geq \left(\sqrt{\alpha_1 P}\sqrt{\alpha_2 P}\right) \tilde{h_{S2}}\Bigg)\Bigg]. \tag{2.29}$$

Utilizing the probability of A event conditioned over B event given as:

$$P(A|B) = \frac{P(A \cap B)}{P(B)}. \tag{2.30}$$

The expression (2.26) and (2.27) can be expressed as

$$P_2(e|correct) = \frac{1}{2}\Bigg[P\left(n + \left(\sqrt{\alpha_1 P} - \sqrt{\alpha_2 P} + \eta_{S2}\right)e + \tilde{h_2}\eta_{S2} \leq -\sqrt{\alpha_2 P}\tilde{h_{S2}}\right) + \\ P\left(\sqrt{\alpha_2 P}\tilde{h_{S2}}\right) \leq n + \left(\sqrt{\alpha_1 P} - \sqrt{\alpha_2 P} + n\right)e + \tilde{h_{S2}}\eta_2 \leq \left(\sqrt{\alpha_1 P} + \sqrt{\alpha_2 P}\right)\tilde{h_{S2}}\Bigg], \tag{2.31}$$

$$P_2(e|error) = \frac{1}{2}\Bigg[P\Bigg(\left(\sqrt{\alpha_1 P} - \sqrt{\alpha_2 P}\right)\tilde{h_{S2}} \leq n + \left(\sqrt{\alpha_1 P} - \sqrt{\alpha_2 P} + \eta_{S2}\right)e + \tilde{h_{S2}}\eta_{S2} \leq \\ \left(2\sqrt{\alpha_1 P} - \sqrt{\alpha_2 P}\right)\tilde{h_{S2}}\Bigg) + P\Bigg(n + \left(\sqrt{\alpha_1 P} + \sqrt{\alpha_2 P} + \eta_{S2}\right)e + \tilde{h_{S2}}\eta_{S2} \leq \\ \left(2\sqrt{\alpha_1 P} + \sqrt{\alpha_2 P}\right)\tilde{h_{S2}}\Bigg)\Bigg]. \tag{2.32}$$

The expression (2.29) and (2.30) writing in terms of Q-function is obtained as:

$$P_2(e|correct) = \frac{1}{2}\Big[Q(\sqrt{\Gamma_3}) + Q(\sqrt{\Gamma_4}) - Q(\sqrt{\Gamma_5})\Big], \tag{2.33}$$

$$P_2(e|error) = \frac{1}{2}\Big[Q(\sqrt{\Gamma_6}) - Q(\sqrt{\Gamma_7}) + Q(\sqrt{\Gamma_8})\Big], \tag{2.34}$$

where

$$\Gamma_3 = \frac{\alpha_2 P|\tilde{h_{S2}}|^2}{\frac{N_o}{2} + ((\sqrt{\alpha_1 P} - \sqrt{\alpha_2 P})^2 + k_{S2}^2 P)\sigma_e^2 + k_{S2}^2 P|\tilde{h_{S2}}|^2}, \ \Gamma_4 = \frac{\alpha_2 P|\tilde{h_{S2}}|^2}{\frac{N_o}{2} + ((\sqrt{\alpha_1 P} + \sqrt{\alpha_2 P})^2 + k_{S2}^2 P)\sigma_e^2 + k_{S2}^2 P|\tilde{h_{S2}}|^2},$$

$$\Gamma_5 = \frac{(\sqrt{\alpha_1 P} + \sqrt{\alpha_1 P})^2|\tilde{h_{S2}}|^2}{\frac{N_o}{2} + ((\sqrt{\alpha_1 P} + \sqrt{\alpha_2 P})^2 + k_{S2}^2 P)\sigma_e^2 + k_{S2}^2 P|\tilde{h_{S2}}|^2}, \ \Gamma_6 = \frac{(\sqrt{\alpha_1 P} - \sqrt{\alpha_1 P})^2|\tilde{h_{S2}}|^2}{\frac{N_o}{2} + ((\sqrt{\alpha_1 P} - \sqrt{\alpha_2 P})^2 + k_{S2}^2 P)\sigma_e^2 + k_{S2}^2 P|\tilde{h_{S2}}|^2},$$

$$\Gamma_7 = \frac{(2\sqrt{\alpha_1 P} - \sqrt{\alpha_1 P})^2|\tilde{h_{S2}}|^2}{\frac{N_o}{2} + ((\sqrt{\alpha_1 P} - \sqrt{\alpha_2 P})^2 + k_{S2}^2 P)\sigma_e^2 + k_{S2}^2 P|\tilde{h_{S2}}|^2}, \ \Gamma_8 = \frac{(2\sqrt{\alpha_1 P} + \sqrt{\alpha_1 P})^2|\tilde{h_{S2}}|^2}{\frac{N_o}{2} + ((\sqrt{\alpha_1 P} + \sqrt{\alpha_2 P})^2 + k_{S2}^2 P)\sigma_e^2 + k_{S2}^2 P|\tilde{h_{S2}}|^2}.$$

The final expression of the average BER at the near user can be described as:

$$P_2^{avg} = \frac{1}{4}\left[2 + \sqrt{\frac{\bar{\Gamma_3}}{2+\bar{\Gamma_3}}} + \sqrt{\frac{\bar{\Gamma_4}}{2+\bar{\Gamma_4}}}\right] - \frac{1}{4}\left[\sqrt{\frac{\bar{\Gamma_5}}{2+\bar{\Gamma_5}}} - \sqrt{\frac{\bar{\Gamma_6}}{2+\bar{\Gamma_6}}} + \sqrt{\frac{\bar{\Gamma_7}}{2+\bar{\Gamma_7}}} - \sqrt{\frac{\bar{\Gamma_8}}{2+\bar{\Gamma_8}}}\right]. \tag{2.35}$$

Proof Please see Appendix B.

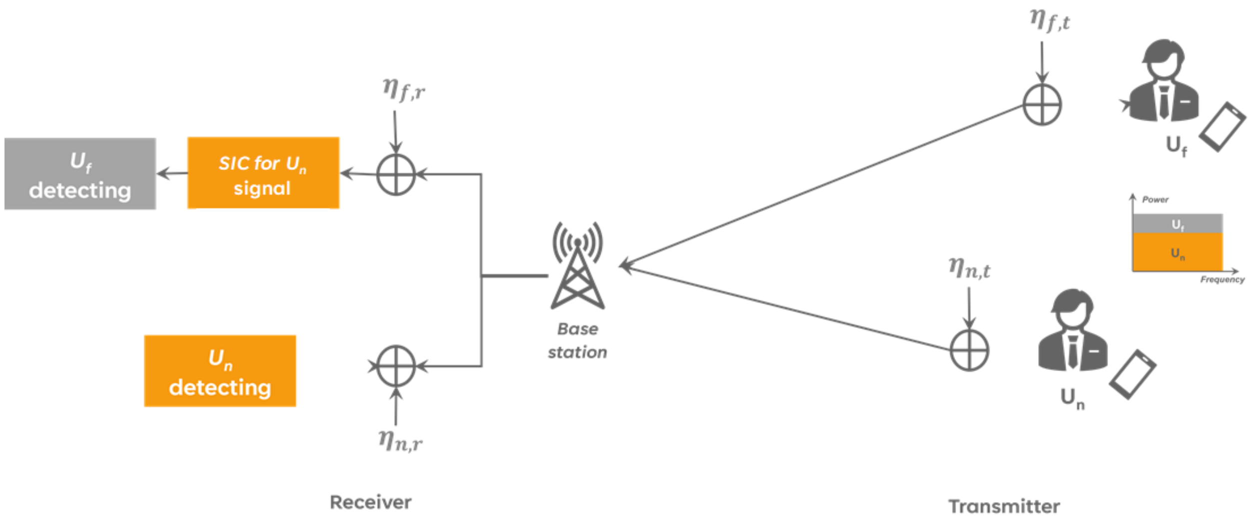

Figure 2.2: System model uplink NOMA with HWI.

2.5 System model of the uplink NOMA

In this section, we consider an uplink NOMA network that consists of a BS and two users i.e. the far user U1, and the near user U2. In the presence of HWI and ipCSI as depicted in Fig. 2.2 All nodes are equipped with a single antenna. According to uplink NOMA protocol, the received signal at the BS under HWI and ipCSI is expressed as:

$$y_{BS} = \sum_{i=1}^{2} (\tilde{h}_i + e)(\sqrt{\alpha_i P} x_i + \eta_i) + n, \tag{2.36}$$

where α_1 and α_2 is the PA coefficient in which $\alpha_2 < \alpha_1$ The SINR for the U_2 is defined as:

$$\gamma_2 = \frac{|\tilde{h}_{S2}|^2 \alpha_2 P}{|\tilde{h}_{S1}|^2 \alpha_1 P + |\tilde{h}_{S1}|^2 k_{S1}^2 P + |\tilde{h}_{S2}|^2 k_{S2}^2 P + \sigma_e^2 k_{S2}^2 P + \sigma_e^2 k_{S1}^2 P + \sigma_e^2 P + N_o}. \tag{2.37}$$

Assuming a perfect SIC, the SINR of the U_1 can be given as:

$$\gamma_1 = \frac{|\tilde{h}_{S1}|^2 \alpha_1 P}{|\tilde{h}_{S1}|^2 k_{S1}^2 P + |\tilde{h}_{S2}|^2 k_{S2}^2 P + \sigma_e^2 k_{S2}^2 P + \sigma_e^2 k_{S1}^2 P + \sigma_e^2 P + N_o}. \tag{2.38}$$

2.6 Performance analysis of the uplink NOMA

2.6.1 Outage probability

In this subsection, we derive the expression of the OP of the uplink NOMA system in the presence of HWI and ipCSI over the Rayleigh fading channel.

The OP of the U_2 under HWI and ipCSI can be expressed as in [63]:

$$\begin{aligned} P_{out,2} &= F_{\gamma_2}(\gamma_{th,2}) \\ &= Pr(\gamma_2 \leq \gamma_{th,2}), \end{aligned} \tag{2.39}$$

where $\gamma_{th,2}$ of the U_2 and F_{γ_i} is the CDF of γ_i

$$\begin{aligned} P_{out,2} &= Pr\left(|\tilde{h}_{S2}|^2 \leq \frac{\gamma_{th,2}[P|\tilde{h}_{S1}|^2(\alpha_1 + k_{S1}^2) + \sigma_e^2(k_{S1}^2 + k_{S2}^2 + 1)P + N_o]}{P(\alpha_2 - k_{S2}^2)}\right) \\ &= 1 - \exp\left(-\frac{\gamma_{th,2}(\sigma_e^2(k_{S1}^2 + k_{S2}^2 + 1)P + N_o)}{P(\alpha_2 - \gamma_{th,2}k_{S2}^2)\phi_{h_{S2}}}\right) \frac{P(\alpha_2 - \gamma_{th,2}k_{S2}^2)\phi_{h_{S2}}}{\gamma_{th,2}P(\alpha_1 + k_{S2}^2)\phi_{h_{S1}} + P(\alpha_2 - \gamma_{th,2}k_{S2}^2)\phi_{h_{S2}}}, \end{aligned} \tag{2.40}$$

where ϕ_{h_i} is the mean of h_i.
Thus the OP of the x_1 at U_1 can be expressed as:

$$\begin{aligned} P_{out,1} &= Pr\left(|\tilde{h}_{S1}|^2 \leq \frac{\gamma_{th,1}[P|\tilde{h}_{S2}|^2 k_{S2}^2 + \sigma_e^2(k_{S1}^2 + k_{S2}^2 + 1)P + N_o]}{P(\alpha_1 - \gamma_{th,1}k_{S1}^2)}\right) \\ &= 1 - \exp\left(-\frac{\gamma_{th,1}(\sigma_e^2(k_{S1}^2 + k_{S2}^2 + 1)P + N_o)}{P(\alpha_1 - \gamma_{th,1}k_{S1}^2)\phi_{S1}}\right) \frac{P(\alpha_1 - \gamma_{th,1}k_{S1}^2)\phi_{S1}}{\gamma_{th,1}Pk_{S2}^2\phi_{S2} + P(\alpha_1 - \gamma_{th,1}k_{S1}^2)\phi_{S1}}. \end{aligned} \tag{2.41}$$

It is worth mentioning that in the event of an outage for U_2, where the SIC cannot be successfully executed, U_1 will also be in the outage. As a result, the outcome reveals that the OP of U_1 is determined as [60, eq. (11)]:

$$\begin{aligned} P_{out,1} = 1 - &\exp\left(-\frac{\gamma_{th,2}(\sigma_e^2(k_{S1}^2 + k_{S2}^2 + 1)P + N_o)}{P(\alpha_2 - \gamma_{th,2}k_{S2}^2)\phi_{h_{S2}}}\right) \frac{P(\alpha_2 - \gamma_{th,2}k_{S2}^2)\phi_{h_{S2}}}{\gamma_{th,2}P(\alpha_1 + k_{S2}^2)\phi_{h_{S1}} + P(\alpha_2 - \gamma_{th,2}k_{S2}^2)\phi_{h_{S2}}} \\ &\times \exp\left(-\frac{\gamma_{th,1}(\sigma_e^2(k_{S1}^2 + k_{S2}^2 + 1)P + N_o)}{P(\alpha_1 - \gamma_{th,1}k_{S1}^2)\phi_{S1}}\right) \frac{P(\alpha_1 - \gamma_{th,1}k_{S1}^2)\phi_{S1}}{\gamma_{th,1}Pk_{S2}^2\phi_{S2} + P(\alpha_1 - \gamma_{th,1}k_{S1}^2)\phi_{S1}}. \end{aligned} \tag{2.42}$$

2.6.2 Ergodic capacity of the uplink NOMA

In this subsection, we analyze the achievable rates of users in the uplink Non-Orthogonal Multiple Access (NOMA) system. Similar to the downlink NOMA, we consider the Shannon limit and provide an analysis of the ergodic capacity. The SINR of each U_2 and U_1 are defined in (2.37) and (2.38), respectively. The EC of the U_2 can be expressed as:

$$C_2 = \int_0^{\infty} log_2(1 + \gamma_2) p_{\delta_2}(\delta_2) d_{\delta_2}, \tag{2.43}$$

where p_{δ_2} is the PDF of δ_2. By applying the technique of integration by parts, it can be represented by (CDF) of δ_2 as:

$$C_i = \frac{1}{ln2} \int_0^{\infty} \frac{1 - F_{\delta_i}}{1 - x},\ i = 1, 2 \tag{2.44}$$

where F_{δ_i} is the CDF of γ_i determined in (2.40) and (2.41) for the U_2 and U_1, respectively.

$$C_2 = \frac{1}{ln2} \int_0^{\frac{\alpha_2}{k_2^2}} \frac{\frac{\exp(x(\sigma_e P + \sigma_e P k_{S2}^2 + \sigma_e P k_{S1}^2 + N_o))}{\phi_{S2}(\alpha_2 - x k_{S2}^2) P} \frac{(\alpha_2 - x k_{S2}^2) P \phi_{S2}}{x(\alpha_1 + k_{S1}^2) P \phi_{S2} + (\alpha_2 - x k_S 2^2) P \phi_{S2}}}{1 + x} dx, \tag{2.45}$$

$$C_1 = \frac{1}{ln2} \int_0^{\frac{\alpha_1}{k_{S1}^2}} \frac{\frac{\exp(x(\sigma_e P + \sigma_e P k_{S2}^2 + \sigma_e P k_{S1}^2 + N_o))}{\phi_{S1}(\alpha_1 - x k_{S1}^2) P} \frac{(\alpha_1 - x k_{S1}^2) P \phi_{S1}}{x k_{S2}^2 P \phi_{S2} + (\alpha_1 - x k_{S1}^2) P \phi_{S1}}}{1 + x} dx, \tag{2.46}$$

where ϕ_i is the mean of h_i. The equation (2.45) and (2.46) currently lack a known analytical solution. Nevertheless, their computations can be effortlessly performed utilizing software tools such as MATLAB, MAPLE, and MATHEMATICA.

2.7 Numerical results

This section presents the OP, EC, and BER performance of a downlink and OP and EC for the uplink NOMA over the Rayleigh fading channel by the numerical results validated through the simulation results. Unless, theoretical curves are represented by markers, while simulation results are depicted using lines in the figures. We set the parameters to $d_1 = 4$, $d_1 = 2$. the ipCSI coefficient is set $\sigma_e^2 = 0.001$ and the HWI distortion level at the transceiver is defined as $k_{S1}^2 = k_{S2}^2 = k$. The average SNR is defined as defined as $SNR = \frac{P}{No}$.
The impact of imperfections, ipCSI and HWI, on the downlink NOMA performance is evaluated as a function of SNR. The HWI factor is set as $k = 0.175$ [64], while σ_e^2 is 0.001. By

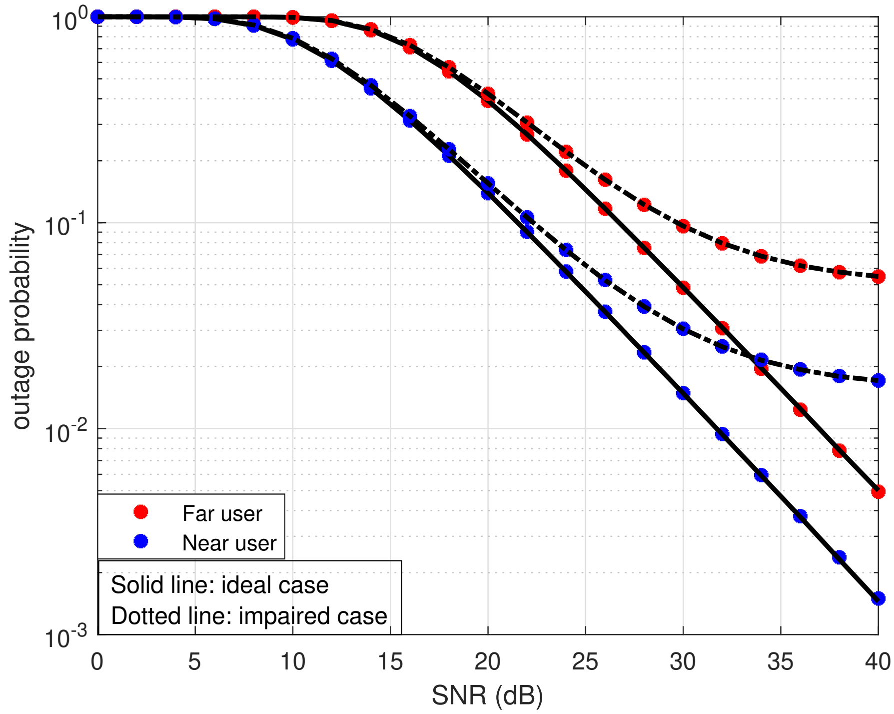

Figure 2.3: OP of the downlink NOMA w.r.t SNR with $k = 0.175$ and $\sigma_e^2 = 0.001$.

examining Figs. 2.3, 2.4, and 2.5, it becomes evident that the ideal scenario (with $k = 0$ and $\sigma_e^2 = 0$) outperforms the impaired scenario. Remarkably, at high SNR values, both users experience an error floor. However, in Figs .2.3 and 2.5 due to the presence of HWI and ipCSI, the near user is relatively less affected compared to the far user due to the SIC process implemented at U_2. This process selectively subtracts only the signal of U_1 and does not consider the presence of imperfections. Hence, the near user experiences a slight impact from imperfections, whereas the far user is more significantly affected.

In Figs. 2.6, 2.7, and 2.8, we examine the impact of the HWI on the direct NOMA system. It can be seen that the OP, EC, and BER performance of both users decreases with the increase of the HWI factor for all SNR values.

Figs. 2.9, 2.10, and 2.11 provide insights into the effect of channel estimation errors on the OP for different SNR values. The results indicate that increasing ipCSI leads to a decrease in the performance of both users, emphasizing the significant impact of channel estimation errors on the NOMA system's performance. Additionally, we observe that the influence of HWI on system performance is comparatively less significant than that of the ipCSI factor.

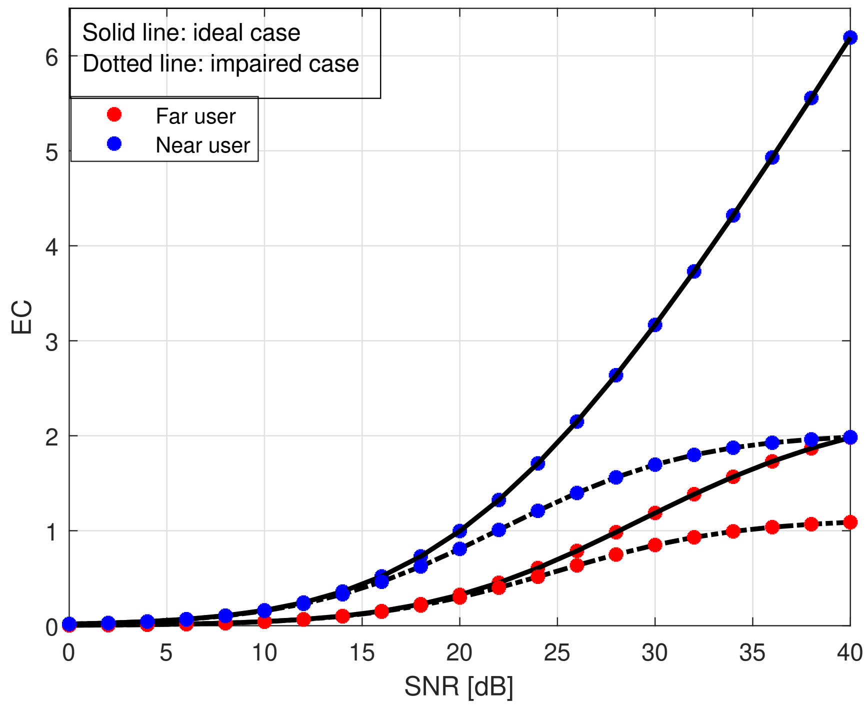

Figure 2.4: EC of the downlink NOMA w.r.t SNR with $k = 0.175$ and $\sigma_e^2 = 0.001$.

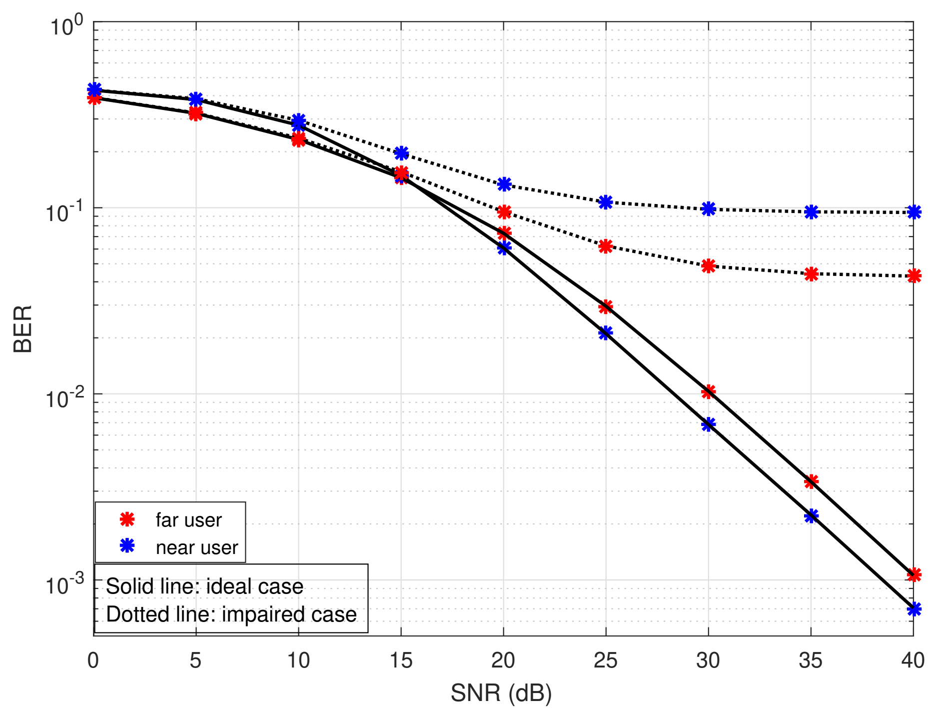

Figure 2.5: BER of the downlink NOMA w.r.t SNR with $k = 0.175$ and $\sigma_e^2 = 0.001$.

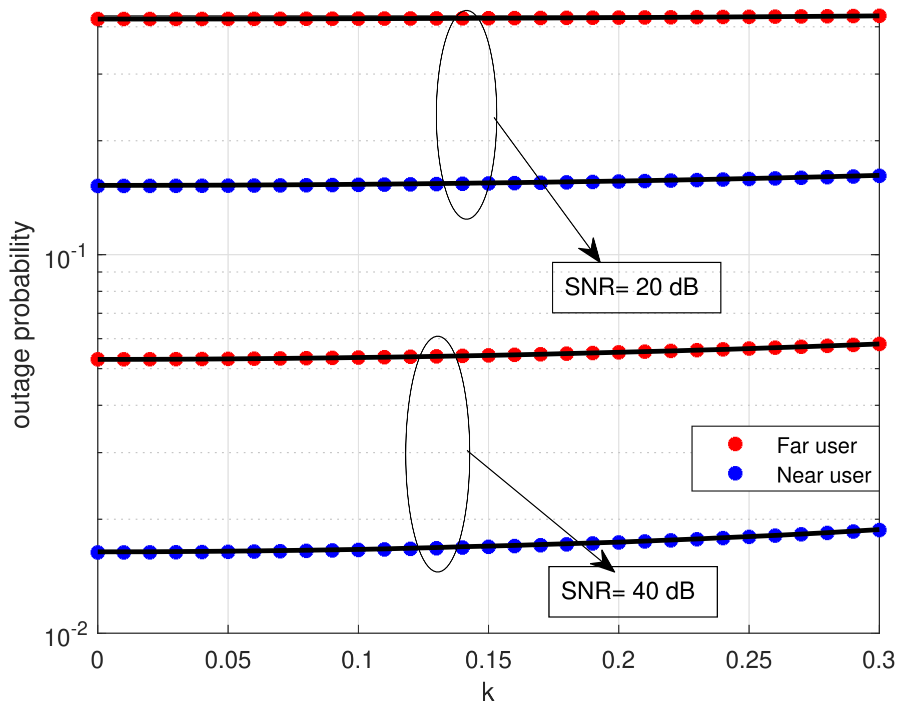

Figure 2.6: OP of downlink NOMA the w.r.t HWI with $\sigma_e^2 = 0.001$.

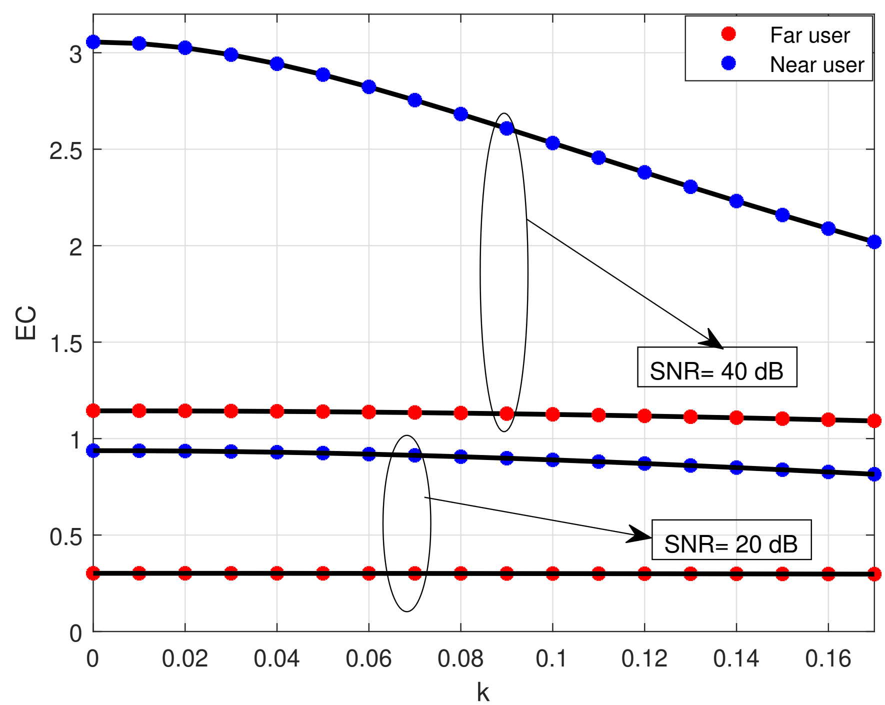

Figure 2.7: EC of the downlink NOMA w.r.t HWIwith $\sigma_e^2 = 0.001$.

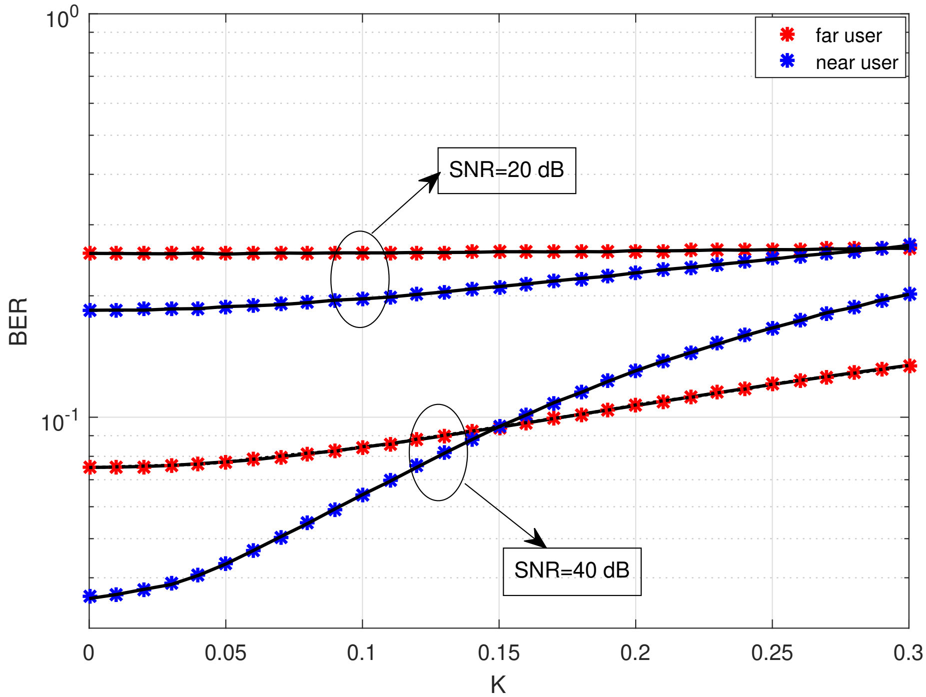

Figure 2.8: BER of the downlink NOMA versus HWI with $\sigma_e^2 = 0.001$.

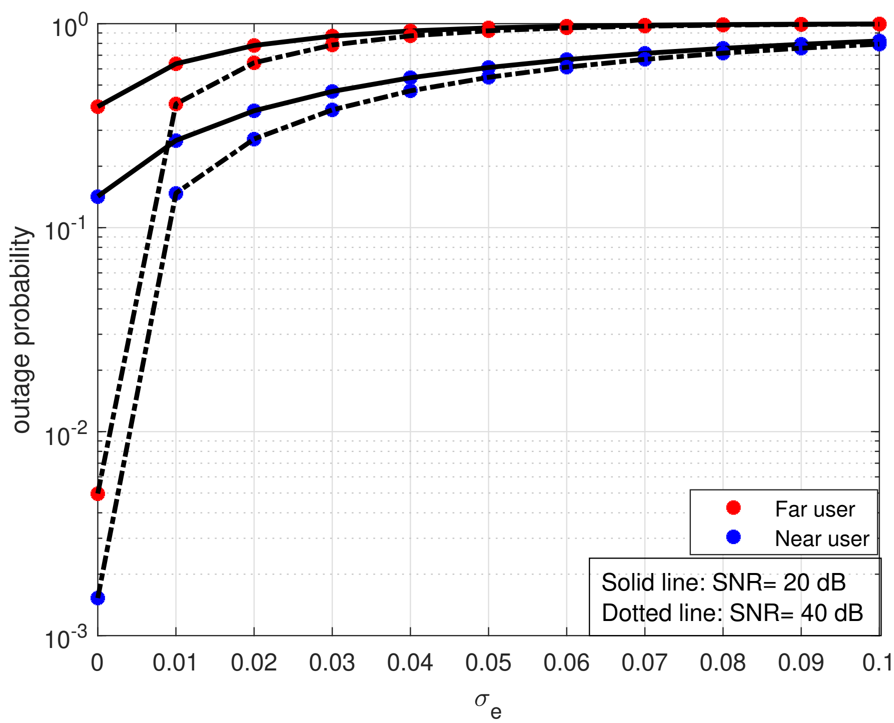

Figure 2.9: OP of the downlink NOMA versus ipCSI with $k = 0.175$.

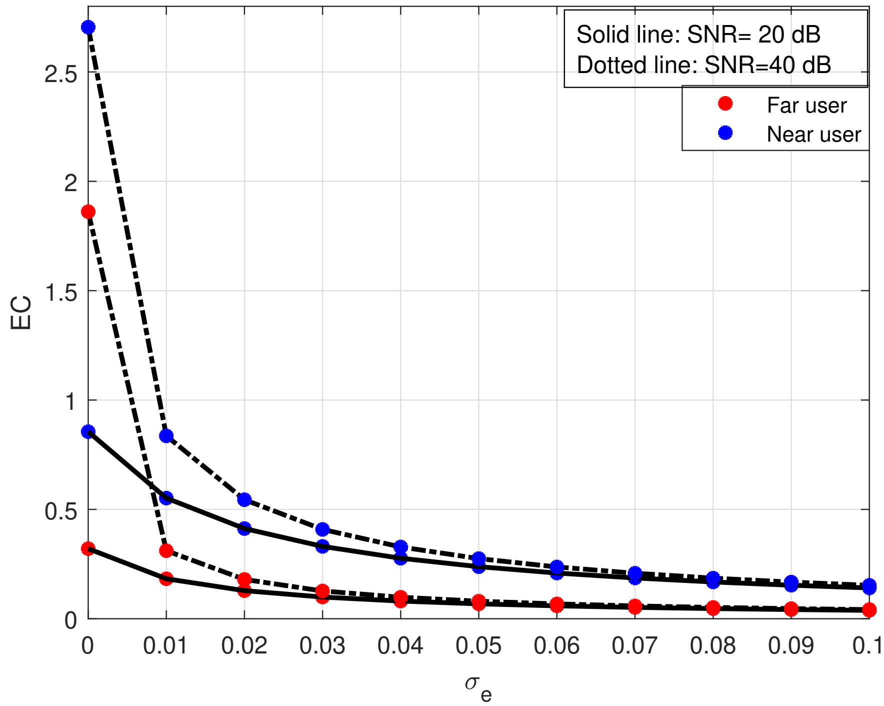

Figure 2.10: EC of the downlink NOMA versus ipCSI with $k = 0.175$.

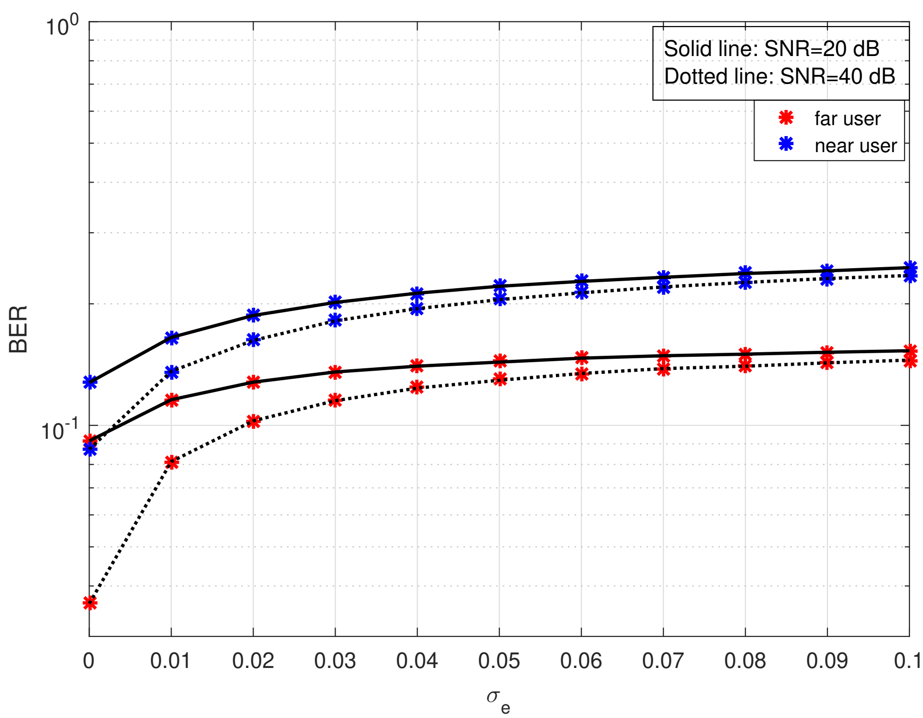

Figure 2.11: BER of the downlink NOMA w.r.t ipCSI with $k = 0.175$.

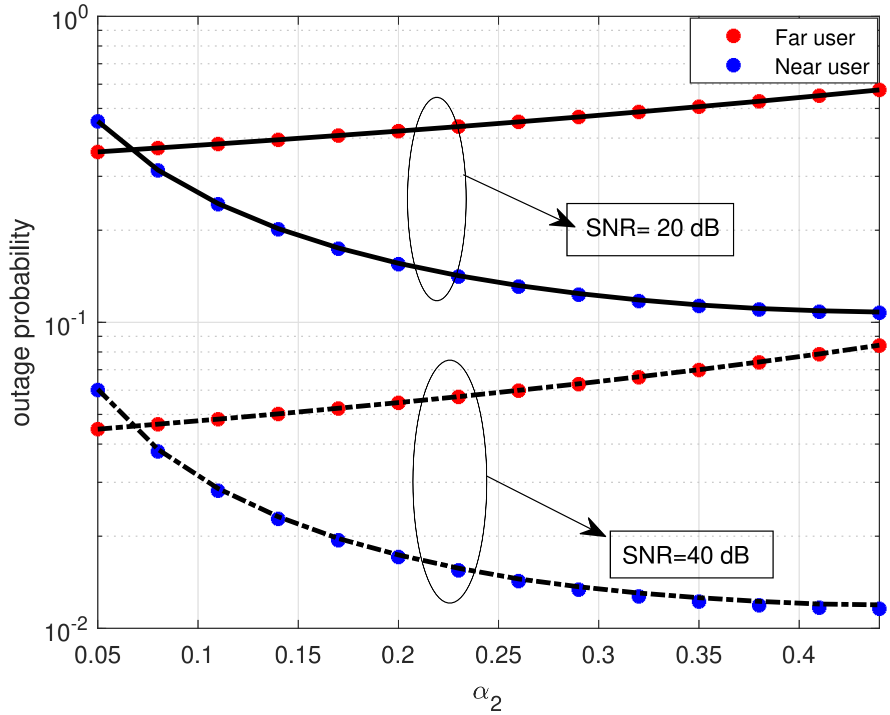

Figure 2.12: OP of the downlink NOMA w.r.t PA with $k = 0.175$ and $\sigma_e^2 = 0.001$.

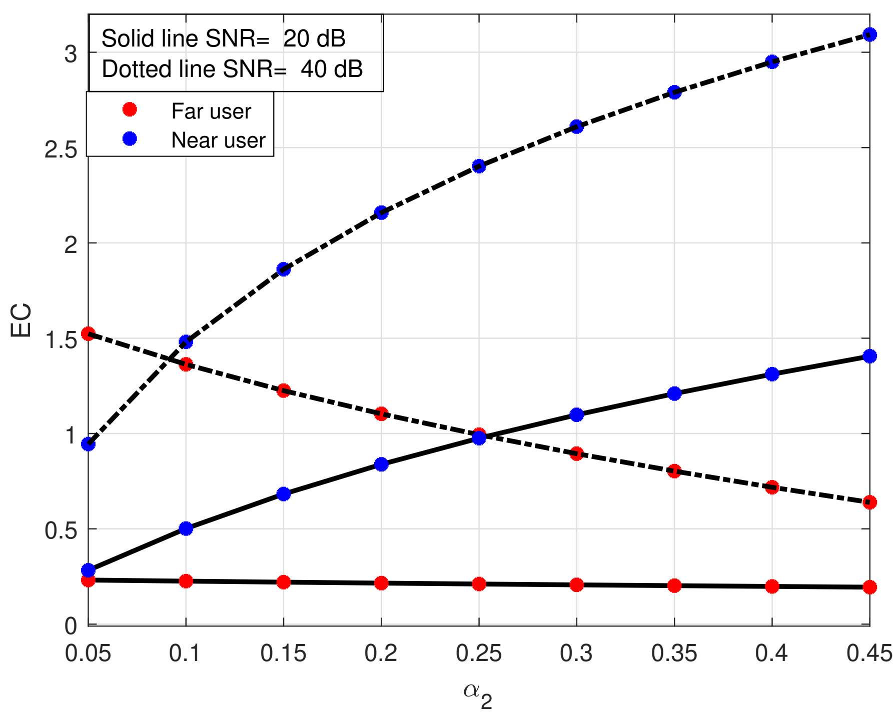

Figure 2.13: EC of the downlink NOMA versus PA with $k = 0.175$ and $\sigma_e^2 = 0.001$.

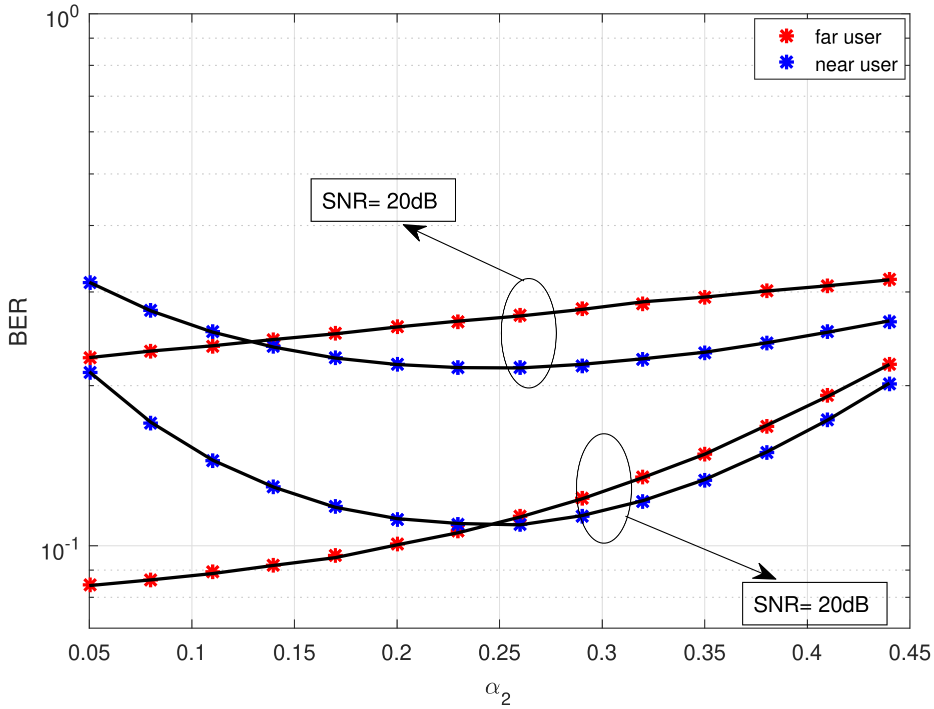

Figure 2.14: BER of the downlink NOMA w.r.t PA with $k = 0.175$ and $\sigma_e^2 = 0.001$.

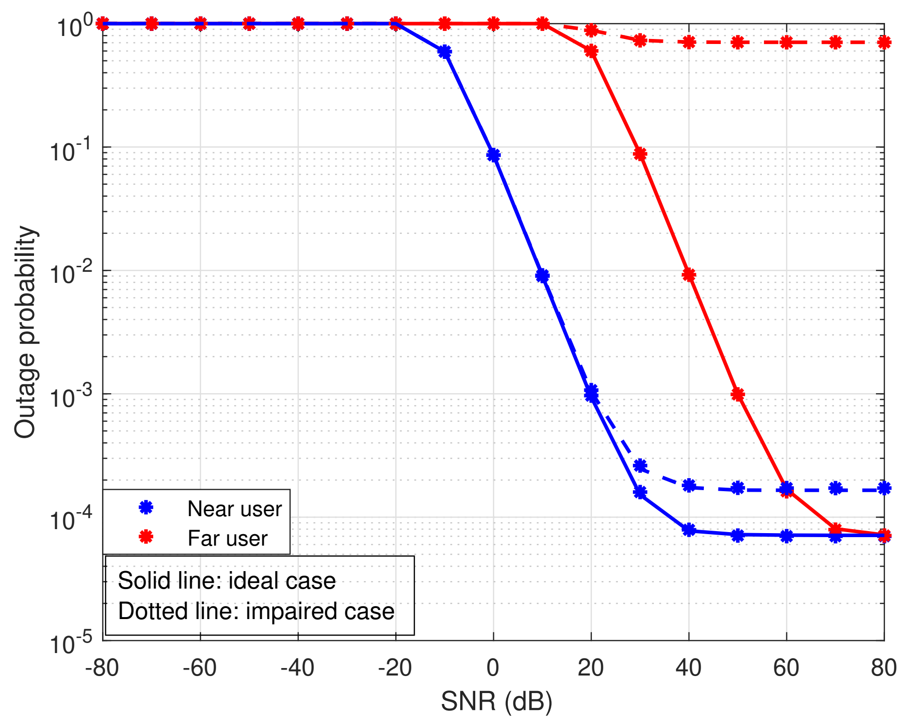

Figure 2.15: OP of the uplink NOMA versus SNR with $k = 0.175$ and $\sigma_e^2 = 0.001$.

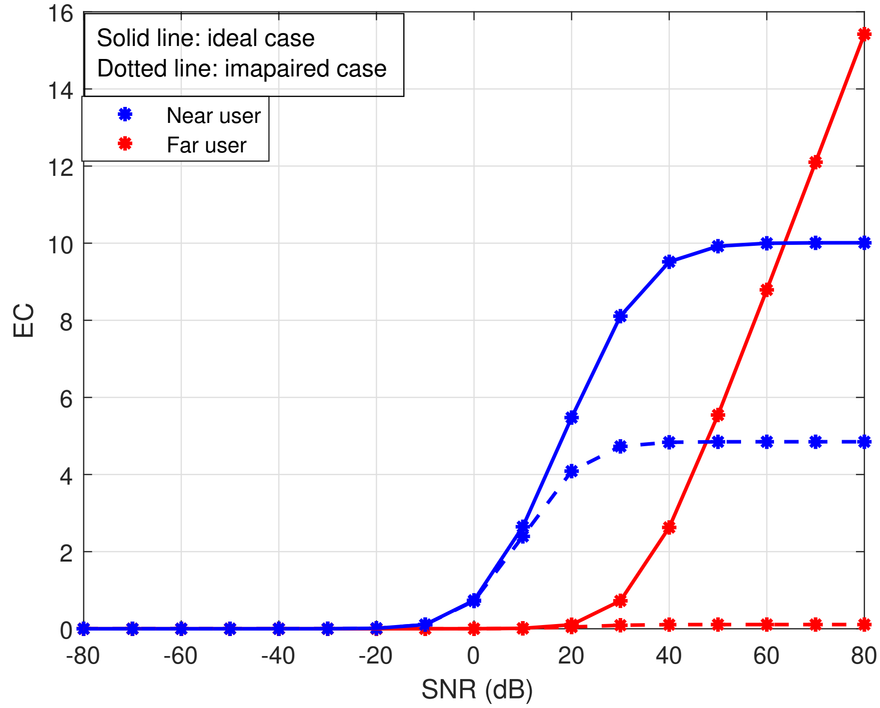

Figure 2.16: EC of the uplink NOMA versus SNR with $k = 0.175$ and $\sigma_e^2 = 0.001$.

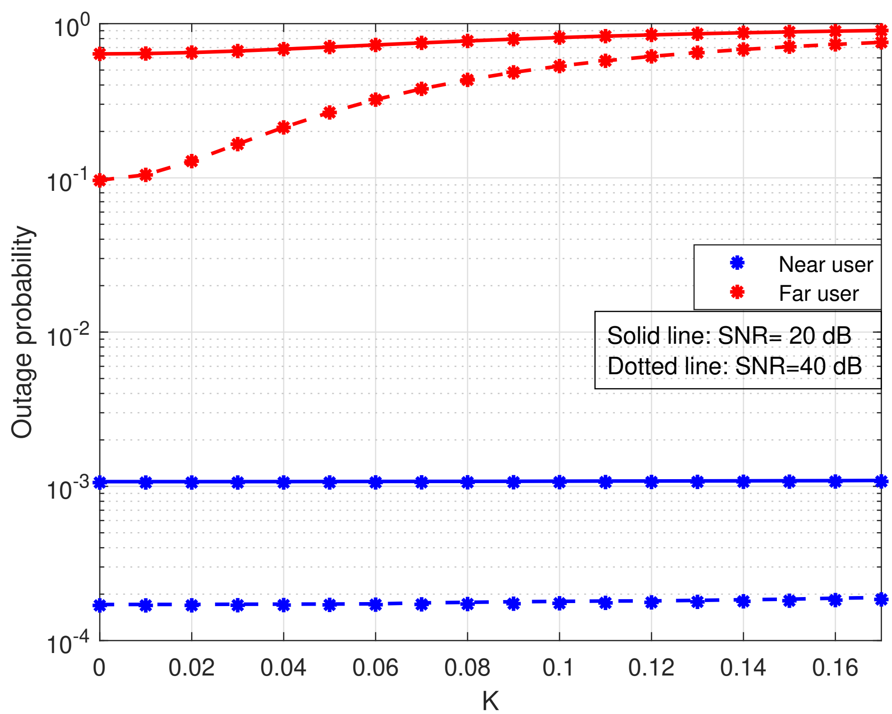

Figure 2.17: OP of the uplink NOMA w.r.t HWI with $\sigma_e^2 = 0.001$.

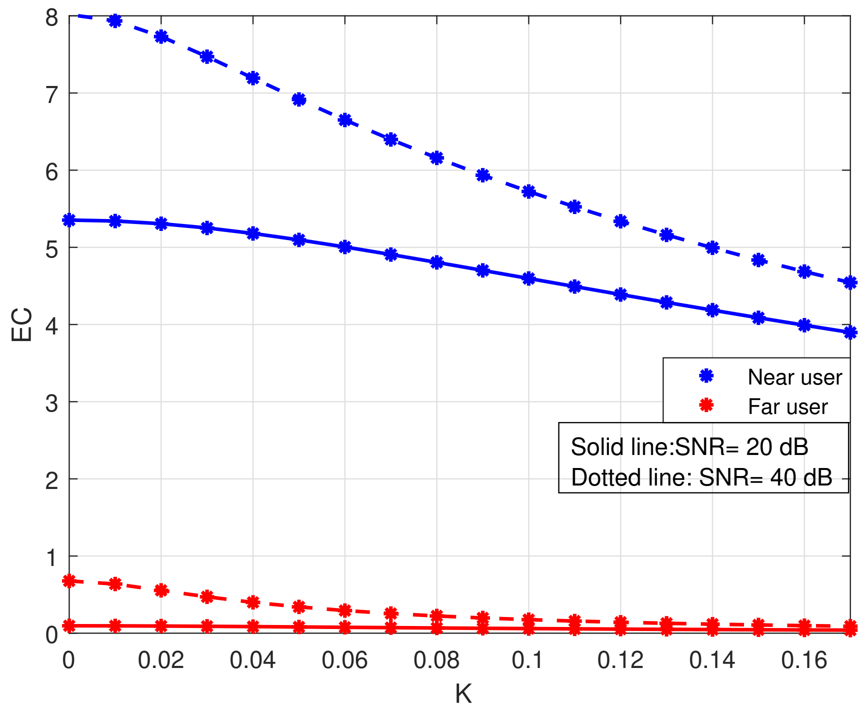

Figure 2.18: EC of the uplink NOMA w.r.t HWI with $\sigma_e^2 = 0.001$.

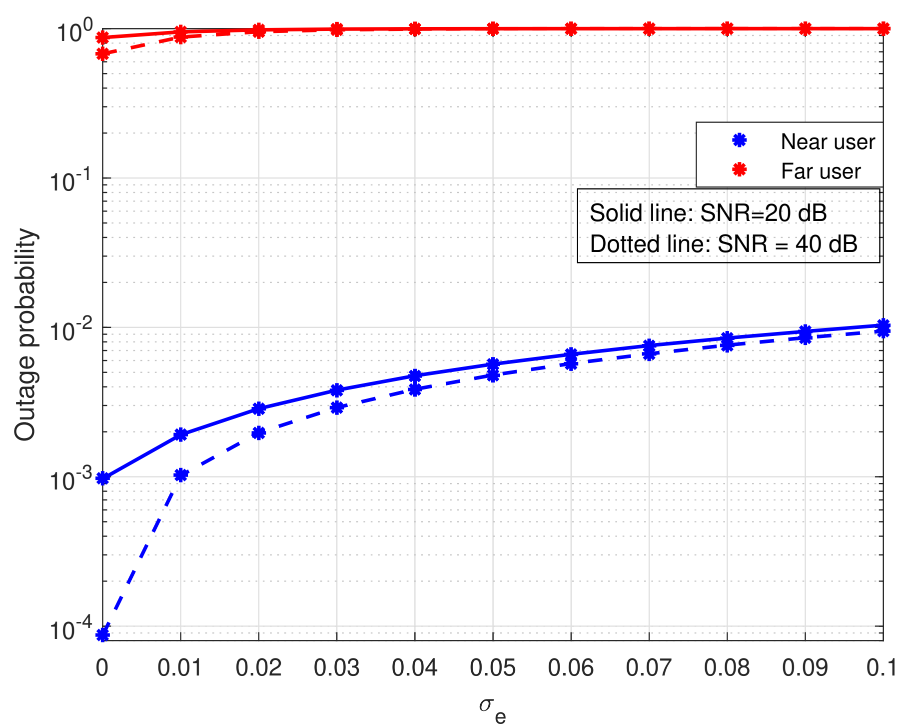

Figure 2.19: OP of the uplink NOMA w.r.t ipCSI with $k = 0.175$.

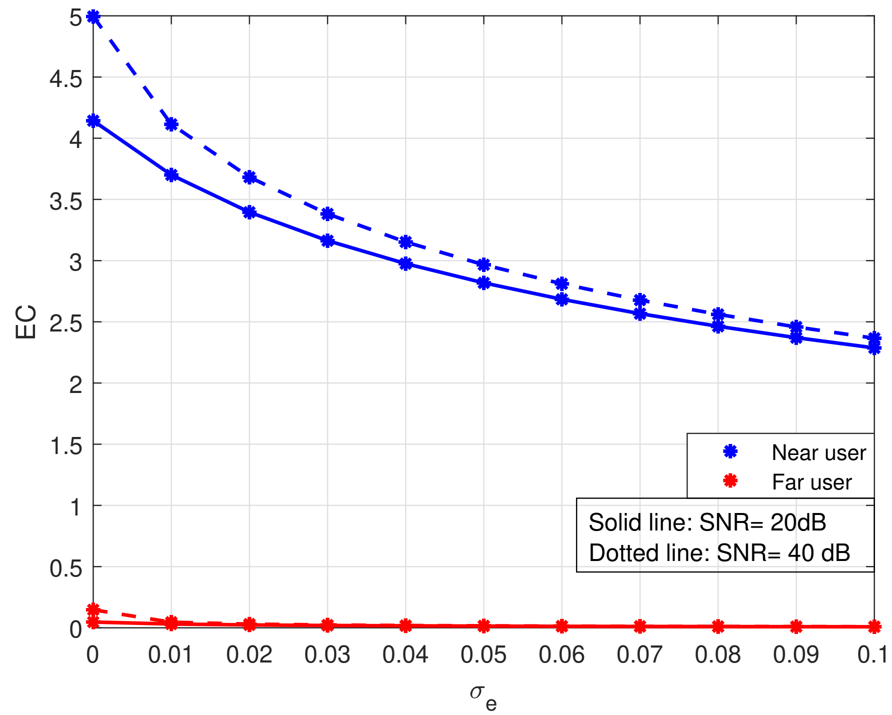

Figure 2.20: EC of the uplink NOMA versus ipCSI with $k = 0.175$.

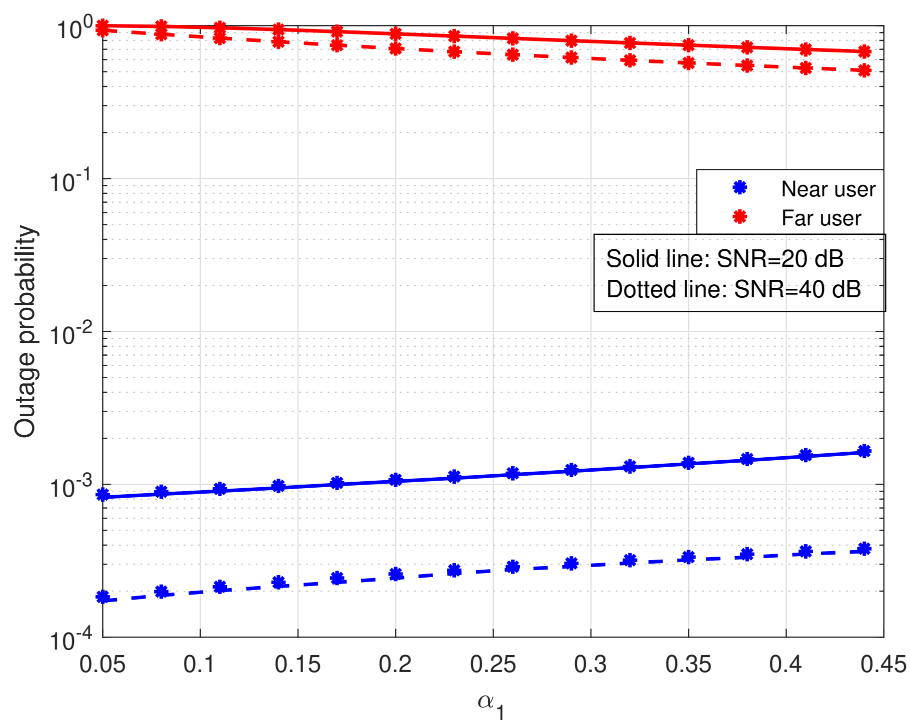

Figure 2.21: OP of the uplink NOMA w.r.t Power allocation with $k = 0.175$ and $\sigma_e^2 = 0.001$.

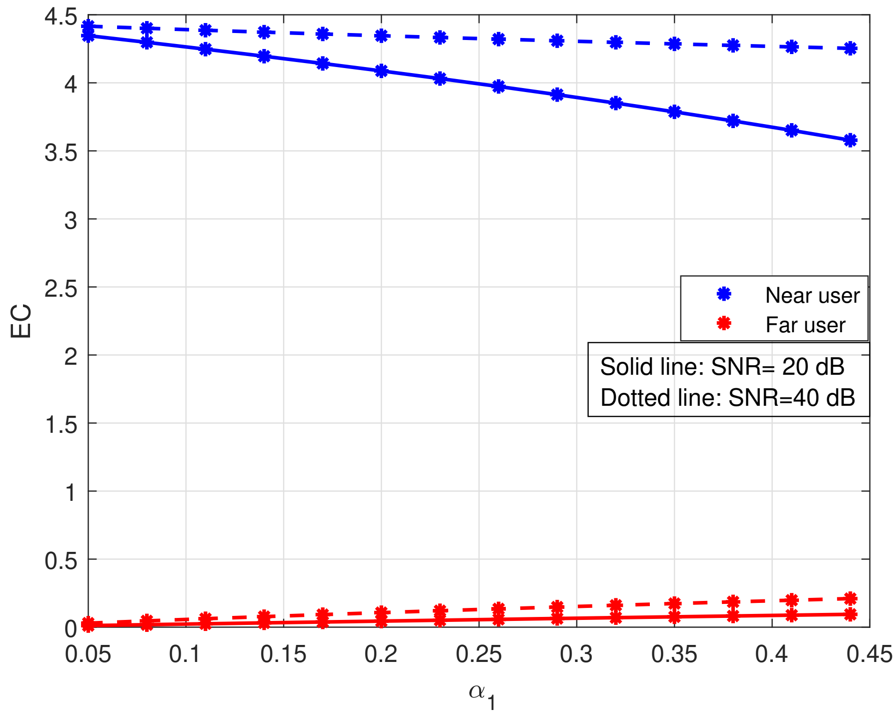

Figure 2.22: EC of the uplink NOMA versus Power allocation with $k = 0.175$ and $\sigma_e^2 = 0.001$.

The effect of the power allocation (α_2) on the NOMA system is presented in Figs. 2.12, 2.13, and 2.14 with different SNRs. By increasing PA α_2, we can observe that U_1's performance deteriorates while U_2's performance improves.

To evaluate the performance of the uplink NOMA system considering HWI and ipCSI, we consider $\sigma_e^2 = 0.001$ and $k = 0.175$, as defined in the downlink scenario. The power allocation is set as $\alpha_1 = 0.2$ and $\alpha_2 = 0.8$.

Figs. 2.15 and 2.16 illustrate the results, demonstrating a perfect match between the simulation results and theoretical curves. The ideal case outperforms the impaired case in terms of performance. Furthermore, in the uplink NOMA system, the near user exhibits superior performance compared to the far user. This can be attributed to PA attributed to the near user. Notably, the presence of HWI and ipCSI at high SNR levels leads to the emergence of an error floor.

Figs. 2.17 and 2.18 depict the impact of HWI on the performance of the uplink NOMA with different levels of SNR. It can be shown that as the HWI factor increases the OP and decreases the EC. However, increasing the SNR improves the performance of the users. Figs. 2.19 and 2.20 illustrate the influence of the ipCSI on the uplink NOMA system, considering different levels of SNR. The results indicate a decrease in both the OP and EC performance for both users as the ipCSI increases. This observation highlights the significance of accurate channel estimation for the NOMA system. However, it is worth noting that the system performance can still improve with higher SNR levels, even when imperfections are present.

Figs 2.21 and 2.22 evaluate the effect of the PA on the uplink NOMA. We can notice that the PA has a different effect on the users' performance, augmenting the PA enhances the performance of U_1, but degrades the performance of U_2.

2.8 Conclusion

This chapter investigates the performance of a downlink and uplink NOMA network while considering practical system constraints, including HWI and ipCSI. We derived an exact closed-form expression for the OP, EC, and BER for the downlink NOMA and OP, EC performance for the uplink NOMA. Our results indicate that the impact of HWI on user performance varies due to its influence on the SIC process. Additionally, the performance of the system is significantly influenced by the channel estimation errors. Furthermore, the joint effect of these imperfections leads to significant deterioration in the NOMA networks.

Chapter 3

Effect of the IQI on the downlink and uplink NOMA system

3.1 Introduction

The emergence of Non-Orthogonal Multiple Access (NOMA) has heralded a highly promising breakthrough in the domain of wireless communication systems. This innovative technique holds the potential to not only meet but excel in addressing the rigorous demands posed by 5G networks. It brings to the table extensive connectivity, low latency, and exceptional spectral efficiency, all of which are paramount in the contemporary landscape of wireless communication.

In practical communication scenarios, monolithic architectures face challenges stemming from RF frontend imperfections, driven by component mismatches and manufacturing non-idealities. These imperfections, particularly in-phase (I) and quadrature-phase (Q) imbalance (IQI), result in amplitude and phase discrepancies between the I and Q branches of the transceiver. IQI, responsible for imperfect image rejection, severely hampers the overall system's performance. While, in an ideal scenario, mixers exhibit perfectly balanced I and Q branches with a 90 phase shift, achieving flawless image band attenuation. In a realistic scenario, the direct-conversion transceivers are susceptible to analog front-end impairments. These impairments introduce errors in phase shifts and amplitude mismatches between I and Q branches, leading to corruption of the down-converted signal constellation and a subsequent increase in the error rate

3.2 Related works

Driven by this practical consideration, recent studies have sought to either create models for, reduce the impact of, or even take advantage of IQI. The authors referenced in [65] formulate the Signal-to-Interference-plus-Noise Ratio (SINR), considering the correlation between subcarriers within the framework of Orthogonal Frequency Division Multiplexing (OFDM) systems. The authors in [66] have developed a precise analytical estimate for the average subcarrier SINR in beamforming OFDM systems, taking into account the presence of joint transmit-receive IQI This derived equation sheds new light on how various system parameters impact overall system performance. The authors of [67] conduct an extensive investigation into the impacts of IQI, to accentuate their significant manifestations. These effects, contingent upon the specific scenario, can lead to both detrimental and, on occasion, advantageous outcomes. The impact of joint IQI and PHN on beamforming OFDM direct-conversion transceivers is examined in [68], where an exact normalized mean squared error expression and several special and asymptotic cases to gain insights are also analyzed. The presence of IQI imbalance in the performance of amplify and forward relaying (AF) in the OFDM system is investigated in [69], where the analytical approximation of Outage Probability (OP) and Error Vector Magnitude is derived. In the context of the NOMA, the effect of the RF impairment in the NOMA system was investigated [70]. To evaluate the system performance, the closed form of conditional Pairwise Error Probability is derived for two users in the downlink NOMA system [71]. The outage probability of IQI impairment NOMA at the radio frequency front end in the Nakagami-m fading channel is evaluated in [6, 72, 73]. However, the security performance of multi-antenna is presented in [74]. Furthermore, [75] investigated the impact of IQI imperfection on the security of the ambient backscatter (AmBC) NOMA system, where outage probability in the presence of an eavesdropper is derived for two NOMA users. Nevertheless, the authors of [76, 77, 78] devoted their works to the NOMA performance in terms of OP for each cooperative, cognitive radio, and vehicle-to-vehicle system.

3.3 Motivations and Contributions

Inspired by this motivation, the current study is focused on quantifying and examining the impacts of IQI on downlink and uplink direct NOMA systems. The primary objective of this article is to establish a comprehensive framework for analyzing both downlink and uplink NOMA systems in various IQI scenarios. This framework addresses cases involving: Transmit (TX) IQI, Receive (RX) IQI, and the combined TX/RX IQI. Specifically, we derive the

SINR for uplink and downlink NOMA systems operating in the presence of TX and/or RX IQI.

This chapter is dedicated to a thorough analysis of the OP and Ergodic Capacity (EC) performance of both the downlink and uplink NOMA systems when confronted with the presence of IQI. The investigation takes place over the Rayleigh fading channel and assumes a scenario of direct transmission between the source and the users. Through this exploration, we aim to gain a comprehensive understanding of how IQI impacts the performance of NOMA in practical communication scenarios, shedding light on potential strategies for mitigating its effects and maximizing the benefits of this transformative technology.

3.4 System Model of downlink NOMA with IQI

We consider a downlink NOMA system, specifically a direct transmission scenario. The system comprises three elements: a Source (S), a far user (U_1), and a near user (U_2). To simplify the analysis, we assume that all nodes operate in half duplex (HD) mode and that the communication links are over the Rayleigh fading. All nodes are equipped with a single antenna, as illustrated in Fig. 3.1. In the downlink NOMA scenario, the power allocation

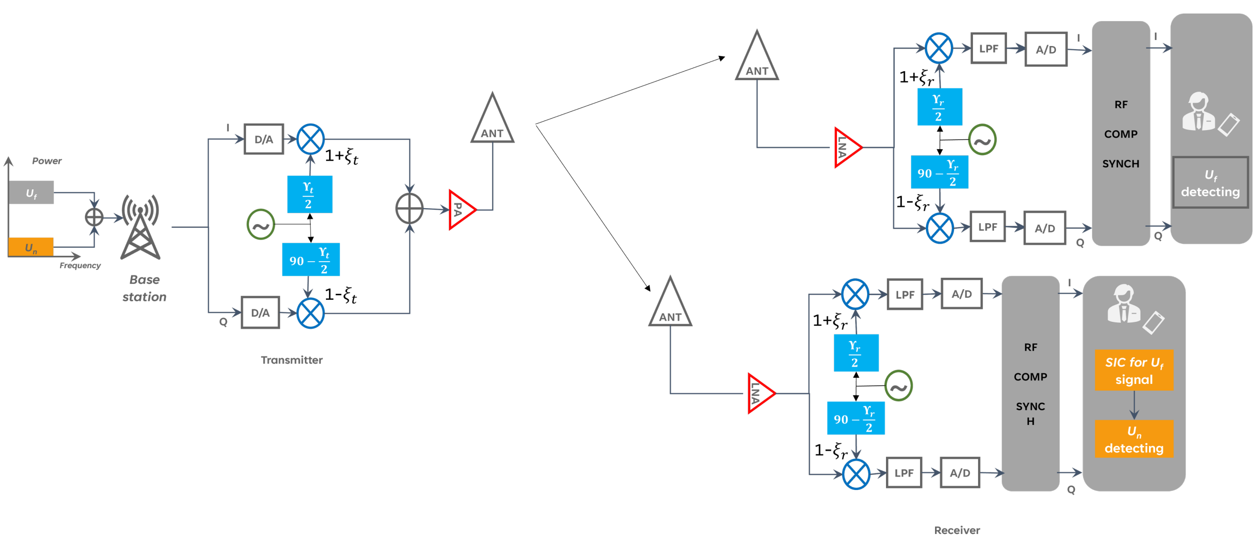

Figure 3.1: System model of the downlink NOMA under IQI.

(PA) assigned to each user is determined based on the channel gain between S and the respective users. As a result, a higher PA is specifically designated for the U_1 in comparison to the U_2. The complex flat fading channel coefficient of the S-U_1 and S-U_2 are defined respectively as: h_i where $i = 1, 2$. Assuming an ideal RF front end, the receiver signal at the user i can be given as:

$$y = h_i(\sqrt{\alpha_1 P}x_1 + \sqrt{\alpha_2 P}x_2) + n, \tag{3.1}$$

where P is the total transmission power, α_i is the power factor allocated to the user i and x_i is the information signal from AP to the user i, $n \sim \mathcal{CN}(0, N_o)$ is the additive white Gaussian noise (AWGN). Additionally, we assume that the RF carriers are converted to the baseband using direct conversion architectures. Consequently, the resulting baseband representation of the signal is impacted by IQI and can be expressed as [48]:

$$y_{IQI} = \mu_{t/r}S + \nu_{t/r}S^*, \tag{3.2}$$

where S is the transmitted signal and $\mu_{t/r}$, $\nu_{t/r}$ are the IQI coefficient presented as in [30]:

$$\begin{aligned} \mu_t &= \frac{1}{2}(1 + \xi_t \exp(j\Upsilon_t)), \\ \nu_t &= \frac{1}{2}(1 - \xi_t \exp(-j\Upsilon_t)), \\ \mu_r &= \frac{1}{2}(1 + \xi_r \exp(-j\Upsilon_r)), \\ \nu_r &= \frac{1}{2}(1 - \xi_r \exp(j\Upsilon_r)), \end{aligned} \tag{3.3}$$

where $j = \sqrt{-1}$ and $\xi_{t/r}$ and $\Upsilon_{t/r}$ are the amplitude and phase of TX and RX respectively. Furthermore, the image rejection ratio (IRR) at the transmitter (TX) and receiver (RX) can be described as:

$$IRR_{t/r} = \frac{|\mu_{t/r}|^2}{|\nu_{t/r}|^2}. \tag{3.4}$$

In the following sections, we present the signal model for NOMA systems, considering the presence of IQI at the transmitter (TX) and/or receiver (RX).

1)NOMA TX impaired IQI

In this scenario, we consider the RF front end of the RX to be ideal, while TX is affected by

IQI. Under this assumption, we can formulate the received signal as:

$$y_{IQI,i}^{TX} = \mu_t h_i \left(\sqrt{\alpha_1 P} x_1 + \sqrt{\alpha_2 P} x_2\right) + \nu_t h_i^* \left(\sqrt{\alpha_1 P} x_1 + \sqrt{\alpha_2 P} x_2\right)^* + n. \tag{3.5}$$

Assuming a perfect CSI, the received signal-to-interference-plus-noise ratio (SINR) of the U_1 is presented as:

$$\gamma_1^{TX} = \frac{\mu_t^2 |h_1|^2 P \alpha_1}{\mu_t^2 |h_1|^2 P \alpha_2 + \nu_t^2 |h_1|^2 P + N_0}. \tag{3.6}$$

The SINR of U_2 for decoding a U_1 signal is defined as:

$$\gamma_{2\to1}^{TX} = \frac{\mu_t^2 |h_2|^2 P \alpha_1}{\mu_t^2 |h_2|^2 P \alpha_2 + \nu_t^2 |h_2|^2 P + N_0}. \tag{3.7}$$

The SINR for U_2 can be obtained as:

$$\gamma_2^{TX} = \frac{\mu_t^2 |h_2|^2 P \alpha_2}{\nu_t^2 |h_2|^2 P + N_0}. \tag{3.8}$$

2)NOMA RX impaired IQI

In this case, we consider the RF front-end of the TX to be ideal, while the receiver RX is impacted by IQI. Consequently, we can express the receiver signal as:

$$y_{IQI,i}^{RX} = \mu_r h_i \left(\sqrt{\alpha_1 P} x_1 + \sqrt{\alpha_2 P} x_2\right) + \nu_r h_i^* \left(\sqrt{\alpha_1 P} x_1 + \sqrt{\alpha_2 P} x_2\right)^* + \left(\mu_r + \nu_r\right) n. \tag{3.9}$$

Similar to the TX-impaired IQI, the received SINR of the U_1 is obtained as:

$$\gamma_1^{RX} = \frac{\mu_r^2 |h_1|^2 P \alpha_1}{\mu_r^2 |h_1|^2 P \alpha_2 + \nu_r^2 |h_1|^2 P + (\mu_r^2 + \mu_r^2) N_0}. \tag{3.10}$$

The SINR of U_2 for coding a U_1 can be expressed as:

$$\gamma_{2\to1}^{RX} = \frac{\mu_r^2 |h_2|^2 P \alpha_1}{\mu_r^2 |h_2|^2 P \alpha_2 + \nu_r^2 |h_2|^2 P + (\mu_r^2 + \nu_r^2) N_0}. \tag{3.11}$$

The SINR for U_2 can be obtained as:

$$\gamma_2^{RX} = \frac{\mu_r^2|h_2|^2 P\alpha_1}{\nu_r^2|h_2|^2 P + (\mu_r^2 + \nu_r^2)N_0}. \tag{3.12}$$

3) NOMA joint TX and RX impaired by IQI

In this case, both the TX and RX components are affected by the impact of IQI. Consequently, the received signal can be given as:

$$\begin{aligned} y_{IQI,i}^{TX/RX} =& \mu_r(\mu_t h_i(\sqrt{\alpha_1 P}x_1 + \sqrt{\alpha_2 P}x_2) + \nu_t h_i^*(\sqrt{\alpha_1 P}x_1 + \sqrt{\alpha_2 P}x_2)^* + n) + \\ & \nu_r(\mu_t h_i(\sqrt{\alpha_1 P}x_1 + \sqrt{\alpha_2 P}x_2) + \nu_t h_i^*(\sqrt{\alpha_1 P}x_1 + \sqrt{\alpha_2 P}x_2)^* + n)^*. \end{aligned} \tag{3.13}$$

The SINR of the $U1$, considering the impairment of both the TX and RX, can be represented as:

$$\gamma_1^{TX/RX} = \frac{(\mu_r^2\mu_t^2 + \nu_r^2\nu_t^2)|h_1|^2 P\alpha_1}{(\mu_r^2\mu_t^2 + \nu_r^2\nu_t^2)|h_1|^2 P\alpha_2 + (\mu_r^2\nu_t^2 + \mu_t^2\nu_r^2)|h_1|^2 P + (\mu_r^2 + \nu_r^2)N_0}. \tag{3.14}$$

The SINR of the U_1 at U_2 in the presence of IQI can be expressed as:

$$\gamma_{2\to 1}^{TX/RX} = \frac{(\mu_r^2\mu_t^2 + \nu_r^2\nu_t^2)|h_2|^2 P\alpha_1}{(\mu_r^2\mu_t^2 + \nu_r^2\nu_t^2)|h_2|^2 P\alpha_2 + (\mu_r^2\nu_t^2 + \mu_t^2\nu_r^2)|h_2|^2 P + (\mu_r^2 + \nu_r^2)N_0}. \tag{3.15}$$

Assuming a perfect SIC, the SINR of the U_2 is obtained as:

$$\gamma_2^{TX/RX} = \frac{(\mu_r^2\mu_t^2 + \nu_r^2\nu_t^2)|h_2|^2 P\alpha_1}{(\mu_r^2\nu_t^2 + \mu_t^2\nu_r^2)|h_2|^2 P + (\mu_r^2 + \nu_r^2)N_0}. \tag{3.16}$$

3.5 Perfromance Analysis of the downlink NOMA with IQI

3.5.1 Outage probability

The OP is the probability that the symbol error rate exceeds a predefined threshold [71]. In this section, we derive the analytical expression of OP for the downlink NOMA system in the presence of IQI for two users.

1) NOMA TX impaired IQI

In the context of a downlink NOMA system, we take into account the impact of IQI on TX, the OP of U_1 can be represented as:

$$\begin{aligned} P_{out,1}^{TX} &= Pr(\gamma_1^{TX} \leq \gamma_{th,1}) \\ &= Pr\left(|\tilde{h}_1|^2 \leq \frac{\gamma_{th,1} N_o}{(\mu_t^2\alpha_1 - \gamma_{th,1}\mu_t^2\alpha_2 - \gamma_{th,1}\nu_t^2)P}\right), \end{aligned} \tag{3.17}$$

where $\gamma_{th,1}$ is the threshold at the U_1.
We can alternatively express the OP using the cumulative distribution function as in [60]:.

$$P_{out} = F_{\gamma_i}(\gamma). \tag{3.18}$$

Based on the PDF and CDF of channel power gain given in (2.8) and (2.9), respectively. The OP of the U_1 can be expressed as:

$$P_{out,1}^{TX} = 1 - \exp\left(-\frac{1}{\phi_1}\frac{\gamma_{th,1} N_o}{(\mu_t^2\alpha_1 - \gamma_{th,1}\mu_t^2\alpha_2 - \gamma_{th,1}\nu_t^2)P}\right), \tag{3.19}$$

where $\phi_i = E(h_i)$ is the channel mean power. In the case of the U_2, the outage occurs when the transmitted signal from the S to U_2 cannot be successfully decoded. Thus, the OP for the U_2 can be expressed as [60]:

$$P_{out,2}^{TX} = F_{\gamma_{2\to1}^{TX}}(\gamma) + [1 - F_{\gamma_{2\to1}^{TX}}]F_{\gamma_2^{TX}}(\gamma), \tag{3.20}$$

where the $F_{\gamma_{2\to1}^{TX}}$ and $F_{\gamma_2^{TX}}$ can be given respectively as:

$$F_{\gamma_{2\to1}^{TX}}(\gamma) = 1 - \exp\left(-\frac{1}{\phi_2}\frac{\gamma_{th,2} N_o}{(\mu_t^2\alpha_1 - \gamma_{th,2}\mu_t^2\alpha_2 - \gamma_{th,2}\nu_t^2)P}\right), \tag{3.21}$$

$$F_{\gamma_2^{TX}}(\gamma) = 1 - \exp\left(-\frac{1}{\phi_2}\frac{\gamma_{th,2}N_o}{(\mu_t^2\alpha_2 - \gamma_{th,2}\nu_t^2)P}\right). \tag{3.22}$$

By substituting (3.21) and (3.22) in (3.20), we get the OP of the U_2 as:

$$P_{out,2}^{TX} = 1 - \exp\left(-\frac{1}{\phi_2}\frac{\gamma_{th,2}N_o}{(\mu_t^2\alpha_1 - \gamma_{th,1}\mu_t^2\alpha_2 - \gamma_{th,1}\nu_t^2)P}\right)\exp\left(-\frac{1}{\phi_2}\frac{\gamma_{th,1}N_o}{(\mu_t^2\alpha_1 - \gamma_{th,1}\mu_t^2\alpha_2 - \gamma_{th,1}\nu_t^2)P}\right). \tag{3.23}$$

2) NOMA RX impaired by IQI

Similar to the OP of the NOMA TX impaired by IQI, the OP of the U_1 when the TX is ideal and the RX is impaired can be defined respectively as:

$$P_{out,1}^{RX} = 1 - \exp\left(-\frac{1}{\phi_1}\frac{(\mu_r^2 + \nu_r^2)\gamma_{th,1}N_o}{(\mu_r^2\alpha_1 - \gamma_{th,1}\mu_r^2\alpha_2 - \gamma_{th,1}\nu_r^2)P}\right). \tag{3.24}$$

Furthermore, we can represent the OP of U_2 as:

$$P_{out,2}^{RX} = 1 - \exp\left(-\frac{1}{\phi_2}\frac{(\mu_r^2 + \nu_r^2)\gamma_{th,2}N_o}{(\mu_r^2\alpha_1 - \gamma_{th,2}\mu_r^2\alpha_2 - \gamma_{th,2}\nu_r^2)P}\right)\exp\left(-\frac{1}{\phi_2}\frac{(\mu_r^2 + \nu_r^2)\gamma_{th,2}N_o}{(\mu_r^2\alpha_2 - \gamma_{th,2}\nu_r^2)P}\right). \tag{3.25}$$

3) NOMA joint TX and RX impaired by IQI

The OP of the U_1 and U_2 for the case that both the TX and RX are impaired care given respectively as:

$$P_{out,1}^{TX/RX} = 1 - \exp\left(-\frac{1}{\phi_1}\frac{(\mu_r^2 + \nu_r^2)\gamma_{th,1}N_o}{(\epsilon_1\alpha_1 - \gamma_{th,1}\epsilon_1\alpha_2 - \gamma_{th,1}\epsilon_2)P}\right), \tag{3.26}$$

$$P_{out,2}^{TX/RX} = 1 - \exp\left(-\frac{1}{\phi_2}\frac{(\mu_r^2 + \nu_r^2)\gamma_{th,2}N_o}{(\epsilon_1\alpha_1 - \gamma_{th,2}\epsilon_1\alpha_2 - \gamma_{th,2}\epsilon_1)P}\right)\exp\left(-\frac{1}{\phi_2}\frac{(\mu_r^2 + \nu_r^2)\gamma_{th,2}N_o}{(\epsilon_1\alpha_2 - \gamma_{th,2}\epsilon_1)P}\right), \tag{3.27}$$

where $\epsilon_1 = (\mu_t^2\mu_r^2 + \nu_t^2\nu_r^2)$ and $\epsilon_2 = (\mu_r^2\nu_t^2 + \nu_t^2\nu_r^2)$.

3.5.2 Ergodic Capacity of the downlink NOMA with IQI

In this subsection, we derive the EC performance of the downlink NOMA in the presence of the IQI for different scenarios: TX, RX, and both the TX and RX impaired.

1) NOMA TX impaired IQI

The Shannon capacity of signals x_1 and x_2 should be considered based on both the $S-U_1$ and $S-U_2$ links, respectively. As a result, the Shannon capacity of U_1 and U_2 is given by the following expressions, respectively

$$C_1^{TX} = \frac{1}{2} log_2 \left(1+\gamma_1^{TX}\right), \tag{3.28}$$

$$C_2^{TX} = \frac{1}{2} log_2 \left(1+\gamma_2^{TX}\right). \tag{3.29}$$

By averaging The achievable rates over instantaneous channel coefficients in (3.28) and (3.29), we obtain

$$C_1^{TX} = \int_0^\infty log_2(1+\gamma_1^{TX}) p_{\delta_1}(\delta_1) d_{\delta_1}, \tag{3.30}$$

$$C_2^{TX} = \int_0^\infty log_2(1+\gamma_2^{TX}) p_{\delta_2}(\delta_2) d_{\delta_2}, \tag{3.31}$$

where $\delta_i|\tilde{h_i}|^2$ and $p_{\delta_i}(\delta_i)$ is the PDF of δ_i.
Remembering that $\int_0^\infty = log_2(1+x)f_x(x)dx = \frac{1}{ln2}\int_0^\infty \frac{1-F_X(x)}{1+x}dx$, where $F_X(.)$ is are the CDFs of X.
Therefore, the EC of the U_1 and U_2 when the TX is impaired is given, respectively as:

$$C_1^{TX} = \frac{1}{ln2}\int_0^{\frac{\mu_t^2\alpha_1}{\mu_t^2\alpha_2+\nu_t^2}} \frac{\exp\left(-\frac{1}{\phi_1}\frac{xN_o}{(\mu_t^2\alpha_1 - x\mu_t^2\alpha_2 - x\nu_t^2)P}\right)}{1+x}dx, \tag{3.32}$$

$$C_2^{TX} = \frac{1}{ln2}\int_0^{\frac{\mu_t^2\alpha_2}{\nu_t^2}} \frac{\exp\left(-\frac{1}{\phi_2}\frac{xN_o}{(\mu_t^2\alpha_2 - x\nu_t^2)P}\right)}{1+x}dx, \tag{3.33}$$

As far as the author's knowledge extends, there is currently no known analytical solution available for equations (3.32) and (3.33). Nevertheless, these equations can be efficiently computed using various software tools such as MATLAB, MATHEMATICA.

2) NOMA RX impaired IQI

Similar to TX impaired, the EC of the U_1 and U_2 in the presence of IQI using some algebraic manipulation can be obtained, respectively as:

$$C_1^{RX} = \frac{1}{ln2}\int_0^{\frac{\mu_r^2\alpha_1}{\mu_r^2\alpha_2+\nu_r^2}} \frac{\exp\left(-\frac{1}{\phi_1}\frac{(\mu_r^2+\nu_r^2)xN_o}{(\mu_r^2\alpha_1-x\mu_r^2\alpha_2-x\nu_r^2)P}\right)}{1+x}dx, \tag{3.34}$$

$$C_2^{RX} = \frac{1}{ln2}\int_0^{\frac{\mu_r^2\alpha_2}{\nu_r^2}} \frac{\exp\left(-\frac{1}{\phi_2}\frac{(\mu_r^2+\nu_r^2)xN_o}{(\mu_r^2\alpha_2-x\nu_r^2)P}\right)}{1+x}dx. \tag{3.35}$$

3) NOMA joint TX and RX impaired IQI

By employing algebraic manipulation, the EC of U_1 and U_2 when both the TX and RX are impaired can be presented as

$$C_1^{TX/RX} = \frac{1}{ln2}\int_0^{\frac{\epsilon_1\alpha_1}{\epsilon_1\alpha_2+\epsilon_2)}} \frac{\exp\left(-\frac{1}{\phi_1}\frac{(\mu_r^2+\nu_r^2)\gamma_{th,1}N_o}{(\epsilon_1\alpha_1-\gamma_{th,1}\epsilon_1\alpha_2-\gamma_{th,1}\epsilon_2)P}\right)}{1+x}dx, \tag{3.36}$$

$$C_2^{TX/RX} = \frac{1}{ln2}\int_0^{\frac{(\epsilon_1\alpha_2}{\epsilon_1)}} \frac{\exp\left(-\frac{1}{\phi_1}\frac{(\mu_r^2+\nu_r^2)\gamma_{th,2}N_o}{(\epsilon_1\alpha_2-\gamma_{th,2}\epsilon_2)P}\right)}{1+x}dx. \tag{3.37}$$

3.6 System model of the uplink NOMA with IQI

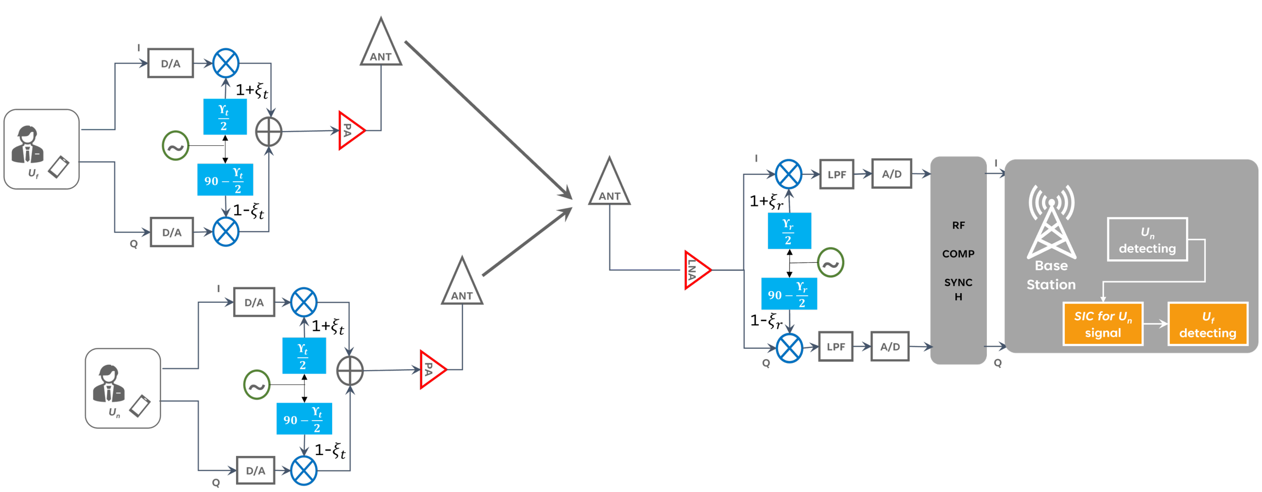

Figure 3.2: System model of the uplink NOMA under IQI.

Instead of the downlink direct NOMA, the uplink NOMA allows multiple transmitters to transmit their signals to an access point using the same time and frequency resources. The key feature of uplink NOMA is the power allocation strategy, where the signal from the near user transmitter is assigned a higher power level compared to the signal from the far user transmitter. We consider that the system model consists of an access point (AP), far user (U_1), and near user (U_2) as depicted in Fig. 3.2. We assume that all nodes are equipped with a single antenna and are impaired by IQI.

1) NOMA TX impaired IQI

The received signal of the uplink NOMA when the TX is impaired can be presented as:

$$y_{IQI}^{TX} = u_t \left(h_1 \sqrt{\alpha_1 P} x_1 + h_2 \sqrt{\alpha_2 P} x_2 \right) + v_t \left(h_1 \sqrt{\alpha_1 P} x_1 + h_2 \sqrt{\alpha_2 P} x_2 \right)^* + n. \tag{3.38}$$

The SINR of the U_2 assuming a perfect CSI can be expressed as

$$\gamma_2^{TX} = \frac{\mu_t^2 |h_2|^2 P \alpha_2}{\mu_t^2 |h_1|^2 P \alpha_1 + \nu_t^2 |h_1|^2 P \alpha_1 + \nu_t^2 |h_2|^2 P \alpha_2 + N_0}. \tag{3.39}$$

According to the uplink NOMA protocol, U_1 will perform the SIC process to cancel the interference from the U_2. Hence, assuming a perfect SIC and CSI, the SINR of the U_1 is given as:

$$\gamma_1^{TX} = \frac{\mu_t^2 |h_1|^2 P \alpha_1}{\nu_t^2 |h_1|^2 P \alpha_1 + N_0}. \tag{3.40}$$

2) NOMA RX impaired IQI

The received signal of the uplink NOMA when the TX is ideal and RX is impaired can be obtained as:

$$y_{IQI}^{RX} = u_r \left(h_1 \sqrt{\alpha_1 P} x_1 + h_2 \sqrt{\alpha_2 P} x_2 \right) + v_r \left(h_1 \sqrt{\alpha_1 P} x_1 + h_2 \sqrt{\alpha_2 P} x_2 \right)^* + u_r n + v_r n^*. \tag{3.41}$$

The SINR of the U_2 and U_1 can be presented, respectively as:

$$\gamma_2^{RX} = \frac{\mu_r^2 |h_2|^2 P \alpha_2}{\mu_r^2 |h_1|^2 P \alpha_1 + \nu_r^2 |h_1|^2 P \alpha_1 + \nu_r^2 |h_2|^2 P \alpha_2 + (\mu_r^2 + \nu_r^2) N_0}, \tag{3.42}$$

$$\gamma_1^{RX} = \frac{\mu_r^2|h_1|^2 P\alpha_1}{\nu_r^2|h_1|^2 P\alpha_1 + (\mu_r^2 + \nu_r^2)N_0}. \tag{3.43}$$

3) NOMA joint TX and RX impaired IQI

The received signal for the uplink NOMA when both TX and RX are impaired can be defined as:

$$\begin{aligned} y_{IQI}^{TX/RX} &= u_r\left(u_t\left(h_1\sqrt{\alpha_1 P}x_1 + h_2\sqrt{\alpha_2 P}x_2\right) + v_t\left(h_1\sqrt{\alpha_1 P}x_1 + h_2\sqrt{\alpha_2 P}x_2\right)^* + n\right) \\ &+ v_r\left(u_t\left(h_1\sqrt{\alpha_1 P}x_1 + h_2\sqrt{\alpha_2 P}x_2\right) + v_t\left(h_1\sqrt{\alpha_1 P}x_1 + h_2\sqrt{\alpha_2 P}x_2\right)^* + n\right)^*. \end{aligned} \tag{3.44}$$

The SINR of the U_2 and U_2 while both the TX and RX are impaired can be given as:

$$\gamma_2^{TX/RX} = \frac{\epsilon_1|h_2|^2 P\alpha_2}{\epsilon_1|h_1|^2 P\alpha_1 + \epsilon_2|h_1|^2 P\alpha_1 + \epsilon_2|h_2|^2 P\alpha_2 + (\mu_r^2 + \nu_r^2)N_0}, \tag{3.45}$$

$$\gamma_1^{TX/RX} = \frac{\epsilon_1|h_1|^2 P\alpha_1}{\epsilon_2|h_1|^2 P\alpha_1 + (\mu_r^2 + \nu_r^2)N_0}. \tag{3.46}$$

3.7 Performance Analysis of the uplink NOMA with IQI

3.7.1 Outage probability

In this subsection, the OP of the uplink NOMA in the presence of different scenarios IQI over the Rayleigh fading channel for the two users.

1) NOMA TX impaired IQI

The OP of the U_2 and U_1 when the TX is impaired can be given, respectively as:

$$
\begin{aligned}
P_{out,2}^{TX} &= \left(|h_2|^2 \leq \frac{\gamma_{th,2}\Big((\mu_t^2+\nu_t^2)\alpha_1|h_1|^2 P + N_o\Big)}{(\mu_t^2+\nu_t^2)\alpha_2|h_1|^2 P} \right) \\
&= 1-\exp\left(-\frac{\gamma_{th,2}N_o}{P\left(\mu_t^2\alpha_2-\gamma_{th,2}\nu_t^2\alpha_2\right)\phi_2}\right)\frac{P\left(\mu_t^2\alpha_2-\gamma_{th,2}\nu_t^2\alpha_2\right)\phi_2}{\gamma_{th,2}(\mu_t^2+\nu_t^2)\alpha_1 P\phi_1 + P\left(\mu_t^2\alpha_2-\gamma_{th,2}\nu_t^2\alpha_2\right)\phi_2},
\end{aligned} \tag{3.47}
$$

$$
\begin{aligned}
P_{out,1}^{TX} &= \left(|h_1|^2 \leq \frac{\gamma_{th,1}N_o}{(\mu_t^2+\nu_t^2)\alpha_1|h_1|^2 P} \right) \\
&= 1-\exp\left(-\frac{\gamma_{th,1}N_o}{P\left(\mu_t^2\alpha_1-\gamma_{th,1}\nu_t^2\alpha_1\right)\phi_1}\right),
\end{aligned} \tag{3.48}
$$

the outage of x_2 occurs if one of the two events occurs: If U_1 fails to detect x_2 and if x_2 is successfully detected and fails to detect x_1. By using PDF and CDF. the OP of x_1 at U_1 can be determined as:

$$
\begin{aligned}
P_{out,1}^{TX} =& 1-\exp\left(-\frac{\gamma_{th,2}N_o}{P\left(\mu_t^2\alpha_2-\gamma_{th,2}\nu_t^2\alpha_2\right)\phi_2}\right)\frac{P\left(\mu_t^2\alpha_2-\gamma_{th,2}\nu_t^2\alpha_2\right)\phi_2}{\gamma_{th,2}(\mu_t^2+\nu_t^2)\alpha_1 P\phi_1 + P\left(\mu_t^2\alpha_2-\gamma_{th,2}\nu_t^2\alpha_2\right)\phi_2} \\
&\times \exp\left(-\frac{\gamma_{th,1}N_o}{P\left(\mu_t^2\alpha_1-\gamma_{th,1}\nu_t^2\alpha_1\right)\phi_1}\right).
\end{aligned} \tag{3.49}
$$

2) NOMA RX impaired IQI

Assuming an ideal TX, the OP of the U_2 and U_1 while the RX is impaired can be expressed, respectively as:

$$
\begin{aligned}
&P_{out,2}^{RX} = \\
&1-\exp\left(-\frac{\gamma_{th,2}(\mu_r^2+\nu_r^2)N_o}{P\left(\mu_r^2\alpha_2-\gamma_{th,2}\nu_r^2\alpha_2\right)\phi_2}\right)\frac{P\left(\mu_r^2\alpha_2-\gamma_{th,2}\nu_r^2\alpha_2\right)\phi_2}{\gamma_{th,2}(\mu_r^2+\nu_r^2)\alpha_1 P\phi_1 + P\left(\mu_r^2\alpha_2-\gamma_{th,2}\nu_r^2\alpha_2\right)\phi_2},
\end{aligned} \tag{3.50}
$$

$$
P_{out,1}^{RX} = 1-\exp\left(-\frac{\gamma_{th,1}(\mu_r^2+\nu_r^2)N_o}{P\left(\mu_r^2\alpha_1-\gamma_{th,1}\nu_r^2\alpha_1\right)\phi_1}\right). \tag{3.51}
$$

The OP of x_1 at the U_1 can be defined as:

$$
\begin{aligned}
P_{out,1}^{RX} =& 1-\exp\left(-\frac{\gamma_{th,2}(\mu_r^2+\nu_r^2)N_o}{P\left(\mu_r^2\alpha_2-\gamma_{th,2}\nu_r^2\alpha_2\right)\phi_2}\right)\frac{P\left(\mu_r^2\alpha_2-\gamma_{th,2}\nu_r^2\alpha_2\right)\phi_2}{\gamma_{th,2}(\mu_r^2+\nu_r^2)\alpha_1 P\phi_1 + P\left(\mu_r^2\alpha_2-\gamma_{th,2}\nu_r^2\alpha_2\right)\phi_2} \\
&\times \exp\left(-\frac{\gamma_{th,1}(\mu_r^2+\nu_r^2)N_o}{P\left(\mu_r^2\alpha_1-\gamma_{th,1}\nu_r^2\alpha_1\right)\phi_1}\right).
\end{aligned} \tag{3.52}
$$

3) NOMA joint TX and RX impaired IQI

In the case of the joint TX and RX impaired, similar to the previous derivation. The OP of U_2 and U_1 is obtained, respectively as:

$$P_{out,2}^{TX/RX} = 1 - \exp\left(-\frac{\gamma_{th,2}(\mu_r^2+\nu_r^2)N_o}{P\Big(\epsilon_1\alpha_2-\gamma_{th,2}\epsilon_2\alpha_2\Big)\phi_2}\right)\frac{P\Big(\epsilon_1\alpha_2-\gamma_{th,2}\epsilon_2\alpha_2\Big)\phi_2}{\gamma_{th,2}\Big(\epsilon_1+\epsilon_2\Big)\alpha_1 P\phi_1+P\Big(\epsilon_1\alpha_2-\gamma_{th,2}\epsilon_2\alpha_2\Big)\phi_2}, \tag{3.53}$$

$$P_{out,1}^{TX/RX} = 1 - \exp\left(-\frac{\gamma_{th,1}(\mu_r^2+\nu_r^2)N_o}{P\Big(\epsilon_1\alpha_1-\gamma_{th,1}\epsilon_2\alpha_1\Big)\phi_1}\right). \tag{3.54}$$

The OP of the x_1 at the U_1 can be given as:

$$P_{out,1}^{TX/RX} = 1 - \exp\left(-\frac{\gamma_{th,2}(\mu_r^2+\nu_r^2)N_o}{P\Big(\epsilon_1\alpha_2-\gamma_{th,2}\epsilon_2\alpha_2\Big)\phi_2}\right)\frac{P\Big(\epsilon_1\alpha_2-\gamma_{th,2}\epsilon_2\alpha_2\Big)\phi_2}{\gamma_{th,2}\Big(\epsilon_1+\epsilon_2\Big)\alpha_1 P\phi_1+P\Big(\epsilon_1\alpha_2-\gamma_{th,2}\epsilon_2\alpha_2\Big)\phi_2}$$
$$\times \exp\left(-\frac{\gamma_{th,1}(\mu_r^2+\nu_r^2)N_o}{P\Big(\epsilon_1\alpha_1-\gamma_{th,1}\epsilon_2\alpha_1\Big)\phi_1}\right). \tag{3.55}$$

3.7.2 Ergodic Capacity of the uplink NOMA with IQI

In this subsection, we analyze the uplink NOMA in terms of EC performance considering various scenarios of the IQI.

1) NOMA TX impaired IQI

the Shannon capacity of U_2 and U_1 is presented, respectively as:

$$C_2^{TX} = \frac{1}{2}log_2\left(1+\gamma_2^{TX}\right), \tag{3.56}$$
$$C_1^{TX} = \frac{1}{2}log_2\left(1+\gamma_1^{TX}\right). \tag{3.57}$$

By averaging the achievable rates over instantaneous channel coefficients, we get

$$C_2^{TX} = \int_0^{\infty} log_2(1+\gamma_2^{TX})p_{\delta_2}(\delta_2)d_{\delta_2}, \tag{3.58}$$

$$C_1^{TX} = \int_0^{\infty} log_2(1+\gamma_1^{TX}) p_{\delta_1}(\delta_1) d_{\delta_1}, \tag{3.59}$$

where $p_{\delta_i}(\delta_i)$ is the PDF of δ_i. Similar to the previous derivation. The EC of the U_2 and U_1 when the TX is impaired can be expressed as:

$$C_2^{TX} = \frac{1}{ln2} \int_0^{\frac{\mu_t^2}{\nu_t^2}} \frac{\exp\left(-\frac{xN_o}{P\left(\mu_t^2\alpha_2 - x\nu_t^2\alpha_2\right)\phi_2}\right) \frac{P\left(\mu_t^2\alpha_2 - x\nu_t^2\alpha_2\right)\phi_2}{x(\mu_t^2+\nu_t^2)\alpha_1 P\phi_1 + P\left(\mu_t^2\alpha_2 - x\nu_t^2\alpha_2\right)\phi_2}}{1+x} dx, \tag{3.60}$$

$$C_1^{TX} = \frac{1}{ln2} \int_0^{\frac{\mu_t^2}{\nu_t^2}} \frac{\exp\left(-\frac{xN_o}{P\left(\mu_t^2\alpha_1 - x\nu_t^2\alpha_1\right)\phi_1}\right)}{1+x} dx. \tag{3.61}$$

2) NOMA RX impaired IQI

The EC of U_2 and U_1 when the TX is ideal and RX is impaired can be obtained, respectively as:

$$C_2^{RX} = \frac{1}{ln2} \int_0^{\frac{\mu_r^2}{\nu_r^2}} \frac{\exp\left(-\frac{x(\mu_r^2+\nu_r^2)N_o}{P(\mu_r^2\alpha_2 - x\nu_r^2\alpha_2)\phi_2}\right) \frac{P\left(\mu_r^2\alpha_2 - x\nu_r^2\alpha_2\right)\phi_2}{x(\mu_r^2+\nu_r^2)\alpha_1 P\phi_1 + P(\mu_r^2\alpha_2 - x\nu_r^2\alpha_2)\phi_2}}{1+x} dx, \tag{3.62}$$

$$C_1^{RX} = \frac{1}{ln2} \int_0^{\frac{\mu_r^2}{\nu_r^2}} \frac{\exp\left(-\frac{x(\mu_r^2+\nu_r^2)N_o}{P(\mu_r^2\alpha_1 - x\nu_r^2\alpha_1)\phi_1}\right)}{1+x} dx. \tag{3.63}$$

3) NOMA joint TX and RX impaired IQI

The EC of U_2 and U_1 when both the TX and RX are impaired can be obtained, respectively as:

$$C_2^{TX/RX} = \frac{1}{ln2} \int_0^{\frac{\epsilon_1}{\epsilon_2}} \frac{\exp\left(-\frac{x(\mu_r^2+\nu_r^2)N_o}{P\left(\epsilon_1\alpha_2 - x\epsilon_2\alpha_2\right)\phi_2}\right) \frac{P\left(\epsilon_1\alpha_2 - x\epsilon_2\alpha_2\right)\phi_2}{x\left((\epsilon_1+\epsilon_2\right)\alpha_1 P\phi_1 + P\left(\epsilon_1\alpha_2 - x\epsilon_2\alpha_2\right)\phi_2}}{1+x} dx, \tag{3.64}$$

$$C_1^{TX/RX} = \frac{1}{ln2} \int_0^{\frac{\epsilon_1}{\epsilon_2}} \frac{\exp\left(-\frac{x(\mu_r^2+\nu_r^2)N_o}{P\left(\epsilon_1\alpha_1 - x\epsilon_2\alpha_1\right)\phi_1}\right)}{1+x} dx, \tag{3.65}$$

3.8 Numerical Results

In this section, we present the OP and EC performance for a downlink and uplink NOMA under IQI over the Rayleigh fading channel. The figures present theoretical curves as markers and simulation results as lines. The distance between the users and S is set as $d_1 = 5m$, $d_2 = 1.5m$, In the case of the downlink, the PA is set at $\alpha_1 = 0.8$ and $\alpha_2 = 0.2$.

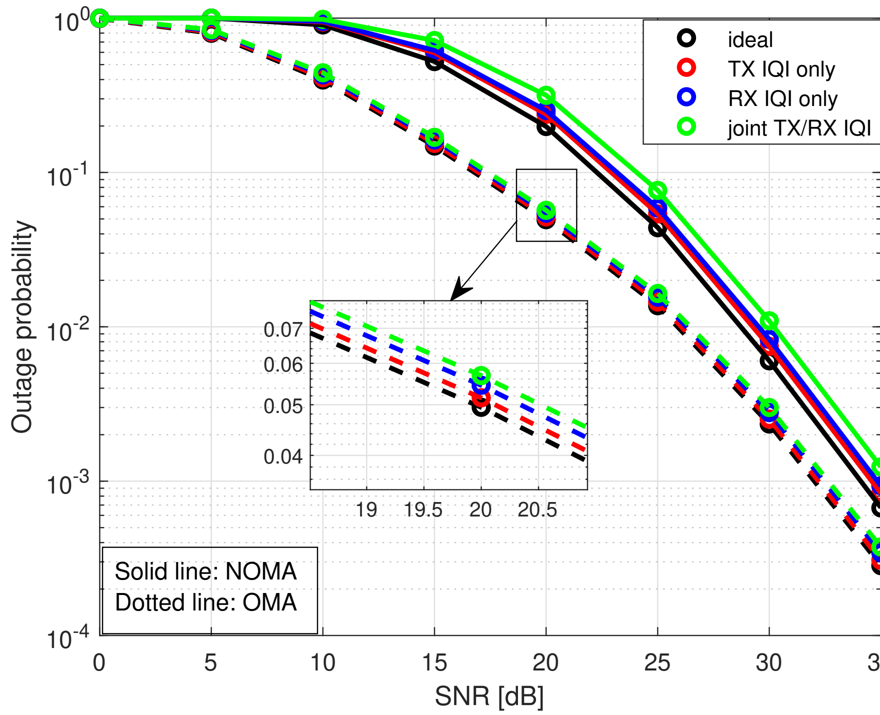

Figure 3.3: Comparison between downlink NOMA and OMA in terms of OP.

In Fig. 3.3, we analyze the OP versus SNR for different scenarios: TX, RX, and joint TX/RX. Comparing the results with the ideal case, it is evident that the system without IQI outperforms the system with IQI in terms of outage performance. Moreover, an OMA system performs better than a NOMA system. However, the impact of IQI on system performance is more pronounced when it manifests in the receiver. This difference arises because the receiver is influenced by IQI, signal, channel conditions, and noise, while the transmitter is only impacted by the IQI.

In Figs. 3.4 and 3.5, we illustrate the OP and EC of users in the downlink NOMA systems

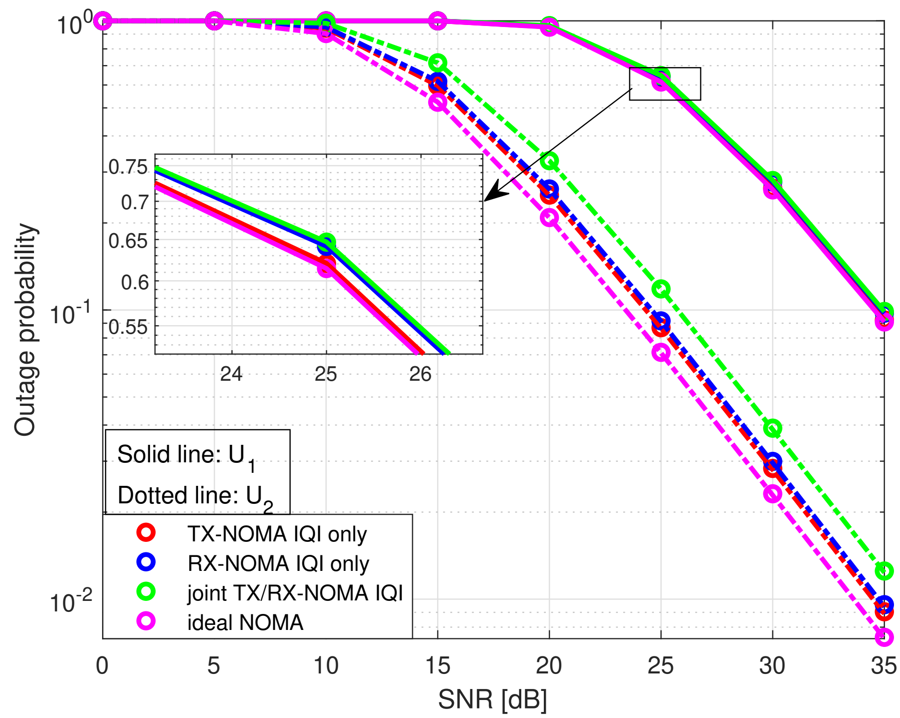

Figure 3.4: OP of the downlink NOMA under IQI w.r.t SNR with $IRR_t = IRR_r = 20dB$.

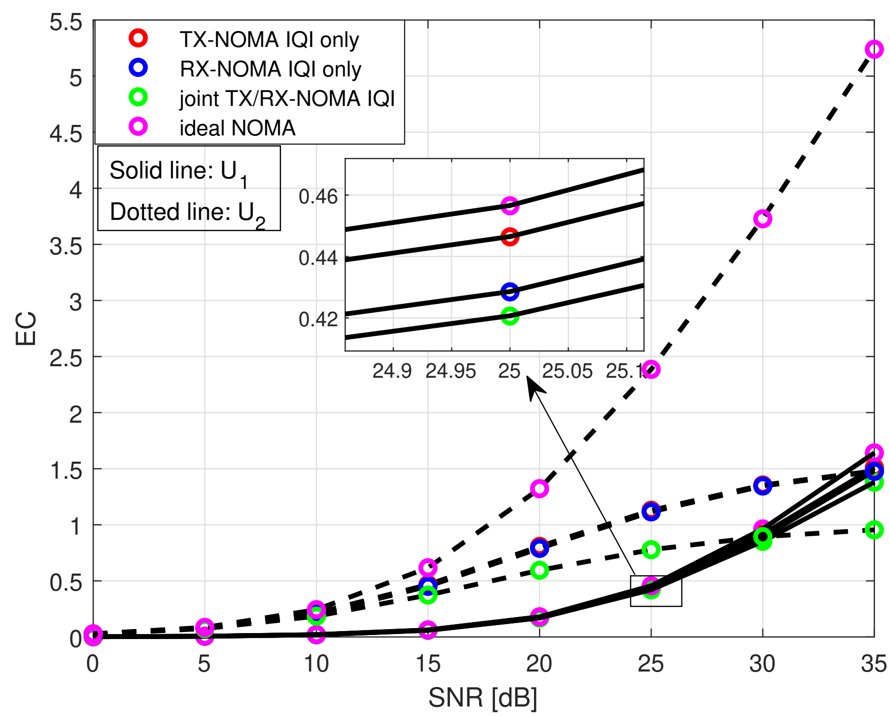

Figure 3.5: EC of the downlink NOMAunder IQI versus SNR with $IRR_t = IRR_r = 20dB$.

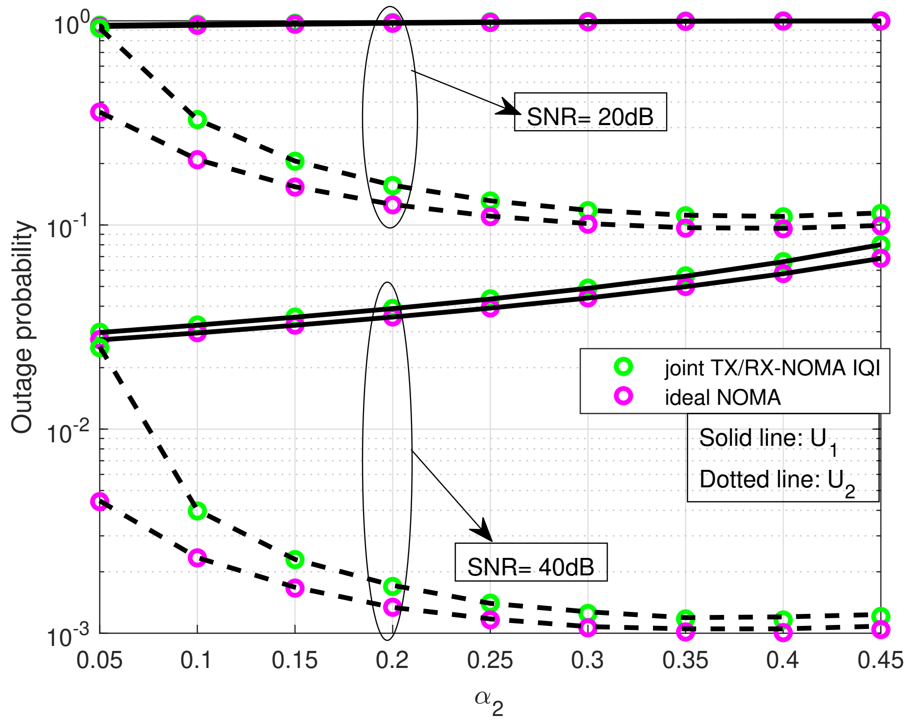

Figure 3.6: OP of the downlink NOMA under IQI w.r.t PA with $IRR_t = IRR_r = 20dB$.

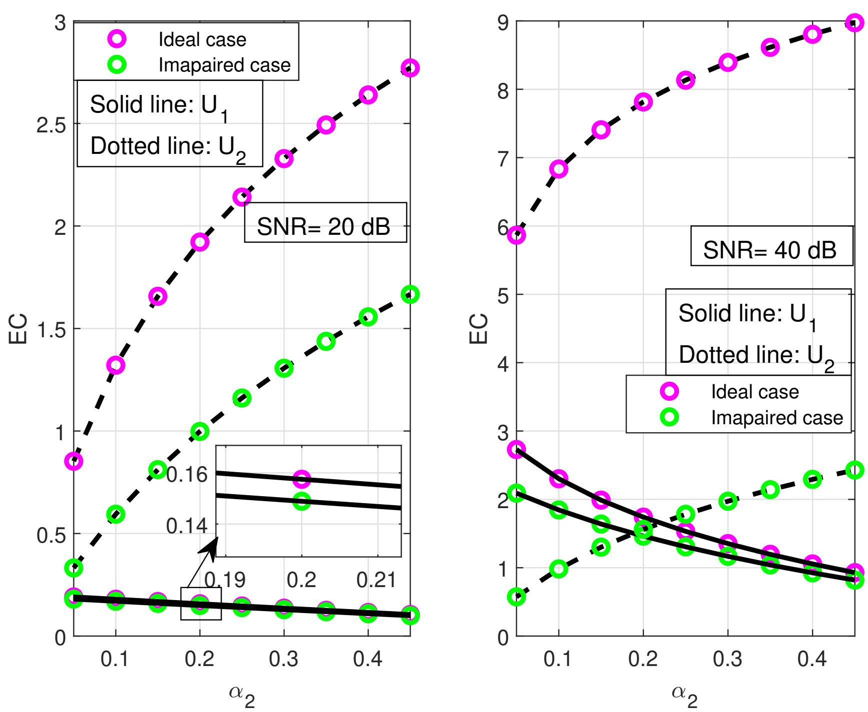

Figure 3.7: EC of the downlink, NOMA under IQI w.r.t of PA with $IRR_t = IRR_r = 20dB$.

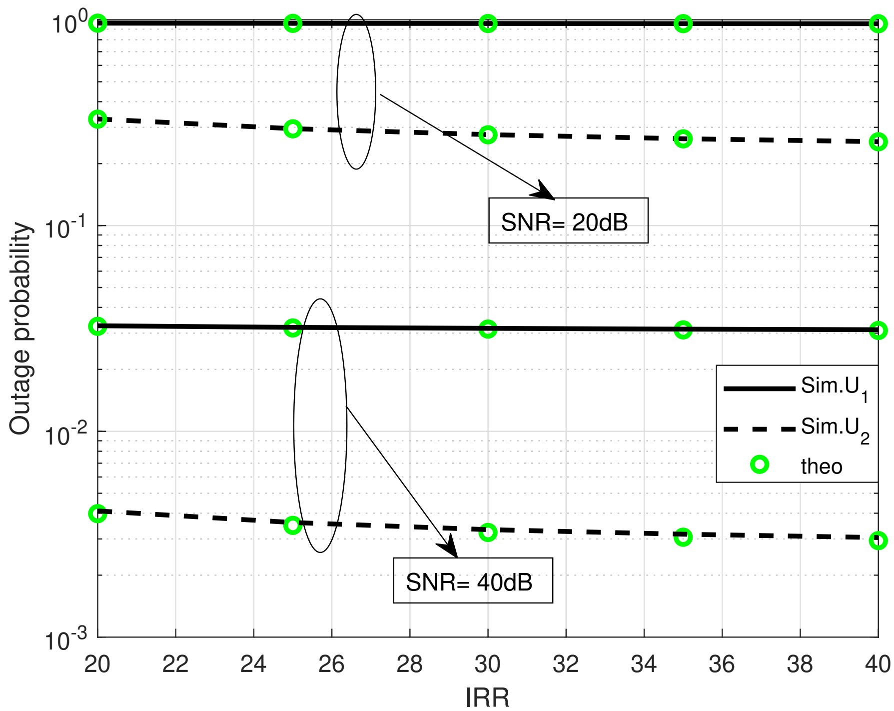

Figure 3.8: OP of the downlink NOMA under IQI w.r.t of IRR.

where joint TX and RX are affected by IQI with $IRR_t = IRR_r = 20dB$. The performance of users with ideal IQI demonstrates better performance compared to those in a non-ideal IQI condition. Therefore, the U_1 exhibits superior performance, due to the high PA allocated to U_1. Furthermore, as the SNR increases, the system performance improves for both users.

The impact of PA is evaluated in Figs. 3.6 and 3.7, where both TX and RX are affected by IQI with different SNR values. As the α_2 increases, we can observe that the performance of U_1 degrades, while the performance of U_2 improves. Furthermore, as the SNR increases, the performance of the two users improves.

In Figs. 3.8 and 3.9, we present the OP and EC performance of the downlink NOMA versus IRR with different levels of SNR. As IRR increases, there is a noticeable improvement in both the OP and EC performance for the users.

To assess the performance of the uplink NOMA system, we consider the impairment of both the transmitter (TX) and receiver (RX) by IQI with $\alpha_1 = 0.2$ and $\alpha_2 = 0.8$.

Figs. 3.10 and 3.11 depict the effect of the IQI on the uplink NOMA in the function of

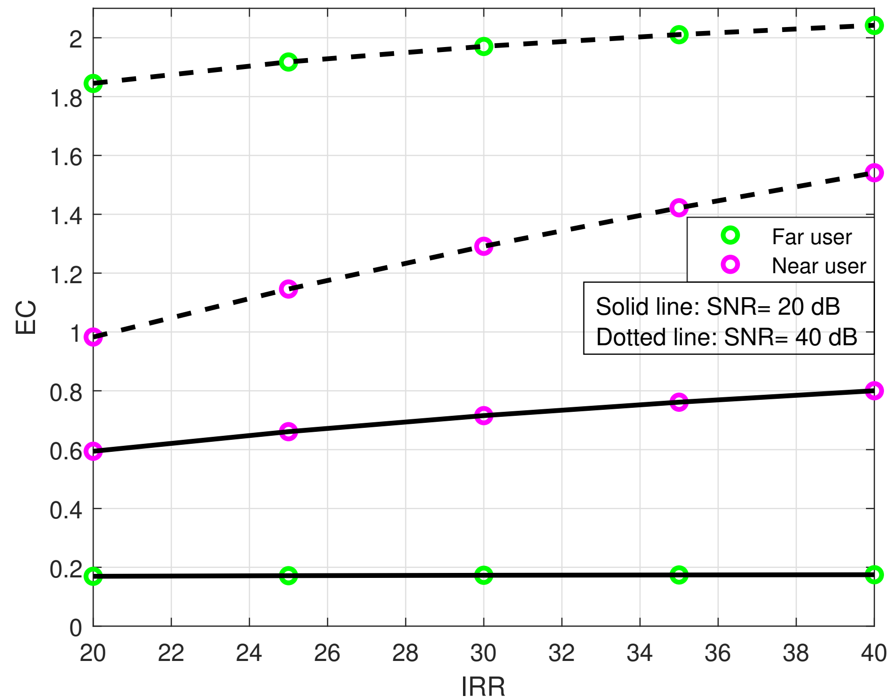

Figure 3.9: EC of the downlink NOMA under IQI w.r.t of IRR.

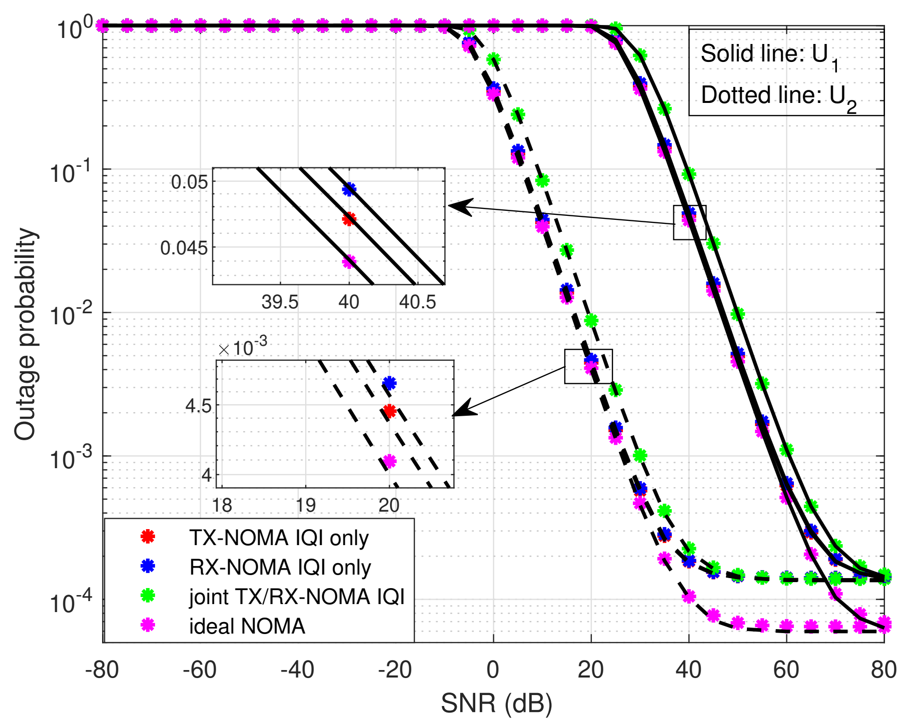

Figure 3.10: OP of the uplink NOMA under IQI versus SNR with $IRR_t = IRR_r = 20dB$.

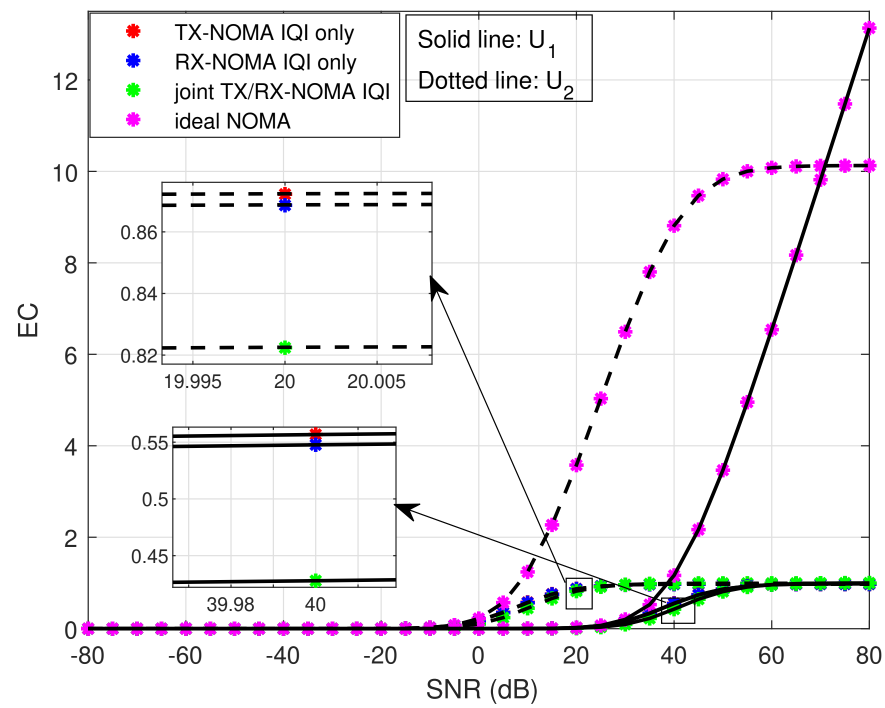

Figure 3.11: EC of the uplink NOMA under IQI w.r.t SNR with $IRR_t = IRR_r = 20dB$.

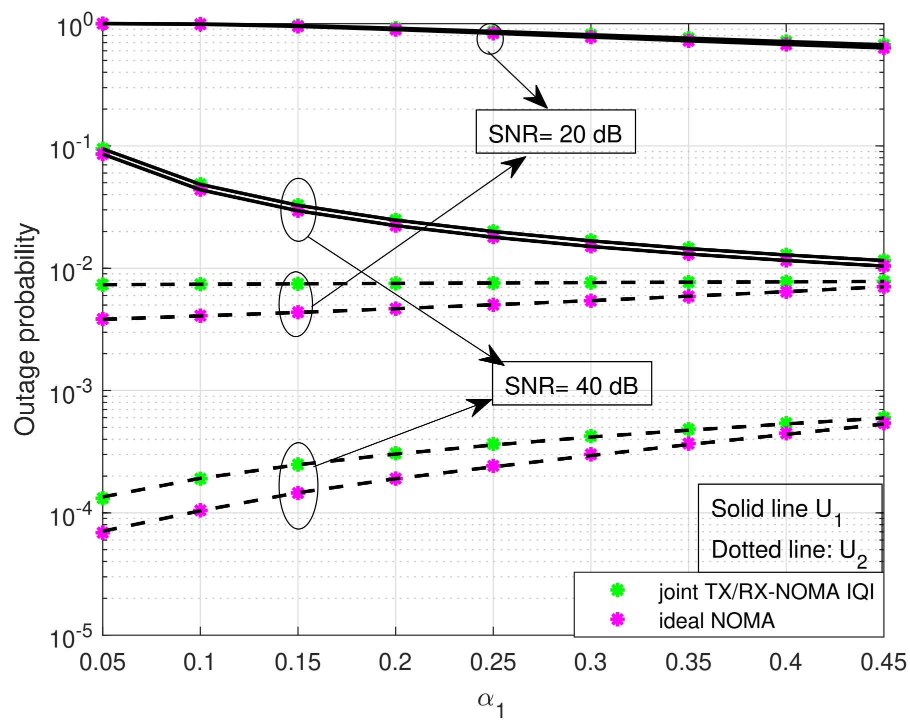

Figure 3.12: OP of the uplink NOMA under IQI versus PA with $IRR_t = IRR_r = 20dB$.

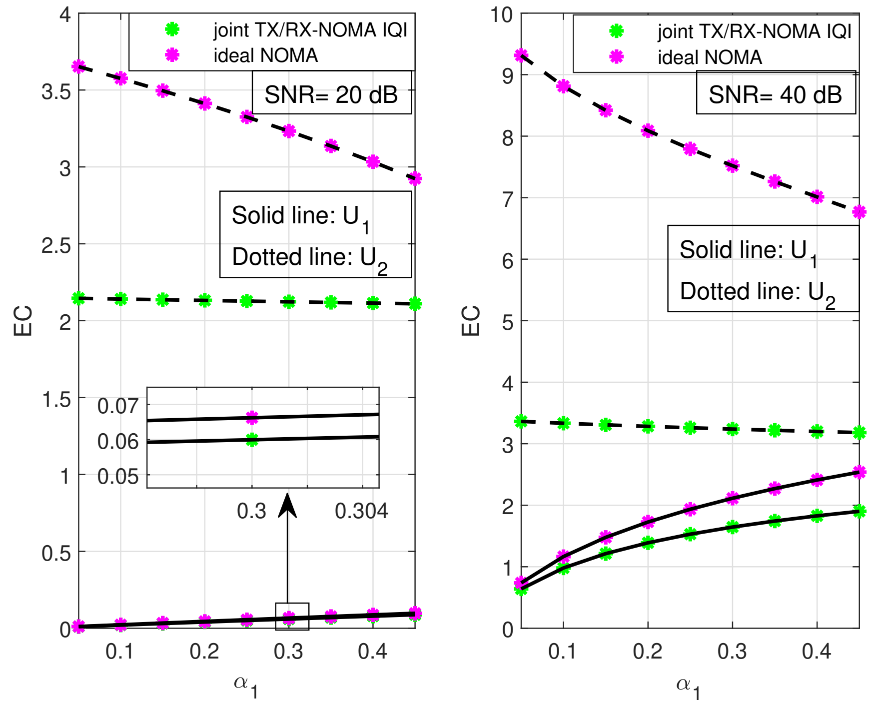

Figure 3.13: EC of the uplink NOMA under IQI versus PA with $IRR_t = IRR_r = 20dB$.

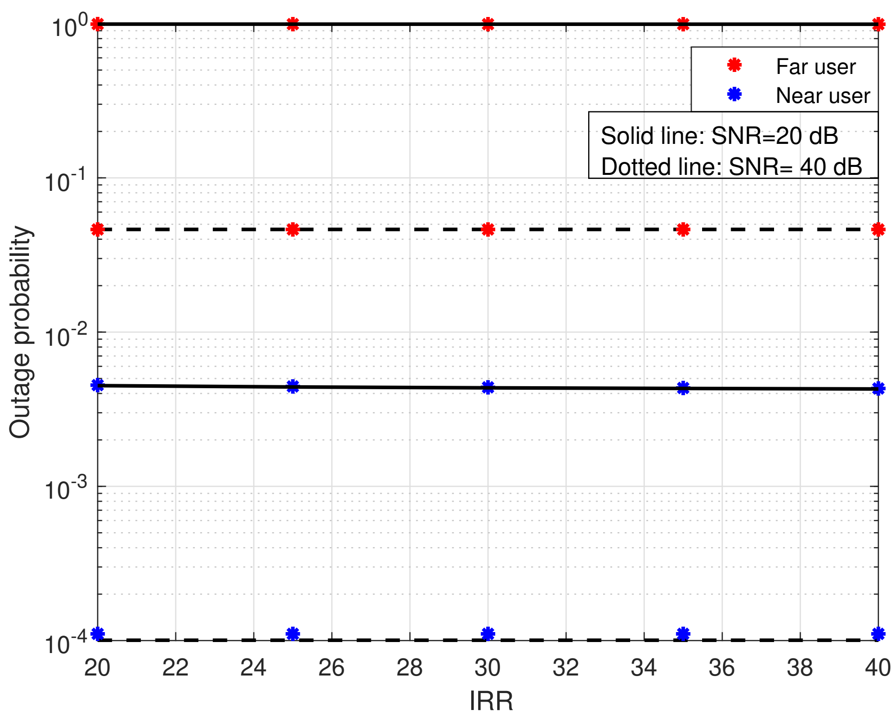

Figure 3.14: OP of the uplink NOMA under IQI w.r.t IRR.

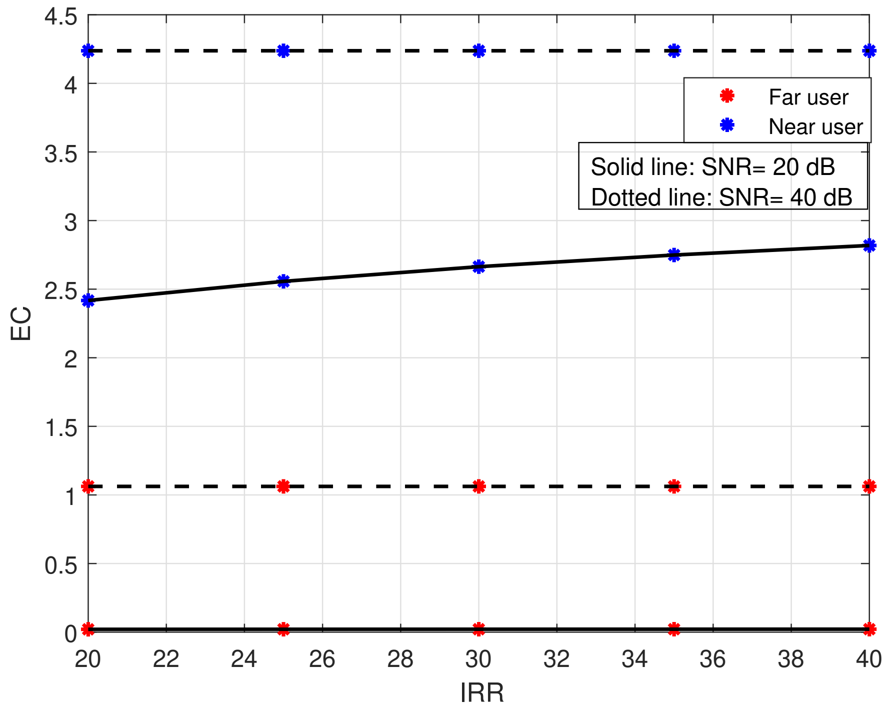

Figure 3.15: OP of the uplink NOMA under IQI w.r.t of IRR.

SNR with $IRR_t = IRR_r = 20dB$ in terms of OP and EC. The results demonstrate that the joint TX/RX impaired IQI significantly influences the system's performance. Moreover, U_2 outperforms user U_1 due to the uplink NOMA system allocating more Power Allocation (PA) resources to the near user than the far one.

The impact of PA on the uplink NOMA is presented in Figs. 3.12 and 3.13 in terms of OP and EC performance with different values of SNR. The influence of PA on user performance is distinct for each user. Increasing the α_1 improves the performance of user U_1, while it simultaneously degrades the performance of user U_2.

Fig. 3.14 and 3.15 illustrate the effect of IRR on the uplink of direct NOMA with different levels of SNR. It can be seen that as the IRR increases the performance of both users increase. Besides, despite the presence of imperfections, the system's performance can still improve with higher SNR levels.

3.9 Conclusion

This chapter investigated the impact of IQI on a downlink and uplink NOMA system in terms of OP and EC over a Rayleigh fading channel. The analysis considered three scenarios: IQI impairment in the transmitter, IQI impairment in the receiver, and IQI impairment in both the transmitter and receiver simultaneously. However, the findings reveal that IQI impairment significantly diminishes the OP and EC performance of both the downlink and uplink NOMA systems. This highlights the importance of devising compensation and optimization methods to enhance the overall performance and efficiency of NOMA systems.

Chapter 4

Impact of Hardware Impairment on the Cooperative NOMA system

4.1 Introduction

Non-orthogonal multiple access (NOMA) is a promising solution to satisfy the demands for spectrum efficiency and network density in the next generations of wireless access. Therefore, the integration of the NOMA with cooperative relaying (CNOMA) networks has attracted recent attention to improve transmission reliability and extend network coverage and increase spectral efficiency [79]. In CNOMA schemes, there are two possible configurations depending on whether direct links are available between the source and users or not. In the first, the relay node(s) improves the key performance indicators (KPIs), e.g., capacity, outage probability (OP) and bit error rate (BER), while in the second, the relay node(s) extends the coverage.

4.1.1 Related work

Nevertheless, almost all literature is devoted to the second scenario where the direct links (DLs) are blocked by some obstacles. To enhance the outage performance of the users, the authors in [80] presented the CNOMA with the aid of a decode-and-forward (DF) relay with different relaying schemes by using both direct and relaying links. In [81], the impact of the DF selection relay on the performance of CNOMA is analyzed with two types of relay selection in terms of OP over the Rayleigh fading channel. The authors in [82] examined the outage performance of the amplify-and-forward (AF) relay CNOMA network over the Rayleigh fading channel. The ergodic sum rate and OP of CNOMA with DF and AF protocols over the Nakagami-m fading channels have been analyzed in [83]. Therefore, to improve the performance of the DF CNOMA system, the hybrid relaying scheme that switches between full and half duplex (FD/HD) has been investigated in [84, 85]. For a more realistic system, the authors in [86] analyzed the residual self-interference and residual multiple access interferences due to imperfect co-channel interference cancellation on the FD-CNOMA over Nakagami-channel in terms of OP and ergodic capacity. The FD/HD coordinated direct and DF relay transmission in the NOMA system is analyzed in terms of OP and ergodic sum rate under imperfect channel state information (ipCSI) and imperfect successive interference cancellation (ipSIC) in [87]. Additionally, the authors in [88] presented a dual-hop multi-relay NOMA using the DF system over the Nakagami-m fading channel in terms of OP. A novel two-stage power allocation (PA) scheme with NOMA was proposed to improve the sum rate and the OP of the dual-hop relay system in [89]. The authors in [90] presented the sum rate analysis of the CNOMA scheme with dual-hop hybrid wireless-power line communication. In [91], the performance of the dual-hop DF relay system using NOMA under the assumption of statistical CSI is evaluated. The authors in [92] studied and compared the performance of dual-hop relaying systems adopting DF and AF forwarding strategies. Moreover, a unified framework of NOMA networks that applied the code-domain NOMA (CD-NOMA) and power-domain NOMA (PD-NOMA) NOMA with ipSIC and perfect SIC in terms of OP and throughput is investigated in [93]. The authors in [94] examined the impact of physical layer secrecy on the performance of a unified NOMA framework, where both external and internal eavesdropping scenarios are evaluated in terms of secrecy OP for both CD-NOMA and PD-NOMA under ipSIC and perfect SIC. To model the locations of NOMA users within the networks, a unified downlink NOMA transmission scenario has been investigated in [95].

On the other hand, radio-frequency (RF) equipment is one of the most significant components of the massive network of interconnected devices that facilitates communication between individual devices and/or their base station (BS). Therefore, the direct conversion transceivers seem to be the RF front-end solution to stringent design goals such as low cost, low power dissipation, improved efficiency and performance [13]. However, in a realistic communication scenario, the RF component suffers from various types of hardware impairment (HWI) that limit the performance of the overall system, such as oscillator phase noise (PN), high power amplifier (HPA) and in-phase and quadrature-phase imbalance (IQI)[34, 48]. The effect of individual HWI on the system's performance has been examined in [96, 97, 98], where the authors in [96, 98] analyzed throughput and OP performance with the impacts of IQI on the transceiver front-end of the AF two-hop relay node with different IQI levels. The impact of non-linear HPA has been studied in [97], where the OP, ergodic capacity (EC) and BER performance deteriorated compared to linear HPA. In [99], the achievable rate has been examined for the massive multiple-input-multiple-output (MIMO) FD relaying in the presence of HWI. In [100], the effect of HWI on one and two ways AF systems in terms of OP expressions has been performed.

As well as other communication techniques [97, 99, 100] given above, the effects of such imperfections on the performance of CNOMA schemes have been examined in several studies [43, 49, 50, 58, 101, 102, 103]. The performance of NOMA dual-hop AF relaying networks is examined over the Nakagami-m fading channel in terms of OP and ergodic sum rate in [49]. An AF CNOMA system with HWI is analyzed in terms of OP and intercept probability over the multipath fading channel in [102]. The impact of HWI is investigated on the NOMA-based AF relaying network in terms of OP, EC and ergodic sum rate. The authors in [50] investigate the OP and ergodic rate performance of the FD-CNOMA with the presence of HWI over the Rician fading channels. Furthermore, the effect of the simultaneous wireless information and power transfer NOMA system has been analyzed in terms of OP [101]. However, the CNOMA network suffers also from imperfect successive interference cancellation (ipSIC) and imperfect channel state information (ipCSI). The authors in [58] study the impacts of HWI on the NOMA with ipCSI, where both cooperative and non-cooperative NOMA are analyzed in terms of OP, EC and energy efficiency. In [103], the OP of the cognitive radio NOMA network is analyzed under HWI, ipCSI and ipSIC. On the other hand, BER performances of FD-CNOMA have been investigated in [104] with ipSIC where perfect CSI and no HWI are considered. Then, the BER and OP performances of a two-hop and multi-hop DF CNOMA with ipCSI have been investigated in [55, 56, 105]. The pairwise error probability is derived for the AF-CNOMA by considering HWI with no ipCSI [43]. Besides, the BER of the NOMA arbitrary number of users and modulation orders has been analyzed in [106, 107, 108], which proved that the increase in number of users or modulations order causes infeasible PA. In those cases, some of the users need to get very low power coefficients.

4.1.2 Motivations and contributions

All the aforementioned CNOMA studies investigate the performances of CNOMA without direct link (DL) and CNOMA with DL has not been investigated with imperfections in terms of any performance metrics. Besides, most of the above papers [79, 80, 87, 93, 94, 50, 58, 102, 103] analyze the effects of one or multiple imperfections only in terms of achievable rate and/or OP whilst the BER performance is considered in very limited studies [43, 56, 104, 105].

Furthermore, the effects of HWI on the BER performances of NOMA with/without cooperative relaying have not been studied well although its effects on capacity and OP performances have been evaluated in [50, 58, 102, 103]. Also, the OP with the effect of HWI on CNOMA, when maximum ratio combining (MRC) is implemented at the receiver in the presence of ipSIC and ipCSI, has not been performed. As discussed above, to the best of our knowledge, the BER and OP performance of NOMA schemes (with/without cooperative relaying) has not been investigated with practical constraints (i.e., ipSIC, ipCSI and HWI). Besides, the BER performance of NOMA with/without cooperation has not been revealed with all imperfections in the open literature.

Motivated by this, this chapter provides a comprehensive analytical framework for the BER and OP performances of NOMA schemes under practical constraints where the consideration of ipSIC, ipCSI and HWI. Therefore, the main contributions of the chapter can be summarized as follows:

- Three different schemes of the NOMA system (downlink NOMA, CNOMA without direct link, CNOMA with direct link) are presented with practical constraints (i.e., ipSIC, ipCSI and HWI).
- The exact BER expressions of the three considered systems are derived under HWI in the presence of ipSIC and ipCSI and the analytical results are validated via computer simulations.
- The outage performance for the different NOMA schemes is also investigated and exact OP expressions are derived under HWI, ipCSI and ipSIC. The asymptotic analysis of OP at high SNR regions is performed to reveal the insights of the parameters for HWI, ipCSI, and ipSIC on system performance and the results show that the OP is affected by HWI, ipCSI and ipSIC in the high SNR. In addition, the computer simulations show a perfect match with theoretical results.
- For comparisons, extensive computer simulations are presented to reveal the effects of HWI, ipCSI and ipSIC on the BER and OP performance of the considered systems with different scenarios (e.g., PA, and distance between nodes).
- The conventional OMA schemes are considered as a benchmark for comparison with

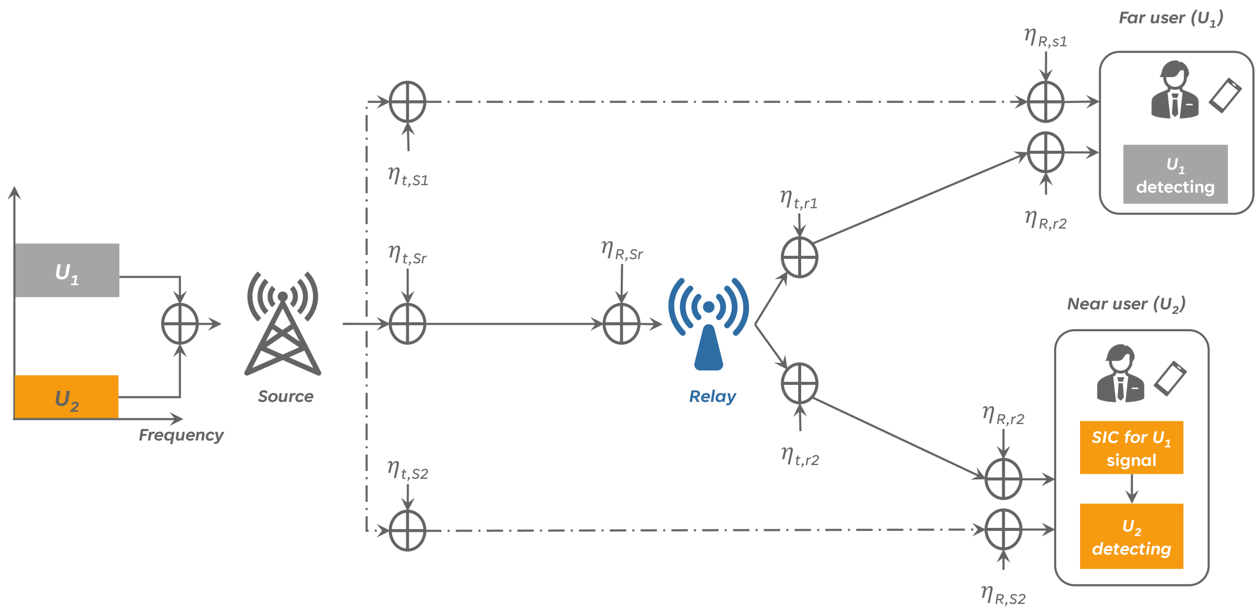

Figure 4.1: System model CNOMA schemes with HWI.

proposed NOMA schemes. Therefore, the BER and OP system analysis is obtained for our three NOMA schemes in the presence of HWI, ipCSI and ipSIC.

4.2 System model

A downlink CNOMA system is presented in Fig. 4.1. The system comprises a source (S), a DF relay (R), and two users: user 1 (U_1) and user 2 (U_2). All nodes are equipped with a single antenna and the R operates in HD mode. Three different scenarios of the considered system which are:

1. Downlink NOMA (NOMA) S transmits directly the signal to the users.
2. Cooperative NOMA without direct link (CNOMA) S communicates with the users through R, as there is no direct link between S and the users.
3. Cooperative NOMA with a direct link (CNOMA-WDL) S employs R and utilizes the direct links to transmit the signal to the users. In a two-phase process, the users combine the signals received from both sources using the maximum ratio combining (MRC).

The complex flat fading channel coefficients between S-users are represented as The received signals at U_1, U_2 and R ath the first phase are presented as [42, 109]:

$$y_i = (\tilde{h}_i \ + e)(\sqrt{P_s} s_{sc} + \eta_i) + n, \tag{4.1}$$

where $s_{sc} = \sqrt{\alpha_1} x_1 + \sqrt{\alpha_2} x_2$, α_1 and α_2 are the PA coefficient and s_1, s_2 are the message of the U_1 and U_2, respectively. η_i is the independent distortion noise defined as $\eta_i \sim \mathcal{CN}(0,\ k_i^2 P_s)$, k_i^2 is the HWI level at the transceivers. n is the Additive White Gaussian Noise (AWGN) $\mathbf{n} \sim \mathcal{CN}(0,\ N_o)$.

The received signal-to-interference plus noise ratio (SINR) for the x_1 in the first phase at the U_1, U_2 and R

$$\gamma_1^{S1} = \frac{\alpha_1 P_s |\tilde{h}_{S1}|^2}{\alpha_2 P_s |\tilde{h}_{S1}|^2 + \sigma_\epsilon^2 P_s + \sigma_\epsilon^2 P_s k_{S1}^2 + |\tilde{h}_{S1}|^2 P_s k_{S1}^2 + N_0}, \tag{4.2}$$

$$\gamma_1^{S2} = \frac{\alpha_1 P_s |\tilde{h}_{S2}|^2}{\alpha_2 P_s |\tilde{h}_{S2}|^2 + \sigma_\epsilon^2 P_s + \sigma_\epsilon^2 P_s k_{S2}^2 + |\tilde{h}_{S2}|^2 P_s k_{S2}^2 + N_0}, \tag{4.3}$$

$$\gamma_1^{Sr} = \frac{\alpha_1 P_s |\tilde{h}_{Sr}|^2}{\alpha_2 P_s |\tilde{h}_{Sr}|^2 + \sigma_\epsilon^2 P_s + \sigma_\epsilon^2 P_s k_{Sr}^2 + |\tilde{h}_{Sr}|^2 P_s k_{Sr}^2 + N_0}. \tag{4.4}$$

Although both U2 and R implement SIC to detect x_2, the SINR of x_2 at U_2 and R is provided respectively as:

$$\gamma_2^{S2} = \frac{\alpha_2 P_s |\tilde{h}_{S2}|^2}{\varsigma \alpha_1 P_s |\tilde{h}_{S2}|^2 + \sigma_\epsilon^2 P_s + \sigma_\epsilon^2 P_s k_{S2}^2 + |\tilde{h}_{S2}|^2 P_s k_{S2}^2 + N_0}, \tag{4.5}$$

$$\gamma_2^{Sr} = \frac{\alpha_2 P_s |\tilde{h}_{Sr}|^2}{\varsigma \alpha_1 P_s |\tilde{h}_{Sr}|^2 + \sigma_\epsilon^2 P_s + \sigma_\epsilon^2 P_s k_{Sr}^2 + |\tilde{h}_{Sr}|^2 P_s k_{Sr}^2 + N_0}, \tag{4.6}$$

where ς denotes the residual SIC factor. During the second phase of the cooperative schemes, R utilizes SIC for both users. Subsequently, it generates a new superimposed signal SC signal and retransmits it to the users using its own power, similar to R-S. The received signal at U_1 and U_2 in the second phase is presented as:

$$y_j = (\tilde{h}_j \ + e)(\sqrt{P_r} s_{sc} + \eta_j) + n, \tag{4.7}$$

where P_r is the relay transmit power, $\eta_{ri} \sim \mathcal{CN}(0,\ k_{ri}^2 P_r)$. The SINR for x_1 and x_2 in the CNOMA, where the users receive the signal from R only, can be defined as:

$$\gamma_1^{r1} = \frac{\alpha_1 P_r |\tilde{h}_{r1}|^2}{\alpha_2 P_r |\tilde{h}_{r1}|^2 + \sigma_\epsilon^2 P_r + \sigma_\epsilon^2 P_r k_{r1}^2 + |\tilde{h}_{r1}|^2 P_r k_{r1}^2 + N_0}, \tag{4.8}$$

$$\gamma_1^{r2} = \frac{\alpha_1 P_r |\tilde{h}_{r2}|^2}{\alpha_2 P_r |\tilde{h}_{r2}|^2 + \sigma_\epsilon^2 P_r + \sigma_\epsilon^2 P_r k_{r2}^2 + |\tilde{h}_{r2}|^2 P_r k_{r2}^2 + N_0}, \tag{4.9}$$

$$\gamma_2^{r2} = \frac{\alpha_2 P_r |\tilde{h}_{r2}|^2}{\varsigma \alpha_1 P_r |\tilde{h}_{r2}|^2 + \sigma_\epsilon^2 P_r + \sigma_\epsilon^2 P_r k_{r2}^2 + |\tilde{h}_{r2}|^2 P_r k_{r2}^2 + N_0}. \tag{4.10}$$

The SINR for x_1 and x_2 in the context of CNOMA-WDL, where users employ MRC to receive signals, can be expressed as:

$$\gamma_1^{\mathsf{CNOMA-DL-WDL}} = {\gamma_1}^{S1} + {\gamma_1}^{r1}, \tag{4.11}$$

$$\gamma_{2\to 1}^{\mathsf{CNOMA-DL-WDL}} = {\gamma_1}^{S2} + {\gamma_1}^{r2}, \tag{4.12}$$

$$\gamma_2^{\mathsf{CNOMA-DL-WDL}} = {\gamma_2}^{S2} + {\gamma_2}^{r2}. \tag{4.13}$$

4.2.1 Performance Analysis

4.2.1.1 Outage probability anlysis

In this subsection, the expression of OP for the different NOMA schemes: NOMA, CNOMA, and CNOMA-WDL over the Rayleigh fading channel.

1) OP of the NOMA syetem

The OP of the x_1 at the U_1 and R under HWI, ipCSI is given as:

$$\begin{aligned} P_{x_1,m}(out) &= P\left(\gamma_1^m \leq \gamma_{th,1}\right) \\ &= 1 - \exp\left(-\gamma_{th,1}\Theta_1^m\right),\ m = Sr; S1; r1, \end{aligned} \tag{4.14}$$

where

$\Theta_1^{Sr} = \frac{\left(N_0+\sigma_\epsilon^2 P_s+\sigma_\epsilon^2 P_s k_{Sr}{}^2\right)}{\Phi_{Sr}\left(\alpha_1 P_s-\gamma_{th,1}P_s\alpha_2-\gamma_{th,1}P_s k_{Sr}{}^2\right)}$, $\Theta_1^{S1} = \frac{\left(N_0+\sigma_\epsilon^2 P_s+\sigma_\epsilon^2 P_s k_{S1}{}^2\right)}{\Phi_{S1}\left(\alpha_1 P_s-\gamma_{th,1}P_s\alpha_2-\gamma_{th,1}P_s k_{S1}{}^2\right)}$,

$\Theta_1^{r1} = \frac{\left(N_0+\sigma_\epsilon^2 P_r+\sigma_\epsilon^2 P_r k_{r1}{}^2\right)}{\Phi_{r1}\left(\alpha_1 P_r-\gamma_{th,1}P_r\alpha_2-\gamma_{th,1}P_r k_{r1}{}^2\right)}$. $\gamma_{th,1} = 2^{\tau R_1} - 1$ is the threshold of x_1, τ the time slot duration 1 for NOMA 2 for CNOMA and $\Phi_m = \mathrm{E}[|\tilde{h}_m|^2]$ are defined.

Proof Please see Appendix C.

The OP of x_2 at U_2 and R with HWI, ipCSI, and ipSIC is determined as:

$$\begin{aligned} P_{m_2,n}(out) &= P\left(\gamma_1^n \leq \gamma_{th,1}\right) + P\left(\gamma_1^n > \gamma_{th,1}\right) P\left(\gamma_2^n \leq \gamma_{th,2}\right) \\ &= 1 - \exp\left(-\Theta_1^n\gamma_{th,1}\right)\exp\left(-\Theta_2^n\gamma_{th,2}\right),\ n = Sr; S2; r2, \end{aligned} \tag{4.15}$$

where

$\Theta_2^{Sr} = \frac{\left(N_0+\sigma_\epsilon^2 P_s+\sigma_\epsilon^2 P_s k_{Sr}{}^2\right)}{\Phi_{Sr}\left(\alpha_2 P_s-\varsigma\gamma_{th,2}P_s\alpha_1-\gamma_{th,2}P_s k_{Sr}{}^2\right)}$, $\Theta_1^{S2} = \frac{\left(N_0+\sigma_\epsilon^2 P_s+\sigma_\epsilon^2 P_s k_{S2}{}^2\right)}{\Phi_{S2}\left(\alpha_1 P_s-\gamma_{th,1}P_s\alpha_2-\gamma_{th,1}P_s k_{S2}{}^2\right)}$,

$\Theta_2^{S2} = \frac{\left(N_0+\sigma_\epsilon^2 P_s+\sigma_\epsilon^2 P_s k_{S2}{}^2\right)}{\Phi_{S2}\left(P_s\alpha_2-\gamma_{th,2}\varsigma\alpha_1 P_s-\gamma_{th,2}P_s k_{S2}{}^2\right)}$, $\Theta_1^{r2} = \frac{\left(N_0+\sigma_\epsilon^2 P_r+\sigma_\epsilon^2 P_r k_{r2}{}^2\right)}{\Phi_{r2}\left(\alpha_1 P_r-\gamma_{th,1}P_r\alpha_2-\gamma_{th,1}P_r k_{r2}{}^2\right)}$,

$\Theta_2^{r2} = \frac{\left(N_0+\sigma_\epsilon^2 P_r+\sigma_\epsilon^2 P_r k_{r2}{}^2\right)}{\Phi_{r2}\left(P_r\alpha_2-\gamma_{th,2}\varsigma\alpha_1 P_r-\gamma_{th,2}P_r k_{r2}{}^2\right)}$. $\gamma_{th,2} = 2^{\tau R_2} - 1$ is the threshold of m_2, and $\Phi_n = \mathrm{E}[|\tilde{h}_n|^2]$.

2) OP of CNOMA system

The OP of the CNOMA can be obtained as:

$$P_l^{(\mathsf{CNOMA})}(out) = 1 - \left(1 - P_{x_l,Sr}(out)\right)\left(1 - P_{x_l,rl}(out)\right),\ l = 1,\ 2, \tag{4.16}$$

where, the $P_{x_l,Sr}(out)$ and $P_{x_l,rl}(out)$ are defined for the first and second phases, respectively in (4.14) and (4.15).

3) OP of CNOMA-WDL system

The Outage Probability (OP) of CNOMA-WDL for user U_1, who utilizes the MRC to combine the received signals from S and R, can be expressed as [110]:

$$\begin{aligned} &P_1^{\mathsf{CNOMA-WDL}}(out) = \\ &(1 - P({\gamma_1}^{Sr} < \gamma_{th,1}))P((\gamma_1^{S1} + \gamma_1^{r1}) < \gamma_{th,1}) + P({\gamma_1}^{Sr} < \gamma_{th,1})P(\gamma_1^{S1} < \gamma_{th,1}), \end{aligned} \tag{4.17}$$

where $P({\gamma_1}^{Sr} < \gamma_{th,1})$, $P({\gamma_1}^{S1} < \gamma_{th,1})$ and $P({\gamma_1}^{S1} < \gamma_{th,1})$ are obtained in (4.14). employing the CDF of two independent exponential random variables ${\gamma_1}^{S1} \neq \gamma_1^{r1}$.
Then, the term (4.17) can define be as in [110, eq. (6)]
:

$$P((\gamma_1^{S1} + \gamma_1^{r1}) < \gamma_{th,1}) = 1 - \left[\tau_1 \exp\left(-\Theta_1^{S1}\gamma_{th,1}\right) + \tau_2 \exp\left(-\Theta_1^{r1}\gamma_{th,1}\right)\right], \text{where } \Theta_1^{s1} \neq \Theta_1^{r1}, \tag{4.18}$$

where $\tau_1 = \frac{\Theta_1^{S1}}{\Theta_1^{S1} - \Theta_1^{r1}}$ and $\tau_2 = \frac{\Theta_1^{r1}}{\Theta_1^{r1} - \Theta_1^{S1}}$.
Replacing (4.14) and (4.18) into (4.17), the OP of the U_1 for the CNOMA-WDL is given as:

$$\begin{aligned} P_1^{\mathsf{CNOMA-WDL}}(out) &= \exp\left(-\gamma_{th,1}\Theta_1^{Sr}\right)\left(1 - \left[\tau_1 \exp\left(-\Theta_1^{S1}\gamma_{th,1}\right) + \tau_2 \exp\left(-\Theta_1^{r1}\gamma_{th,1}\right)\right]\right) \\ &+ \left(1 - \exp\left(-\gamma_{th,1}\Theta_1^{Sr}\right)\right)\left(1 - \exp\left(-\gamma_{th,1}\Theta_1^{S1}\right)\right). \end{aligned} \tag{4.19}$$

The OP at the output MRC of x_2 at the U_2 which can be presented as:

$$P_2^{CNOMA-WDL}(out) = P_{2\to1}^{\mathsf{CNOMA-WDL}}(out) + \left[1 - P_{2\to1}^{\mathsf{CNOMA-WDL}}(out)\right] P_2(out), \tag{4.20}$$

where $P_{2\to1}^{\mathsf{CNOMA-WDL}}(out)$ and $P_2(out)$ are the OP to detect x_1 and x_2 at U_2 at output MRC that can be defined

$$P_{2\to1}^{\mathsf{CNOMA-WDL}}(out) = (1 - P\left({\gamma_1}^{Sr} < \gamma_{th,1}\right))P\left(({\gamma_1}^{S2} + {\gamma_1}^{Sr}) < \gamma_{th,1}\right) + P\left({\gamma_1}^{Sr} < \gamma_{th,1}\right)P\left(\gamma_1^{S2} < \gamma_{th,1}\right), \tag{4.21}$$

where $P\left({\gamma_1}^{Sr} < \gamma_{th,1}\right))$ is given in (4.14). The other term can be expressed by using the CDF of ${\gamma_1}^{S2} \neq \gamma_1^{r1}$

$$P\left(\gamma_1^{S2} < \gamma_{th,1}\right) = 1 - \exp\left(-\Theta_1^{S2}\gamma_{th,1}\right), \tag{4.22}$$

$$P(({\gamma_1}^{S2} + {\gamma_1}^{Sr}) < \gamma_{th,1}) = 1 - \left[\tau_3 \exp\left(-\Theta_1^{S2}\gamma_{th,1}\right) + \tau_4 \exp\left(-\Theta_1^{r2}\gamma_{th,1}\right)\right], \text{ where } \Theta_1^{S2} \neq \Theta_1^{r2}, \tag{4.23}$$

where $\tau_3 = \frac{\Theta_1^{S2}}{\Theta_1^{S2} - \Theta_1^{r2}}$ and $\tau_4 = \frac{\Theta_1^{r2}}{\Theta_1^{r2} - \Theta_1^{S2}}$.

Replacing (4.14), (4.22), and (4.23) in (4.21), we get:

$$P_{2\to1}^{\mathsf{CNOMA}}(out) = \exp\left(-\Theta_1^{sr}\gamma_{th,1}\right)\left(1 - \left[\tau_3 \exp\left(-\Theta_1^{s2}\gamma_{th,1}\right) + \tau_4 \exp\left(-\Theta_1^{r2}\gamma_{th,1}\right)\right]\right) + \left(1 - \exp\left(-\Theta_1^{sr}\gamma_{th,1}\right)\right)\left(1 - \exp\left(-\Theta_1^{s2}\gamma_{th,1}\right)\right). \tag{4.24}$$

The OP of x_2 at U_2 at output MRC is expressed as:

$$P_2(out) = (1 - P\left({\gamma_2}^{Sr} < \gamma_{th,2}\right))P\left(\gamma_2({\gamma_2}^{S2} + {\gamma_2}^{Sr}) < \gamma_{th,2}\right) + P\left({\gamma_2}^{sr} < \gamma_{th,2}\right)P\left(\gamma_2^{S2} < \gamma_{th,2}\right), \tag{4.25}$$

where $P\left({\gamma_2}^{Sr} < \gamma_{th,2}\right))$ and $P\left({\gamma_2}^{S2} < \gamma_{th,2}\right))$ is defined in (4.15) and

$$P(({\gamma_2}^{S2} + {\gamma_2}^{Sr}) < \gamma_{th,2}) = 1 - \left[\tau_5 \exp\left(-\Theta_2^{s2}\gamma_{th,2}\right) + \tau_6 \exp\left(-\Theta_2^{r2}\gamma_{th,2}\right)\right], \text{ where } \Theta_2^{s2} \neq \Theta_2^{r2}, \tag{4.26}$$

where $\tau_5 = \frac{\Theta_2^{S2}}{\Theta_2^{S2} - \Theta_2^{r2}}$ and $\tau_6 = \frac{\Theta_2^{r2}}{\Theta_2^{r2} - \Theta_2^{S2}}$.

Substituting (4.15) and (4.26) in (4.25), we get the OP of the x_2 at the U_2 at the output as:

$$P_2(out) = \exp\left(-\Theta_2^{Sr}\gamma_{th,2}\right)\left(1 - \left[\tau_5 \exp\left(-\Theta_2^{S2}\gamma_{th,2}\right) + \tau_6 \exp\left(-\Theta_2^{r2}\gamma_{th,2}\right)\right]\right) + \left(1 - \exp\left(-\Theta_2^{Sr}\gamma_{th,2}\right)\right)\left(1 - \exp\left(-\Theta_2^{S2}\gamma_{th,2}\right)\right). \tag{4.27}$$

By Substituting (4.24) and (4.27) in (4.20), we obtain the OP of x_2 at the U_2 at the output MRC.

4.2.1.2 Asymptotic OP anlysis

The asymptotic OP is defined in high SNR regimes where we use $\exp(-x) \approx (1-x)$ in high SNR as in [111]:

1) Asymptotic OP of NOMA system

The asymptotic OP of the first phase the x_1 at R and U_1 can be presented as:

$$P^{asym}_{x_1,m}(out) \approx \gamma_{th,1}\Theta_1^m. \tag{4.28}$$

The asymptotic OP of the second phase the x_2 at R and U_2 can be given as:

$$P^{asym}_{x_2,n}(out) \approx 1-(1-\Theta_1^n\gamma_{th,1})(1-\Theta_2^n\gamma_{th,2}). \tag{4.29}$$

2) Asymptotic OP of CNOMA system

The asymptotic OP of the CNOMA without DL can be presented as:

$$P^{asym,\mathsf{CNOMA}}_{e2e,i}(out) \approx 1-\left(1-P^{asym}_{x_i,Sr}(out)\right)\left(1-P^{asym}_{x_i,r,i}(out)\right),\ i=1,\ 2, \tag{4.30}$$

where $P^{asym}_{x_i,Sr}(out)$ and $P^{asym}_{x_i,r,i}(out)$ are defined in (4.29) and (4.30)

3)Asymptotic OP of CNOMA-WDL system

The asymptotic OP of U_1 for the CNOMA-WDL is given as:

$$\begin{aligned}P_1^{\mathsf{asym,CNOMA-WDL}}(out) &\approx \left(1-\gamma_{th,1}\Theta_1^{Sr}\right)\left(1-\left[\tau_1\left(1-\tau_1^{S1}\gamma_{th,1}\right)+\tau_2\left(1-\Theta_1^{r1}\gamma_{th,1}\right)\right]\right)\\&+\left(\gamma_{th,1}\tau_1^{Sr}\right)\left(\gamma_{th,1}\tau_1^{S1}\right).\end{aligned} \tag{4.31}$$

The asymptotic OP of U_2 for the CNOMA-WDL:

$$\begin{aligned}&P_2^{asym,CNOMA-WDL}(out) = P_{2\to1}^{\mathsf{asym,CNOMA-WDL}}(out)+P_2^{asym}(out)\times\\&\left[1-P_{2\to1}^{\mathsf{asym,CNOMA-WDL}}(out)\right],\end{aligned} \tag{4.32}$$

Each term can be defined as:

$$P_{2\to 1}^{asym,\text{CNOMA}}(out) = (1-\Theta_1^{sr}\gamma_{th,1})\left(1-\left[\tau_3\left(1-\Theta_1^{s2}\gamma_{th,1}\right)+\tau_4\left(1-\Theta_1^{r2}\gamma_{th,1}\right)\right]\right)+ (1-(1-\Theta_1^{sr}\gamma_{th,1}))\left(1-\left(1-\Theta_1^{s2}\gamma_{th,1}\right)\right), \tag{4.33}$$

$$P_2^{asym}(out) = \left(1-\Theta_2^{Sr}\gamma_{th,2}\right)\left(1-\left[\tau_5\left(1-\Theta_2^{S2}\gamma_{th,2}\right)+\tau_6\exp\left(-\Theta_2^{r2}\gamma_{th,2}\right)\right]\right) + \left(1-\left(1-\Theta_2^{Sr}\gamma_{th,2}\right)\right)\left(1-\left(1-\Theta_2^{S2}\gamma_{th,2}\right)\right). \tag{4.34}$$

4.2.1.3 Bit error rate analysis

In this section, we derive the BER expressions for three different schemes, namely NOMA, CNOMA, and CNOMA-WDL. The analysis is performed for both users over the Rayleigh fading channels. To modulate the messages of users U_1 and U_2 at S and R, we employ the Binary Phase-Shift Keying (BPSK) modulation technique.

1) BER of NOMA system

The BER for x_1 symbols in the presence of the effects of HWI and ipCSI is given as:

$$P_{x_1,m} = \frac{1}{2}\sum_{i=1}^{2}\mathrm{Q}\left(\sqrt{2\Delta_{x_1,m,i}}\right),\ m = Sr;\ S1;\ r1, \tag{4.35}$$

where

$\Delta_{x_1,Sr,i} = \frac{P_s\psi_i|\tilde{h}_{Sr}|^2}{N_0+2P_sk_{Sr}^2|\tilde{h}_{Sr}|^2+2(k_{Sr}^2+\psi_i)P_s\sigma_\epsilon^2}$, $\Delta_{x_1,S1,i} = \frac{P_s\Psi_z|\tilde{h}_{S1}|^2}{N_0+2P_sk_{S1}^2|\tilde{h}_{S1}|^2+2(k_{s1}^2+\Psi_i)P_s\sigma_\epsilon^2}$,

$\Delta_{x_1,r1,i} = \frac{P_r\Psi_i|\tilde{h}_{r1}|^2}{N_0+2P_rk_{r1}^2|\tilde{h}_{r1}|^2+2(k_{r1}^2+\Psi_i)P_r\sigma_\epsilon^2}$, with $\Psi_i = [(\sqrt{\alpha_1}+\sqrt{\alpha_2})^2, (\sqrt{\alpha_1}-\sqrt{\alpha_2})^2]$ is given according to modulation order.

Proof: Please see Appendix D.

The average BER (ABER) is given as:

$$P_{e2e,x_1,m} = \frac{1}{4}\sum_{i}^{2}\left(1-\sqrt{\frac{\bar{\Delta}_{x_1,m,i}}{1+\bar{\Delta}_{x_1,m,i}}}\right), \tag{4.36}$$

where $\bar{\Delta}_{x_1,m,i} = \mathrm{E}[\Delta_{x_1,m,i}]$, E[.] is an expectation operator. To detect x_2 symbols, each node utilizes a SIC process. The BER for x_2 symbols at each node is determined by combining both the correct and erroneous detections of the x_1 symbols during the SIC process. Therefore, the BER for x_2 at R and user U_2 can be expressed as:

$$P_{x_2,n} = \frac{1}{4}\sum_{j=1}^{6} g_j \mathrm{Q}\left(\sqrt{2\Delta_{x_2,n,j}}\right), \text{ where } n = Sr,\ S2,\ r2, \tag{4.37}$$

where

$\Delta_{x_2,Sr,j} = \frac{P_s \upsilon_j |\tilde{h}_{Sr}|^2}{N_0 + 2P_s k_{Sr}^2 |\tilde{h}_{Sr}|^2 + 2(k_{Sr}^2 + \omega_j) P_s \sigma_\epsilon^2}$, $\Delta_{x_2,S2,j} = \frac{P_s \upsilon_j |\tilde{h}_{S2}|^2}{N_0 + 2P_s k_{S2}^2 |\tilde{h}_{S2}|^2 + 2(k_{S2}^2 + \omega_j) P_s \sigma_\epsilon^2}$,

$\Delta_{x_2,r2,j} = \frac{P_r \upsilon_j |\tilde{h}_{r2}|^2}{N_0 + 2P_r k_{r2}^2 |\tilde{h}_{r2}|^2 + 2(k_{r2}^2 + \omega_j) P_r \sigma_\epsilon^2}$, $\mathbf{g}_j = [1, 1, -1, 1, 1, -1]$,

$\boldsymbol{\upsilon}_j = [\alpha_2, \alpha_2, (\sqrt{\alpha_1} + \sqrt{\alpha_2})^2, (2\sqrt{\alpha_1} + \sqrt{\alpha_2})^2, (\sqrt{\alpha_1} - \sqrt{\alpha_2})^2, (2\sqrt{\alpha_1} - \sqrt{\alpha_2})^2]$, and
$\boldsymbol{\omega}_j = [(\sqrt{\alpha_1}+\sqrt{\alpha_2})^2, (\sqrt{\alpha_1}-\sqrt{\alpha_2})^2, (\sqrt{\alpha_1}+\sqrt{\alpha_2})^2, (\sqrt{\alpha_1}+\sqrt{\alpha_2})^2, (\sqrt{\alpha_1}-\sqrt{\alpha_2})^2, (\sqrt{\alpha_1}-\sqrt{\alpha_2})^2]$.

Proof: Please see Appendix E

By utilizing the alternate form of Q(.) function and the moment generating function (MGF). the ABER of x_2 at the R and U_2 is expressed as:

$$P_{e2e,x_2,n} = \frac{1}{4}\sum_{j=1}^{6} g_j \left(1 - \sqrt{\frac{\bar{\delta}_{x_2,n,j}}{1 + \bar{\delta}_{x_2,n,j}}}\right), \tag{4.38}$$

where $\bar{\delta}_{x_2,n,j} = \mathrm{E}[\delta_{x_2,n,j}]$.

2) BER of CNOMA system

The e2e BER expressions in the CNOMA for both users are given as [105]:

$$P_{e2e,i}^{(\mathsf{CNOMA})} = P_{e2e,x_i,Sr}\left(1 - P_{e2e,x_i,r,i}\right) + \left(1 - P_{e2e,x_i,Sr}\right) P_{e2e,x_i,r,i},\ i = 1, 2 \tag{4.39}$$

where $P_{e2e,x_i,Sr}$ and $P_{e2e,x_i,r,i}$ are the BER of the U_1 and U_2 symbols in R defined in (4.36) and (4.38).

3) BER of CNOMA-WDL system

The e2e BER expressions in CNOMA-WDL for the users under the HWI and ipCSI are given as [59]:

$$P_{e2e,i}^{(\mathsf{CNOMA-WDL})} = \frac{1}{2}\sum_{f} g_f[P_{x_i}^{\mathsf{err-prop}} \times P_{x_i,Sr} + (1-P_{x_i,Sr})P_{x_i}^{\mathsf{coop-MRC}},\ f=i,\ j, \tag{4.40}$$

where $P_{x_i,Sr}$ is given in (4.36) and (4.38). Each term can be presented as:

BER of cooperative diversity with MRC

The BER of the U_1 with diversity combines the two signals from different sources, one from S and one from R is expressed by [59], [112, pp. 320-321]:

$$P_{x_1}^{\mathsf{coop-MRC}} = \mathrm{Q}\left(\sqrt{2(\Delta_{x_1,S1,i}+\Delta_{x_1,r1,i})}\right). \tag{4.41}$$

The Average Bit Error Rate (ABER) for the cooperative-MRC of two branches at U_1 is considered when the mean Signal-to-Noise Ratios (SNRs) of the two branches are different $\bar{\Delta}_{x_1,S1,i} \neq \bar{\Delta}_{x_1,r1,i}$) is presented as:

$$P_{x_1}^{\mathsf{coop-MRC}} = \frac{1}{2}\left(1-\frac{1}{\bar{\Delta}_{x_1,S1,i}-\bar{\Delta}_{x_1,r1,i}}\left(\bar{\Delta}_{x_1,S1,i}\sqrt{\frac{\bar{\Delta}_{x_1,S1,i}}{1+\bar{\Delta}_{x_1,s1,i}}}-\bar{\Delta}_{x_1,r1,i}\sqrt{\frac{\delta_{x_1,r1,i}}{1+\bar{\Delta}_{x_1,r1,i}}}\right)\right). \tag{4.42}$$

The BER for cooperative-MRC after the SIC process to detect U_2 symbols can be presented [59, 112]:

$$P_{x_2}^{\mathsf{coop-MRC}} = \mathrm{Q}\left(\sqrt{2(\Delta_{x_2,S2,j}+\delta_{x_2,r2,j})}\right). \tag{4.43}$$

The ABER for cooperative-MRC of two signals at U_2 when the mean of the SNRs of branches are different (i.e., $\bar{\Delta}_{x_2,S2,j} \neq \bar{\Delta}_{x_2,r2,j}$) is given by [59, 113] as:

$$P_{x_2}^{\mathsf{coop-MRC}}\{s_{sc}\in j\} = \frac{1}{2}\left(1-\frac{1}{\bar{\Delta}_{x_2,S2,j}-\bar{\Delta}_{x_2,r2,j}}\left(\bar{\Delta}_{x_2,S2,j}\sqrt{\frac{\bar{\Delta}_{x_2,S2,j}}{1+\bar{\Delta}_{x_2,S2,j}}}-\bar{\Delta}_{x_2,r2,j}\sqrt{\frac{\bar{\Delta}_{x_2,r2,j}}{1+\bar{\Delta}_{x_2,r2,j}}}\right)\right). \tag{4.44}$$

After implementing MRC, we characterize the total received signal to assess the BER considering error propagation from U_1 and U_2. In this scenario, we assume that S sent a symbol

(+1) for U_1 and another symbol (+1) for U_2. During the SIC process at the R, the symbol of U_1 is erroneously detected as (-1). Consequently, after the SIC process, symbol U_2 is also erroneously detected as (-1) as [46, 114].

BER of cooperative MRC in the error propagation

The sum of the received signals at U_1 through MRC in the error propagation is given as:

$$\begin{aligned} \lambda_{x_1}^{\mathsf{err-prop}} &= \tilde{h}_{S1}^{*} y_{S1} + \tilde{h}_{r1}^{*} y_{r1} \\ &= (\lambda_{x_1,S1,i} - \lambda_{x_1,r1,i}) + \tilde{n}_1, \end{aligned} \tag{4.45}$$

where $\lambda_{x_1,S1,i} = P_s \Psi_i |\tilde{h}_{S1}|^2$ and $\lambda_{x_1,r1,i} = P_r \Psi_i |\tilde{h}_{r1}|^2$. However, $\tilde{n}_1$ is defined as $\mathbf{E}[\tilde{n}_1] \sim \mathcal{CN}(0, \frac{N_0}{2}[\sigma_{\tilde{h}_{S1}}^2 + \sigma_{\tilde{h}_{r1}}^2] + k_{S1}^2 P_s \sigma_{\tilde{h}_{S1}^2} \sigma_\epsilon^2 + k_{S1}^2 P_s \sigma_{\tilde{h}_{S1}}^2 + k_{r1}^2 P_r \sigma_{\tilde{h}_{r1}}^2 {\sigma_\epsilon}^2 + k_{r1}^2 P_r \sigma_{\tilde{h}_{r1}}^2 + P_s \Psi_i \sigma_{\tilde{h}_{S1}}^2 \sigma_\epsilon^2 + P_r \Psi_i \sigma_{\tilde{h}_{r1}}^2 \sigma_\epsilon^2)$.

Therefore, the BER representing the error propagation for the U_1 symbols can be defined as:

$$\begin{aligned} P_{x_1}^{\mathsf{err-prop}} &= P(\lambda_{x_1,S1,i} - \lambda_{x_1,r1,i} < \tilde{n}_1) \\ &= \mathrm{Q}\left(\frac{\lambda_{x_1,S1,i} - \lambda_{x_1,r1,i}}{\sqrt{\Omega_1}} \right), \end{aligned} \tag{4.46}$$

where $\Omega_1 = \frac{N_0}{2}[\sigma_{\tilde{h}_{S1}}^2 + \sigma_{\tilde{h}_{r1}}^2] + k_{S1}^2 P_s \sigma_{\tilde{h}_{S1}}^2 \sigma_\epsilon^2 + k_{S1}^2 P_s \sigma_{\tilde{h}_{S1}}^2 + k_{r1}^2 P_r \sigma_{\tilde{h}_{r1}}^2 {\sigma_\epsilon}^2 + k_{r1}^2 P_r \sigma_{\tilde{h}_{r1}}^2 + P_s \Psi_i \sigma_{\tilde{h}_{S1}}^2 \sigma_\epsilon^2 + P_r \Psi_i \sigma_{\tilde{h}_{r1}}^2 \sigma_\epsilon^2$.

It is observed that when R forwards an incorrect symbol, the effect of this is more pronounced in causing erroneous detection than the impact of additive noise. Thus, we can approximate the BER as $\lambda_{x_1,S1,i} - \lambda_{x_1,r1,i} < 0$ [59].

The BER considering the error propagation is presented as:

$$P_{x_1}^{\mathsf{err-prop}} = P(\lambda_{x_1,S1,i} - \lambda_{x_1,r1,i} < 0). \tag{4.47}$$

The ABER of x_1 in the error propagation is expressed as:

$$P_{x_1}^{\mathsf{err-prop}} = \frac{\bar{\lambda}_{x_1,r1,i}}{\bar{\lambda}_{x_1,r1,i} + \bar{\lambda}_{x_1,S1,i}}, \tag{4.48}$$

where $\bar{\lambda}_{x_1,S1,i} = \mathrm{E}[\lambda_{x_1,S1,i}] = P_s \Psi_z \sigma^2_{\tilde{h}_{S1}}$ and $\bar{\lambda}_{x_1,r1,i} = \mathrm{E}[\lambda_{x_1,r1,i}] = P_r \psi_z \sigma^2_{\tilde{h}_{r1}}$.

Furthermore, after combining the signals from S and R at U_2, the total received signal at U_2 is defined as:

$$\lambda_{x_2}^{\mathsf{err-prop}} = \tilde{h}^*_{S2} y_{S2} + \tilde{h}^*_{r2} y_{r2}. \tag{4.49}$$

Hence, the summation of the received signal at U_2 after the detection of symbols through the SIC process is given as:

$$\lambda_{x_2}^{\mathsf{err-prop}} = (\lambda_{x_2,S2,j} - \lambda_{x_2,r2,j}) + \tilde{n}_2, \tag{4.50}$$

where $\lambda_{x_2,S2,j} = P_s \upsilon_j |\tilde{h}_{S2}|^2$ and $\lambda_{x_2,r2,j} = P_r \upsilon_j |\tilde{h}_{r2}|^2$. $\tilde{n}_2$ is the effective noise with $\mathbf{E}[\tilde{n}_2] \sim \mathcal{CN}(0, \frac{N_0}{2}[\sigma^2_{\tilde{h}_{S2}} + \sigma^2_{\tilde{h}_{r2}}] + k^2_{S2} P_s \sigma^2_{\tilde{h}_{S2}} \sigma^2_\epsilon + k^2_{S2} P_s \sigma^2_{\tilde{h}_{S2}} + k^2_{r2} P_r,\ \sigma^2_{\tilde{h}_{r2}} {\sigma_\epsilon}^2 + k^2_{r2} P_r \sigma^2_{\tilde{h}_{r2}} + P_s \upsilon_j \sigma^2_{\tilde{h}_{S2}} \sigma^2_\epsilon + P_r \upsilon_j \sigma^2_{\tilde{h}_{r2}} \sigma^2_\epsilon)$.

Therefore, the BER for the U_2 of the error propagation is expressed as:

$$\begin{aligned} P_{x_2}^{\mathsf{err-prop}} &= P(\lambda_{x_2,S2,j} - \lambda_{x_2,r2,j} < \tilde{n}_2) \\ &= \mathrm{Q}\left(\frac{\lambda_{x_2,S2,j} - \lambda_{x_2,r2,j}}{\sqrt{\Omega_2}}\right), \end{aligned} \tag{4.51}$$

where $\Omega_2 = \frac{N_0}{2}[\sigma^2_{\tilde{h}_{S2}} + \sigma_{\tilde{h}^2_{r2}} + k^2_{S2} P_s \sigma^2_{\tilde{h}_{S2}} \sigma^2_\epsilon + k^2_{S2} P_s \sigma^2_{\tilde{h}_{S2}} + k^2_{r2} P_r \sigma^2_{\tilde{h}_{r2}} {\sigma_\epsilon}^2 + k^2_{r2} P_r \sigma^2_{\tilde{h}_{r2}} + P_s \upsilon_j \sigma^2_{\tilde{h}_{s2}} \sigma^2_\epsilon + P_r \upsilon_j \sigma^2_{\tilde{h}_{r2}} \sigma^2_\epsilon$. We can estimate the BER for the SIC to detect x_2 $(\lambda_{x_2,S2,j} - \lambda_{x_2,r2,j} < 0)$.

Therefore, the BER of x_2 in the error propagation is presented as:

$$P_{x_2}^{\mathsf{err-prop}} = P(\lambda_{x_2,S2,j} - \lambda_{x_2,r2,j} < 0). \tag{4.52}$$

The ABER of x_2 in the error propagation is expressed as:

$$P_{x_2}^{\mathsf{err-prop}} = \frac{\bar{\lambda}_{x_2,r2,j}}{\bar{\lambda}_{x_2,r2,j} + \bar{\lambda}_{x_2,S2,j}}, \tag{4.53}$$

where $\bar{\lambda}_{x_2,S2,j} = \mathrm{E}[\lambda_{x_2,S2,j}] = P_s \upsilon_j \sigma^2_{\tilde{h}_{S2}}$ and $\bar{\lambda}_{x_2,S2,j} = \mathrm{E}[\lambda_{x_2,r2,j}] = P_r \upsilon_j \sigma^2_{\tilde{h}_{r2}}$.

Finally, to obtain the e2e BER of the CNOMA-WDL for U_1, we substituted (4.36), (4.42), and (4.48) into (4.39).
Likewise, substituting (4.38), (4.44), and (4.53) into (4.39), we obtain the e2e BER of the CNOMA-WDL for U_2.

4.3 Numerical results

In this section, the performance of the three different scenarios of the NOMA system (i.e. NOMA, CNOMA, and CNOMA-WDL) with practical Constraints: HWI, ipCSI, and ipSIC are evaluated in terms of BER and OP over the Rayleigh fading channel. The parameters are set as the HWI level is defined as [49]:$k_{s,1} = k_{S2} = k_{r1} = k_{r2} = k$, $d_{s,1} = 4$m, $d_{S2} = 2$m, $d_{Sr} = 1$m, $d_{r1} = 3$m, $d_{r2} = 1$m, $P_r = P_s$, $\alpha_1 = 0.8$, and $\alpha_2 = 0.2$.

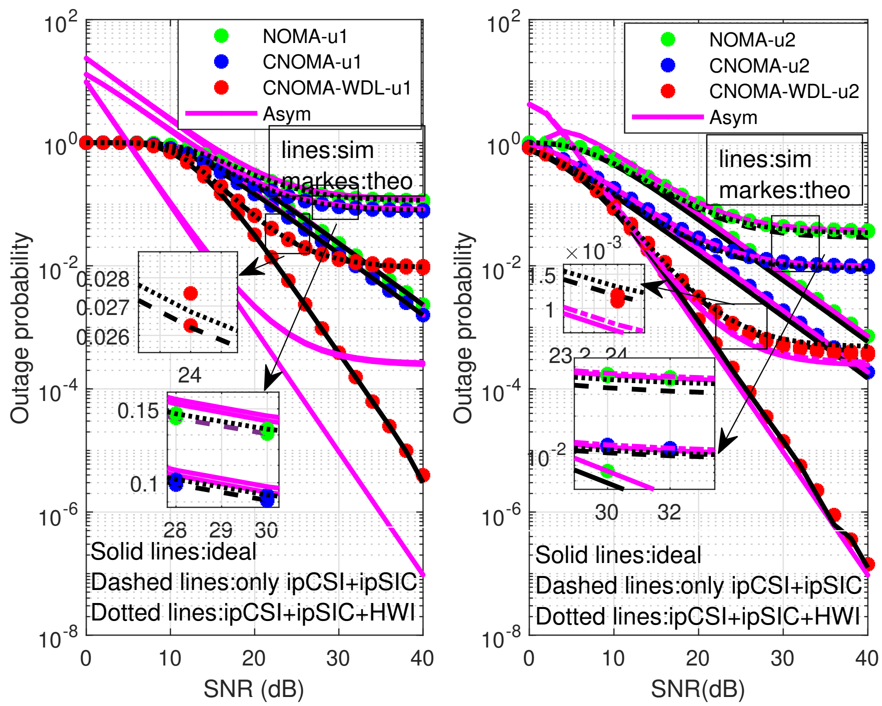

Figure 4.2: OP performances of different NOMA schemes versus SNR with $\sigma_\epsilon^2 = 0.005$.

The OP and BER performance of the different scenarios of the NOMA in the function of the SNR is evaluated in Figs. 4.2 and 4.3, where the HWI is considered as $k = 0.175$ and ipCSI factor $\sigma_\epsilon = 0.005$. It becomes evident that the inclusion of ipCSI and ipSIC leads to a degradation in the OP performance. Additionally, the presence of HWI decreases the

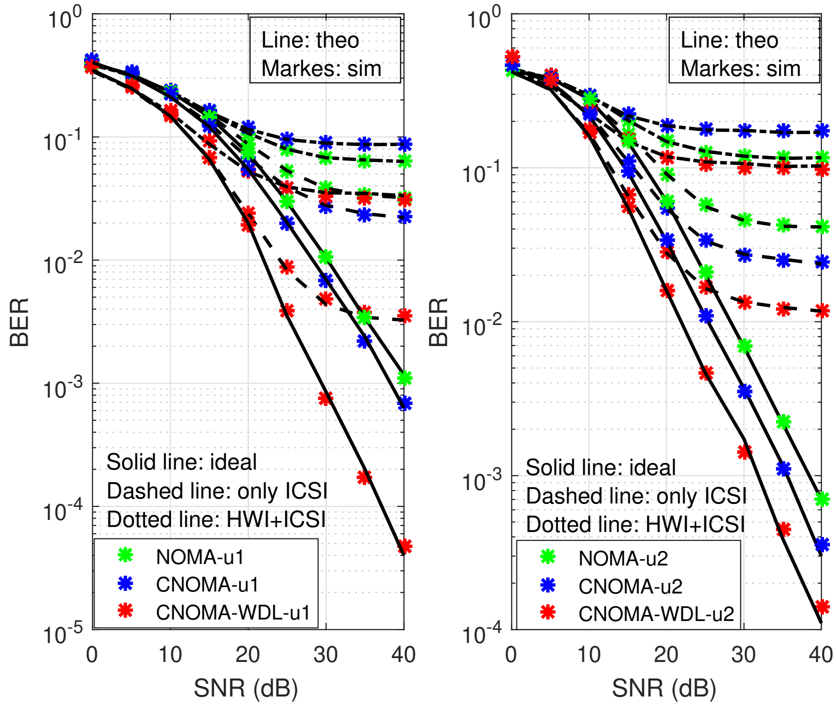

Figure 4.3: BER performances of different NOMA schemes versus SNR, when $\sigma_{\epsilon}^{2} = 0.005$.

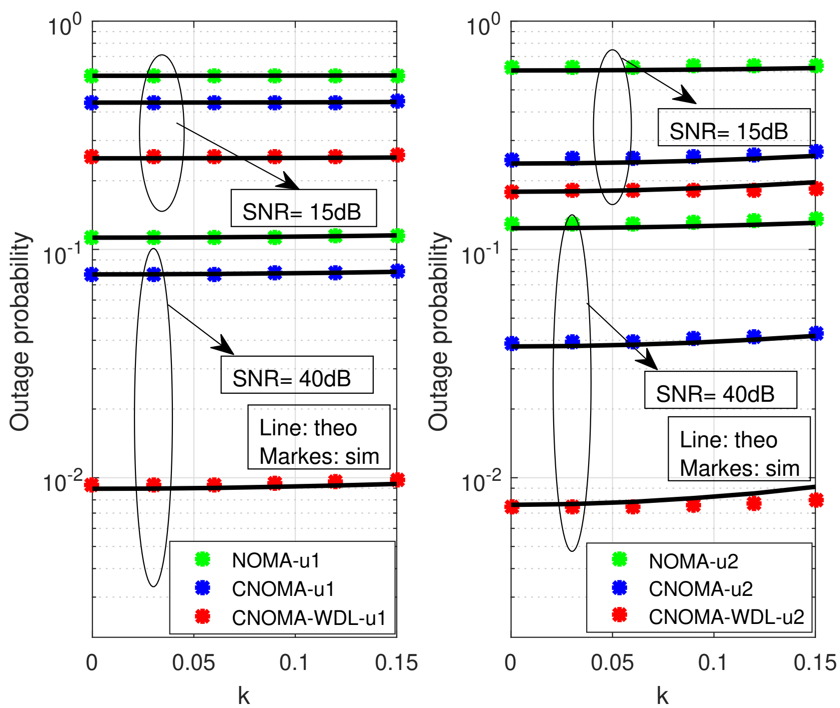

Figure 4.4: OP performances of different NOMA schemes versus HWI, when $\sigma_{\epsilon}^{2} = 0.005$.

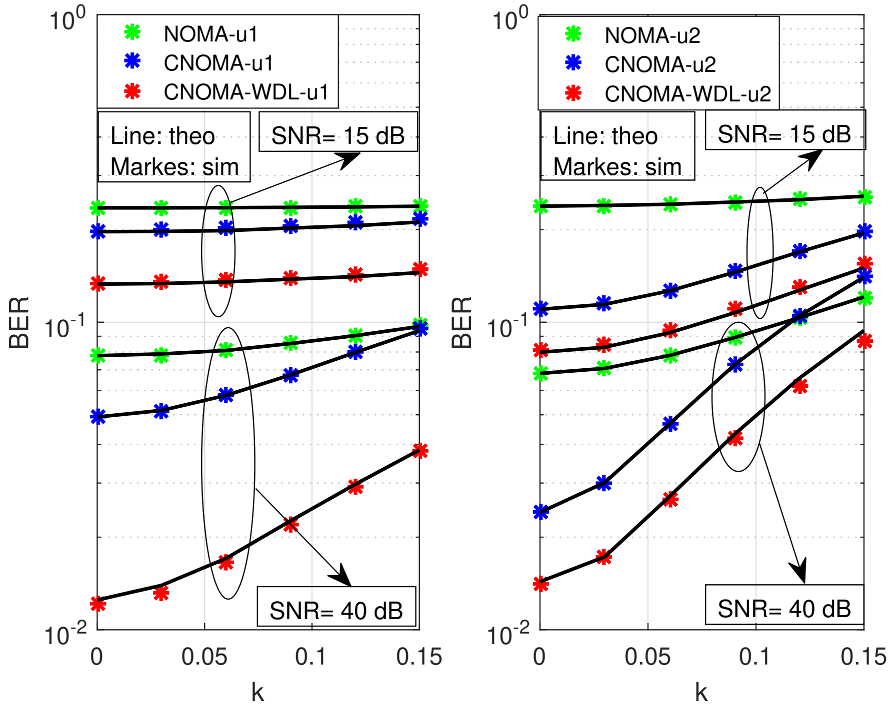

Figure 4.5: BER performances of different NOMA schemes w.r.t HWI level, when $\sigma_\epsilon^2 = 0.005$.

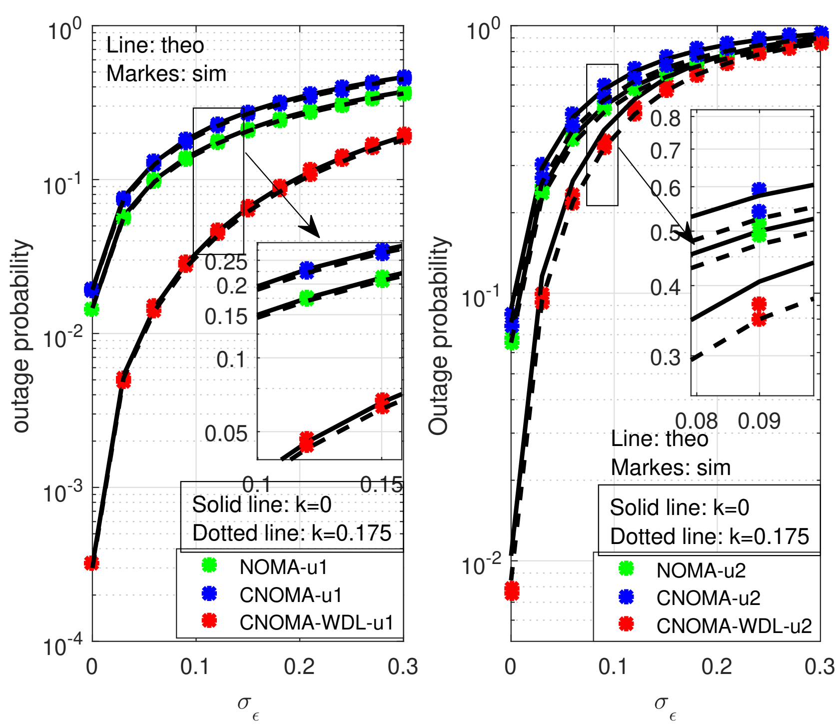

Figure 4.6: OP performances of different NOMA schemes w.r.t ipCSI with SNR= 20 dB.

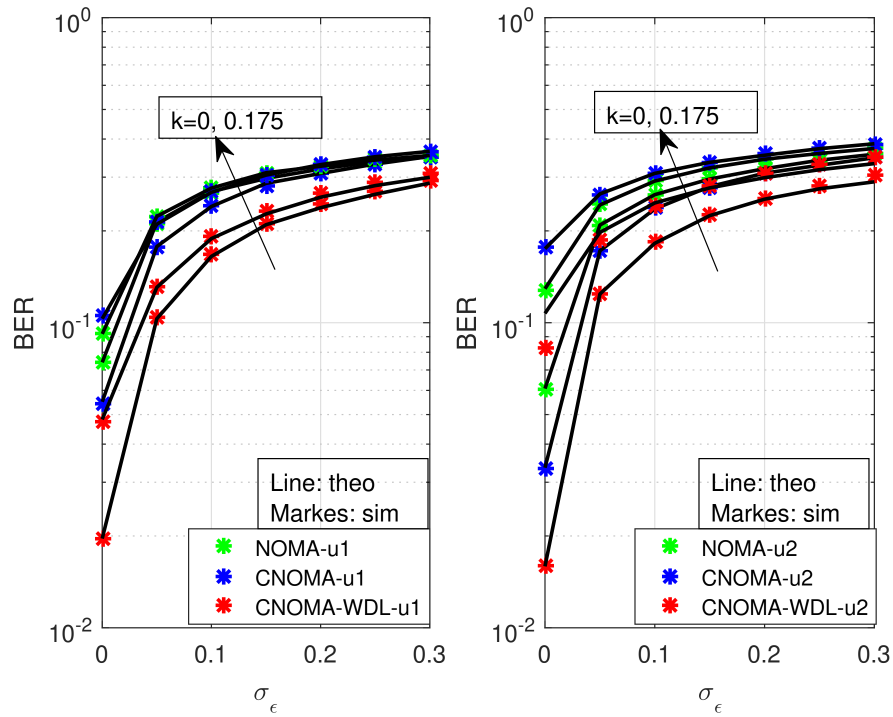

Figure 4.7: BER performances of different NOMA schemes w.r.t σ_ϵ^2, when SNR= 20 dB.

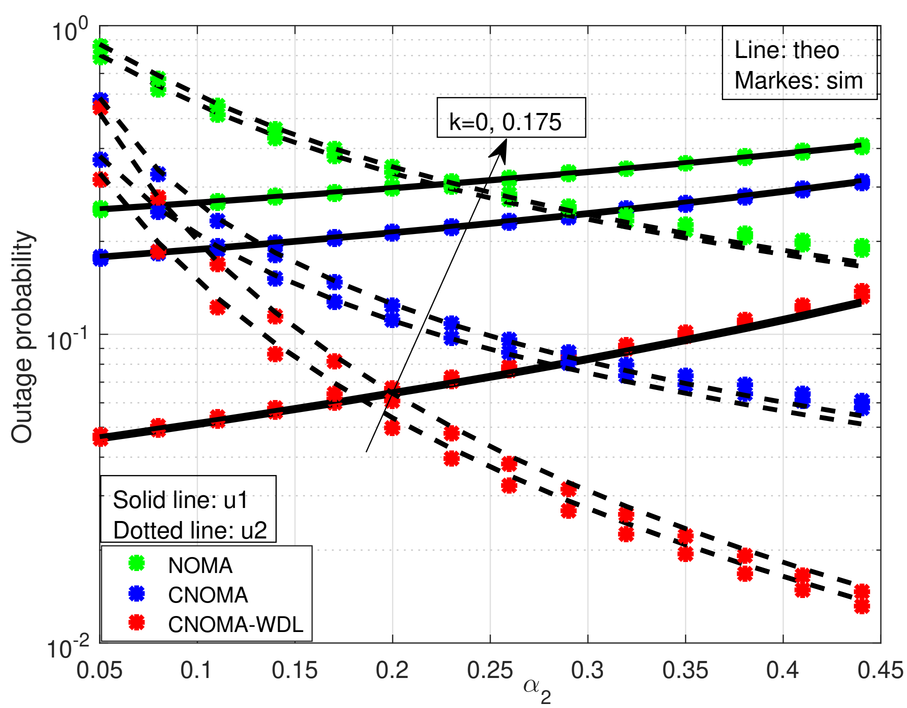

Figure 4.8: OP performances of different NOMA schemes w.r.t of PA, when $\sigma_\epsilon^2 = 0.005$.

OP performance for both users, although its effect is less pronounced when compared to the impact of ipCSI. The performance of CNOMA-WDL surpasses the performance of both CNOMA and NOMA. Also, we notice in Fig. 4.2 that at a high SNR, the asymptotic OP curve is limited compared to the theoretical curves.

The effect of the HWI is examined in Figs. 4.4 and 4.5 in terms of OP and BER performance of the three schemes of the NOMA system. it can be observed that as the level of HWI increases the OP and BER performance of all schemes degrades. Also, the performance of CNOMA surpasses the direct NOMA.

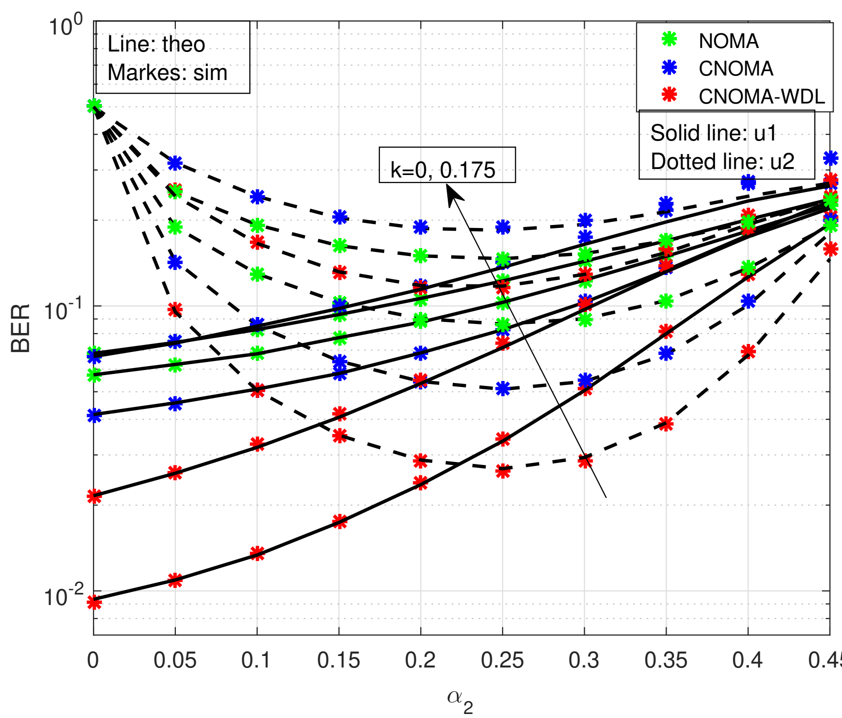

Figure 4.9: BER performances of different NOMA schemes versus σ_ϵ^2, when SNR= 20 dB.

Figs. 4.6 and 4.7 depict the impact of ipCSI on the OP and BER on the different NOMA schemes with different k values and SNR= 20 dB. It can be observed that the performance degrades as the ipCSI factor increases. Additionally, when comparing the impact of ipCSI with that of HWI, the latter has a lesser influence on the outage performance.

The OP and BER performance in the function of the PA with SNR= 20 dB and $\sigma_\epsilon^2 = 0.005$ is presented in Figs. 4.8 and 4.9. With an increase of α_2, the performance of U_2 degrades,

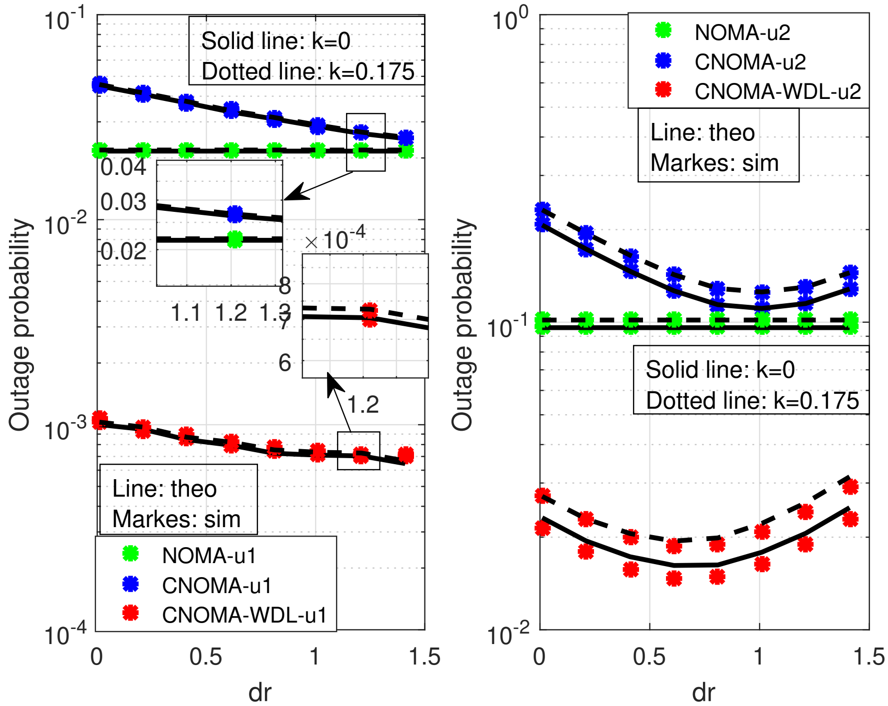

Figure 4.10: OP performances of different NOMA schemes w.r.t d_r when $\sigma_\epsilon^2 = 0.005$.

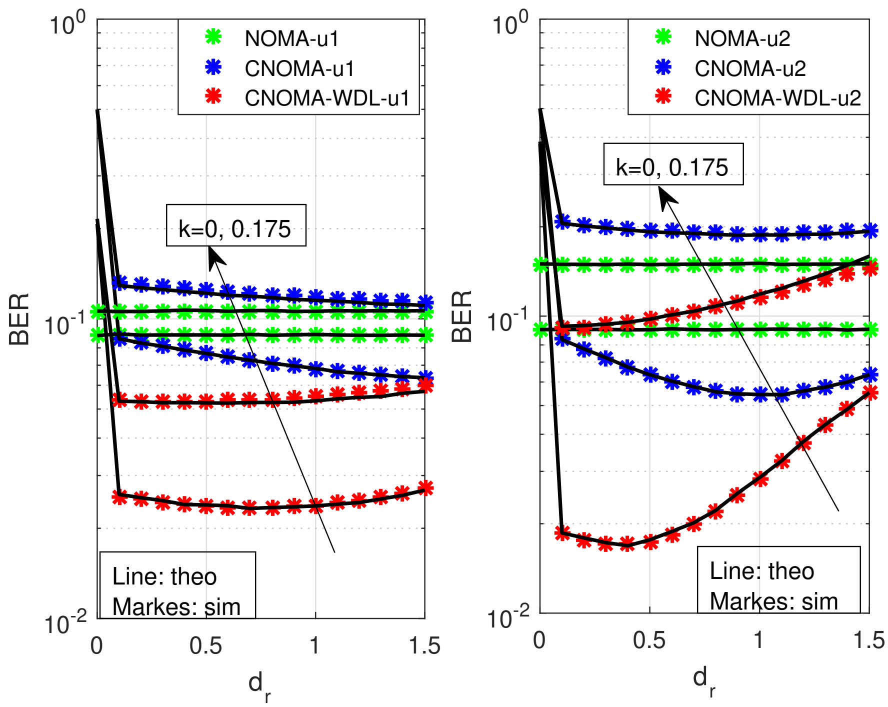

Figure 4.11: BER performances of different NOMA schemes w.r.t d_r, when $\sigma_\epsilon^2 = 0.005$.

while in contrast, the performance of U_1 improves. Hence, with the increase in HWI, the performance of all NOMA schemes deteriorates, particularly impacting U_2 more significantly than U_1 due to the SIC process.

Fig. 4.10 and 4.11 evaluate the OP and BER performance of the different NOMA schemes in the function of the distance of R. It can be observed that when the distance of R is nearer to the middle, both users achieve improved performance. The OP and BER performance in both the first and second phases is influenced by the distance between the S and both users.

4.4 Conclusion

In this chapter, we examined the OP and BER performance of three NOMA schemes: downlink NOMA, and cooperative NOMA with and without direct links under practical assumptions. We considered all imperfections such as HWI, ipCSI and ipSIC. The expressions for the end-to-end OP and BER were derived for all schemes, and their theoretical validity was verified through computer simulations.

Additionally, we delved into the influence of HWI, ipCSI, PA, and distance R on the OP and BER performances. Our findings indicated that each of these parameters played a crucial role in determining the performance of the various NOMA schemes.

Chapter 5

Impact of IQI on the Cooperative NOMA system

5.1 Introduction

With the rapid development of the Internet of things (IoT), the beyond 5G network must support massive user and device connectivity to meet the demand for low latency, spectral efficiency and diverse service types. As a promising solution, non-orthogonal multiple access (NOMA) gets more attention due to its ability to meet these requirements. To improve spectral efficiency, NOMA is integrated with a variety of techniques, including cooperative communication and multiple input multiple outputs (MIMO) [115, 116, 60]. In cooperative NOMA (CNOMA), there are two schemes, CNOMA without the direct links and CNOMA with the direct links. In the CNOMA scheme without the direct links, it is assumed that the users cannot receive the base station (BS) signal, so it is used to extend the coverage area and help the very far users or users who suffer from channel disorders. In the CNOMA with the direct links, it is considered that the users can receive the signal from the BS and relay so the users can improve their performance by employing one of the diversity techniques (e.g., maximum ratio combining (MRC)).

5.1.1 Related works

To evaluate the performance of the CNOMA without the direct links, a reversed decode-forward (DF) CNOMA under the imperfect successive interference canceler (ipSIC) and imperfect channel state information (ipCSI) have been analyzed in terms of the outage probability (OP) and ergodic capacity (EC) [56]. To overcome the problems associated with poor channel quality and disconnection communication between the BS and users, the multi-hop for CNOMA to deliver the signal to the users everywhere has been performed and examined in [105]. In [117], the OP and throughput of the CNOMA over Nakagami-m fading channels were examined.

Also, to evaluate the performance of CNOMA with direct links, the authors in [118, 119] analyzed the system capacity and OP of DF relaying for CNOMA. The OP performance of the three CNOMA schemes have been analyzed in [80]. The incremental relay for CNOMA to improve OP performance has been examined in [120]. The authors of [121, 122] evaluate the OP and achievable rate performance of the CNOMA with and without the direct links under ipCSI over the Nakagami-m fading channels. In [123], the ergodic sum rate has been derived for CNOMA with direct links. A full-duplex (FD) and half-duplex (HD) for CNOMA with the direct links have been analyzed in terms of the OP, EC and energy efficiency [85]. The EC and OP for threshold-based selective CNOMA have been analyzed to provide a reliable alternative for traditional CNOMA networks [124]. The authors of [125] investigate the ergodic sum capacity and OP of the uplink CNOMA over the Rayleigh fading channel. An FD CNOMA-based coordinated direct and relay transmission has been analyzed in terms of the OP and ergodic rate under the effect of the residual interference generated due to the ipSIC [126].

On the other hand, direct-conversion transceivers are an interesting radio frequency (RF) front-end option since they do not require external intermediate frequency filters or image rejection filters [127]. Due to their high-speed data transfer, low costs low power dissipation, and their architectures are assumed to be ideal candidates for wireless technologies [128]. However, in practice, the direct-conversion transceiver suffers from RF front-end due to component mismatch and imperfect manufacturing, such as in-phase and quadrature-phase imbalance (IQI). These refer to the amplitude and phase mismatch between a transceiver's I and Q branches and cause imperfect image rejection with significant performance limits [6].

The I and Q branches of the mixer in an ideal transceiver should have identical amplitude and exactly 90 phase shift, which is not realistic [65]. In practical implementations, IQI exists in the direct-conversion transceiver due to the inadequate analog components employed in the transceiver. In [13], the authors analyze the impact of IQI on the performance of different modulations under multipath fading channels. The effects of IQI on the OP of both single-carrier and multi-carrier systems cascaded Nakagami-m fading channels were evaluated [129]. The exact closed-form expression of the OP and EC of the amplify-and-forward (AF) relay under IQI over the Nakagami-m fading channel has been derived in [130]. An FD CNOMA system under IQI and ipSIC in terms of OP and ergodic sum-rate have been examined [131]. The authors in [30] examine the reliability and security of a cooperative dual-hop NOMA system in the presence of IQI. The effect of IQI and ipSIC in terms of OP has been evaluated on the CNOMA system over the Nakagami-m fading channel in [132]. The OP and intercept probability (IP) have been examined for NOMA with multi-antenna under IQI over the Nakagami-m fading [74]. In [133, 134], the outage performance and ergodic rate for the ambient backscatter communication (AmBC) NOMA system with both IQI and residual hardware impairments (RHIs) has been investigated. To investigate the reliability and security of AmBC NOMA, the OP and the IP have been analyzed in [75, 135]. The authors in [76, 136] evaluate the error performance of downlink NOMA with the effects of IQI and ipSIC.

5.1.2 Motivations and Contributions

As mentioned above, the CNOMA has been analyzed in terms of the OP, EC in the two NOMA schemes with and without the direct links [56, 105, 117, 118, 119, 80, 120, 121, 122, 123, 85, 124, 125, 126]. All these works are considered the ideal case, so this is not practical. The RF front-end impairments are usually ignored in the literature due to their negative influence on the CNOMA system's performance. Hence, it is important to consider this topic, considering the critical significance of this issue to the actual implementation of NOMA/C-NOMA systems. The OP, EC, and throughput for CNOMA in the presence of IQI have been evaluated in [13, 129, 130, 30]. Most of these works consider CNOMA in the presence of IQI without a direct link between the source and users due to long distances or obstacles, etc.

Correspondingly, CNOMA in the presence of IQI when the direct and relay links are available has not been considered to the best of the author's knowledge. Furthermore, all works of NOMA/CNOMA with IQI assumed the perfect CSI [13, 129, 130, 30, 74]. The assumption of the perfect CSI is not a practical and realistic scenario. Motivated by this, this chapter analyzes the effect of the IQI on the CNOMA system when the direct and relay links are available, where the ipCSI is taken into consideration. In this context, the contributions of this chapter are as follows:

- Since users receive signals from different sources, the MRC is used by users to combine the received signals. In this regard, we introduce a CNOMA with direct links under IQI. Also, for more realistic assumptions with the IQI effect, the ipCSI is taken into account in our considered system.

- To illustrate the system's performance, the end-to-end (e2e) OP and throughput are derived for our considered system under the IQI and ipCSI.
- The comparison of this model with conventional NOMA (i.e., NOMA direct link) and the impact of the image rejection ratio (IRR) and power allocation (PA) are examined on the CNOMA/NOMA system performance. Since the distance between the relay and users affects the users' performance, also the evaluation of the impact of the relay's distance on the performance of CNOMA in the presence of IQI and ipCSI. Comprehensive Monte-Carlo simulation results are presented to confirm the derived expressions.

5.2 System model

In our analysis, we examine a downlink CNOMA system where both direct and relay links are available to users, as illustrated in Fig. 5.1. The model system comprises a Source (S), a DF relay (R), and two users identified as the far user (U_1) and the near user (U_2). All nodes work in HD mode and are equipped with a single antenna. The channel coefficient of the links S-users, S-R, and R-users are defined by $h_i \sim \mathcal{CN}(0,\ \sigma_i^2)$ and $h_j \sim \mathcal{CN}(0,\ \sigma_j^2)$, where $i = S1, S2, SR$ and $j = R1, R2$. We also consider that the ipCSI exists for all nodes, where the estimation channel coefficients are defined as $\tilde{h}_i = h_i - e$ and $\tilde{h}_j = h_j - e$, with $e \sim \mathcal{CN}(0,\ \sigma_e^2)$.

The transmission is divided into two separate time slots. In the first time slot, S transmits the superimposed coding (S_{sc}) signal to both R and the users. In the second time slot, R combines the previously encoded signals to create a new S_{sc} signal, following the same method as the source, and forwards it to the users. U_1 directly decodes its signal using MLD, while U_2 employs SIC to decode its signal. as defined in eq.(3.2). According to the NOMA protocol, The received signal at the first phase under IQI and ipCSI is given as:

$$\begin{aligned} {y_i}^{IQI} &= \mu_{r,i}((\tilde{h}_i + e)\sqrt{P_s}(\mu_{t,i}S_{sc} + \nu_{t,i}{S_{sc}}^*) + n) \\ &+ \nu_{r,i}((\tilde{h}_i + e)\sqrt{P_s}(\mu_{t,i}S_{sc} + \nu_{t,i}{S_{sc}}^*) + n)^*,\ i = S1, S2, SR, \end{aligned} \tag{5.1}$$

where $X_{sc} = \sqrt{\alpha_1}x_1 + \sqrt{\alpha_2}x_2$ with α_1, α_2 are the PA coefficient for U_1 and U_2 messages, re-

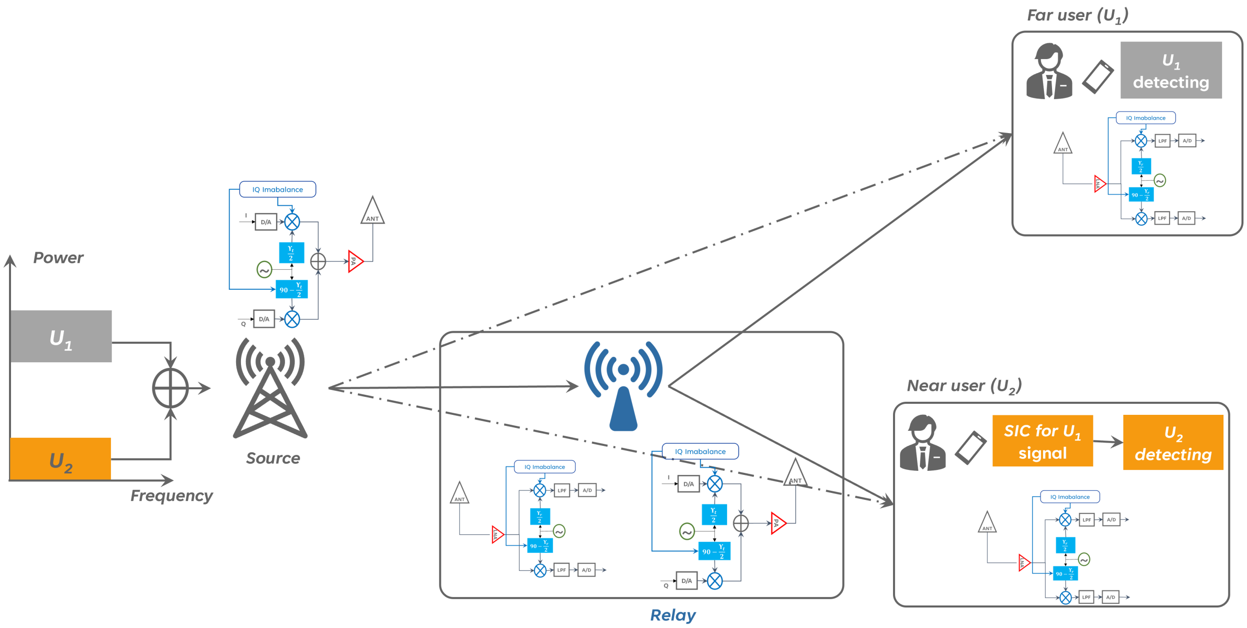

Figure 5.1: System model of the uplink NOMA under IQI.

spectively and P_s is the transmit power of S. n is the additive white Gaussian noise (AWGN) with $CN(0,\ N_0)$, $\mu_{t,i/r,i}$ and $\nu_{t,i/r,i}$ are the IQI coefficients at the TX/RX which are presented in (3.3).
The received SINR of the x_1 at the first time slot (i.e., at R, U_1 and U_2) under ipCSI is given by:

$$\gamma_{x_1}^{S1} = \frac{\delta_{1,S1}\alpha_1\lambda_s|\tilde{h}_{S1}|}{\delta_{1,S1}\alpha_2\lambda_s|\tilde{h}_{S1}| + \delta_{1,S1}\lambda_s\sigma_e^2 + \delta_{2,S1}\lambda_s|\tilde{h}_{S1}| + \delta_{2,S1}\lambda_s\sigma_e^2 + \delta_{3,S1}}, \tag{5.2}$$

$$\gamma_{x_1}^{S2\rightarrow S1} = \frac{\delta_{1,S2}\alpha_1\lambda_s|\tilde{h}_{S2}|}{\delta_{1,S2}\alpha_2\lambda_s|\tilde{h}_{S2}| + \delta_{1,S2}\lambda_s\sigma_e^2 + \delta_{2,S2}\lambda_s|\tilde{h}_{S2}| + \delta_{2,S2}\lambda_s\sigma_e^2 + \delta_{3,S2}}, \tag{5.3}$$

$$\gamma_{x_1}^{SR} = \frac{\delta_{1,SR}\alpha_1\lambda_s|\tilde{h}_{SR}|}{\delta_{1,SR}\alpha_2\lambda_s|\tilde{h}_{SR}| + \delta_{1,SR}\lambda_s\sigma_e^2 + \delta_{2,SR}\lambda_s|\tilde{h}_{SR}| + \delta_{2,sR}\lambda_s\sigma_e^2 + \delta_{3,SR}}, \tag{5.4}$$

where $\delta_{1,i} = \mu_{t,i}^2\mu_{r,i}^2 + \nu_{t,i}^2\nu_{r,i}^2$, $\delta_{2,i} = \mu_{r,i}^2\nu_{t,i}^2 + \nu_{r,i}^2\mu_{t,i}^2$, $\delta_{3,i} = \mu_{r,i}^2 + \nu_{r,i}^2$ and λ_s is the transmit signal to noise ratio (SNR) by S with $\lambda_s = \frac{P_s}{N_0}$.

On the other hand, Un and R employ the SIC process to eliminate the x_1 signal and detect the x_2 signal. Therefore, assuming perfect SIC and ipCSI, the SINR of the x_2 signal at U_2 and R can be defined as follows:

$$\gamma_{x_2}^{S2} = \frac{\delta_{1,S2}\alpha_2\lambda_s|\tilde{h}_{S2}|}{\delta_{1,S2}\lambda_s\sigma_e^2 + \delta_{2,s2}\alpha_2\lambda_s|\tilde{h}_{S2}| + \delta_{2,S2}\lambda_s\sigma_e^2 + \delta_{3,S2}}, \tag{5.5}$$

$$\gamma_{x_2}^{SR} = \frac{\delta_{1,SR}\alpha_2\lambda_s|\tilde{h}_{SR}|}{\delta_{1,SR}\lambda_s\sigma_e^2 + \delta_{2,SR}\alpha_2\lambda_s|\tilde{h}_{SR}| + \delta_{2,SR}\lambda_s\sigma_e^2 + \delta_{3,SR}}. \tag{5.6}$$

Similarly, in the second time slot, we consider that both users, U_1 and U_2, are affected by the presence of both IQI and ipCSI. However, we can express the received signal at U_1 and U_2 as follows

$$\begin{aligned} {y_j}^{IQI} =& \mu_{r,j}((\tilde{h}_j + e)\sqrt{P_R}(\mu_{t,j}S_{sc} + \nu_{t,j}{S_{sc}}^*) + n_j) + \nu_{r,j}((\tilde{h}_j + e) \\ & \times \sqrt{P_R}(\mu_{t,j}S_{sc} + \nu_{t,j}{S_{sc}}^*) + n)^*, \ j = R1, R2, \end{aligned} \tag{5.7}$$

where P_r transmit power of R, n is the AWGN with $CN(0,\ N_0)$.

The received SINR at U_1 and U_2 to decode the signal x_1 symbol is defined, respectively as:

$$\gamma_{x1}^{R1} = \frac{\delta_{1,R1}\alpha_1\lambda_R|\tilde{h}_{R1}|}{\delta_{1,R1}\alpha_2\lambda_R|\tilde{h}_{R1}| + \delta_{1,R1}\lambda_R\sigma_e^2 + \delta_{2,R1}\lambda_R|\tilde{h}_{R1}| + \delta_{2,R1}\lambda_R\sigma_e^2 + \delta_{3,R1}}, \tag{5.8}$$

$$\gamma_{x1}^{R2\to R1} = \frac{\delta_{1,R2}\alpha_1\lambda_R|\tilde{h}_{R2}|}{\delta_{1,R2}\alpha_2\lambda_R|\tilde{h}_{R2}| + \delta_{1,R2}\lambda_R\sigma_e^2 + \delta_{2,R2}\lambda_R|\tilde{h}_{R2}| + \delta_{2,R2}\lambda_R\sigma_e^2 + \delta_{3,R2}}. \tag{5.9}$$

U_2 uses the SIC process to eliminate the interference caused by the x_1 signal. Assuming perfect cancellation, we can obtain the received SINR at U_2 as:

$$\gamma_{x2}^{R2} = \frac{\delta_{1,R2}\alpha_2\lambda_R|\tilde{h}_{R2}|}{\delta_{1,R2}\lambda_R\sigma_e^2 + \delta_{2,R2}\alpha_2\lambda_R|\tilde{h}_{R2}| + \delta_{2,R2}\lambda_R\sigma_e^2 + \delta_{3,R2}}, \tag{5.10}$$

where $\delta_{1,j} = \mu_{t,j}^2\mu_{r,i}^2 + \nu_{t,j}^2\nu_{r,j}^2$, $\delta_{2,j} = \mu_{r,j}^2\nu_{t,j}^2 + \nu_{r,j}^2\mu_{t,j}^2$, $\delta_{3,j} = \mu_{r,j}^2 + \nu_{r,j}^2$ and λ_R is the transmit SNR by R $\lambda_R = \frac{P_r}{N_0}$.

5.3 Performance analysis

In this section, we derive the e2e expression of the Op and throughput of the considered system where the IQI and ipCSI are taken into account over the Rayleigh fading channel.

5.3.1 Outage probability

The outage can be defined as the event when the user or node cannot decode the received signal. The expression of OP of U_1 under IQI and ipCSI using the MRC to combine the two received signals can be given as [110]:

$$P_{out,U_1} = (1 - P(\gamma_{x1}^{SR} < \theta_1))P(\gamma_{x1}^{S1} + \gamma_{x1}^{R1} < \theta_1) + P(\gamma_{x1}^{SR} < \theta_1)P(\gamma_{x1}^{S1} < \theta_1), \tag{5.11}$$

where $P(\gamma_{x1}^{SR} < \theta_1)$ is the OP of x_1 at R, $P(\gamma_{x1}^{S1} < \theta_1)$ is the OP of x_1 at U_1, $P(\gamma_{x1}^{S1} + \gamma_{x1}^{R1} < \theta_1)$ is the OP of x_1 at U_1 when MRC is used and $\theta_1 = 2^{2r1} - 1$ is the threshold to detect x_1, $r1$ is the target rate of x_1. Each term of the eq. (5.11) can be expressed as:

$$P(\gamma_{x1}^{S1} < \theta_1) = 1 - \exp\left(-\Theta_1\theta_1\right), \tag{5.12}$$

$$P(\gamma_{x1}^{SR} < \theta_1) = 1 - \exp\left(-\Theta_2\theta_1\right), \tag{5.13}$$

where

$\Theta_1 = \frac{(\delta_{3,S1}+\delta_{2,S1}\lambda_s\sigma_e^2+\delta_{1,S1}\lambda_s\sigma_e^2)}{\varphi_{S1}(\delta_{1,S1}\alpha_1-\delta_{1,S1}\alpha_2\theta_1-\delta_{2,S1}\theta_1)\lambda_s}$, $\Theta_2 = \frac{(\delta_{3,SR}+\delta_{2,SR}\lambda_s\sigma_e^2+\delta_{1,SR}\lambda_s\sigma_e^2)}{\varphi_{SR}(\delta_{1,SR}\alpha_1-\delta_{1,SR}\alpha_2\theta_1-\delta_{2,SR}\theta_1)\lambda_s}$, and

$\varphi_{S1} = E[|\tilde{h}_{S1}|^2], \varphi_{SR} = E[|\tilde{h}_{SR}|^2]$.

To evaluate the OP of the U_1, it is crucial to determine the distribution of two independent exponential random variables X and Y, with X $\neq$ Y, the CDF of two independent exponential random variables Z=X+Y can be expressed as [110, eq. (6)]:

$$P(X + Y < k) = 1 - \left[\frac{X}{X - Y}\exp\left(-\frac{X}{Y}\right) + \frac{X}{Y - X}\exp\left(-\frac{K}{Y}\right)\right] X \neq Y. \tag{5.14}$$

Given that γ_{x1}^{S1} and γ_{x1}^{R1} are independent exponential random variables, with $\gamma_{x1}^{S1} \neq \gamma_{x1}^{R1}$, we can calculate the probability $P(\gamma_{x1}^{S1} + \gamma_{x1}^{R1} < \theta_1)$ as:

$$P(\gamma_{x1}^{S1} + \gamma_{x1}^{R1} < \theta_1) = 1 - \left[\frac{\Theta_1}{\Theta_1 - \Theta_3}\exp\left(-\Theta_1\theta_1\right) + \frac{\Theta_3}{\Theta_3 - \Theta_1}\exp\left(-\Theta_3\theta_1\right)\right] \Theta_1 \neq \Theta_3, \tag{5.15}$$

where $\Theta_3 = \frac{(\delta_{3,R1}+\delta_{2,R1}\lambda_s\sigma_e^2+\delta_{1,R1}\lambda_s\sigma_e^2)}{\varphi_{R1}(\delta_{1,R1}\alpha_1-\delta_{1,R1}\alpha_2\theta_1-\delta_{2,R1}\theta_1)\lambda_s}$.

Replacing (5.12), (5.13), and (5.15) into (5.11), the P_{out,U_1} can be given as:

$$\begin{aligned} P_{out,U_1} =& \exp\left(-\Theta_2\theta_1\right)\left(1-\left[\frac{\Theta_1}{\Theta_1-\Theta_3}\exp\left(-\Theta_1\theta_1\right)+\frac{\Theta_3}{\Theta_3-\Theta_1}\exp\left(-\Theta_3\theta_1\right)\right]\right)+ \\ & \left(1-\exp\left(-\Theta_2\theta_1\right)\right)\left(1-\exp\left(-\Theta_1\theta_1\right)\right). \end{aligned} \quad (5.16)$$

At U_2, two signals are received from distinct sources: one from the source and the other from R. To combine the two received signals, U_2 employs MRC. The detection of x_2 is based on whether U_2 can successfully detect x_1. Consequently, the OP at U_2, representing the MRC output to detect x_2, can be expressed as:

$$P_{out,U_2} = P^{MRC}_{out,U_2\to U_1} + \left(1 - P^{MRC}_{out,U_2\to U_1}\right) P^{MRC}_{out,U_2}, \quad (5.17)$$

where $P^{MRC}_{out,U_2\to U_1}$ is the OP to detect x_1 at U_2 at output MRC and P^{MRC}_{out,U_2} is the OP at output MRC when the SIC is used at U_2 to detect x_2, it can be presented as:

$$P^{MRC}_{out,U_2\to U_1} = (1 - P\left(\gamma^{SR}_{x1} < \theta_1\right))P\left(\gamma^{S2}_{x1} + \gamma^{SR}_{x1} < \theta_1\right) + P\left(\gamma^{SR}_{x1} < \theta_1\right)P\left(\gamma^{S2}_{x1} < \theta_1\right), \quad (5.18)$$

where $P\left(\gamma^{S2}_{x1} + \gamma^{SR}_{x1} < \theta_1\right)$ is the OP after implentation of MRC of x_1 at U_2, $P\left(\gamma_{SR} < \theta_1\right)$ is defined in (5.13). Each term can be given as:

$$P\left(\gamma^{S2}_{x1} < \theta_1\right) = 1 - \exp\left(-\Theta_4\theta_1\right), \quad (5.19)$$

$$P(\gamma^{S2}_{x1} + \gamma^{SR}_{x1} < \theta_1) = 1 - \left[\frac{\Theta_4}{\Theta_4-\Theta_5}\exp\left(-\Theta_4\theta_1\right) + \frac{\Theta_5}{\Theta_5-\Theta_4}\exp\left(-\Theta_5\theta_1\right)\right]\Theta_4 \neq \Theta_5, \quad (5.20)$$

where

$$\Theta_4 = \frac{(\delta_{3,S2}+\delta_{2,S2}\lambda_s\sigma_e^2+\delta_{1,S2}\lambda_s\sigma_e^2)}{\varphi_{S2}(\delta_{1,S2}\alpha_1-\delta_{1,S2}\alpha_2\theta_1-\delta_{2,S2}\theta_1)\lambda_s},\ \Theta_5 = \frac{(\delta_{3,R2}+\delta_{2,R2}\lambda_s\sigma_e^2+\delta_{1,R2}\lambda_s\sigma_e^2)}{\varphi_{R2}(\delta_{1,R2}\alpha_1-\delta_{1,S2}\alpha_2\theta_1-\delta_{2,R2}\theta_1)\lambda_s}.$$

Replaying (5.13), (5.19) and (5.20), we find the OP of x_1 at U_2 at output MRC as presented as:

$$P_{out,U_2\to U_1}^{MRC} = \exp\left(-\Theta_2\theta_1\right)\left(1-\left[\frac{\Theta_4}{\Theta_4-\Theta_5}\exp\left(-\Theta_4\theta_1\right)+\frac{\Theta_5}{\Theta_5-\Theta_4}\exp\left(-\Theta_5\theta_1\right)\right]\right)+ \\ \left(1-\exp\left(-\Theta_2\theta_1\right)\right)\left(1-\exp\left(-\Theta_4\theta_1\right)\right). \tag{5.21}$$

The OP at the output of MRC, when SIC is implemented at U_2 to detect x_2, is presented as:

$$P_{out,U_2}^{MRC} = (1-P(\gamma_{x2}^{SR}<\theta_2))P(\gamma_{x2}^{S2}+\gamma_{x2}^{R2}<\theta_2)+P(\gamma_{x2}^{SR}<\theta_2)P(\gamma_{s2}<\theta_2), \tag{5.22}$$

where $P(\gamma_{x2}^{S2}+\gamma_{x2}^{R2}<\theta_2)$ is the OP of x_2 at U_2 when MRC is implemented, $P(\gamma_{x2}^{SR}<\theta_2)$ is the OP to detect x_2 at R and $P(\gamma_{x2}^{S2}<\theta_2)$ is the OP of x_2 at U_2. $\theta_2 = 2^{2r2}-1$ is the threshold to detect x_2, $r2$ is the target rate to detect x_2. Each term can be determined as:

$$P(\gamma_{x2}^{S2}<\theta_2) = 1-\exp\left(-\Theta_6\theta_2\right), \tag{5.23}$$

$$P(\gamma_{x2}^{SR}<\theta_2) = 1-\exp\left(-\Theta_7\theta_2\right), \tag{5.24}$$

$$P(\gamma_{x2}^{S2}+\gamma_{x2}^{R2}<\theta_2) = 1-\left[\frac{\Theta_8}{\Theta_8-\Theta_6}\exp\left(-\Theta_8\theta_2\right)+\frac{\Theta_6}{\Theta_6-\Theta_8}\exp\left(-\Theta_6\theta_2\right)\right]\Theta_8\neq\Theta_6, \tag{5.25}$$

where

$\Theta_6 = \frac{(\delta_{3,S2}+\delta_{2,S2}\lambda_s\sigma_e^2+\delta_{1,S2}\lambda_s\sigma_e^2)\theta_2}{\varphi_{S2}(\delta_{1,S2}\alpha_2\theta_2-\delta_{2,s2}\theta_2)\lambda_s}$, $\Theta_7 = \frac{(\delta_{3,SR}+\delta_{2,SR}\lambda_s\sigma_e^2+\delta_{1,SR}\lambda_s\sigma_e^2)\theta_2}{\varphi_{SR}(\Delta_{1,SR}\alpha_2\theta_2-\delta_{2,SR}\theta_2)\lambda_s}$,

$\Theta_8 = \frac{(\delta_{3,R2}+\delta_{2,R2}\lambda_s\sigma_e^2+\delta_{1,R2}\lambda_s\sigma_e^2)}{\varphi_{R2}(\Delta_{1,R2}\alpha_2\theta_2-\delta_{2,R2}\theta_2)\lambda_s}$, and $\varphi_{S2} = E[|\tilde{h}_{S2}|^2]$,

Hence, by substituting (5.23), (5.24), and (5.25), we get the OP of x_2 at U_n at output MRC as:

$$P_{out,U_2}^{MRC} = \exp\left(-\Theta_7\theta_2\right)\left(1-\left[\frac{\Theta_8}{\Theta_8-\Theta_6}\exp\left(-\Theta_8\theta_2\right)+\frac{\Theta_6}{\Theta_6-\Theta_8}\exp\left(-\Theta_6\theta_2\right)\right]\right)+ \\ (1-\exp\left(-\Theta_7\theta_2\right))(1-\exp\left(-\Theta_6\theta_2\right)). \tag{5.26}$$

Therefore, we get the OP of U_2 at output MRC by replacing (5.21) and (5.26) into (5.17).

5.3.2 Throughput performance

This subsection analyses the throughput of the considered system. Hence, the expression of the throughput can be given:

$$\tau = (1 - P_{out,U_2})r2 + (1 - P_{out,U_1})r1, \tag{5.27}$$

where P_{out,U_1} and P_{out,U_2} are the OP of U_2 and U_1 at output MRC expressed in (5.16) and (5.17), respectively.

5.4 Numerical results

In this section, the performance of CNOMA with direct links considering IQI and ipCSI is examined in terms of OP and throughput performance and compared with the performance of the conventional NOMA. The simulation results are validated through the numerical results. The parameters used in the simulations are set to d_{S1}=5m, d_{S2}=2m, d_{SR}=1m, d_{R1}=4m, d_{R2}=1m, $\alpha_1 = 0.9$, α_2=0.1, σ_e^2=0, 0.01 and path loss factor is equal to 3. We also consider that the P_s=P_r and IRR=IRR_t=IRR_r.

Fig. 5.2 illustrates the OP behavior of CNOMA with respect to SNR under IQI and ipCSI conditions. The target rate is set to $R_1 = R_2 = 0.1$ and $IRR = 20dB$. Despite the presence or absence of the IQI and ipCSI, the OP of CNOMA consistently outperforms that of NOMA for both users.

Furthermore, the users under ideal IQI conditions exhibit better OP compared to those in non-ideal conditions. Notably, the introduction of ipCSI detrimentally impacts the OP performance for both users, especially at high SNR levels.

The OP of the CNOMA versus IRR is presented in Fig. 5.3 when the parameters are set as $R_1 = 0.1$ and $R_2 = 0.4$ and $SNR = 20$ dB. As the IRR increases, the performance of OP for users improves, gradually approaching a level of the ideal scenario without IQI. The differences observed in the gaps between the ideal IQ-matching and IQI curves highlight the diverse effects of IQI on the OP performance among different users in the system. Moreover, the presence of ipCSI negatively affects the performance of the OP in both scenarios (ideal

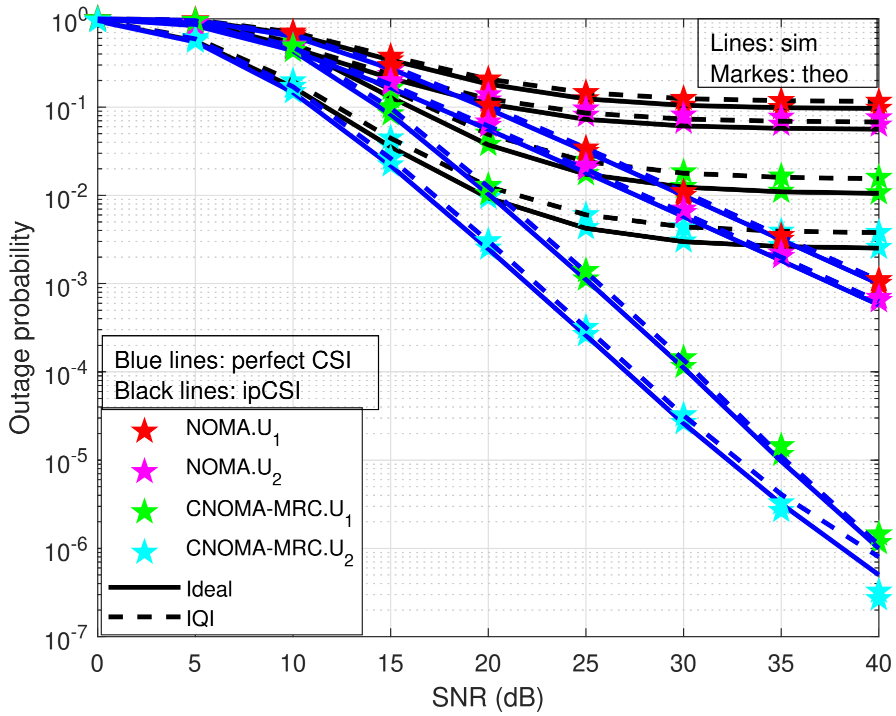

Figure 5.2: OP of CNOMA w.r.t SNR when $IRR = 20$ dB.

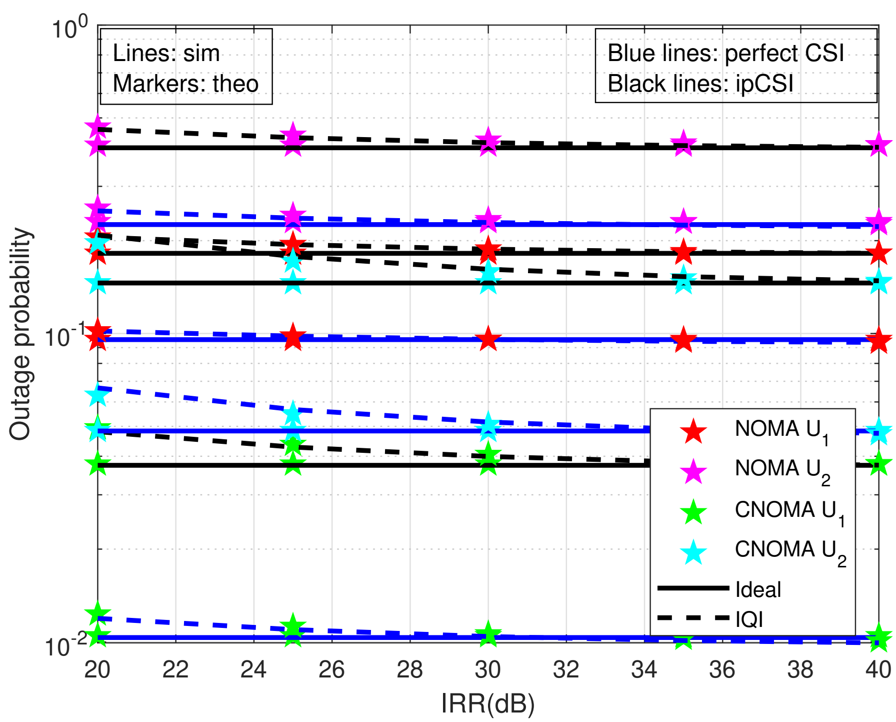

Figure 5.3: OP of CNOMA w.r.t IRR when $SNR = 20$ dB.

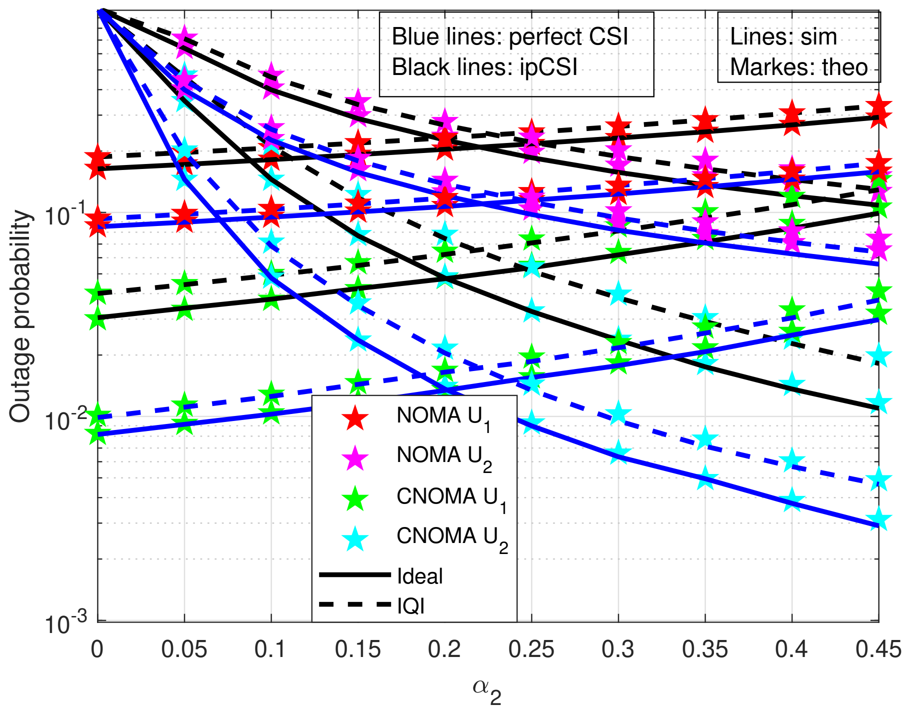

Figure 5.4: OP of CNOMA w.r.t PA when $IRR = 20$ dB.

and non-ideal IQI).

Fig. 5.4 illustrates the OP of the CNOMA in the function of PA when $R_1 = 0.1$ and $R_2 = 0.4$, SNR= $20dB$, and IRR=$20dB$. In the presence or absence of the IQI and ipCSI, With the increase of α_2, the performance of one user deteriorates, whereas the performance of the other user improves. Therefore, the PA coefficient plays a crucial role in determining the system's performance in the presence of imperfections.

Fig. 5.5 presents the OP performance of the CNOMA in the function of the distance of R, the parameters are set as SNR= $20dB$, $IRR = 20dB$ and $R_1 = R_2 = 0.1$. It can be observed that both users experience improved performance when R is situated closer to the middle distance between S and the users. Increased or decreased distance between the source and both users leads to a higher level of outage performance in both the first and second phases.

On the other hand, in Fig. 5.6, we present the CNOMA performance in the function of the SNR, where the parameters are considered as $SNR = 20$ dB, $R_1 = R_2 = 0.1$ and $\sigma_e^2 = 0.001$. As we can see, in both ideal and non-ideal scenarios, the CNOMA system demonstrates

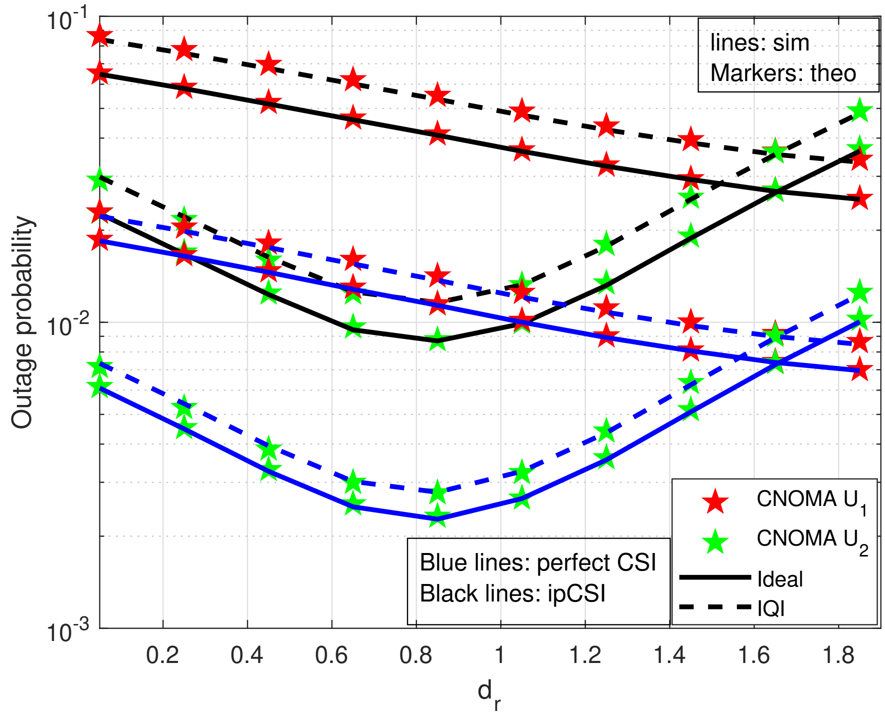

Figure 5.5: OP of CNOMA w.r.t d_r when $IRR = 20$ dB.

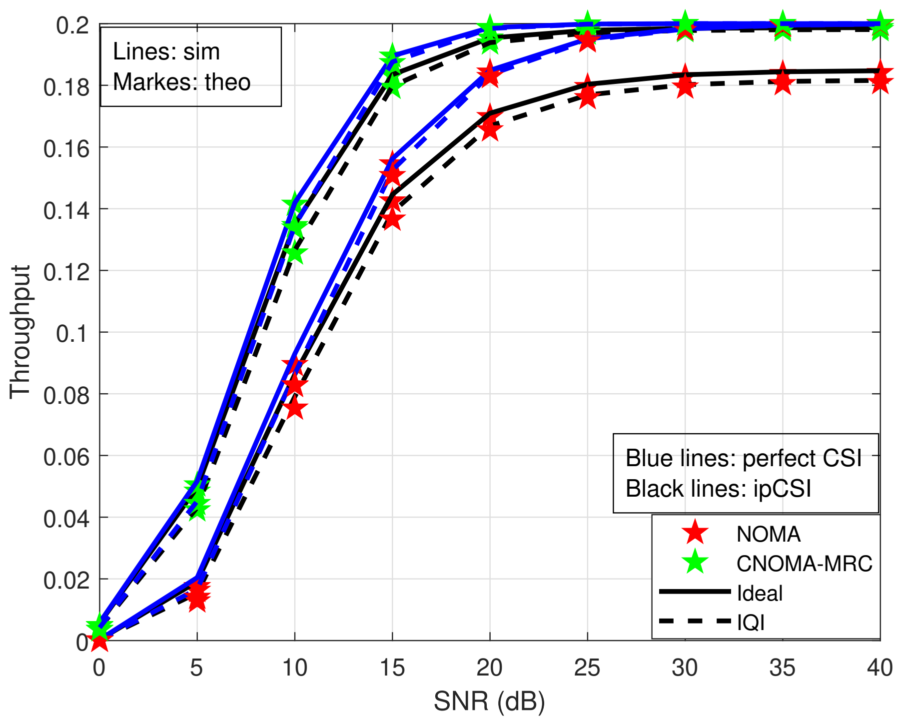

Figure 5.6: Throughput of CNOMA w.r.t SNR when $IRR = 20$ dB.

superior throughput performance compared to the NOMA system. Also, it is evident that the ideal IQI exhibits a greater performance improvement in throughput compared to the non-ideal condition. Also, the ipCSI has a negative impact on the throughput performance in both ideal and non-ideal IQI scenarios.

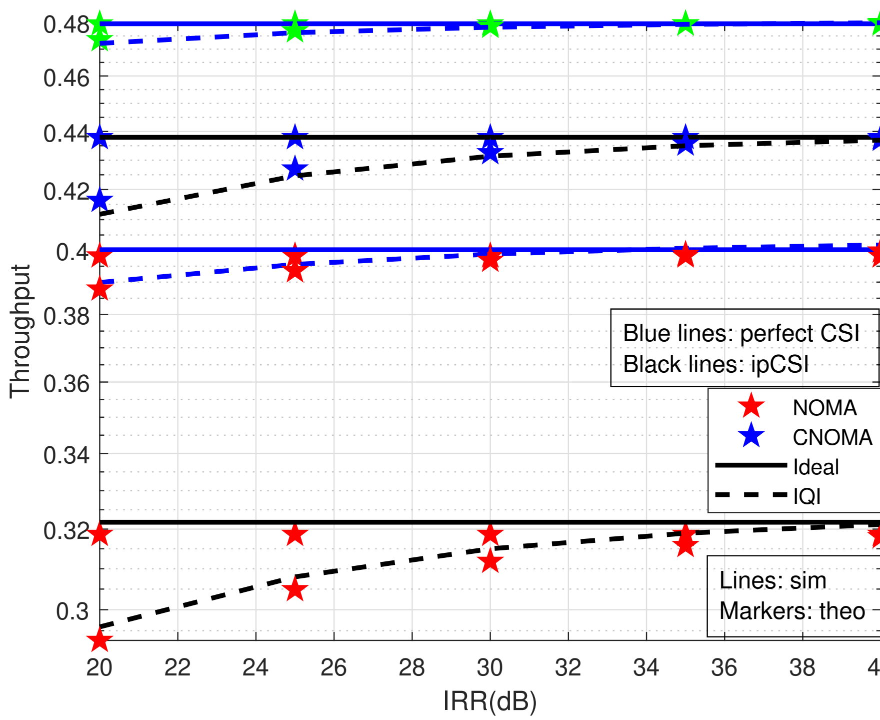

Figure 5.7: Throughput of CNOMA w.r.t IRR when $SNR = 20$ dB.

The throughput of the CNOMA w.r.t IRR is presented in Fig. 5.7 when $SNR = 20$ dB, $R_1 = 0.1$ and $R_2 = 0.4$. As the IRR increases, the throughput of the NOMA and CNOMA increases approaching performance levels similar to the ideal case (without IQI) at higher IRR values. the presence of ipCSI has a negative effect on the throughput performance in both ideal and non-ideal IQI. Therefore, the CNOMA enhances the throughput of NOMA in both ideal/non-ideal scenarios.

The impact of the PA is depicted in Fig. 5.8 with $IRR = 20dB$ and $SNR = 20dB$, it can be observed that As α_2 increases, one user's performance degrades, while the other user's performance improves, regardless of the presence or absence of imperfections. Also, the performance of the CNOMA is better than the NOMA system in all cases.

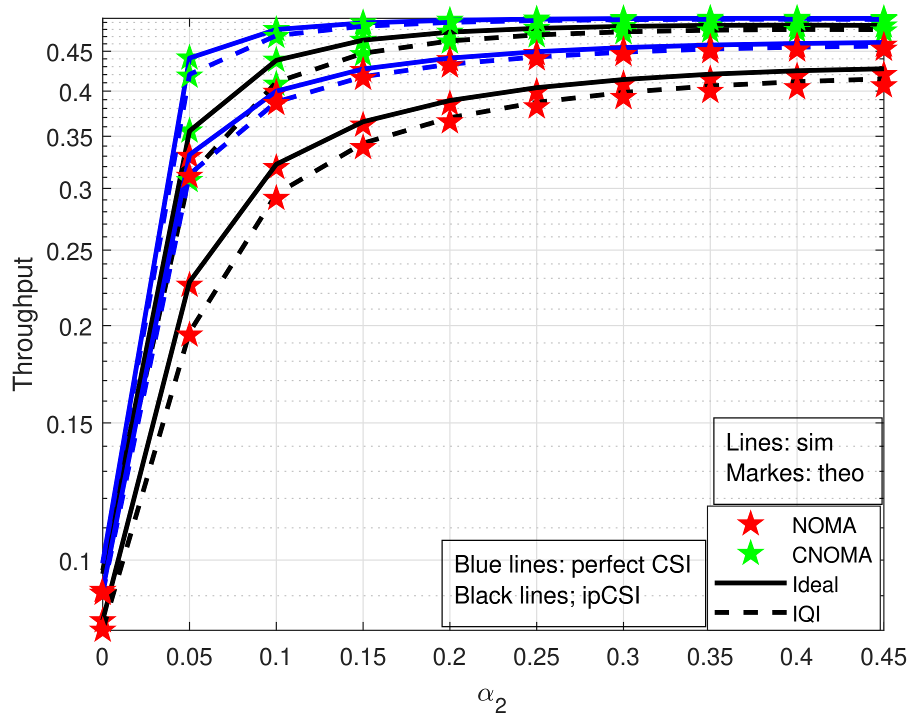

Figure 5.8: Throughput of CNOMA w.r.t PA when $SNR = 20$ dB.

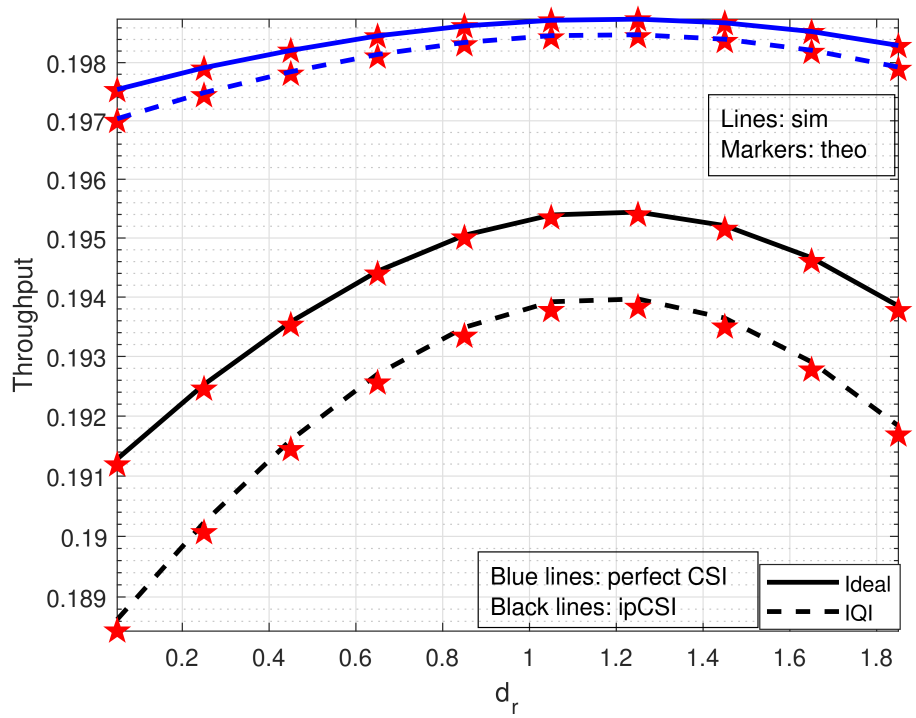

Figure 5.9: Throughput of CNOMA w.r.t d_r when $IRR = SNR = 20$ dB.

To illustrate the influence of the distance of R on the throughput performance of CNOMA in the presence of IQI and ipCSI, Fig. 5.9 presents the throughput performance is notably influenced by the distance between S and R. Increasing the distance between these points results in a decrease in throughput performance, leading to an augmentation occurrence of signal detection errors at R. Consequently, the transmission of information during the second phase will involve a higher rate of errors. It is worth noting that the optimal throughput performance is achieved when point R is positioned at an intermediate distance.

5.5 Conclusion

In this chapter, we examined the influence of IQI on the performance of CNOMA with direct links using MRC under ipCSI. We derived the expressions for the OP and throughput, to evaluate the imperfections on the performance of the system. The simulation results validated the accuracy of our mathematical analyses. The results of this study demonstrate a degradation in system performance with the coexistence of joint imperfections (IQI and ipCSI). Specifically, the performance of the system was significantly affected by the presence of ipCSI. Consequently, it becomes essential to utilize effective models, optimization approaches, and adaptable compensation techniques while deploying NOMA and CNOMA systems. These measures are essential for mitigating the negative effects of imperfections and enhancing the overall performance of the systems.

Chapter 6

Impact of Hardware Impairment on uplink SIMO Cooperative NOMA

6.1 Introduction

Meeting the demands of the 6th-generation (6G) and beyond wireless communication networks, which support a vast number of connected devices with low communication latencies and improved data rates, poses a significant challenge. To address this, researchers are exploring new communication technologies and system designs. Among these technologies, non-orthogonal multiple access (NOMA) has captured the attention of the research community as a promising solution to meet the requirements of 6G networks [137, 138]. The NOMA is based on the concept of utilizing the power domain for multiple access, which enables multiple users to be multiplexed at the same time, frequency, or code resources but at different power levels. This technique employs successive interference cancellation (SIC) to separate overlapping messages at the receiver, resulting in significant improvements in both spectrum efficiency and user fairness compared to the conventional orthogonal multiple access (OMA)[139, 140, 71]. The evaluation of performance in uplink NOMA systems is extensively discussed in [44, 141, 142, 53], where metrics such as outage probability (OP) and ergodic capacity (EC) are commonly utilized, taking into account both perfect and imperfect channel state information (CSI).

On the other hand, cooperative communication is a successful strategy for addressing issues related to multipath propagation, extending coverage, and improving the reliability of communication systems [105].

6.1.1 Related works

A combination of cooperative communication and NOMA has resulted in the development of cooperative NOMA (CNOMA) systems, which have garnered significant attention in recent papers. The OP and throughput performance of the downlink CNOMA over the Nakagami-m fading channels are evaluated in [117]. The authors in [143] evaluate the OP performance of CNOMA over the Rayleigh fading. The authors in [144] examine the effectiveness of hybrid downlink-uplink NOMA cooperative relay networks by analyzing the OP, diversity order, and throughput. In [145], underlay cognitive hybrid satellite-terrestrial for CNOMA has been analyzed for OP over Rician fading and Nakagami-m fading. Furthermore, multi-relay in NOMA systems can improve wireless network coverage, capacity, reliability, and interference reduction. These systems also enhance network resilience through redundancy and diversity. The effect of the relay selection on the performance of CNOMA is investigated in [81]. The authors of [146] present the performance of the NOMA system with the aid of multiple relays where two-stage relay selection with decode-and-forward (DF) and amplify-and-forward (AF) relaying protocols. The performance of the multiple relays assisted NOMA over the Nakagami-m fading channels is investigated in [147]. In addition, advanced approaches related to NOMA are being considered through the adoption of emerging transmission techniques, such as full-duplex communications and multi-antenna systems. The authors in [148] explore the use of NOMA with a multiple-antenna AF relaying network as a means of enhancing system performance. The performance of a two-user with simultaneous wireless information and power transfer (SWIPT) of the cooperative multiple-input single-output (MISO) NOMA system is examined in [149]. In [150], the authors study the performance of the uplink single-input multiple-output (SIMO) NOMA with joint maximum likelihood detector in terms of bit error rate.

6.1.2 Motivations and contributions

The aforementioned studies assume ideal hardware, perfect CSI, and SIC. In realistic communication systems, the hardware transceivers suffer from several imperfections due to in-phase and quadrature imbalance (IQI) in modulators, phase noise in local oscillators, and non-linearity power amplifiers [48, 151, 75]. The effect of the hardware impairment (HWI) on the NOMA-based relay systems over the Nakagami-m channels in terms of OP and ergodic sum rate performance is evaluated in [152, 153]. The BER and OP performance of the CNOMA under practical assumptions where the imperfect SIC (ipSIC), imperfect CSI (ipCSI), and hardware impairments (HWI) are investigated in [154]. In [155, 156], downlink NOMA with cognitive radio-assisted satellite-terrestrial relay networks under joint effects of channel estimation errors and HWI has been investigated in terms of secrecy OP. In [135], the OP and intercept probability of cognitive ambient backscatter downlink NOMA internet-of-vehicle enabled maritime transportation systems communication with HWI has been examined. The ambient backscatter downlink NOMA communication with both IQI and residual HWI has been analyzed in terms of OP and ergodic rate [134]. The authors of [151, 157] evaluate the performance of OP and system throughput of downlink and uplink CNOMA with ipCSI and IQI.

As previously mentioned, considerable attention has been given to the downlink CNOMA system with multiple relays and/or antennas in previous literature, as in [105, 117, 143, 144, 145, 81, 146, 147, 148, 149]. However, the uplink NOMA and CNOMA system has not garnered an equivalent level of focus. The evaluation of the uplink NOMA with and without ipCSI has been analyzed in [44, 141, 142, 53]. Moreover, multi-antenna technology plays a crucial role in enhancing the performance of NOMA and CNOMA schemes. These schemes have been predominantly investigated for downlink improvements [150, 149], while their potential in the uplink remains absent. Also, most papers consider the effect of HWI for downlink NOMA and CNOMA schemes [155, 156, 135, 134], while it is missing in the uplink NOMA and CNOMA schemes. To the best of the authors' knowledge, the investigation of uplink SIMO-CNOMA, both with and without multiple relays has not been investigated. Besides, the practical constraints have been neglected in all previous studies of the uplink of NOMA and CNOMA. Therefore, it is important to consider the practical constraints in the uplink CNOMA for realistic evaluations. Motivated by this, the performance of the uplink SIMO-CNOMA with the aid of multiple relays and an arbitrary number of users is studied in this chapter in the presence of HWI, ipCSI, and ipSIC. The OP and system throughput of our considered system is analyzed.

Accordingly, the main contributions of this work can be summarized as follows:

- A practical multi-user uplink NOMA scheme affected by HWI, ipCSI, and ipSIC is examined. Our analysis includes the multi-relay scenario with the selection relay (SR) technique and explores the use of SIMO to enhance performance. The transmitter has a single antenna, while the receiver uses multiple antennas during the cooperative scheme's two transmission phases.

- The derivation of the OP and system throughput of our proposed system with multiple relays and SIMO. We take into account practical constraints such as HWI, ipCSI, and ipSIC. The analytical expressions are validated by computer simulations. An asymptotic analysis of the system's performance is examined in high SNR regions. The objective of this analysis is to uncover valuable insights regarding the effects of HWI, ipCSI, and ipSIC parameters on the system's performance. The results reveal an impact of HWI, ipCSI, and ipSIC parameters on the system's performance in high SNR regions.

- The impact of the system parameters, such as HWI, ipCSI, number of the relays and antennas on the OP, and system throughput performance of the considered schemes are extensively investigated. Numerical results show that the systems are limited by the effects of HWI and ipCSI which have a degradation on the system performance despite increases in the number of antennas and relays.

6.2 System model

We examine an uplink CNOMA which comprises three key components: an access point AP, J users and R_L denoted respectively, as $\{U_j,\ j \in [1, J]\}$ and $\{R_l \in [1, R_L]\}$, as illustrated in Fig. 6.1 where R_l is the selected relay. In the considered system, we assume to employ the selection combining (SC), to choose the best-received signal. It is assumed that the AP and relays are equipped with receive antennas presented as $\{N_r, m \in [1, N_r]\}$. Also, we assume that all nodes work in half-duplex (HD) mode. Due to obstructions in the environment, direct communication links between the users and the AP are disregarded. Instead, the relays are employed to facilitate the transmission of user signals to the AP. The complex Rayleigh channel coefficients between the users-relays and relays-AP are presented as $h_j^{\{m,R_l\}} \sim \mathcal{CN}(0,\ \gamma_j^{\{m,R_l\}})$ and $g^{\{m,R_l\}} \sim \mathcal{CN}(0,\ \gamma^{\{m,R_l\}})$, respectively. We assume that CSI between all nodes is imperfect. The estimated channel coefficients are given as $\tilde{h}_j^{\{m,R_l\}} = h_j^{\{m,R_l\}} - e$ and $\tilde{g}_j^{\{m,R_l\}} = g_j^{\{m,R_l\}} - e$, where e is the channel estimation error [22]. In the context of uplink CNOMA, during the first phase, the users transmit their signals concurrently to R_l. As a result, the received considering both HWI and ipCSI.

$$y_I^{\{m,R_l\}} = \sum_{j=1} (\tilde{h}_j^{\{m,R_l\}} + e)(\sqrt{\alpha_j P} x_j + \eta_I^{\{m,R_l\}}) + n, \tag{6.1}$$

where x_j is the users signal, α_j is power allocation (PA) coefficients in which $\alpha_J < ... < \alpha_{J_1} < ... < \alpha_1$, P is the total transmit power, n is the additive white Gaussian noise (AWGN)

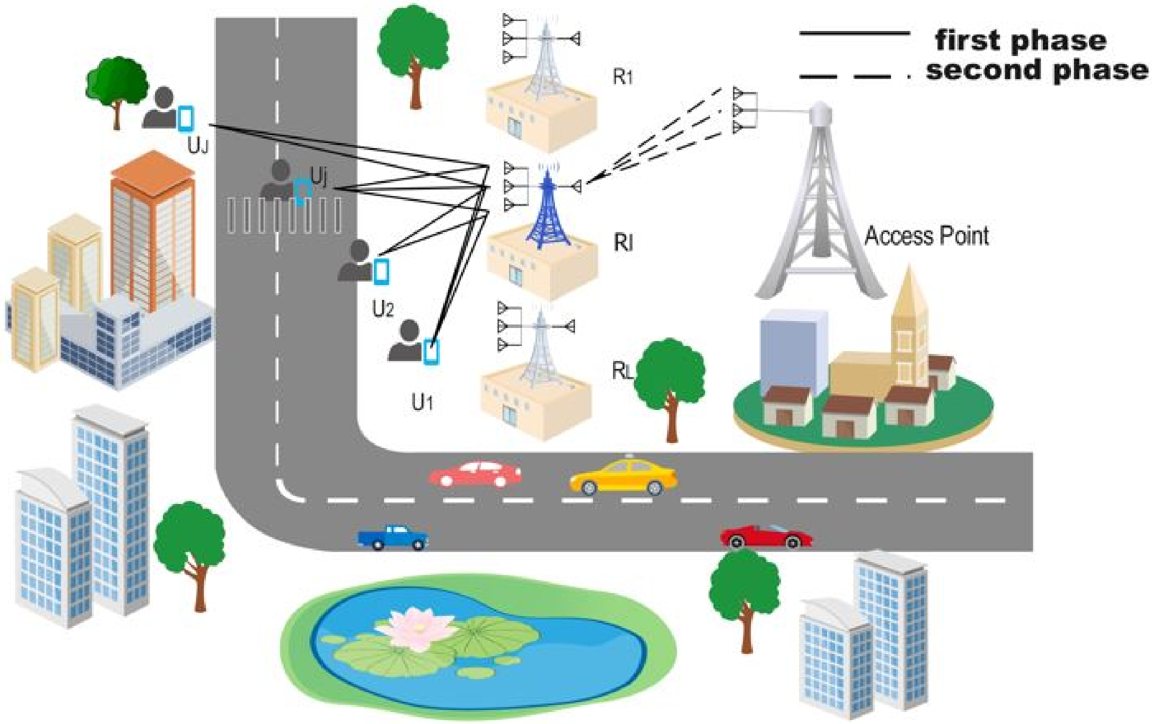

Figure 6.1: System model of uplink SIMO-CNOMA with selection relays.

$n \sim \mathcal{CN}(0, \sigma_n^2)$. Given the presence of N_r antennas at the receiver of the R_l node, for each signal, the SIC for each antenna is used. Then, R_l decodes firstly the signal of the highest power (U_1 signal). In the first phase, the SINRs for the transmitted signal by U_j to R_l is given as:

$$\gamma_{j,I}^{\{m,R_l\}} = \frac{\alpha_j P|\tilde{h}_j^{\{m,R_l\}}|^2}{\sum\limits_{j+1} \alpha_{j+1} P|\tilde{h}_{j+1}^{\{m,R_l\}}|^2 + \sum\limits_{i=1}^{j-1} \varsigma \alpha_i P|\tilde{h}_i^{\{m,R_l\}}|^2 + \sum\limits_{j=1} |\tilde{h}_j^{\{m,R_l\}}|^2 {k_j^{\{m,R_l\}}}^2 P + \epsilon_1}, \tag{6.2}$$

where ς is the residual SIC, $\epsilon_I = \sum\limits_{j=1} {k_j^{\{m,R_L\}}}^2 \sigma_e^2 P + \sigma_e^2 P + \sigma_n^2$. In the second phase, R_l combines the signals decoded during the first phase into new superimposed coding signals and transmits them to the AP. Notably, we consider the distribution of power in this second phase to be identical to that of the first phase. The received signal in the second phase under HWI and ipCSI can be expressed as:

$$y_j^{II\{m,R_l\}} = (\tilde{g}_j^{\{m,R_l\}} + e)\left(\sum_{j=1} \sqrt{\alpha_j P} x_j + \eta_{II}^{\{m,R_l\}}\right) + n, \tag{6.3}$$

where $\eta_I^{\{m,R_l\}}$ and $\eta_{II}^{\{m,R_l\}}$ are the HWI distortion term as (1.10) and (1.11) at the first and the second phase, respectively, and can be presented as:

$$\begin{aligned} \eta_I^{\{m,R_l\}} &\sim \mathcal{CN}(0,\ k_I^{\{m,R_l\}^2}P), \\ \eta_{II}^{\{m,R_l\}} &\sim \mathcal{CN}(0,\ k_{II}^{\{m,R_l\}^2}P). \end{aligned} \tag{6.4}$$

Furthermore, the SINR in the second phase at AP is expressed as:

$$\gamma_{j,II}^{\{m,R_l\}} = \frac{\alpha_j P|\tilde{g}^{m,R_l}|^2}{\sum\limits_{j+1} \alpha_j P|\tilde{g}^{m,R_l}|^2 + \sum\limits_{i=1}^{j-1} \varsigma \alpha_i P|\tilde{g}^{\{m,R_l\}}|^2 + |\tilde{g}^{m,R_l}|^2 K^{\{m,R_l\}^2} P + \epsilon_{II}}, \tag{6.5}$$

where $\epsilon_{II} = K^{\{m,R_l\}^2}\sigma_e^2 P + \sigma_e^2 P + \sigma_n^2$.
At both R_l and AP, the SC technique is employed to select the optimal SINR. Considering the implementation of SR technology, only one relay is permitted to transmit the signal to the users. Therefore, The SINR of the R_l for U_j is determined through the principle of max-min relay selection as in [158]:

$$\Omega_{R_l}^{SR} = \max_{1,\dots,R_L} \{\min\ \{\Omega_{j,I}^{\{m,R_l\}}\}, \{\Omega_{j,II}^{\{m,R_l\}}\}\}, \tag{6.6}$$

with

$$\Omega_{j,I}^{\{m,R_l\}} = \max_{m=1,\dots,N_r} (\Omega_{j,I}^{\{m,R_l\}}), \tag{6.7}$$

$$\Omega_{j,II}^{\{m,R_l\}} = \max_{m=1,\dots,N_r} (\Omega_{j,II}^{\{m,R_l\}}). \tag{6.8}$$

6.3 Performance analysis

In this section, we derive the OP and throughput expression of the uplink SIMO-CNOMA in the presence of HWI, ipCSI, and ipSIC over the Rayleigh fading channel.

6.3.1 Outage probability

1) OP of two users

Outage probability of the U_1: The end-2-end (e2e) OP of U_1 signal, when SR and SC are implemented under HWI and ipCSI is expressed as:

$$P_1(out) = \prod_{1}^{R_L}\left[1-\left(1-\prod_{m=1}^{Nr} Pr\left(\gamma_{1,I}^{m,R_l} < \gamma_{th,1}\right)\right)\left(1-\prod_{m=1}^{Nr} Pr\left(\gamma_{1,II}^{\{m,R_l\}} < \gamma_{th,1}\right)\right)\right]. \tag{6.9}$$

Each term can be calculated as:

$$\begin{aligned}\prod_{m=1}^{Nr} Pr\left(\gamma_{1,I}^{m,R_l} < \gamma_{th,1}\right) &= \prod_{m=1}^{Nr} Pr\left(|\tilde{h}_1^{m,R_l}|^2 < \frac{\gamma_{th,1}\left[\beta_1|\tilde{h}_2^{m,R_l}|^2+\triangle_1\right]}{\rho_1}\right)\\ &= \prod_{m=1}^{Nr}\left(1-\exp\left(-\frac{\triangle_1\gamma_{th,1}}{\rho_1\lambda_{h_1^{m,l}}}\right)\frac{\rho_1\lambda_{h_1^{m,l}}}{\beta_1\gamma_{th,1}\lambda_{h_2^{m,l}}+\rho_1\lambda_{h_1^{m,l}}}\right),\end{aligned} \tag{6.10}$$

$$\begin{aligned}\prod_{m=1}^{Nr} Pr\left(\gamma_{1,II}^{\{m,R_l\}} < \gamma_{th,1}\right) &= \prod_{m=1}^{Nr} Pr\left(|\tilde{g}_1^{\{m,R_l\}}|^2 < \frac{\gamma_{th,1}\epsilon_{II}}{\left(\alpha_1P-\gamma_{th,1}\alpha_2P-\gamma_{th,1}K_{II}^{\{m,R_l\}^2}P\right)}\right)\\ &= \prod_{m=1}^{Nr}\left(1-\exp\left(-\frac{\gamma_{th,1}\epsilon_{II}}{\lambda_{g_1^{\{m,R_l\}}}\left(\alpha_1P-\gamma_{th,1}\alpha_2P-\gamma_{th,1}K_{II}^{\{m,R_l\}^2}P\right)}\right)\right),\end{aligned} \tag{6.11}$$

where
$\rho_1 = P\left(\alpha_1-\gamma_{th,1}K_{1,I}^{\{m,l\}^2}\right)$, $\beta_1 = P\left(\alpha_2+K_{2,I}^{\{m,l\}^2}\right)$, and $\triangle_1 = \left(\sigma_e^2PK_{2,I}^{\{m,l\}^2}+\sigma_e^2P+\sigma_n^2\right)$.

By replacing the (6.10) and (6.11) in (6.9), the e2e OP of U_1 can be given as:

$$\begin{aligned}P_1(out) = \prod_{1}^{R_L}\Bigg[1-&\left(1-\prod_{m=1}^{Nr}\left(1-\exp\left(-\frac{\triangle_1\gamma_{th,1}}{\rho_1\lambda_{h_1^{m,R}}}\right)\frac{\rho_1\lambda_{h_1^{m,R_l}}}{\beta_1\gamma_{th,1}\lambda_{h_{2,I}^{m,R_l}}+\rho_1\lambda_{h_1^{m,R_l}}}\right)\right)\\ &\times\left(1-\prod_{m=1}^{Nr}\left(1-\exp\left(-\frac{\gamma_{th,1}\left(\sigma_e^2P\left(K_{II}^{\{m,R_l\}^2}+1\right)+\sigma_n^2\right)}{\lambda_{g_1^{\{m,R_l\}}}\left(\alpha_1P-\gamma_{th,1}\alpha_2P-\gamma_{th,1}K_{II}^{\{m,R_l\}^2}P\right)}\right)\right)\right)\Bigg].\end{aligned} \tag{6.12}$$

Outage probability of the U_2: The outage of the U2 occurs if the U1 and U2 signals cannot be successfully decoded. Therefore, the e2e OP of the U_2 in the presence of HWI, ipCSI, and ipSIC. is given as

$$P_2(out) = \prod_{1}^{R_L}\Big[1 - P_{2,I}(out)P_{2,II}(out)\Big], \tag{6.13}$$

The OP of the U_2 in the first phase can be given as

$$P_{2,I}(out) = \left[1 - \left(1 - \prod_{m=1}^{Nr} Pr\left(\gamma_{1,I}^{\{m,R_l\}} < \gamma_{th,1}\right)\right)\left(1 - \prod_{m=1}^{Nr} Pr\left(\gamma_{2,I}^{\{m,R_l\}} < \gamma_{th,2}\right)\right)\right], \tag{6.14}$$

where

$$Pr\left(\gamma_{1,I}^{\{m,R_l\}} < \gamma_{th,1}\right) = \prod_{m=1}^{Nr}\left[1 - \exp\left(-\frac{\triangle_1\gamma_{th,1}}{\rho_1\lambda_{h_1^{m,R_l}}}\right)\frac{\rho_1\lambda_{h_1^{\{m,R_l\}}}}{\beta_1\gamma_{th,1}\lambda_{h_2^{\{m,R_l\}}} + \rho_1\lambda_{h_1^{\{m,R_l\}}}}\right], \tag{6.15}$$

and

$$\Pr\left(\gamma_{2,I}^{\{m,R_l\}} < \gamma_{th,2}\right) = \prod_{m=1}^{Nr}\left[1 - \exp\left(-\frac{\triangle_2\gamma_{th,2}}{\rho_2\lambda_{h_2^{m,R_l}}}\right)\frac{\rho_2\lambda_{h_2^{\{m,R_l\}}}}{\beta_2\gamma_{th,2}\lambda_{h_1^{\{m,R_l\}}} + \rho_2\lambda_{h_2^{\{m,R_l\}}}}\right], \tag{6.16}$$

where
$\triangle_2 = \left(\sigma_e^2 P {K_{1,I}^{\{m,R_l\}}}^2 + \sigma_e^2 P + \sigma_n^2\right)$, $\rho_2 = P\left(\alpha_2 - \gamma_{th,1}{K_{2,I}^{\{m,R_l\}}}^2\right)$, and $\beta_2 = P\left(\varsigma\alpha_1 + {K_{1,I}^{\{m,R_l\}}}^2\right)$.

By substituting (6.15) and (6.16) into (6.14), we get

$$P_{2,I}(out) = 1 - \left(1 - \prod_{m=1}^{Nr}\left[1 - \exp\left(-\frac{\triangle_1\gamma_{th,1}}{\rho_1\lambda_{h_1^{m,l}}}\right)\frac{\rho_1\lambda_{h_1^{\{m,R_l\}}}}{\beta_1\gamma_{th,1}\lambda_{h_2^{\{m,R_l\}}} + \rho_1\lambda_{h_1^{\{m,R_l\}}}}\right]\right)\times$$
$$\left(1 - \prod_{m=1}^{Nr}\left[1 - \exp\left(-\frac{\triangle_2\gamma_{th,2}}{\rho_2\lambda_{h_2^{m,R_l}}}\right)\frac{\rho_2\lambda_{h_2^{\{m,R_l\}}}}{\beta_2\gamma_{th,2}\lambda_{h_1^{\{m,R_l\}}} + \rho_2\lambda_{h_2^{\{m,R_l\}}}}\right]\right). \tag{6.17}$$

Likewise (6.14), the OP of U_2 in the second phase can be expressed

$$P_{2,II}(out) = \left[1 - \left(1 - \prod_{m=1}^{Nr} Pr\left(\gamma_{1,II}^{\{m,R_l\}} < \gamma_{th,1}\right)\right)\left(1 - \prod_{m=1}^{Nr} Pr\left(\gamma_{2,II}^{\{m,R_l\}} < \gamma_{th,2}\right)\right)\right]. \tag{6.18}$$

where

$$Pr\left(\gamma_{1,II}^{\{m,R_l\}} < \gamma_{th,1}\right) = \prod_{m=1}^{Nr}\left[1 - \exp\left(-\frac{\gamma_{th,1}\epsilon_{II}}{\lambda_{g_{\{m,R_l\}}}\left(\alpha_1 P - \gamma_{th,1}\alpha_2 P - \gamma_{th,1}{K_{II}^{\{m,R_l\}}}^2 P\right)}\right)\right], \tag{6.19}$$

and

$$\Pr\left(\gamma_{2,II}^{\{m,R_l\}} < \gamma_{th,2}\right) = \prod_{m=1}^{Nr}\left[1 - \exp\left(-\frac{\gamma_{th,2}\epsilon_{II}}{\lambda_{g_j^{\{m,R_l\}}}\left(\alpha_2 P - \gamma_{th,2}\varsigma\alpha_1 P - \gamma_{th,2}{K_{II}^{\{m,R_l\}}}^2 P\right)}\right)\right]. \tag{6.20}$$

By substituting (6.19) and (6.20) in (6.18), the OP of U_2 in the second phase can be presented as:

$$\begin{aligned} P_{2,II}(out) = 1 - &\left(1 - \prod_{m=1}^{Nr}\left[1 - \exp\left(-\frac{\gamma_{th,1}\epsilon_{II}}{\lambda_{g_j^{\{m,R_l\}}}}\left(\alpha_1 P - \gamma_{th,1}\alpha_2 P - \gamma_{th,1}{K_{II}^{\{m,R_l\}}}^2 P\right)\right)\right]\right) \\ &\times\left(1 - \prod_{m=1}^{Nr}\left[1 - \exp\left(-\frac{\gamma_{th,2}\epsilon_{II}}{\lambda_{g_j^{\{m,R_l\}}}\left(\alpha_2 P - \gamma_{th,2}\varsigma\alpha_1 P - \gamma_{th,2}{K_{II}^{\{m,R_l\}}}^2 P\right)}\right)\right]\right). \end{aligned} \tag{6.21}$$

To obtain the e2e OP of the U_2, we replace (6.17) and (6.21) into (6.13).

2) OP of an arbitrary number of users

The e2e OP of U_j under HWI, ipCSI, and ipSIC can be defined as:

$$P_j(out) = \prod_{1}^{R_L}\left[1 - \prod_{j=1}^{J} P_{j,I}(out)\prod_{j=1}^{J} P_{j,II}(out)\right]. \tag{6.22}$$

The OP of the U_j in the first phase can be obtained as:

$$P_{j,I}(out) = 1 - \prod_{j=1}^{J}\left(1 - \prod_{m=1}^{Nr} Pr\left(\gamma_{j,I}^{\{m,R_l\}} < \gamma_{th,j}\right)\right), \tag{6.23}$$

where

$$\prod_{m=1}^{Nr} Pr\left(\gamma_{j,I}^{\{m,R_l\}} < \gamma_{th,j}\right) = \prod_{m=1}^{Nr}\left(1-\exp\left(-\frac{\gamma_{th,j}\triangle_j}{P(\alpha_j-\gamma_{th,j}{k_j^{\{m,R_l\}}}^2)\lambda_{h_j^{\{m,R_l\}}}}\right)\right.$$
$$\times \frac{P(\alpha_j-\gamma_{th,j}{k_j^{\{m,R_l\}}}^2)\lambda_{h_j^{\{m,R_l\}}}}{P(\alpha_j-\gamma_{th,j}{k_j^{\{m,R_l\}}}^2)\lambda_{h_j^{\{m,R_l\}}}+\gamma_{th,j}(\alpha_{j+1}+{k_{j+1}^{\{m,R_l\}}}^2)\ P\ \lambda_{h_{j+1}^{\{m,R_l\}}}}$$
$$\times \frac{P(\alpha_j-\gamma_{th,j}{k_j^{\{mR_l\}}}^2)\lambda_{h_j^{\{m,R_l\}}}}{P(\alpha_j-\gamma_{th,j}{k_j^{\{m,R_l\}}}^2)\lambda_{h_j^{\{m,R_l\}}}+\gamma_{th,j}(\varsigma\alpha_{(j-1)}+{k_{(j-1)}^{\{m,R_l\}}}^2)\ P\ \lambda_{h_{j-1}^{\{m,R_l\}}}}$$
$$\times \frac{P(\alpha_j-\gamma_{th,j}{k_j^{\{m,R_l\}}}^2)\lambda_{h_j^{\{m,R_l\}}}}{P(\alpha_j-\gamma_{th,j}{k_j^{\{m,R_l\}}}^2)\lambda_{h_j^{\{m,R_l\}}}+\gamma_{th,j}(\alpha_{j+2}+{k_{j+2}^{\{m,R_l\}}}^2)\ P\ \lambda_{h_{j+2}^{\{m,R_l\}}}} \quad (6.24)$$
$$\times \frac{P(\alpha_j-\gamma_{th,j}{k_j^{\{m,R_l\}}}^2)\lambda_{h_j^{\{m,R_l\}}}}{P(\alpha_j-\gamma_{th,j}{k_j^{\{m,R_l\}}}^2)\lambda_{h_j^{\{m,R_l\}}}+\gamma_{th,j}(\varsigma\alpha_{j-2}+{k_{j-2}^{\{m,R_l\}}}^2)\ P\ \lambda_{h_{j-2}^{\{m,R_l\}}}}$$
$$\ldots\times \frac{P(\alpha_j-\gamma_{th,j}{k_j^{\{m,R_l\}}}^2)\lambda_{h_j^{\{m,R_l\}}}}{P(\alpha_j-\gamma_{th,j}{k_j^{\{m,R_l\}}}^2)\lambda_{h_j^{\{m,R_l\}}}+\gamma_{th,j}(\alpha_J+{k_J^{\{m,R_l\}}}^2)\ P\ \lambda_{h_J^{\{m,R_l\}}}}$$
$$\left.\times \frac{P(\alpha_j-\gamma_{th,j}{k_j^{\{m,R_l\}}}^2)\lambda_{h_j}^{\{m,R_l\}}}{P(\alpha_j-\gamma_{th,j}{k_j^{\{m,R_l\}}}^2)\lambda_{h_j}^{\{m,R_l\}}+\gamma_{th,j}(\varsigma\alpha_{(J-1)}+{k_{J-1}}^{\{m,R_l\}2})\ P\ \lambda_{h_{J-1}^{\{m,R_l\}}}}\right).$$

Substituting (6.24) into (6.23), the U_j in the first phase can be given as:

$$
\begin{aligned}
P_{j,I}(out) =& 1-\prod_{j=1}^{J}\left(1-\prod_{m=1}^{Nr}\left(1-\exp\left(-\frac{\gamma_{th,j}\triangle_j}{P(\alpha_j-\gamma_{th,j}k_j^{\{m,R_l\}^2})\lambda_{h_j^{\{m,R_l\}}}}\right)\right.\right.\\
&\times\frac{P(\alpha_j-\gamma_{th,j}k_j^{\{m,R_l\}^2})\lambda_{h_j^{\{m,R_l\}}}}{P(\alpha_j-\gamma_{th,j}k_j^{\{m,R_l\}^2})\lambda_{h_j^{\{m,R_l\}}}+\gamma_{th,j}(\alpha_{j+1}+k_{j+1}^{\{m,R_l\}^2})\ P\ \lambda_{h_{j+1}^{\{m,R_l\}}}}\\
&\times\frac{P(\alpha_j-\gamma_{th,j}k_j^{\{mR_l\}^2})\lambda_{h_j^{\{m,R_l\}}}}{P(\alpha_j-\gamma_{th,j}k_j^{\{m,R_l\}^2})\lambda_{h_j^{\{m,R_l\}}}+\gamma_{th,j}(\varsigma\alpha_{(j-1)}+k_{(j-1)}^{\{m,R_l\}^2})\ P\ \lambda_{h_{j-1}^{\{m,R_l\}}}}\\
&\times\frac{P(\alpha_j-\gamma_{th,j}k_j^{\{m,R_l\}^2})\lambda_{h_j^{\{m,R_l\}}}}{P(\alpha_j-\gamma_{th,j}k_j^{\{m,R_l\}^2})\lambda_{h_j^{\{m,R_l\}}}+\gamma_{th,j}(\alpha_{j+2}+k_{j+2}^{\{m,R_l\}^2})\ P\ \lambda_{h_{j+2}^{\{m,R_l\}}}}\\
&\times\frac{P(\alpha_j-\gamma_{th,j}k_j^{\{m,R_l\}^2})\lambda_{h_j^{\{m,R_l\}}}}{P(\alpha_j-\gamma_{th,j}k_j^{\{m,R_l\}^2})\lambda_{h_j^{\{m,R_l\}}}+\gamma_{th,j}(\varsigma\alpha_{j-2}+k_{j-2}^{\{m,R_l\}^2})\ P\ \lambda_{h_{j-2}^{\{m,R_l\}}}}\\
&\ldots\times\frac{P(\alpha_j-\gamma_{th,j}k_j^{\{m,R_l\}^2})\lambda_{h_j^{\{m,R_l\}}}}{P(\alpha_j-\gamma_{th,j}k_j^{\{m,R_l\}^2})\lambda_{h_j^{\{m,R_l\}}}+\gamma_{th,j}(\alpha_J+k_J^{\{m,R_l\}^2})\ P\ \lambda_{h_J^{\{m,R_l\}}}}\\
&\left.\left.\times\frac{P(\alpha_j-\gamma_{th,j}k_j^{\{m,R_l\}^2})\lambda_{h_j}^{\{m,R_l\}}}{P(\alpha_j-\gamma_{th,j}k_j^{\{m,R_l\}^2})\lambda_{h_j}^{\{m,R_l\}}+\gamma_{th,j}(\varsigma\alpha_{(J-1)}+k_{J-1}{}^{\{m,R_l\}2})\ P\ \lambda_{h_{J-1}^{\{m,R_l\}}}}\right)\right).
\end{aligned}
\tag{6.25}
$$

The OP of the U_j in the second phase can be given as:

$$
P_{j,II}(out)=1-\prod_{j=1}^{J}\left(1-\prod_{m=1}^{Nr}Pr\left(\gamma_{j,II}^{\{m,R_l\}}<\gamma_{th,j}\right)\right), \tag{6.26}
$$

where

$$
\prod_{m=1}^{Nr}Pr\left(\gamma_{j,II}^{\{m,R_l\}}<\gamma_{th,j}\right)=\prod_{m=1}^{Nr}Pr\left(|\tilde{g}_j^{m,R_l}|^2<\frac{\gamma_{th,j}\epsilon_{II}}{P(\alpha_j-\gamma_{th,j}\sum\limits_{j+1}\alpha_{j+1}-\gamma_{th,j}\sum\limits_{i=1}^{j+1}\varsigma\alpha_i-\gamma_{th,j}K_{II}^{\{m,R_l\}^2})}\right). \tag{6.27}
$$

Using some manipulation as in [105], (6.26) can be written as:

$$\prod_{m=1}^{Nr} Pr\left(\gamma_{j,II}^{\{m,R_l\}} < \gamma_{th,j}\right) = \prod_{m=1}^{Nr}\left(1-\exp\left(-\frac{\gamma_{th,j}\epsilon_{II}}{P(\alpha_j - \gamma_{th,j}\sum_{j+1}\alpha_{j+1} - \gamma_{th,j}\sum_{i=1}^{j+1}\varsigma\alpha_i - \gamma_{th,j}K^{\{m,R_l\}^2})\lambda_{g_j^{\{m,R_l\}}}}\right)\right). \tag{6.28}$$

Replacing (6.28) in (6.26), the OP U_j in the second phase can be presented as:

$$P_{j,II}(out) = 1-\prod_{j=1}^{J}\left(1-\prod_{m=1}^{Nr}\left(1-\exp\left(-\frac{\gamma_{th,j}\epsilon_{II}}{P(\alpha_j - \gamma_{th,j}\sum_{j+1}\alpha_{j+1} - \gamma_{th,j}\sum_{i=1}^{j+1}\varsigma\alpha_i - \gamma_{th,j}K^{\{m,R_l\}^2})\lambda_{g_j^{\{m,R_l\}}}}\right)\right)\right). \tag{6.29}$$

Thus, to obtain the e2e OP of U_j, we replace the (6.25) and (6.29) in (6.22).

6.3.2 Asymptotic outage probability

In this subsection, we analyze the performance of the asymptotic OP under high SNR conditions to attain a deeper understanding of the scenarios under consideration.

1) Asymptotic OP of two users

The asymptotic OP of the U_1 under HWI and ipCSI can be expressed as:

$$P_1^{asy}(out) \approx \prod_{1}^{R_l}\left[1-\left(1-\prod_{m=1}^{Nr}\left(\left(\frac{\triangle_1\gamma_{th,1}}{\rho_1\lambda_{h_1^{m,R_l}}}\right)\frac{\rho_1\lambda_{h_1^{m,R_l}}}{\beta_1\gamma_{th,1}\lambda_{h_2^{m,R_l}}+\rho_1\lambda_{h_1^{m,R_l}}}\right)\right)\times\left(1-\prod_{m=1}^{Nr}\left(\frac{\gamma_{th,1}\epsilon_{II}}{\lambda_{h_1^{\{m,R_l\}}}\left(\alpha_1 P - \gamma_{th,1}\alpha_2 P - \gamma_{th,1}K_{II}^{\{m,R_l\}^2}P\right)}\right)\right)\right]. \tag{6.30}$$

The asymptotic OP of the U_2 at the first and second phases under HWI, ipCSI, and ipSIC can be presented, respectively as:

$$P_{2,I}^{asy}(out) \approx 1 - \left(1 - \prod_{m=1}^{Nr}\left(\left(\frac{\triangle_1\gamma_{th,1}}{\rho_1\lambda_{h_1^{m,R_l}}}\right)\frac{\rho_1\lambda_{h_1^{\{m,R_l\}}}}{\beta_1\gamma_{th,1}\lambda_{h_2^{\{m,R_l\}}}+\rho_1\lambda_{h_1^{\{m,R_l\}}}}\right)\right) \times\left(1 - \prod_{m=1}^{Nr}\left(\left(\frac{\triangle_2\gamma_{th,2}}{\rho_2\lambda_{h_2^{m,R_l}}}\right)\frac{\rho_2\lambda_{h_2^{\{m,R_l\}}}}{\beta_2\gamma_{th,2}\lambda_{h_1^{\{m,R_l\}}}+\rho_2\lambda_{h_2^{\{m,R_l\}}}}\right)\right). \tag{6.31}$$

$$P_{2,II}^{asy}(out) \approx 1 - \left(1 - \prod_{m=1}^{Nr}\left(\frac{\gamma_{th,1}\epsilon_{II}}{\lambda_{g_{\{m,R_l\}}}\left(\alpha_1 P - \gamma_{th,1}\alpha_2 P - \gamma_{th,1}{K_{II}^{\{m,R_l\}}}^2 P\right)}\right)\right) \times\left(1 - \prod_{m=1}^{Nr}\left(\frac{\gamma_{th,2}\epsilon_{II}}{\lambda_{g_j^{\{m,R_l\}}}\left(\alpha_2 P - \gamma_{th,2}\varsigma\alpha_1 P - \gamma_{th,2}{K_{II}^{\{m,R_l\}}}^2 P\right)}\right)\right). \tag{6.32}$$

2) Asymptotic OP of an arbitrary number of users

The asymptotic OP of Uj at the first and second phases can be obtained, respectively as:

$$
\begin{aligned}
P_{j,I}(out) \approx & 1-\prod_{j=1}^{J}\Bigg(1-\prod_{m=1}^{Nr}\Bigg(\Bigg(\frac{\gamma_{th,j}\triangle_j}{P(\alpha_j-\gamma_{th,j}{k_j^{\{m,R_l\}}}^2)\lambda_{h_j^{\{m,R_l\}}}}\Bigg) \\
& \times\frac{P(\alpha_j-\gamma_{th,j}{k_j^{\{m,R_l\}}}^2)\lambda_{h_j^{\{m,R_l\}}}}{P(\alpha_j-\gamma_{th,j}{k_j^{\{m,R_l\}}}^2)\lambda_{h_j^{\{m,R_l\}}}+\gamma_{th,j}(\alpha_{j+1}+{k_{j+1}^{\{m,R_l\}}}^2)\ P\ \lambda_{h_{j+1}^{\{m,R_l\}}}} \\
& \times\frac{P(\alpha_j-\gamma_{th,j}{k_j^{\{m,R_l\}}}^2)\lambda_{h_j^{\{m,R_l\}}}}{P(\alpha_j-\gamma_{th,j}{k_j^{\{m,R_l\}}}^2)\lambda_{h_j^{\{m,R_l\}}}+\gamma_{th,j}(\varsigma\alpha_{j-1}+{k_{j-1}^{\{m,R_l\}}}^2)\ P\ \lambda_{h_{j-1}^{\{m,R_l\}}}} \\
& \times\frac{P(\alpha_j-\gamma_{th,j}{k_j^{\{m,R_l\}}}^2)\lambda_{h_j^{\{m,R_l\}}}}{P(\alpha_j-\gamma_{th,j}{k_j^{\{m,R_l\}}}^2)\lambda_{h_j^{\{m,R_l\}}}+\gamma_{th,j}(\alpha_{j+2}+{k_{j+2}^{\{m,R_l\}}}^2)\ P\ \lambda_{h_{j+2}^{\{m,R_l\}}}} \\
& \times\frac{P(\alpha_j-\gamma_{th,j}{k_j^{\{m,R_l\}}}^2)\lambda_{h_j^{\{m,R_l\}}}}{P(\alpha_j-\gamma_{th,j}{k_j^{\{m,R_l\}}}^2)\lambda_{h_j^{\{m,R_l\}}}+\gamma_{th,j}(\varsigma\alpha_{j-2}+{k_{j-2}^{\{m,R_l\}}}^2)\ P\ \lambda_{h_{j-2}^{\{m,R_l\}}}} \\
& \ldots\times\frac{P(\alpha_j-\gamma_{th,j}{k_j^{\{m,R_l\}}}^2)\lambda_{h_j^{\{m,R_l\}}}}{P(\alpha_j-\gamma_{th,j}{k_j^{\{m,R_l\}}}^2)\lambda_{h_j^{\{m,R_l\}}}+\gamma_{th,j}(\alpha_{J}+{k_{J}^{\{m,R_l\}}}^2)\ P\ \lambda_{h_{J}^{\{m,R_l\}}}} \\
& \times\frac{P(\alpha_j-\gamma_{th,j}{k_j^{\{m,R_l\}}}^2)\lambda_{h_j^{\{m,R_l\}}}}{P(\alpha_j-\gamma_{th,j}{k_j^{\{m,R_l\}}}^2)\lambda_{h_j^{\{m,R_l\}}}+\gamma_{th,j}(\varsigma\alpha_{(J-1)}+{k_{J-1}^{\{m,R_l\}}}^2)\ P\ \lambda_{h_{J-1}^{\{m,R_l\}}}}\Bigg)\Bigg).
\end{aligned} \tag{6.33}
$$

$$
\begin{aligned}
&\prod_{m=1}^{Nr} Pr\left(\gamma_{j,II}^{\{m,R_l\}}<\gamma_{th,j}\right)\approx \\
&1-\prod_{j=1}^{J}\Bigg(1-\prod_{m=1}^{Nr}\Bigg(\frac{\gamma_{th,j}\psi_{II}}{P(\alpha_j-\gamma_{th,j}\sum\limits_{j+1}\alpha_{j+1}-\gamma_{th,j}\sum\limits_{i=1}^{j+1}\varsigma\alpha_i-\gamma_{th,j}{K^{\{m,R\}}}^2)\lambda_{g_j^{\{m,R_l\}}}}\Bigg).
\end{aligned} \tag{6.34}
$$

To obtain the asymptotic OP of the U_2, substitute (6.33) and (6.34) into (6.13).

6.3.3 System Throughput

In this subsection, the analytical expression of the system throughput is given in the presence of the HWI, ipCSI, and ipSIC can be provided as [151]:

$$\tau = \sum_{j=1}^{J}(1 - P_j(out))r_j, \tag{6.35}$$

where $P_j(out)$ is the e2e OP of U_j and r_j is the target rate of U_j.

6.4 Numerical results

This section analyses the uplink SIMO-CNOMA performance in the presence of HWI, ipCSI, and ipSIC. The numerical results are validated through the simulation results. The parameters are set as In the case of the two users $d_1 = 3m$ and $d_2 = 5m$, and $\alpha_1 = 0.75$, $\alpha_2 = 0.25$. In the case of the three users $d_1 = 3m$, $d_2 = 4m$ and $d_3 = 5m$, and $\alpha_1 = 0.7$, $\alpha_2 = 0.2$ and $\alpha_3 = 0.1$.The Distance between the relays and AP $d_r = 4m$. The HWI coefficient ${K_{j,I}^{m,L}}^2 = {K_{II}^{m,L}}^2 = 0.05$, the channel estimation error $\sigma_e^2 = 0.001$, and the residual SIC factor $\varsigma = 0.001$.

The OP performance of the uplink SIMO-CNOMA system under HWI, ipCSI, and ipSIC with different numbers of users is presented in Figs. 6.2, and 6.3. It is evident from the figures that as the number of relays and antennas increases, the OP performance of the users exhibits improvement. However, even with the growing number of relays and antennas, an error floor is consistently present across all user curves, particularly at high SNR. This error floor can be attributed to the presence of imperfections in the system (HWI, ipCSI, and ipSIC) and the interference between the channels of the users. Therefore, The increasing number of users affects the distribution of power to the rest of the users, which affects the SIC process. The growing number of users has a direct influence on the allocation of power among all users, by impacting the efficiency of the SIC process. Additionally, The asymptotic OP curves are limited over the theoretical curves at the high SNR.

Figs. 6.4 and 6.5 evaluate the effect of the HWI and channel estimation system of the considered system when $l = 3$ and $j = 3$. It's apparent that augmenting HWI and the channel estimation error factors leads to a reduction in the OP performance for all users. Notably, it's observable that HWI has a relatively lesser impact on the outage performance compared to the effects of ipCSI across all antennas. Consequently, it can be concluded that the system's performance is more significantly influenced by channel estimation errors than by HWI.

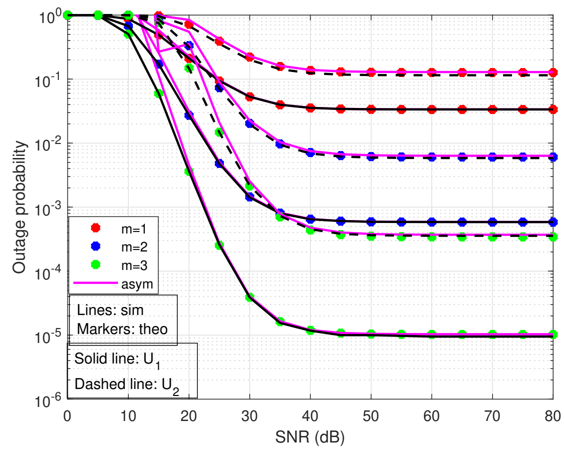

(a) Case of one relay.

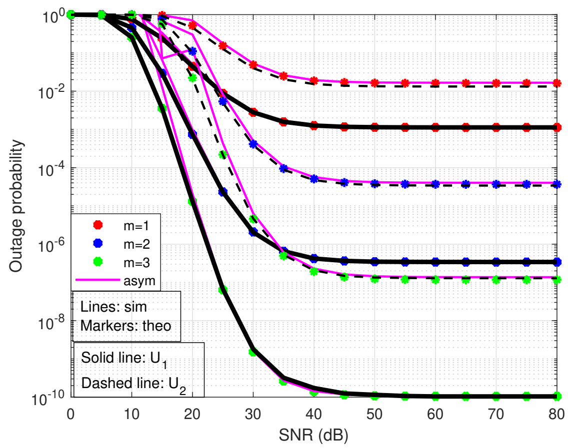

(b) Case of two relays.

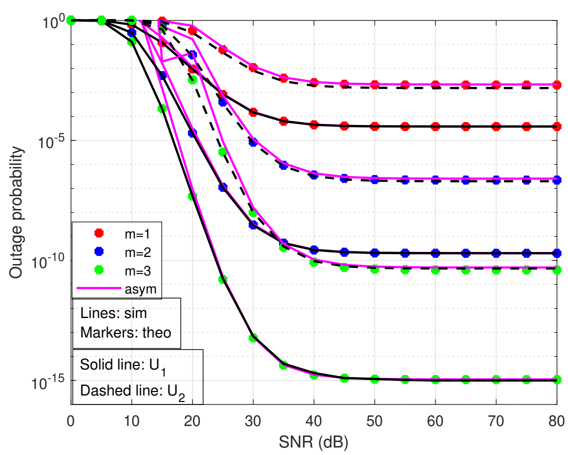

(c) Case of three relays.

Figure 6.2: OP w.r.t. SNR for uplink SIMO-CNOMA with SR of two users.

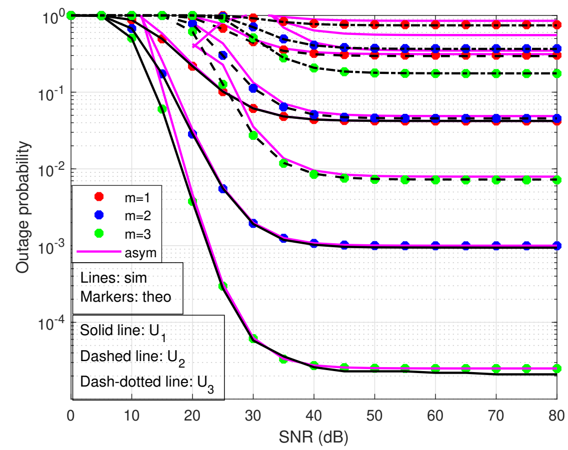

(a) Case of one relay.

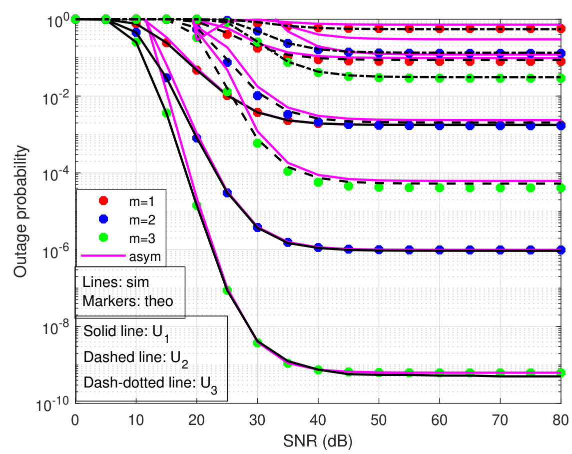

(b) Case of two relays.

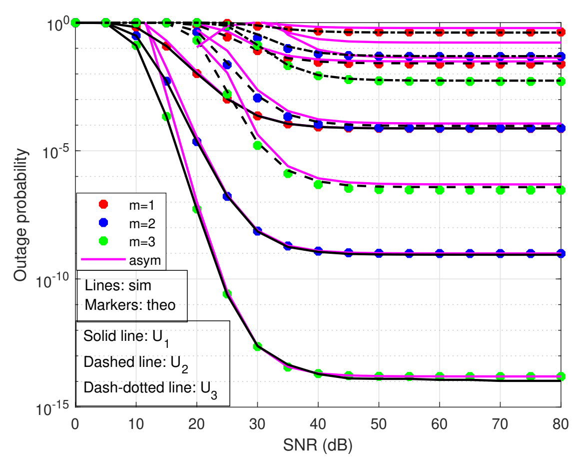

(c) Case of three relays.

Figure 6.3: OP w.r.t. SNR for uplink SIMO-CNOMA with SR of three users.

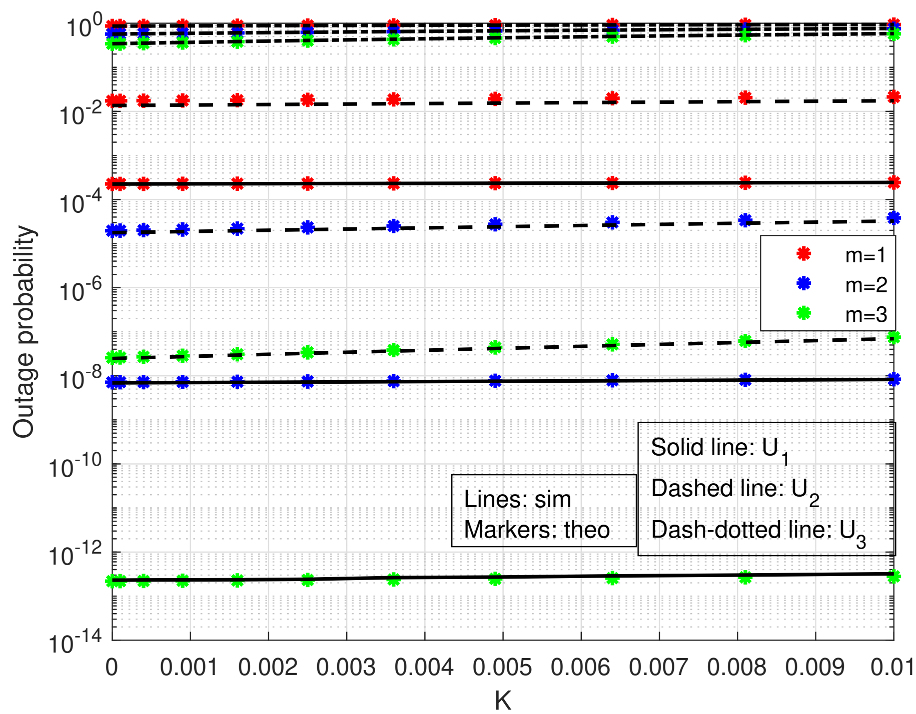

(a) OP w.r.t HWI.

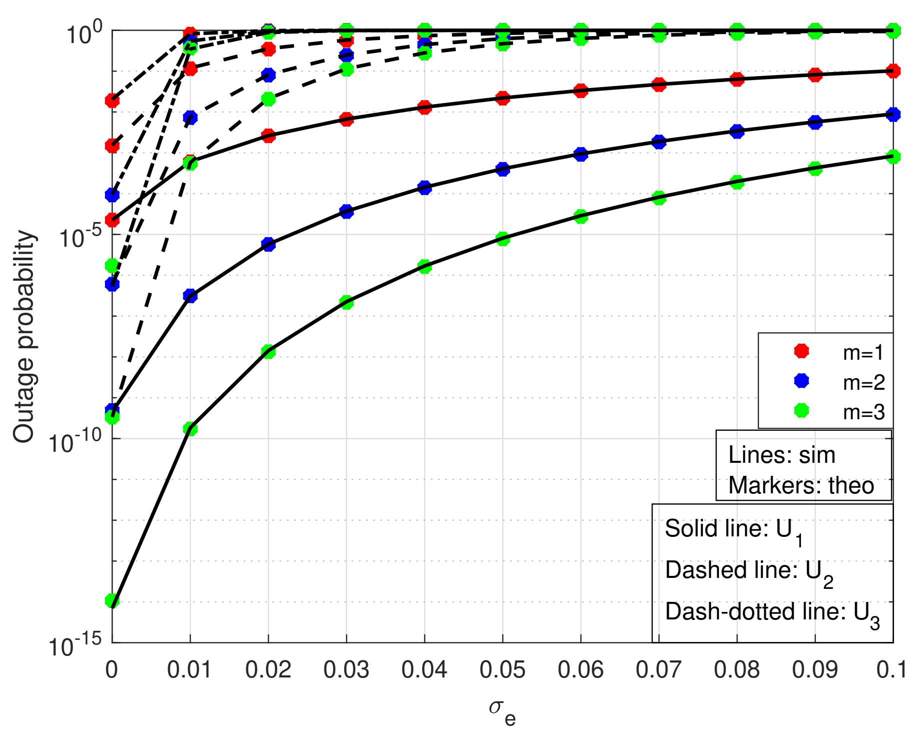

(b) OP w.r.t ipCSI.

Figure 6.4: OP performance evaluation for HWI and ipCSI for uplink SIMO-CNOMA.

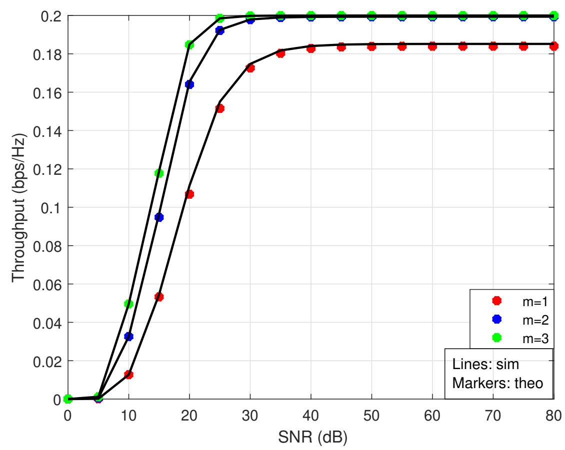

(a) Case of one relay.

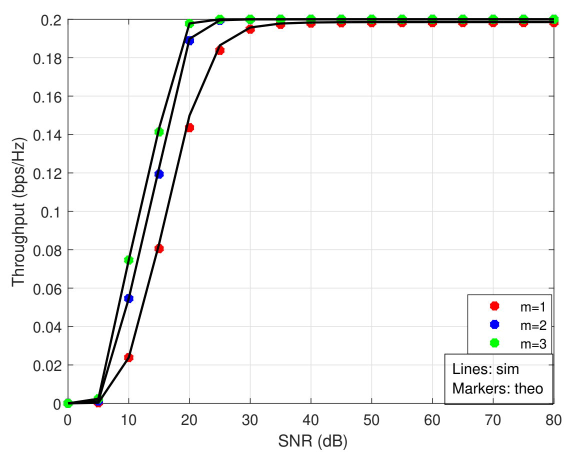

(b) Case of two relays.

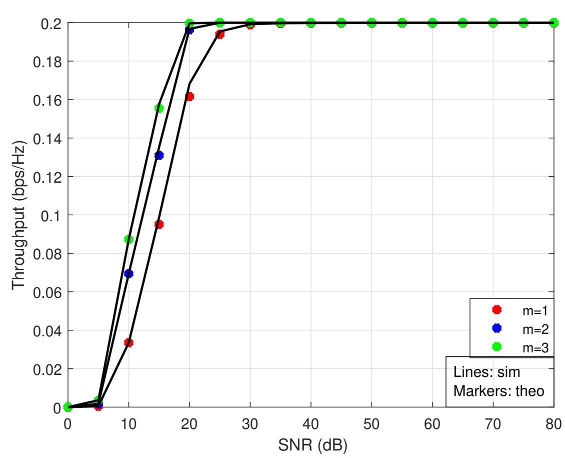

(c) Case of three relays.

Figure 6.5: Throughput w.r.t. SNR for uplink SIMO-CNOMA with SR of two users.

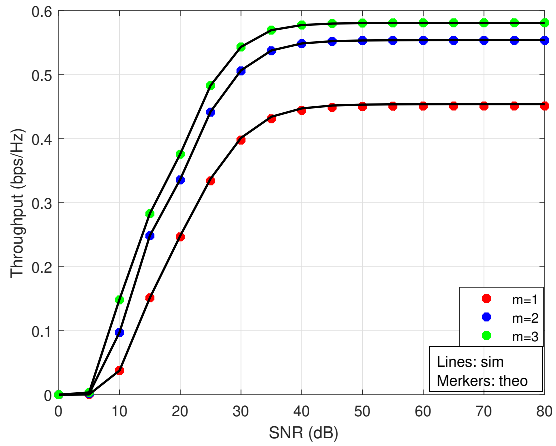

(a) Case of one relay.

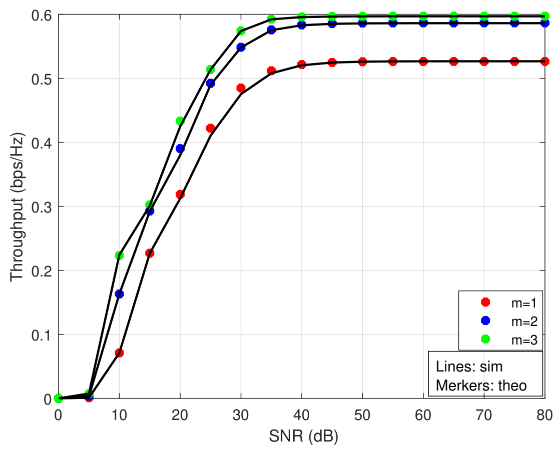

(b) Case of two relays.

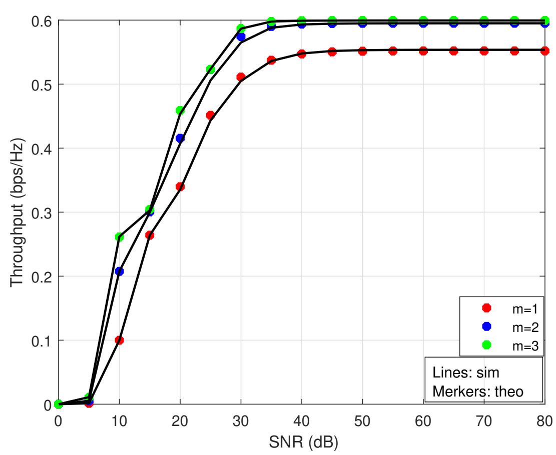

(c) Case of three relays.

Figure 6.6: Throughput w.r.t. SNR for uplink SIMO-CNOMA with SR of three users.

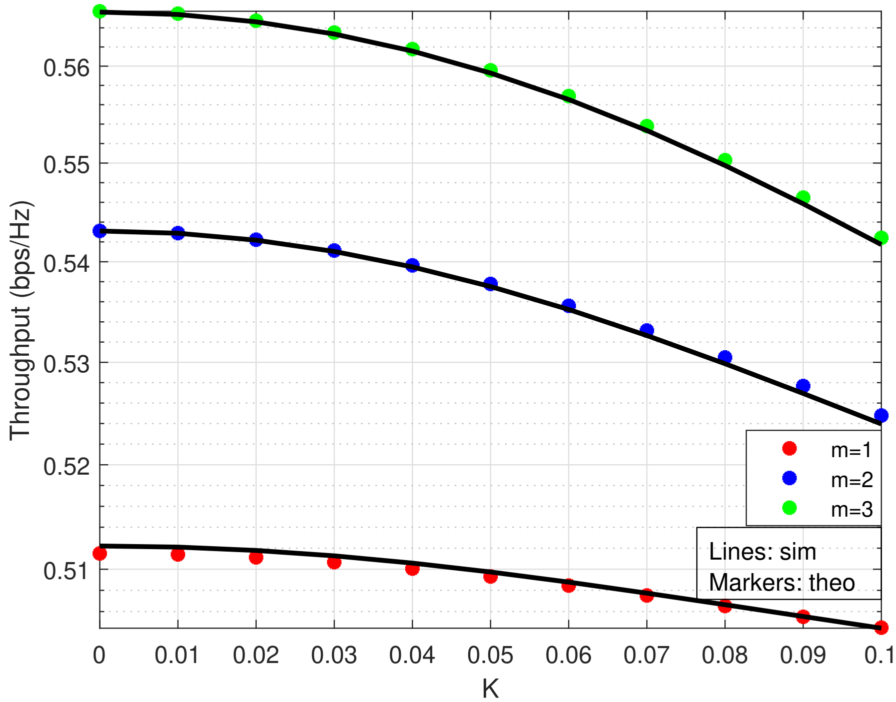

(a) Throughput w.r.t. HWI.

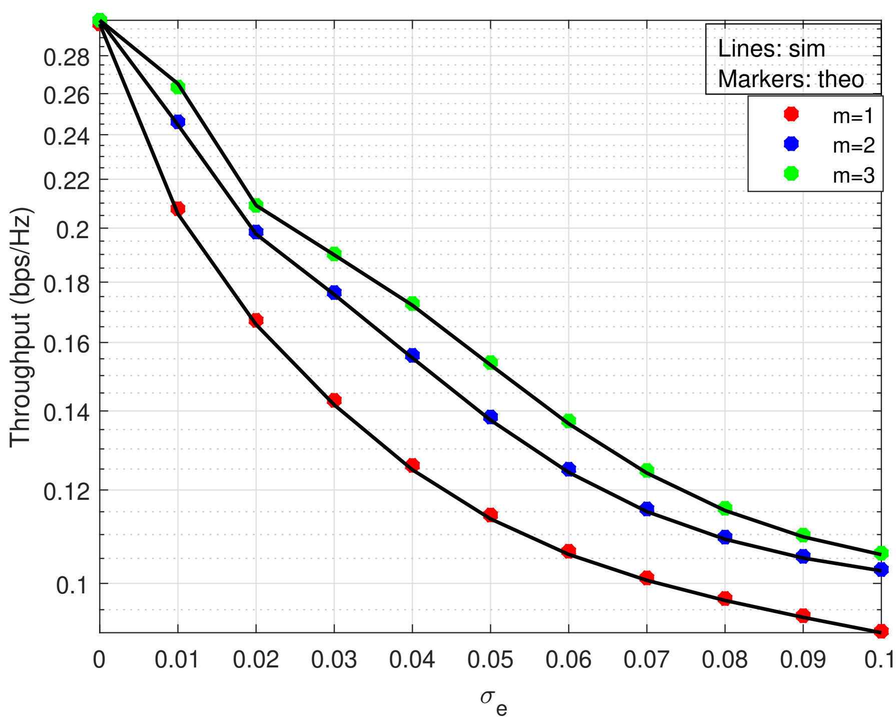

(b) Throughput w.r.t. ipCSI.

Figure 6.7: Throughput performance evaluation for ipCSI and HWI.

The system throughput of the uplink SIMO-CNOMA with different numbers of relays and antennas in the function of SNR is presented in Figs. 6.6 and 6.7 where the HWI, ipCSI, and ipSIC are taken into consideration. From the figures, it can be shown that the augmentation of the number of relays and antennas leads to an improvement in the system's throughput. Likewise, it becomes evident that an increase in the number of users is directly linked to enhanced system throughput performance.

The impact of HWI and channel estimation error are illustrated in Fig. 6.8, we evaluate the impact of the HWI and ipCSI on the uplink SIMO CNOMA in the presence of ipSIC where l = 3 and j = 3 on the system throughput. An increase in the HWI factor has a relatively less impact on system performance, whereas it is apparent that increasing the ipCSI factor leads to a more rapid decrease in system throughput. Our observations indicate that both HWI and ipCSI negatively affect system throughput performance. Consequently, it becomes evident that channel estimation error has a significantly greater impact on system performance compared to HWI.

6.5 Conclusion

In this chapter, the effect of the HWI on the uplink SIMO-CNOMA under ipCSI and ipSIC is examined in terms of OP and system throughput over the Rayleigh fading channel. By deriving The mathematical expressions for the OP and system throughput are derived and validated through computer simulations. The findings results demonstrate that, regardless of the number of relays and antennas in use, an increased number of users leads to a degradation in performance when HWI and ipCSI are present. the channel estimation error has a more significant influence on performance than HWI within the analyzed system. Nevertheless, as the number of antennas and relays increases, the system's performance shows improvement.

General conclusion

The emergence of Non-Orthogonal Multiple Access (NOMA) marks a significant and promising development in the field of wireless communication systems. This innovative approach holds the potential to meet the demanding requirements of 5G networks and beyond, offering robust connectivity, minimal latency, and exceptional spectral efficiency.

Within communication systems, transceivers play a pivotal role in both transmitting and receiving signals. However, owing to the inherent complexity of their internal components and the intricacies of the manufacturing process, transceivers often exhibit hardware imperfections and non-ideal behavior. Various factors contribute to these non-ideal operations, particularly in radio frequency (RF) transceivers.

This thesis focused on evaluating the impact of hardware impairments (HWI) on the NOMA system, seeking to understand how imperfections and non-ideal behavior in hardware components in a communication system can affect the performance and reliability of NOMA as a communication technique. Our research aimed to assess how HWIs influence NOMA's efficiency, reliability, and overall capabilities in wireless communication systems.

To create a more realistic scenario within communication systems, we considered imperfect channel state information (ipCSI) and imperfect successive interference (ipSIC). This approach helps us comprehend the challenges and interactions among these factors, enabling the development of mitigation strategies and performance benchmarking for NOMA in practical scenarios.

In the first chapter, we provided a general overview of NOMA and cooperative NOMA (CNOMA) systems. This chapter offered an introduction to the fundamental principles of the NOMA and CNOMA system, including its system model and the principles of communication. We also explored different links, both downlink and uplink. Additionally, we discussed various types of HWI, such as phase noise (PHN), high-power amplifier (HPA) issues, and in-phase and quadrature imbalance (IQI). The primary goal of this chapter was to establish a comprehensive understanding of NOMA systems.

In the second chapter of our study, we delved into the influence of HWIs and ipCSI on direct NOMA. We began by analyzing direct downlink NOMA and derived essential performance metrics, including outage probability (OP), ergodic capacity (EC), and bit error rate (BER). Subsequently, we shifted our focus to direct uplink NOMA, evaluating its performance in terms of OP and EC. The analytical analysis was validated through simulation results. It was demonstrated that ipCSI had a higher impact on performance than HWI in the two links of the NOMA system. This chapter provided crucial insights into the real-world challenges and potential enhancements of NOMA in wireless communication systems. A part of this chapter has been published in [57].

In the third chapter, we delved into a crucial aspect of wireless communication systems, specifically examining the downlink and uplink of NOMA techniques in the presence of IQI. We assumed that the communication link between users and the source was established through direct transmission. The mathematical analysis of the OP and EC was derived and validated through simulation. The results revealed that the impact of IQI on system performance was more pronounced when it manifested in the joint transmitter and receive.

The fourth chapter delved into the practical evaluation of OP and BER performance across three NOMA schemes: downlink NOMA, CNOMA with and without direct links considering realistic assumptions and accounting for imperfections such as ipSIC, ipCSI, and HWI. Exact expressions for end-to-end BER and OP were derived for each scheme and subsequently validated through computer simulations. Notably, our findings showed that the HWI exhibited a lesser impact on OP performance compared to ipCSI across all schemes. Interestingly, the BER of the NOMA could outperform CNOMA, particularly when HWI levels were relatively high. The discussion was extended to the influential role of power allocation (PA) on OP and BER, emphasizing the importance of prudent PA selection to prevent error propagation. Our work offers valuable insights for the practical implementation of NOMA schemes, providing a foundation for researchers to further analyze additional NOMA schemes under realistic conditions. This chapter has been published in [109].

Chapter Five investigated the impact of IQI on the performance of the CNOMA with direct links in the presence of ipCSI. We derived the OP and throughput expressions to evaluate the effects of imperfections on the performance of the considered systems. The mathematical analysis was validated using the simulation results. The results revealed that joint imperfections degraded significantly the performance of the systems. The presence of ipCSI degraded the performance of the ideal and non-ideal IQI. To this end, it was crucial to apply an efficient model, optimization, and dynamic compensation for the implementation of the NOMA and CNOMA systems. This chapter has been published in [151].

Chapter six of this thesis investigated the performance of the uplink SIMO-NOMA system with multiple relays, considering practical factors like HWI, ipCSI, and ipSIC. Mathematical expressions for OP and system throughput were derived, demonstrating alignment with simulation results. The study discussed the impact of HWI, ipCSI, and ipSIC on the performance of the uplink SIMO-CNOMA, emphasizing their critical role. Results indicated that, regardless of relay and antenna numbers, a higher number of users reduced system performance, favoring a lower number of users for better performance with fewer errors. Notably, ipCSI had a greater impact than HWI. Nevertheless, performance improved with more antennas and relays. The chapter offered insights for practical implementation of the uplink SIMO-CNOMA. Future work should explore multiple-input multiple-output (MIMO) technology in both phases of uplink CNOMA for enhanced system performance. This chapter has been published in [159].

Anticipated directions in NOMA research revolve around the critical consideration of HWI effects. This involves the integration of deep learning for adaptive optimization, specifically addressing the challenges imposed by hardware imperfections in uncrewed aerial vehicles (UAVs) and reconfigurable intelligent surfaces (RIS). The exploration extends to dynamic compensation strategies that intricately tackle hardware impairment complexities, ensuring the robustness of NOMA systems. The research emphasis lies not only on the adaptability of NOMA in diverse multi-modal scenarios but also on fortifying security and privacy measures in the face of hardware vulnerabilities. The practical implementation and standardization efforts are aligned with this focus, recognizing the need for resilient NOMA systems in real-world hardware conditions. Additionally, the exploration of HWI-MIMO technologies in NOMA and the pursuit of energy-efficient designs for UAV-powered NOMA systems underscore the commitment to overcoming HWI challenges, thereby fostering the continued evolution and widespread adoption of NOMA in wireless communication.

Bibliography

[1] SM Riazul Islam, Nurilla Avazov, Octavia A Dobre, and Kyung-Sup Kwak. Power-domain non-orthogonal multiple access (NOMA) in 5G systems: Potentials and challenges. *IEEE Communications Surveys & Tutorials*, 19(2):721–742, 2016.

[2] Mamta Agiwal, Abhishek Roy, and Navrati Saxena. Next generation 5G wireless networks: A comprehensive survey. *IEEE communications surveys & tutorials*, 18(3):1617–1655, 2016.

[3] Klein S Gilhousen, Irwin M Jacobs, Roberto Padovani, Andrew J Viterbi, Lindsay A Weaver, and Charles E Wheatley. On the capacity of a cellular CDMA system. *IEEE transactions on vehicular technology*, 40(2):303–312, 1991.

[4] Hina Tabassum, Md Shipon Ali, Ekram Hossain, Md Jahangir Hossain, and Dong In Kim. Non-orthogonal multiple access (NOMA) in cellular uplink and downlink: Challenges and enabling techniques. *arXiv preprint arXiv:1608.05783*, 2016.

[5] SM Islam, Ming Zeng, Octavia A Dobre, and Kyung-Sup Kwak. Non-orthogonal multiple access (NOMA): How it meets 5G and beyond. *arXiv preprint arXiv:1907.10001*, 2019.

[6] Bassant Selim, Sami Muhaidat, Paschalis C Sofotasios, Bayan S Sharif, Thanos Stouraitis, George K Karagiannidis, and Naofal Al-Dhahir. Outage probability of single carrier NOMA systems under I/Q imbalance. In *2018 IEEE Wireless Communications and Networking Conference (WCNC)*, pages 1–6. IEEE, 2018.

[7] Yuanwei Liu, Zhijin Qin, and Zhiguo Ding. *Non-orthogonal multiple access for massive connectivity*. Springer, 2020.

[8] Zhiguo Ding, Yuanwei Liu, Jinho Choi, Qi Sun, Maged Elkashlan, I Chih-Lin, and H Vincent Poor. Application of non-orthogonal multiple access in LTE and 5G networks. *IEEE Communications Magazine*, 55(2):185–191, 2017.

[9] Yuanwei Liu, Zhijin Qin, Maged Elkashlan, Zhiguo Ding, Arumugam Nallanathan, and Lajos Hanzo. Non-orthogonal multiple access for 5G and beyond. *Proceedings of the IEEE*, 105(12):2347–2381, 2017.

[10] Yingmin Wang, Bin Ren, Shaohui Sun, Shaoli Kang, and Xinwei Yue. Analysis of non-orthogonal multiple access for 5G. *China Communications*, 13(2):52–66, 2016.

[11] Ming Zeng, Animesh Yadav, Octavia A Dobre, and H Vincent Poor. Energy-efficient joint user-RB association and power allocation for uplink hybrid NOMA-OMA. *IEEE Internet of Things Journal*, 6(3):5119–5131, 2019.

[12] J Nicholas Laneman, David NC Tse, and Gregory W Wornell. Cooperative diversity in wireless networks: Efficient protocols and outage behavior. *IEEE Transactions on Information theory*, 50(12):3062–3080, 2004.

[13] Bassant Selim, Sami Muhaidat, Paschalis C Sofotasios, Bayan S Sharif, Thanos Stouraitis, George K Karagiannidis, and Naofal Al-Dhahir. Performance analysis of non-orthogonal multiple access under I/Q imbalance. *IEEE Access*, 6:18453–18468, 2018.

[14] François Horlin and André Bourdoux. *Digital compensation for analog front-ends: a new approach to wireless transceiver design*. John Wiley & Sons, 2008.

[15] Dong-Sun Kim, Sung-Joon Jang, and Tae-Ho Hwang. A fully integrated sensor SoC with digital calibration hardware and wireless transceiver at 2.4 GHz. *Sensors*, 13(5):6775–6792, 2013.

[16] Fernando Gregorio, Gustavo González, Christian Schmidt, and Juan Cousseau. Signal processing techniques for power efficient wireless communication systems. *Practical Approaches for RF Impairments Reduction*, 2020.

[17] Ali Soltani Tehrani. *Behavioral modeling of radio frequency transmitters*. Chalmers Tekniska Hogskola (Sweden), 2009.

[18] Mikko Valkama. *Advanced I/Q signal processing for wideband receivers models and algorithms*. Tampere University of Technology, 2001.

[19] Alper Demir, Amit Mehrotra, and Jaijeet Roychowdhury. Phase noise in oscillators: A unifying theory and numerical methods for characterisation. In *Proceedings of the 35th annual Design Automation Conference*, pages 26–31, 1998.

[20] Mohammad Reza Khanzadi. *Phase Noise in Communication Systems–Modeling, Compensation, and Performance Analysis.* Chalmers University of Technology, 2015.

[21] Dinh-Thuan Do and Tu-Trinh Thi Nguyen. Impacts of imperfect SIC and imperfect hardware in performance analysis on AF non-orthogonal multiple access network. *Telecommunication Systems*, 72(4):579–593, 2019.

[22] Ali Afana, Najah Abu-Ali, and Salama Ikki. On the joint impact of hardware and channel imperfections on cognitive spatial modulation MIMO systems: Cramer–Rao bound approach. *IEEE Systems Journal*, 13(2):1250–1261, 2018.

[23] Emil Bjornson, Michail Matthaiou, and Merouane Debbah. A new look at dual-hop relaying: Performance limits with hardware impairments. *IEEE Transactions on Communications*, 61(11):4512–4525, 2013.

[24] Davide Dardari, Velio Tralli, and Alessandro Vaccari. A theoretical characterization of nonlinear distortion effects in OFDM systems. *IEEE transactions on Communications*, 48(10):1755–1764, 2000.

[25] Basuki E Priyanto, Troels B Sorensen, Ole K Jensen, Torben Larsen, Troels Kolding, and Preben Mogensen. Assessing and modeling the effect of RF impairments on UTRA LTE uplink performance. In *2007 IEEE 66th Vehicular Technology Conference*, pages 1213–1217. IEEE, 2007.

[26] Asma Bouhlel and Anis Sakly. Impact of IQ Imbalance on RIS-Assisted SISO Communication Systems. *Wireless Communications and Mobile Computing*, 2021:1–12, 2021.

[27] Aly Mahmoud AbdEllatif, Ahmed Hesham Mehana, and Yasmine Fahmy. IQ imbalance analysis and compensation in multiple antenna systems. *IET Communications*, 14(11):1748–1758, 2020.

[28] Amirhossein Mohammadian and Chintha Tellambura. RF impairments in wireless transceivers: Phase noise, CFO, and IQ imbalance–A survey. *IEEE Access*, 9:111718–111791, 2021.

[29] Chang Zheng et al. OFDM Interference Analysis with'Dirty RF'. Master's thesis, Helsinki University of Technology, 2009.

[30] Xingwang Li, Mengle Zhao, Xiang-Chuan Gao, Lihua Li, Dinh-Thuan Do, Khaled M Rabie, and Rupak Kharel. Physical layer security of cooperative NOMA for IoT networks under I/Q imbalance. *IEEE Access*, 8:51189–51199, 2020.

[31] Denis Petrovic, Wolfgang Rave, and Gerhard Fettweis. Effects of phase noise on OFDM systems with and without PLL: Characterization and compensation. *IEEE Transactions on communications*, 55(8):1607–1616, 2007.

[32] Huseyin Arslan. *Wireless communication signals: A laboratory-based approach*. John Wiley & Sons, 2021.

[33] Steve C Cripps et al. *RF power amplifiers for wireless communications*, volume 250. Artech house Norwood, MA, 2006.

[34] Lydi Smaini. *Rf analog impairments modeling for communication systems simulation: application to OFDM-based transceivers*. John Wiley & Sons, 2012.

[35] Praveen Kumar Singya, Nagendra Kumar, and Vimal Bhatia. Mitigating NLD for wireless networks: Effect of nonlinear power amplifiers on future wireless communication networks. *IEEE Microwave Magazine*, 18(5):73–90, 2017.

[36] Truman S Gray. *Applied Electronics*. Asia, 1958.

[37] Siavash M Alamouti. A simple transmit diversity technique for wireless communications. *IEEE Journal on selected areas in communications*, 16(8):1451–1458, 1998.

[38] Seung Hee Han and Jae Hong Lee. An overview of peak-to-average power ratio reduction techniques for multicarrier transmission. *IEEE wireless communications*, 12(2):56–65, 2005.

[39] Robert E Collin. *Foundations for microwave engineering*. John Wiley & Sons, 2007.

[40] Shimin Gong, Xiao Lu, Dinh Thai Hoang, Dusit Niyato, Lei Shu, Dong In Kim, and Ying-Chang Liang. Toward smart wireless communications via intelligent reflecting surfaces: A contemporary survey. *IEEE Communications Surveys & Tutorials*, 22(4):2283–2314, 2020.

[41] *Analog Electronics: circuits, systems and signal processing, author=Crecraft, David and Gergely, Stephen*. Elsevier, 2002.

[42] Xingwang Li, Jingjing Li, P Takis Mathiopoulos, Di Zhang, Lihua Li, and Jin Jin. Joint impact of hardware impairments and imperfect CSI on cooperative SWIPT NOMA multi-relaying systems. In *2018 IEEE/CIC International Conference on Communications in China (ICCC)*, pages 95–99. IEEE, 2018.

[43] Lina Mohjazi, Lina Bariah, Sami Muhaidat, Paschalis C Sofotasios, Oluwakayode Onireti, and Muhammad Ali Imran. Error probability analysis of non-orthogonal multiple access for relaying networks with residual hardware impairments. In *IEEE 30th Annual Internat. Symp. Pers., Mob. Radio Commun. (PIMRC)*, 2019.

[44] Akash Agarwal, Rishabh Chaurasiya, Sudhakar Rai, and Aditya K Jagannatham. Outage probability analysis for NOMA downlink and uplink communication systems with generalized fading channels. *IEEE Access*, 8:220461–220481, 2020.

[45] Refik Caglar Kizilirmak and Hossein Khaleghi Bizaki. Non-orthogonal multiple access (NOMA) for 5G networks. *Towards 5G Wireless Networks-A Physical Layer Perspective*, 83:83–98, 2016.

[46] Monika Jain, Sandhya Soni, Nikhil Sharma, and Divyang Rawal. Performance analysis at far and near user in NOMA based system in presence of SIC error. *AEU-International Journal of Electronics and Communications*, 114:152993, 2020.

[47] Ferdi Kara and Hakan Kaya. BER performances of downlink and uplink NOMA in the presence of SIC errors over fading channels. *IET Communications*, 12(15):1834–1844, 2018.

[48] Tim Schenk. *RF imperfections in high-rate wireless systems: impact and digital compensation*. Springer Science & Business Media, 2008.

[49] Chao Deng, Xiaoya Zhao, Di Zhang, Xingwang Li, Jingjing Li, and Charles Casimiro Cavalcante. Performance analysis of NOMA-based relaying networks with transceiver hardware impairments. 2018.

[50] Chao Deng, Meng Liu, Xingwang Li, and Yuanwei Liu. Hardware impairments aware full-duplex NOMA networks over Rician fading channels. *IEEE Systems Journal*, 15(2):2515–2518, 2020.

[51] Zheng Yang, Zhiguo Ding, Pingzhi Fan, and George K Karagiannidis. On the performance of non-orthogonal multiple access systems with partial channel information. *IEEE Transactions on Communications*, 64(2):654–667, 2015.

[52] Dinh-Thuan Do, Mojtaba Vaezi, and Thanh-Luan Nguyen. Wireless powered cooperative relaying using NOMA with imperfect CSI. In *2018 IEEE Globecom Workshops (GC Wkshps)*, pages 1–6. IEEE, 2018.

[53] Yichen Gao, Bin Xia, Yingbin Liu, Yao Yao, Kexin Xiao, and Guanping Lu. Analysis of the dynamic ordered decoding for uplink NOMA systems with imperfect CSI. *IEEE Transactions on Vehicular Technology*, 67(7):6647–6651, 2018.

[54] Kyuhyuk Chung. Impact of Channel Estimation Errors on BER Performance of Single-User Decoding NOMA System. *International Journal of Internet, Broadcasting and Communication*, 12(4):18–25, 2020.

[55] KARA Ferdi and KAYA Hakan. Error probability analysis of non-orthogonal multiple access with channel estimation errors. In *2020 IEEE International Black Sea Conference on Communications and Networking (BlackSeaCom)*, pages 1–5. IEEE, 2020.

[56] Ferdi Kara and Hakan Kaya. Improved user fairness in decode-forward relaying non-orthogonal multiple access schemes with imperfect SIC and CSI. *IEEE Access*, 8:97540–97556, 2020.

[57] Safia Beddiaf and Abdellatif Khelil. Performance analysis of the NOMA network under joint hardware impairment and imperfect channel state information. *Telecommunications and Radio Engineering*.

[58] Xingwang Li, Jingjing Li, Yuanwei Liu, Zhiguo Ding, and Arumugam Nallanathan. Residual transceiver hardware impairments on cooperative NOMA networks. *IEEE Transactions on Wireless Communications*, 19(1):680–695, 2019.

[59] Ferdi Kara and Hakan Kaya. On the error performance of cooperative-NOMA with statistical CSIT. *IEEE Communications Letters*, 23(1):128–131, 2018.

[60] Thi My Chinh Chu and Hans-Jürgen Zepernick. Outage probability and secrecy capacity of a non-orthogonal multiple access system. In *2017 11th International Conference on Signal Processing and Communication Systems (ICSPCS)*, pages 1–6. IEEE, 2017.

[61] Shailendra Singh and Matadeen Bansal. Outage analysis of NOMA-based cooperative relay systems with imperfect SIC. *Physical Communication*, 43:101219, 2020.

[62] Izrail Solomonovich Gradshteyn and Iosif Moiseevich Ryzhik. *Table of integrals, series, and products*. Academic press, 2014.

[63] Xianbin Xie, Jinhua Liu, Jiawen Huang, and Shiwei Zhao. Ergodic capacity and outage performance analysis of uplink full-duplex cooperative NOMA system. *IEEE Access*, 8:164786–164794, 2020.

[64] Nguyen Tien Tung, Pham Minh Nam, and Phu Tran Tin. Performance evaluation of a two-way relay network with energy harvesting and hardware noises. *Digital Communications and Networks*, 7(1):45–54, 2021.

[65] Özgür Özdemir, Ridha Hamila, and Naofal Al-Dhahir. Exact average OFDM subcarrier SINR analysis under joint transmit–receive I/Q imbalance. *IEEE Trans. Veh. Tech.*, 63(8):4125–4130, 2014.

[66] Ozgur Ozdemir, Ridha Hamila, and Naofal Al-Dhahir. I/Q imbalance in multiple beamforming {OFDM} transceivers: SINR analysis and digital baseband compensation. *IEEE transactions on communications*, 61(5):1914–1925, 2013.

[67] Bassant Selim, Paschalis C Sofotasios, Sami Muhaidat, and George K Karagiannidis. The effects of I/Q imbalance on wireless communications: A survey. In *2016 IEEE 59th International Midwest Symposium on Circuits and Systems (MWSCAS)*, pages 1–4. IEEE, 2016.

[68] Ridha Hamila, Özgür Özdemir, and Naofal Al-Dhahir. Beamforming OFDM performance under joint phase noise and I/Q imbalance. *IEEE Transactions on Vehicular Technology*, 65(5):2978–2989, 2015.

[69] Mohamed Mokhtar, Ahmad Gomaa, and Naofal Al-Dhahir. OFDM AF relaying under I/Q imbalance: Performance analysis and baseband compensation. *IEEE Transactions on Communications*, 61(4):1304–1313, 2013.

[70] Bassant Selim, Sami Muhaidat, Paschalis C Sofotasios, Arafat Al-Dweik, Bayan S Sharif, and Thanos Stouraitis. Radio-frequency front-end impairments: Performance degradation in nonorthogonal multiple access communication systems. *IEEE Vehicular Technology Magazine*, 14(1):89–97, 2019.

[71] Xinji Tian, Qianqian Li, Xingwang Li, Hongxing Peng, Changsen Zhang, Khaled M Rabie, and Rupak Kharel. I/Q imbalance and imperfect SIC on two-way relay NOMA systems. *Electronics*, 9(2):249, 2020.

[72] Alexandros-Apostolos A Boulogeorgos, Paschalis C Sofotasios, Bassant Selim, Sami Muhaidat, George K Karagiannidis, and Mikko Valkama. Effects of RF impairments in communications over cascaded fading channels. *IEEE Transactions on Vehicular Technology*, 65(11):8878–8894, 2016.

[73] Zhiguo Ding, Zheng Yang, Pingzhi Fan, and H Vincent Poor. On the performance of non-orthogonal multiple access in 5G systems with randomly deployed users. *IEEE signal processing letters*, 21(12):1501–1505, 2014.

[74] Xingwang Li, Mengle Zhao, Changsen Zhang, Wali Ullah Khan, Jun Wu, Khaled M Rabie, and Rupak Kharel. Security analysis of multi-antenna NOMA networks under I/Q imbalance. *Electronics*, 8(11):1327, 2019.

[75] Xingwang Li, Mengle Zhao, Yuanwei Liu, Lihua Li, Zhiguo Ding, and Arumugam Nallanathan. Secrecy analysis of ambient backscatter NOMA systems under I/Q imbalance. *IEEE Transactions on Vehicular Technology*, 69(10):12286–12290, 2020.

[76] Malek M Alsmadi, Najah Abu Ali, Mohammed Hayajneh, and Salama S Ikki. Downlink NOMA networks in the presence of IQI and imperfect SIC: Receiver design and performance analysis. *IEEE Transactions on Vehicular Technology*, 69(6):6793–6797, 2020.

[77] Seyed Ali Mohajeran and Seyed Mohammad Sajad Sadough. Outage performance analysis of secondary user under Tx/Rx IQI in cognitive radio systems. In *2015 5th International Conference on Computer and Knowledge Engineering (ICCKE)*, pages 246–250. IEEE, 2015.

[78] Alexandros-Apostolos A Boulogeorgos, Paschalis C Sofotasios, Sami Muhaidat, Mikko Valkama, and George K Karagiannidis. The effects of RF impairments in vehicle-to-vehicle communications. In *2015 IEEE 26th Annual International Symposium on Personal, Indoor, and Mobile Radio Communications (PIMRC)*, pages 840–845. IEEE, 2015.

[79] Ming Zeng, Wanming Hao, Octavia A Dobre, and Zhiguo Ding. Cooperative NOMA: State of the art, key techniques, and open challenges. *IEEE Netwowrk Magazine*, 34(5):205–211, 2020.

[80] Hongwu Liu, Zhiguo Ding, Kyeong Jin Kim, Kyung Sup Kwak, and H Vincent Poor. Decode-and-forward relaying for cooperative NOMA systems with direct links. *IEEE Transactions on Wireless Communications*, 17(12):8077–8093, 2018.

[81] Relay selection for cooperative NOMA, author=Ding, Zhiguo and Dai, Huaiyu and Poor, H Vincent. *IEEE Wireless Communications Letters*, 5(4):416–419, 2016.

[82] Xuesong Liang, Yongpeng Wu, Derrick Wing Kwan Ng, Yiping Zuo, Shi Jin, and Hongbo Zhu. Outage performance for cooperative NOMA transmission with an AF relay. *IEEE Communications Letters*, 21(11):2428–2431, 2017.

[83] Dehuan Wan, Miaowen Wen, Fei Ji, Yun Liu, and Yu Huang. Cooperative NOMA systems with partial channel state information over Nakagami-m fading channels. *IEEE Transactions on Communications*, 66(3):947–958, 2017.

[84] Ningning Guo, Jianhua Ge, Qifei Bu, and Chensi Zhang. Multi-user cooperative non-orthogonal multiple access scheme with hybrid full/half-duplex user-assisted relaying. *IEEE Access*, 7:39207–39226, 2019.

[85] Xinwei Yue, Yuanwei Liu, Shaoli Kang, Arumugam Nallanathan, and Zhiguo Ding. Exploiting full/half-duplex user relaying in NOMA systems. *IEEE Transactions on Communications*, 66(2):560–575, 2017.

[86] Hang-Thi-Thu Nguyen, Thuy Nguyen, and Xuan Nam Tran. Full-duplex cooperative NOMA system under impacts of residual SI and MAI. *International Journal of Electronics*, 108(5):858–875, 2021.

[87] V Aswathi and AV Babu. Full/half duplex cooperative NOMA under imperfect successive interference cancellation and channel state estimation errors. *IEEE Access*, 7:179961–179984, 2019.

[88] Tu-Trinh Thi Nguyen, Dinh-Thuan Do, Yeong-Chin Chen, Chakchai So-In, and Md Arafatur Rahman. New look on relay selection strategies for full-duplex multiple-relay NOMA over Nakagami-m fading channels. *Wireless Networks*, 27(6):3827–3843, 2021.

[89] Wei Duan, Miaowen Wen, Zixiang Xiong, and Moon Ho Lee. Two-stage power allocation for dual-hop relaying systems with non-orthogonal multiple access. *IEEE Access*, 5:2254–2261, 2017.

[90] Roopesh Ramesh and Sanjeev Gurugopinath. Sum rate analysis of cooperative NOMA over dual-hop wireless-power line communication. In *2021 IEEE 18th India Council International Conference (INDICON)*, pages 1–6, 2021.

[91] Dehuan Wan, Miaowen Wen, Fei Ji, and Ronglan Huang. Non-orthogonal multiple access for dual-hop decode-and-forward relay-aided X channel. In *IEEE 85th Vehicular Technology Conference (VTC Spring)*, pages 1–5, 2017.

[92] Yue Xiao, Li Hao, Zheng Ma, Zhiguo Ding, Zhengquan Zhang, and Pingzhi Fan. Forwarding strategy selection in dual-hop NOMA relaying systems. *IEEE Communications Letters*, 22(8):1644–1647, 2018.

[93] Xinwei Yue, Zhijin Qin, Yuanwei Liu, Xiaoming Dai, and Yue Chen. Outage performance of a unified non-orthogonal multiple access framework. In *IEEE International Conference on Communications (ICC)*, pages 1–6, 2018.

[94] Xinwei Yue, Yuanwei Liu, Yuanyuan Yao, Xuehua Li, Rongke Liu, and Arumugam Nallanathan. Secure communications in a unified non-orthogonal multiple access framework. *IEEE Transactions on Wireless Communications*, 19(3):2163–2178, 2020.

[95] Xinwei Yue, Zhijin Qin, Yuanwei Liu, Shaoli Kang, and Yue Chen. A unified framework for non-orthogonal multiple access. *IEEE Transactions on Communications*, 66(11):5346–5359, 2018.

[96] Tan Phuoc Huynh, Tam Nguyen Kieu, Thuan Do Dinh, Miroslav Voznak, and Dominik Uhrin. A performance analysis about impact of I/Q imbalance in AF two-hop relay system. In *2016 IEEE XI Internat. Symp. Telecommun. (BIHTEL)*, pages 1–4.

[97] N Maletić, M Čabarkapa, and N Nešković. Performance of fixed-gain amplify-and-forward nonlinear relaying with hardware impairments. *International Journal of Communications Systems*, 30(6):e3102, 2017.

[98] Xingwang Li, Meng Liu, Chao Deng, Di Zhang, Xiang-Chuan Gao, Khaled M. Rabie, and Rupak Kharel. Joint effects of residual hardware impairments and channel estimation errors on SWIPT assisted cooperative NOMA networks. *IEEE Access*, 7:135499–135513, 2019.

[99] Wei Xie, Xiaochen Xia, Youyun Xu, Kui Xu, and Yurong Wang. Massive MIMO full-duplex relaying with hardware impairments. *Journal of Communications and Networking*, 19(4):351–362, 2017.

[100] Ba Cao Nguyen, Xuan Nam Tran, Dinh Tan Tran, Xuan Nghia Pham, et al. Impact of hardware impairments on the outage probability and ergodic capacity of one-way and two-way full-duplex relaying systems. *IEEE Transactions on Vehicular Technology*, 69(8):8555–8567, 2020.

[101] Xingwang Li, Jingjing Li, and Lihua Li. Performance analysis of impaired SWIPT NOMA relaying networks over imperfect Weibull channels. *IEEE Systems Journal*, 14(1):669–672, 2019.

[102] Meiling Li, Bassant Selim, Sami Muhaidat, Paschalis C Sofotasios, Mehrdad Dianati, Paul D Yoo, Jie Liang, and Anhong Wang. Effects of residual hardware impairments on secure NOMA-based cooperative systems. *IEEE Access*, 8:2524–2536, 2019.

[103] Sultangali Arzykulov, Galymzhan Nauryzbayev, Abdulkadir Celik, and Ahmed M Eltawil. Hardware and interference limited cooperative CR-NOMA networks under imperfect SIC and CSI. *IEEE Open Journal of Communications Society*, 2:1473–1485, 2021.

[104] Anis Amazigh Hamza, Iyad Dayoub, Ihsen Alouani, and Abderrahmane Amrouche. On the error rate performance of full-duplex cooperative NOMA in wireless networks. *IEEE Transactions on Communications*, 70(3):1742–1758, 2022.

[105] Faical Khennoufa, Khelil Abdellatif, and Ferdi Kara. Bit error rate and outage probability analysis for multi-hop decode-and-forward relay-aided NOMA with imperfect SIC and imperfect CSI. *AEU-International Journal of Electronics and Communications*, 147:154124, 2022.

[106] KARA Ferdi and KAYA Hakan. A true power allocation constraint for non-orthogonal multiple access with M-QAM signalling. In *IEEE Microwave Theory and Techniques in Wireless Communications (MTTW)*, volume 1, pages 7–12, 2020.

[107] Hamad Yahya, Emad Alsusa, and Arafat Al-Dweik. Exact BER analysis of NOMA with arbitrary number of users and modulation orders. *IEEE Transactions on Communications*, 69(9):6330–6344, 2021.

[108] Tasneem Assaf, Arafat Al-Dweik, Mohamed El Moursi, and Hatem Zeineldin. Exact BER performance analysis for downlink NOMA systems over Nakagami-m fading channels. *IEEE Access*, 7:134539–134555, 2019.

[109] Safia Beddiaf, Abdellatif Khelil, Faical Khennoufa, Ferdi Kara, Hakan Kaya, Xingwang Li, Khaled Rabie, and Halim Yanikomeroglu. A unified performance analysis of cooperative NOMA with practical constraints: hardware impairment, imperfect SIC and CSI. *IEEE Access*, 10:132931–132948, 2022.

[110] Stefan Valentin, Dereje H Woldegebreal, Tobias Volkhausen, and Holger Karl. Combining for cooperative WLANs-a reality check based on prototype measurements. In *2009 IEEE Internat. Conf. Commun. Workshops*, pages 1–5.

[111] Galymzhan Nauryzbayev, Sultangali Arzykulov, Theodoros A Tsiftsis, and Mohamed Abdallah. Performance of cooperative underlay CR-NOMA networks over Nakagami-m channels. In *2018 IEEE International Conference on Communications Workshops (ICC Workshops)*, pages 1–6. IEEE, 2018.

[112] Marvin K Simon and Mohamed-Slim Alouini. *Digital communications over Fading Channels* . John-Wiley & Sons, 2004.

[113] John G. Proakis and Masoud Salehi. *Digital communications*. McGraw-Hill, 2008.

[114] Furuzan Atay Onat, Abdulkareem Adinoyi, Yijia Fan, Halim Yanikomeroglu, John S Thompson, and Ian D Marsland. Threshold selection for SNR-based selective digital relaying in cooperative wireless networks. *IEEE Transactions on Wireless Communications*, 7(11):4226–4237, 2008.

[115] Zhenling Wang, Zhangyou Peng, Yongsheng Pei, and Haojia Wang. Performance analysis of cooperative NOMA systems with incremental relaying. *Wirel. Commun. Mob. Comp.*, 2020, 2020.

[116] Xingwang Li, Meng Liu, Chao Deng, Di Zhang, Xiang-Chuan Gao, Khaled M Rabie, and Rupak Kharel. Joint effects of residual hardware impairments and channel estimation errors on SWIPT assisted cooperative NOMA networks. *IEEE Access*, 7:135499–135513, 2019.

[117] Shady M Ibraheem, Walid Bedawy, Waleed Saad, and Mona Shokair. Outage performance of NOMA-based DF relay sharing networks over Nakagami-m fading channels. In *2018 13th International Conference on Computer Engineering and Systems (ICCES)*, pages 512–517. IEEE, 2018.

[118] Jung-Bin Kim and In-Ho Lee. Non-orthogonal multiple access in coordinated direct and relay transmission. *IEEE Commun. Lett.*, 19(11):2037–2040, 2015.

[119] Galymzhan Nauryzbayev, Orken Omarov, Sultangali Arzykulov, Khaled M Rabie, Xingwang Li, and Ahmed M Eltawil. Performance limits of wireless powered cooperative NOMA over generalized fading. *Trans. Emerg. Telecommun. Tech.*, 33(4):e4415, 2022.

[120] Guoxin Li, Deepak Mishra, and Hai Jiang. Cooperative NOMA with incremental relaying: Performance analysis and optimization. *IEEE Transactions on Vehicular Technology*, 67(11):11291–11295, 2018.

[121] Xianli Gong, Xinwei Yue, and Feng Liu. Performance analysis of cooperative NOMA networks with imperfect CSI over Nakagami-m fading channels. *Sensors*, 20(2):424, 2020.

[122] Jiayi Zhang, Linglong Dai, Ruicheng Jiao, Xu Li, and Ying Liu. Performance analysis of relay assisted cooperative non-orthogonal multiple access systems. *submitted to IEEE Wireless Commun. Lett*, 2017.

[123] Wei Duan, Guoan Zhang, Qiang Sun, Jia Hou, Yancheng Ji, and Jeaho Choi. On the performance of an enhanced transmission scheme for cooperative relay networks with NOMA. *EURASIP Journal on Wireless Communications and Networking*, 2018:1–14, 2018.

[124] Ferdi Kara and Hakan Kaya. Threshold-based selective cooperative NOMA: Capacity/outage analysis and a joint power allocation-threshold selection optimization. *IEEE Communications Letters*, 24(9):1929–1933, 2020.

[125] Mohammed Belal Uddin, Md Fazlul Kader, and Soo Young Shin. Uplink cooperative diversity using power-domain nonorthogonal multiple access. *Transactions on Emerging Telecommunications Technologies*, 30(12):e3678, 2019.

[126] Yingying Zhang, Zhen Yang, Youhong Feng, and Shihao Yan. Performance analysis of a novel uplink cooperative NOMA system with full-duplex relaying. *IET Communications*, 12(19):2408–2417, 2018.

[127] Asad A Abidi. Direct-conversion radio transceivers for digital communications. *IEEE Journal of solid-state circuits*, 30(12):1399–1410, 1995.

[128] Shahriar Mirabbasi and Ken Martin. Classical and modern receiver architectures. *IEEE Communications Magazine*, 38(11):132–139, 2000.

[129] Alexandros-Apostolos A Boulogeorgos, Paschalis C Sofotasios, Bassant Selim, Sami Muhaidat, George K Karagiannidis, and Mikko Valkama. Outage probability under I/Q imbalance and cascaded fading effects. In *2016 23rd Intern. Conf. Tel. (ICT)*, pages 1–5. IEEE, 2016.

[130] Jingya Li, Michail Matthaiou, and Tommy Svensson. I/Q imbalance in AF dual-hop relaying: Performance analysis in Nakagami-m fading. *IEEE Trans. Commun.*, 62(3):836–847, 2014.

[131] Xingwang Li, Meng Liu, Chao Deng, P Takis Mathiopoulos, Zhiguo Ding, and Yuanwei Liu. Full-duplex cooperative NOMA relaying systems with I/Q imbalance and imperfect SIC. *IEEE Wirel. Commun. Lett.*, 9(1):17–20, 2019.

[132] Hui Guo, Xuejiao Guo, Chao Deng, and Shangqing Zhao. Performance analysis of IQI impaired cooperative NOMA for 5G-enabled Internet of Things. *Wirel. Commun. Mob. Comp.*, 2020, 2020.

[133] Dongkai Cui, Xingwang Li, Gaojian Huang, Khaled Rabie, Galymzhan Nauryzbayev, and Basem M ElHalawany. Outage Probability of ABCom NOMA Systems for 6G with IQI and RHIs. In *2022 13th International Symposium on Communication Systems, Networks and Digital Signal Processing (CSNDSP)*, pages 384–389. IEEE, 2022.

[134] Dongkai Cui, Gaojian Huang, Yike Zheng, Hui Guo, Junxia Li, and Xingwang Li. Performance analysis of ABCom NOMA systems for 6G with generalized hardware impairments. *Physical Communication*, 54:101851, 2022.

[135] Xingwang Li, Yike Zheng, Mohammad Dahman Alshehri, Linpeng Hai, Venki Balasubramanian, Ming Zeng, and Gaofeng Nie. Cognitive AmBC-NOMA IoV-MTS networks with IQI: reliability and security analysis. *IEEE Transactions on Intelligent Transportation Systems*, 2021.

[136] Lina Bariah, Bassant Selim, Lina Mohjazi, Sami Muhaidat, Paschalis C Sofotasios, and Walaa Hamouda. Pairwise error probability of non-orthogonal multiple access with I/Q imbalance. In *2019 UK/China Emerging Technologies (UCET)*, pages 1–4. IEEE, 2019.

[137] Linglong Dai, Bichai Wang, Zhiguo Ding, Zhaocheng Wang, Sheng Chen, and Lajos Hanzo. A survey of non-orthogonal multiple access for 5G. *IEEE Communications Surveys & Tutorials*, 20(3):2294–2323, Third Quarter 2018.

[138] Wonjae Shin, Mojtaba Vaezi, Byungju Lee, David J Love, Jungwoo Lee, and H Vincent Poor. Non-orthogonal multiple access in multi-cell networks: Theory, performance, and practical challenges. *IEEE Communications Magazine*, 55(10):176–183, Oct 2017.

[139] Yuya Saito, Anass Benjebbour, Yoshihisa Kishiyama, and Takehiro Nakamura. System-level performance evaluation of downlink non-orthogonal multiple access (NOMA). In *2013 IEEE 24th Annual International Symposium on Personal, Indoor, and Mobile Radio Communications (PIMRC)*, pages 611–615. IEEE, Sep 2013.

[140] Zheng Yang, Zhiguo Ding, Pingzhi Fan, and Naofal Al-Dhahir. A general power allocation scheme to guarantee quality of service in downlink and uplink NOMA systems. *IEEE Transactions on Wireless Communications*, 15(11):7244–7257, Nov 2016.

[141] Jinglun Wang, Bin Xia, Kexin Xiao, Yichen Gao, and Shaodan Ma. Outage performance analysis for wireless non-orthogonal multiple access systems. *IEEE Access*, 6:3611–3618, Feb 2018.

[142] Sotiris A Tegos, Panagiotis D Diamantoulakis, Junjuan Xia, Lisheng Fan, and George K Karagiannidis. Outage performance of uplink NOMA in land mobile satellite communications. *IEEE Wireless Communications Letters*, 9(10):1710–1714, Oct 2020.

[143] Zhiguo Ding, Mugen Peng, and H Vincent Poor. Cooperative non-orthogonal multiple access in 5G systems. *IEEE Communications Letters*, 19(8):1462–1465, 2015.

[144] Zhiqiang Wei, Linglong Dai, Derrick Wing Kwan Ng, and Jinhong Yuan. Performance analysis of a hybrid downlink-uplink cooperative NOMA scheme. In *2017 IEEE 85th Vehicular Technology Conference (VTC Spring)*, pages 1–7. IEEE, Jun 2017.

[145] Vibhum Singh, Vinay Bankey, and Prabhat K Upadhyay. Underlay cognitive hybrid satellite-terrestrial networks with cooperative-NOMA. In *2020 IEEE Wireless Communications and Networking Conference (WCNC)*, pages 1–6. IEEE, 2020.

[146] Zheng Yang, Zhiguo Ding, Yi Wu, and Pingzhi Fan. Novel relay selection strategies for cooperative NOMA. *IEEE Transactions on Vehicular Technology*, 66(11):10114–10123, Nov 2017.

[147] Hongjiang Lei, Zixuan Yang, Ki-Hong Park, Imran Shafique Ansari, Yongcai Guo, Gaofeng Pan, and Mohamed-Slim Alouini. Secrecy outage analysis for cooperative NOMA systems with relay selection schemes. *IEEE Transactions on Communications*, 67(9):6282–6298, Sep 2019.

[148] Jinjin Men and Jianhua Ge. Non-orthogonal multiple access for multiple-antenna relaying networks. *IEEE Communications Letters*, 19(10):1686–1689, Oct 2015.

[149] Tri Nhu Do, Daniel Benevides da Costa, Trung Q Duong, and Beongku An. Improving the performance of cell-edge users in MISO-NOMA systems using TAS and SWIPT-based cooperative transmissions. *IEEE Transactions on Green Communications and Networking*, 2(1):49–62, Mar 2017.

[150] Hichem Semira and Ferdi Kara. Error performance of uplink SIMO-NOMA with joint maximum-likelihood and adaptive M-PSK. In *2021 IEEE International Black Sea Conference on Communications and Networking (BlackSeaCom)*, pages 1–6. IEEE, May 2021.

[151] Safia Beddiaf, Abdellatif Khelil, Faical Khennoufa, and Khaled Rabie. On the impact of IQI on cooperative NOMA with direct links in the presence of imperfect CSI. *Physical Communication*, 56:101952, 2023.

[152] Fan Ding, Hui Wang, Shengli Zhang, and Mingjun Dai. Impact of residual hardware impairments on non-orthogonal multiple access based amplify-and-forward relaying networks. *IEEE Access*, 6:15117–15131, Apr 2018.

[153] X Li, J Li, J Jin, and L Li. Performance analysis of relaying systems over Nakagami-m fading with transceiver hardware impairments. *Journal of Xidian university*, 45(3), Jun 2018.

[154] Safia Beddiaf, Abdellatif Khelil, Faical Khennoufa, Ferdi Kara, Hakan Kaya, Xingwang Li, Khaled Rabie, and Halim Yanikomeroglu. A Unified Performance Analysis of Cooperative NOMA With Practical Constraints: Hardware Impairment, Imperfect SIC and CSI. *IEEE Access*, 10:132931–132948, Dec 2022.

[155] Kefeng Guo, Chao Dong, and Kang An. NOMA-based cognitive satellite terrestrial relay network: Secrecy performance under channel estimation errors and hardware impairments. *IEEE Internet of Things Journal*, 9(18):17334–17347, 2022.

[156] Yerassyl Akhmetkaziyev, Galymzhan Nauryzbayev, Sultangali Arzykulov, Ahmed M Eltawil, Khaled M Rabie, and Xingwang Li. Performance of NOMA-enabled cognitive satellite-terrestrial networks with non-ideal system limitations. *IEEE Access*, 9:35932–35946, 2021.

[157] Faical Khennoufa, Abdellatif Khelil, Safia Beddiaf, Ferdi Kara, Khaled Rabie, Hakan Kaya, Ahmet Emir, Salama Ikki, and Halim Yanikomeroglu. Wireless powered cooperative communication network for dual-hop uplink NOMA with IQI and SIC imperfections. *IEEE Access*, 2023.

[158] Meng Shen, Zihao Huang, Xianfu Lei, and Lisheng Fan. BER analysis of NOMA with max-min relay selection. *China Communications*, 18(7):172–182, Jul 2021.

[159] Safia Beddiaf, Abdellatif Khelil, Faical Khennoufa, Ferdi Kara, Khaled Rabie, Xingwang Li, Hakan Kaya, Ahmet Emir, and Halim Yanikomeroglu. Impact of hardware impairment on the uplink SIMO Cooperative NOMA with selection relay under imperfect CSI. *IEEE Access*, 2023.

[160] Marvin K Simon and Mohamed-Slim Alouini. *Digital communication over fading channels*. New York: Wiley, 2001.

[161] John W Craig. A new, simple and exact result for calculating the probability of error for two-dimensional signal constellations. In *MILCOM 91-Conference record*, pages 571–575. IEEE, 1991.

Scientific Production

Authored paper- Published

- «Performance Analysis of the NOMA Network under Joint Hardware Impairment and Imperfect Channel State Information» Telecommunications and Radio Engineering.
- « A Unified Performance Analysis of Cooperative NOMA with Practical Constraints: Hardware Impairment, Imperfect SIC, and CSI » IEEE Access, 2022, vol. 10, p. 132931-132948.
- « On the Impact of IQI on Cooperative NOMA with Direct Links in the Presence of Imperfect CSI» Physical Communication, 2023, vol. 56, p. 101952.
- « Impact of Hardware Impairment on the Uplink SIMO Cooperative NOMA with Selection Relay under Imperfect CSI» IEEE Access, 2023.

Co-Authored paper- Published

- «Wireless Powered Cooperative Communication Network for Dual-Hop Uplink NOMA with IQI and SIC Imperfections» IEEE Access, 2023.

Conference paper- Published

- « Outage probability performance of NOMA in the presence of I/Q imbalance » The International Conference on Advances in Communication Technology, Computing and Engineering, Morocco, 2021.

Appendix A

The average bit error rate (ABER) at the U_1 can be presented as in [160]

$$P_1 = \frac{1}{2}\Bigg[\sum_{i=1}^{2}\bigg(\int_0^\infty Q(\Gamma_i) f_{\Gamma_i}(\Gamma_i) d_{\Gamma_i}\bigg)\Bigg], \tag{A.1}$$

where $f_{\Gamma_i}(\Gamma_i)$ is the Rayleigh distributed probability density function which is given as

$$f_{\Gamma_i}(\Gamma_i) = \frac{1}{\bar{\Gamma_i}} \exp\left(\frac{-\Gamma_i}{\bar{\Gamma_i}}\right) \tag{A.2}$$

An alternative representation of the Q-function as defined by Craig's formulation as in [161].

$$Q(x) = \frac{1}{\pi}\int_0^{\frac{\pi}{2}} \exp\left(\frac{-x^2}{2sin^2(\theta)}\right) \tag{A.3}$$

Furthermore, the moment-generating function (MGF) is provided as follows

$$MGF_\Gamma(x) = \int_0^\infty \exp(x\Gamma) f_\Gamma(\Gamma) d_\Gamma \tag{A.4}$$

Then, the ABER can be given as:

$$P_1 = \frac{1}{2}\Bigg[\sum_{i=1}^{2}\left(\frac{1}{\pi}\int_0^{\frac{\pi}{2}} MGF_{\Gamma_i}\left(\frac{-1}{2sin^2(\theta)}\right) d\theta\right)\Bigg] \tag{A.5}$$

with

$$MGF_{\Gamma_i}(x) = (1 - x\bar{\Gamma_i})^{-1} \tag{A.6}$$

Replacing (A.6) into (A.5), it becomes

$$P_1 = \frac{1}{2}\Bigg[\sum_{i=1}^{2}\left(\frac{1}{\pi}\int_0^{\frac{\pi}{2}} \left(1 + \frac{\bar{\Gamma_i}}{2sin^2(\theta)}\right)^{-1}\right)\Bigg] \tag{A.7}$$

However, according to [160], the term of (A.7) can be presented as

$$\frac{1}{\pi}\int_0^{\frac{\pi}{2}} \left(1 + \frac{\bar{\Gamma_i}}{2sin^2(\theta)}\right)^{-1} d\theta = \frac{1}{2}\left[1 - \sqrt{\frac{\frac{\bar{\Gamma_i}}{2}}{1 + \frac{\bar{\Gamma_i}}{2}}}\right] \tag{A.8}$$

Appendix B

The ABER at the U_2 can be presented as

$$P_2 = \frac{1}{2}\Bigg[\int_0^{\infty} Q(\Gamma_3) f_{\Gamma_3}(\Gamma_3) d_{\Gamma_3} + \int_0^{\infty} Q(\Gamma_4) f_{\Gamma_4}(\Gamma_4) d_{\Gamma_4} + \int_0^{\infty} Q(\Gamma_5) f_{\Gamma_5}(\Gamma_5) d_{\Gamma_5} + \int_0^{\infty} Q(\Gamma_6) f_{\Gamma_6}(\Gamma_6) d_{\Gamma_6} + \int_0^{\infty} Q(\Gamma_7) f_{\Gamma_7}(\Gamma_7) d_{\Gamma_7} + \int_0^{\infty} Q(\Gamma_8) f_{\Gamma_8}(\Gamma_8) d_{\Gamma_8}\Bigg], \tag{B.1}$$

According to (A.3) we can write (B.1) as

$$P_2 = \frac{1}{2}\Bigg[\int_0^{\infty} \frac{1}{\pi}\int_0^{\frac{\pi}{2}} \exp\left(\frac{-\Gamma_3}{2sin^2(\theta)}\right) f_{\Gamma_3}(\Gamma_3) d_{\Gamma_3} + \int_0^{\infty} \frac{1}{\pi}\int_0^{\frac{\pi}{2}} \exp\left(\frac{-\Gamma_4}{2sin^2(\theta)}\right) f_{\Gamma_4}(\Gamma_4) d_{\Gamma_4} + \int_0^{\infty} \frac{1}{\pi}\int_0^{\frac{\pi}{2}} \exp\left(\frac{-\Gamma_5}{2sin^2(\theta)}\right) f_{\Gamma_5}(\Gamma_5) d_{\Gamma_5} + \int_0^{\infty} \frac{1}{\pi}\int_0^{\frac{\pi}{2}} \exp\left(\frac{-\Gamma_6}{2sin^2(\theta)}\right) f_{\Gamma_6}(\Gamma_6) d_{\Gamma_6} + \int_0^{\infty} \frac{1}{\pi}\int_0^{\frac{\pi}{2}} \exp\left(\frac{-\Gamma_7}{2sin^2(\theta)}\right) f_{\Gamma_7}(\Gamma_7) d_{\Gamma_7} + \int_0^{\infty} \frac{1}{\pi}\int_0^{\frac{\pi}{2}} \exp\left(\frac{-\Gamma_8}{2sin^2(\theta)}\right) f_{\Gamma_8}(\Gamma_8) d_{\Gamma_8}\Bigg] \tag{B.2}$$

Using MGF and some manipulation mathematics, we can obtain

$$P_2 = \frac{1}{2}\Bigg[\frac{1}{\pi}\int_0^{\frac{\pi}{2}} \left(1 + \frac{\bar{\Gamma}_3}{2sin^2(\theta)}\right)^{-1} d\theta + \frac{1}{\pi}\int_0^{\frac{\pi}{2}} \left(1 + \frac{\bar{\Gamma}_4}{2sin^2(\theta)}\right)^{-1} d\theta + \frac{1}{\pi}\int_0^{\frac{\pi}{2}} \left(1 + \frac{\bar{\Gamma}_5}{2sin^2(\theta)}\right)^{-1} d\theta + \frac{1}{\pi}\int_0^{\frac{\pi}{2}} \left(1 + \frac{\bar{\Gamma}_6}{2sin^2(\theta)}\right)^{-1} d\theta + \frac{1}{\pi}\int_0^{\frac{\pi}{2}} \left(1 + \frac{\bar{\Gamma}_7}{2sin^2(\theta)}\right)^{-1} d\theta + \frac{1}{\pi}\int_0^{\frac{\pi}{2}} \left(1 + \frac{\bar{\Gamma}_8}{2sin^2(\theta)}\right)^{-1} d\theta\Bigg] \tag{B.3}$$

Using (A.8) we can define the (2.35).

Appendix C

The outage of x_1 at U_1 and R occurs if the received SINR of x_1 is less than the threshold $\gamma_{th,1}$. Therefore, using PDF and CDF as [60], the OP of the x_1 at U_1 and R under HWI and ipCSI is computed as

$$
\begin{aligned}
&P_{x_1,m}(out) = P(\gamma_1^m \geq \gamma_{th,1}) \\
&= P(\frac{\alpha_1 P_s|\tilde{h}_{s,1}|^2}{\alpha_2 P_s|\tilde{h}_{s,1}|^2 + \sigma_\epsilon^2 P_s + \sigma_\epsilon^2 P_s k_{s,1}^2 + |\tilde{h}_{s,1}|^2 P_s k_{s,1}^2 + N_0} \geq \gamma_{th,1}) \\
&= P(|\tilde{h}_{s,1}|^2 \geq (\frac{\gamma_{th,1}\left(N_0 + \sigma_\epsilon^2 P_s + \sigma_\epsilon^2 P_s {k_{s,1}}^2\right)}{\Phi_{s,1}(\alpha_1 P_s - \gamma_{th,1} P_s \alpha_2 - \gamma_{th,1} P_s k_s 1^2)})) \\
&= \int_0^{\frac{\gamma_{th,1}\left(N_0+\sigma_\epsilon^2 P_s+\sigma_\epsilon^2 P_s {k_{s,1}}^2\right)}{\Phi_{s,1}\left(\alpha_1 P_s-\gamma_{th,1} P_s \alpha_2-\gamma_{th,1} P_s {k_{s,1}}^2\right)}} \frac{1}{\Phi_{s,1}} \exp \frac{-y}{\Phi_{s,1}}\, dy.
\end{aligned}
\tag{C.1}
$$

Appendix D

The error probability for the x_1 symbols at U_1 under HWI and ipCSI is given as

$$\begin{aligned} P_{x_1,s,1} =& \frac{1}{2}\Big((P(n+(\sqrt{P}_s(\sqrt{\alpha_1}+\sqrt{\alpha_2})+\eta_{s,1})e+\tilde{h}_{s,1}\eta_{s,1}) \geq \sqrt{P}_s(\sqrt{\alpha_1}+\sqrt{\alpha_2})\tilde{h}_{s,1})+ \\ & ((P(n+(\sqrt{P}_s(\sqrt{\alpha_1}-\sqrt{\alpha_2})+\eta_{s,1})e+\tilde{h}_{s,1}\eta_{s,1}) \geq \sqrt{P}_s(\sqrt{\alpha_1}-\sqrt{\alpha_2})\tilde{h}_{s,1})\Big). \end{aligned} \tag{D.1}$$

By using Q-function and PDF in as in [47]

$$P_{x_1,s,1} = \frac{1}{2}\sum_{i=1}^{2}\Big(\mathrm{Q}(\sqrt{2\Delta_{x_1,s,1,i}})\Big). \tag{D.2}$$

The ABER of the U_1 can be expressed

$$P_{x_1,s,1} = \frac{1}{2}\Bigg[\sum_{i=1}^{2}\int_0^\infty \mathrm{Q}\left(\sqrt{2\delta_{m1,s1,i}}\right) f_{\delta_{m1,s1,i}}(\delta_{m1,s1,i}) d_{\delta_{m1,s1,i}}\Bigg], \tag{D.3}$$

where $f_{\Delta_{x_1,s,1,i}}$ is the PDF for the Rayleigh distribution which is presented in [112]. After performing some algebraic computations, we determine the ABER for U_1 using HWI and ipCSI as in (4.14)

Appendix E

The BER of x_2 at U_2 under HWI and ipCSI is given as

$$P_{x_2,s,2} = P^{\text{correct}}_{x_2,s,2} + P^{\text{error}}_{x_2,s,2}, \tag{E.1}$$

where $P^{\text{correct}}_{x_2,s,2}$ is the probability when the x_1 is detected correctly at U_2 and $P^{\text{error}}_{x_2,s,2}$ is the probability when the x_1 is detected erroneously at U_2. Each term can be defined as

$$\begin{aligned} P^{\text{correct}}_{x_2,s2} = \frac{1}{4}\Bigg[& \Big(P(n + (\sqrt{P_s}(\sqrt{\alpha_1} + \sqrt{\alpha_2}) + \eta_{s,2})e + \tilde{h}_{s,2}\eta_{s,2} \leq \sqrt{P_s}(\sqrt{\alpha_1} + \sqrt{\alpha_2})\tilde{h}_{s,2})\Big) \times \\ & \Big(P(n + (\sqrt{P_s}(\sqrt{\alpha_1} + \sqrt{\alpha_2}) + \eta_{s,2})e + \tilde{h}_{s,2}\eta_{s,2} \geq \\ & \sqrt{P_s}\sqrt{\alpha_2}\tilde{h}_{s,2}|n + (\sqrt{P_s}(\sqrt{\alpha_1} + \sqrt{\alpha_2}) + \eta_{s,2})e + \tilde{h}_{s,2}\eta_{s,2})\Big) + \\ & \Big(P(n + (\sqrt{P_s}(\sqrt{\alpha_1} - \sqrt{\alpha_2}) + \eta_{s,2})e + \tilde{h}_{s,2}\eta_{s,2} \leq \sqrt{P_s}(\sqrt{\alpha_1} - \sqrt{\alpha_2})\tilde{h}_{s,2})\Big) \times \\ & \Big(P(n + (\sqrt{P_s}(\sqrt{\alpha_1} - \sqrt{\alpha_2}) + \eta_{s,2})e + \tilde{h}_{s2}\eta_{s,2} \geq \\ & \sqrt{P_s}\sqrt{-\alpha_2}\tilde{h}_{s,2}|n + (\sqrt{P_s}(\sqrt{\alpha_1} - \sqrt{\alpha_2}) + \eta_{s,2})e + \tilde{h}_{s,2}\eta_{s,2})\Big)\Bigg]. \end{aligned} \tag{E.2}$$

And

$$P^{\text{error}}_{m_2,s,2} = \frac{1}{2}\Bigg(P(n + (\sqrt{P_s}(\sqrt{\alpha_1} + \sqrt{\alpha_2}) + \eta_{s2})e + \tilde{h}_l\eta_{s2} \geq \sqrt{P_s}(\sqrt{\alpha_1} + \sqrt{\alpha_2})\tilde{h}_{s2})\Bigg)\times$$
$$\Bigg(P(n + (\sqrt{P_s}(\sqrt{\alpha_1} + \sqrt{\alpha_2}) + \eta_{s2})e + \tilde{h}_{s2}\eta_{s2} \geq$$
$$\sqrt{P_s}(2\sqrt{\alpha_1} + \alpha_2)|n + (\sqrt{P_s}(\sqrt{\alpha_1} + \sqrt{\alpha_2}) + \eta_{s2})e + \tilde{h}_{s2}\eta_{s2} \geq \sqrt{P_s}(\sqrt{\alpha_1} + \sqrt{\alpha_2})\tilde{h}_{s2})\Bigg)+$$
$$\Bigg(P(n + (\sqrt{P_s}(\sqrt{\alpha_1} - \sqrt{\alpha_2}) + \eta_{s2})e + \tilde{h}_{s2}\eta_{s2} \geq \sqrt{P_s}(\sqrt{\alpha_1} - \sqrt{\alpha_2})\tilde{h}_{s2})\Bigg)\times$$
$$\Bigg(P(n + (\sqrt{P_s}(\sqrt{\alpha_1} - \sqrt{\alpha_2}) + \eta_{s2})e + \tilde{h}_{s2}\eta_{s2} \leq$$
$$\sqrt{P_s}(2\sqrt{\alpha_1} - \alpha_2)|n + (\sqrt{P_s}(\sqrt{\alpha_1} - \sqrt{\alpha_2}) + \eta_{s2})e + \tilde{h}_{s2}\eta_{s2} \geq \sqrt{P_s}(\sqrt{\alpha_1} - \sqrt{\alpha_2})\tilde{h}_{s2})\Bigg). \tag{E.3}$$

Replacing (E.2) and (E.3) into (E.1) and using the PDF, Q-function, and some algebraic manipulation we get the ABER of U_2 as in (4.37).